INVESTIGATION OF HIGH CONCENTRATION SLURRY DISPOSAL THROUGH PIPE BEND

A thesis submitted in fulfillment of the requirements for the award of the degree of

DOCTOR OF PHILOSOPHY

By

Jatinder Pal Singh

(Enrollment No.: 901608004)

Under the supervision of

Dr. Satish Kumar
(Associate Professor)
Mechanical Engineering Department,
National Institute of Technology,
Jamshedpur, India

Prof. S. K. Mohapatra
(Senior Professor)
Mechanical Engineering Department,
Thapar Institute of Engineering and Technology,
Patiala, India

Mechanical Engineering Department

THAPAR INSTITUTE OF ENGINEERING AND TECHNOLOGY

PATIALA-147004, INDIA

October 2019

Dedicated to my parents

&

Friends

THAPAR INSTITUTE OF ENGINEERING AND TECHNOLOGY,

PATIALA, INDIA

(Established in 1956)

CERTIFICATE

This is to certify that the work presented in dissertation entitled **"Investigation of high concentration slurry disposal through pipe bend"** is submitted in partial fulfillment of the requirements for the award of degree of **Doctor of Philosophy** under the supervision of **Dr. Satish Kumar**, (Associate Professor, Mechanical Engineering Department, National Institute of Technology, Jamshedpur, India) and **Prof. S. K. Mohapatra** (Senior Professor and Former Head, Mechanical Engineering Department, Thapar Institute of Engineering and Technology, Patiala). The contents of this thesis, in full or in parts, have not been submitted to any other Institute or University for the award of any degree or diploma.

Jatinder Pal Singh

Enrolment No.: 901608004

Date: 18|10|19

This is certified that the above statement made by **Mr. Jatinder Pal Singh** is correct to the best of our knowledge and belief.

Supervisor
Dr. Satish Kumar
(Associate Professor)
Mechanical Engineering Department
National Institute of Technology
Jamshedpur, Jharkhand, India

Supervisor
Prof. S. K. Mohapatra
(Senior Professor)
Mechanical Engineering Department
Thapar Institute of Engineering and Technology
Patiala, Punjab, India

ACKNOWLEDGEMENT

I accord my recondite gratitude to the Almighty God, whose grace enabled me to achieve the chosen ambition and for whatever I am today. No words can suffice my feelings of gratitude towards my father, my mother whose blessings and unconditional love were the driving force during the entire period of my study.

The most pleasant part of work is the opportunity to express my gratitude to *Dr. Satish Kumar* (Associate Professor, Department of Mechanical Engineering, National Institute of Technology, Jamshedpur, India) and *Prof. S.K. Mohapatra* (Senior Professor, Mechanical Engineering Department, Thapar Institute of Engineering and Technology, Patiala, India) for being my guide under his constant supervision, able guidance, concrete suggestions, constructive criticism and sustained encouragement this work was planned and successfully completed. I owe a deep sense of gratitude to him for his untiring efforts at each and every step.

I am eternally grateful to *Prof. Prakash Gopalan* (Director, Thapar Institute of Engineering and Technology, Patiala, India) and *Dr. Rafat Siddique* (Dean of Research and Sponsored Projects, Thapar Institute of Engineering and Technology, Patiala, India) for providing an environment conductive to quality research and learning. I am also grateful to the members of Doctoral committee for their valuable feedback.

The work is not possible without the help of *Dr. Jashanpreet Singh*, *Dr. Mani Kanwar Singh*, and *Dr. Gurprit Singh* who stand with me at every stage of work to solve different problems during experimentation. Last but not the least, I would like to thank my other labmates, *Dr. Kaushal Kumar*, *Mr. Mandeep Singh*, and *Mr. Sagar Kumar* have also contributed a lot at various phases during work.

I am also thankful to *Mr. Satwinder Singh (Malhi)* and *Mr. Sukhbir Singh*, Lab Technicians, Fluid Machinery Lab, Mechanical Engineering Department, Thapar Institute of Engineering and Technology, Patiala, India for their instructions and advice during all experimentation conducted for dissertation work.

I would like to acknowledge Mechanical Engineering Department, Thapar Institute of Engineering and Technology, Patiala and Sophisticated Analytics Laboratories, Patiala for providing the necessary facilities to carry out the various testing and experiments.

Jatinder Pal Singh

ABSTRACT

The present investigation is carried out to investigate the head loss characteristics across 90˚ pipe bends for the flow of concentrated coal and coal-ash slurries. Before head loss experiments, different bench-scale tests are carried out to analyze the physical and chemical characteristic of solid particles. The specific gravity of coal, fly and bottom ash sample is determined as 1.46±2%, 2.27±0.5% and 2.09±1.6%. The maximum settled concentration for coal, fly ash and bottom slurry is observed as in range 65.37-76.55%, 59.67-73.92% and 53.79-68.58% for a solid concentration range of 30-60% respectively. The *pH* of coal-water slurry varies in the range of 6.38-5.93 as solid concentration is increased from 10-60% (by weight). The pH value for fly and bottom ash suspensions are lies in the range of 7.62-7.42 and 7.68-7.45 respectively for the solid concentration range of 30-60%.

Extensive rheological experimentation is performed to analyze flow characteristics of coal-water slurry with and without the use of the additive. The coal-water slurry exhibits Newtonian behaviour at a solid concentration of 30% (by weight). The coal-water slurry exhibits shear thinning behaviour at higher solid concentrations (i.e. above 30%) that show its pseudo-plastic nature. The addition of a small amount of sulphonic acid resulted in an improvement in the rheological properties of the coal-water slurry suspension. Similarly, the rheological experiments are carried out for fly and bottom ash slurry with and without the use of additive (sodium triphosphate). The fly ash slurry exhibits Newtonian behaviour for a solid concentration of 30%. Fly ash slurry shows Bingham plastic behaviour for a solid concentration range of 40-60% (by weight). The bottom ash slurry exhibits Newtonian behaviour for solid suspension up to a solid concentration of 30%. The bottom ash slurry shows Bingham flow behaviour above 40% solid concentration. The addition of sodium triphosphate results in a decrease in viscosity of bottom and fly ash slurry. The maximum percentage decrease in apparent viscosity is observed with 4% addition of sodium triphosphate in fly and bottom ash slurry.

After the rheological analysis of slurry, the head loss experiments are conducted with slurries of different solid concentrations, varying from 30-60% (by weight). During experimentation, the average flow velocity is kept in the range of 2-5 m/s. The *r/D* ratio for the pipe bend varied within the range of 1.5-2.5. Pulverized coal sample having particle size less than 53 µm is used to prepare the coal-water slurry whereas the as-collected samples fly and bottom ash are directly used to prepare the coal-ash slurries. From results, it is found that

the head loss across 90° pipe bend increases with the increase in the solid concentration of coal and coal-ash slurries. The head loss across pipe bends is a function of the solid concentration and *r/D* ratio. A sudden drop in head loss is found as the *r/D* ratio is increased from 1.5 to 2.0. The optimum *r/D* ratio for minimum head loss in a 90˚ pipe bend is 2.0; beyond this, the increase in head loss is seen due to increase in effective length of pipe bend. The head loss across pipe bends for fly ash slurry is more than coal and bottom ash slurry. The maximum reduction in head loss is observed with a 3% (by weight) addition of sulfonic acid in coal-water slurry and 4% addition of sodium triphosphate in coal-ash slurry. Thus, the addition of additive is one of the economical ways to convey the coal and coal-ash slurry at higher solid concentrations.

Computational fluid dynamics (CFD) simulations are also carried out to obtain the head loss, flow patterns and contours for the flow of coal and coal-ash slurry. An Eulerian multiphase model with an SST k-ω approach is used for carrying out the numerical simulations for 50 mm pipe bend geometry. The effect of flow separation and secondary flows on turbulence, flow velocity and distribution of the solid suspension inside the bend geometry is also studied with the help of contours. The *r/D* ratio of 90˚ and 45˚ pipe bend is varied within the range of 1.5-3.0. The minimum head loss is observed across 45˚ bend. The optimum *r/D* ratio for minimum head loss across 45˚ and 90˚ pipe bend is observed as 1.5 and 2.0 respectively. The detailed phenomenon of flow in pipe bends is also discussed with the help of volume fraction, turbulence intensity and velocity contours at different locations in pipe bend.

TABLE OF CONTENTS

Chapter 1 INTRODUCTION 2

1.1 SLURRY TRANSPORTATION SYSTEM 2

1.1.1 Basic components and layout of the slurry transportation system 4

1.2 SLURRY PIPELINE SYSTEM 5

1.3 TYPES OF MEDIA FLOWS INSIDE PIPELINES 6

1.4 FLOW REGIMES IN TWO-PHASE SLURRY FLOW 7

1.5.1 Fully dispersed-symmetric or homogeneous flow 7

1.5.2 Fully dispersed-asymmetric or heterogeneous flow 7

1.5.3 Asymmetric flow with rolling & saltation motion 7

1.5.4 Sliding or moving bed flow 9

1.5.5 Stationary or fixed bed flow 9

1.5 COMPLEXITIES DUE TO TWO-PHASE FLOW INSIDE PIPE BEND 9

1.6 MOTIVATION BEHIND PRESENT STUDY 10

1.7 THESIS OUTLINES 12

Chapter 2 LITERATURE REVIEW 15

2.1 RHEOLOGICAL CHARACTERISTICS OF VARIOUS MINERAL AND SOLID WASTE SLURRIES 16

2.2 EXPERIMENTAL ANALYSIS OF HEAD LOSS FOR DIFFERENT SLURRIES 20

2.3 COMPUTATIONAL ANALYSIS OF HEAD LOSS CHARACTERISTICS ... 33

2.4 GAPS IN LITERATURE 41

2.5 PROBLEM STATEMENT AND METHODOLOGY 41

2.6 OBJECTIVES OF PRESENT WORK 42

Chapter 3 CHARACTERIZATION OF COAL, FLY AND BOTTOM ASH 45

3.1 COLLECTION OF COAL, FLY AND BOTTOM ASH SAMPLES 46

3.2 SURFACE MORPHOLOGY OF COAL AND COAL ASH SAMPLES 48

3.2.1 Surface morphology or microstructure analysis 49

3.3 BENCH SCALE INVESTIGATIONS 53

3.3.1 Particle size distribution 53

3.3.2 Specific gravity of coal and coal-ash sample 56

3.3.3 Potential of hydrogen (pH) 57
3.3.4 Static settled concentration 58
3.4 REMARKS 60

Chapter 4 RHEOLOGY OF COAL AND COAL-ASH SLURRIES 63
4.1 SPECIFICATIONS OF RHEOMETER 64
4.2 SAMPLE PREPARATION AND PROCEDURE 67
4.3 RHEOLOGICAL BEHAVIOUR OF COAL-WATER SLURRY 67
4.4.1 Rheological characteristics of fine particulate (< 53μm) coal-water slurry 69
4.4.2 Effect of an additive on the rheological behaviour of coal-water suspension 69
4.4 RHEOLOGY OF COAL-ASH SLURRY 72
4.5.1 Rheological characteristics of fly ash slurry 73
4.5.2 Effect of an additive on the rheological behaviour of fly ash suspension 75
4.5.3 Rheological characteristics of bottom ash-water slurry 76
4.5.4 Effect of an additive on the rheological behaviour of bottom ash suspension 78
4.5 REMARKS 79

Chapter 5 EXPERIMENTAL INVESTIGATION OF HEAD LOSS CHARCTERSTICS INSIDE PIPE BEND 82
5.1 DETAILS OF PILOT PLANT TEST LOOP 82
5.2 INSTRUMENTATION 83
5.2.1 Flow rate measurement *86*
5.2.2 Pressure measurement *86*
5.4 EXPERIMENTAL PROCEDURE 88
5.5 RANGE OF PARAMETERS 89
5.6 HEAD LOSS CHARACTERISTICS OF COAL AND COAL-ASH WATER SLURRY ACROSS 90° PIPE BEND 90
5.7 EFFECT OF ADDITIVES ON HEAD LOSS CHARACTERISTICS OF COAL AND COAL-ASH SLURRIES 95
5.8 BEND LOSS COEFFICIENT (K_b) IN PIPE BEND 98
5.9 SPECIFIC ENERGY CONSUMPTION (*SEC*) 101
5.10 REMARKS 103

Chapter 6 NUMERICAL SIMULATIONS OF HEAD LOSS CHARCTERSTICS INSIDE PIPELINE 105
6.1 MULTIPHASE FLOW MODEL 105
6.2 EULERIAN–MULTIPHASE MODEL 107
6.2.1 Conservation of Mass 107
6.2.2 Conservation of Momentum 107
6.2.3 Solid–liquid momentum equations 108
6.2.4 Shear stress in solid particles 109
6.3.1 SST k–ω turbulence Model 111
6.3.2 Standard k–ε turbulence Model 112
6.3.3 RNG k–ε turbulence Model 113
6.3.4 Realizable k–ε turbulence Model 113
6.4.1 Boundary Conditions 115
6.4.2 Grid independence test 115
6.5 VALIDATION OF NUMERICAL MODEL 117
6.6 HEAD LOSS CHARACTERSTICS OF 90˚ PIPE BEND FOR COAL AND COAL–ASH SLURRY 118
6.6.1 Influence of solid concentration on head loss characteristics 118
6.6.2 Influence of r/D ratio on head loss characteristics 122
6.6.3 Volume fraction contours 124
6.6.4 Turbulence intensity contours 132
6.6.5 Velocity distribution vectors and contours 139
6.7 EFFECT OF BEND ANGLE ON HEAD LOSS CHARACTERSTICS OF COAL AND COAL–ASH SLURRY 143
6.7.1 Volume fraction contours *146*
6.7.2 Turbulence intensity contours *148*
6.8 REMARKS 150

Chapter 7 CONCLUSIONS AND FUTURE SCOPES 153
7.1 SUMMARY 153
7.2 CONCLUSIONS 153
7.3 KEY RECOMMENDATIONS 156
7.4 SCOPE FOR FUTURE 156
7.5 ACKNOWLEDGEMENT 157

REFERENCES..158

LIST OF PUBLICATIONS 176

LIST OF FIGURES

Figure 1.1: Different types of slurry pipelines 3
Figure 1.2: Schematic layout of the slurry transportation system 4
Figure 1.3: Various types of flow regimes or patterns...8
Figure 2.1: Dispersion of solid phase under action of shear rate in two phase slurries..........16
Figure 2.2: Schematic illustration of viscosity meter used by Yoon et al. (2009)..................18
Figure 2.3: Schematic diagram of pilot test rig developed by Fangary et al. (1997)...............21
Figure 2.4: Schematic diagram of slurry loop at NCPP, Dadri (Kumar et al. 2000)...............22
Figure 2.5: Experimental test loop developed by Lu et al. (2002) 22
Figure 2.6: Schematic illustration of pilot plant test loop developed by Kumar et al. (2003).23
Figure 2.7: Experimental test facility developed by Azzi and Fridel (2005)...........................24
Figure 2.8: Schematic view of test loop developed by Kaushal et al. (2005)..........................24
Figure 2.9: Schematic representation of bend used by Spedding and Benard (2007) 25
Figure 2.10: Schematic illustration of pilot plant test rig developed by Verma et al. (2006)..26
Figure 2.11: Schematic diagram of experimental test loop developed by Chen et al. (2009) .26
Figure 2.12: Schematic illustration of experimental setup developed by EI-Nahhas et al. (2009)..27
Figure 2.13: Schematic diagram of pilot plant test rig developed by Chandel et al. (2010) ...28
Figure 2.14: Layout of experimental test loop developed by Vlasak and Chara (2011) 28
Figure 2.15: Schematic illustration of test rig developed by Slatter (2011) 29
Figure 2.16: Schematic layout of horizontal pipe-loop developed by Hashemi et al. (2014) .30
Figure 2.17: The test facility developed by Saidj et al. (2014)..30
Figure 2.18: Layout of experimental test rig developed by Wu et al. (2015)..........................31
Figure 2. 19: Schematic representation of test setup used by Autee and Giri (2016).............32
Figure 2.20: Unstructured meshing of horizontal pipe done by Ling et al. (2003) 34
Figure 2.21: Volume fraction profile for straight pipeline studied by Lahiri and Ghanta (2008) 34
Figure 2.22: Solid concentration contours for volume fraction of 40% in straight pipeline studied by Kaushal et al. (2012) 36
Figure 2.23: Schematic layout of experimental test loop developed by Nabil et al. (2013)....37
Figure 2.24. Schematic illustration of pilot plant test loop developed by Mazumdar (2012) .40
Figure 2.25: Flow chart of experimental methodology 43

Figure 3.1: Location of source of coal sample (Jharia coal field, Jharkhand, India) [Image is taken from Google Earth, 2018] 46
Figure 3.2: Location of source of bottom ash sample (Deen Bandhu Chhotu Ram Thermal Power Plant, Yamunanagar, Haryana, India) [Image is taken from Google Earth, 2018] 47
Figure 3.3: Generation and utilization of coal ash in last years at Deen Bandhu Chhotu Ram Thermal Power Plant, Yamunanagar, Haryana, India [Source: www.hpgcl.org.in] 47
Figure 3.4: Location of source of bottom ash sample (Deen Bandhu Chhotu Ram Thermal Power Plant, Yamunanagar, Haryana, India) [Image is taken from Google Earth, 2018] 48
Figure 3.5: (a) Carbon tape coated sample holders (b) Auto fine coating machine manufactured by JEOL, Netherlands 49
Figure 3.6: Schematic line diagram of scanning electron microcopy (SEM) unit (Skoog *et al.* 2007) 50
Figure 3.7: Surface morphology of coal sample (particle size < 53 μm)................................51
Figure 3.8: SEM micrograph of fly ash 52
Figure 3.9: Surface morphology of bottom ash 53
Figure 3.10: Schematic line diagram of laser diffraction particle size apparatus 54
Figure 3.11: Particle size distribution of coal, fly and bottom ash samples 55
Figure 3.12: Effect of solid concentration on static settled concentration for coal-water slurry 58
Figure 3.13 Effect of solid concentration on static settled concentration for fly ash slurry 59
Figure 3.14: Effect of solid concentration on static settled concentration for bottom ash slurry 60
Figure 4.1: Photographic view of Rhelolab Q-C rheometer 64
Figure 4.2: Various types of rheometer arrangements 65
Figure 4.3: Uniform mixing of coal sample with stirrer 66
Figure 4.4: Rheogram of < 53μm fine coal-water slurry 68
Figure 4.5: Variation in apparent viscosity with shear rate of coal-water slurry.....................68
Figure 4.6: Effect of additive on the apparent viscosity of fine coal-water slurry 70
Figure 4.7: Variation shear stress-shear rate behaviour of coal-water slurry after addition of additive..71
Figure 4.8: Shear stress versus shear rate plot of fly ash slurry at different solid concentrations 72
Figure 4.9: Variation in apparent viscosity with shear rate of fly ash slurry...........................73
Figure 4.10: Variation of viscosity with shear rate (Perez et al. 2000) 74

Figure 4.11: Effect of additive on the apparent viscosity of fly ash-water slurry 75
Figure 4.12: Rheogram of bottom ash slurry at different solid concentrations 76
Figure 4.13: Variation in apparent viscosity with shear rate for bottom ash slurry.................77
Figure 4.14: Effect of additive on the apparent viscosity of bottom ash slurry.......................78
Figure 5.1: Schematic 3D view of pilot plant test loop 84
Figure 5.2: Photographic view of pilot plant test setup 85
Figure 5.3: Calibration of the flow meter 86
Figure 5.4: Calibration of the pressure transducer..87
Figure 5.5: Photographic view of slurry preparation tank 89
Figure 5.6: Samples collected from slurry sampler 89
Figure 5.7: Head loss characteristics of <53 μm coal-water slurry at (a) 30.27%, (b) 41.90%, (c) 50.73% and (d) 61.56% 91
Figure 5.8: Head loss characteristics of fly ash slurry at (a) 31.24%, (b) 40.96%, (c) 50.92% and (d) 60.42%...92
Figure 5.9: Head loss characteristics of bottom ash slurry (a) 29.98%, (b) 41.62%, (c) 50.42% and (d) 61.18%...94
Figure 5.10: Effect of additive on head loss of coal-water slurry...95
Figure 5.11: Effect of additive on head loss of (a) fly ash and (b) bottom ash slurries...........96
Figure 5.12: Phenomena of flow separation in 90˚ bends 97
Figure 5.13: Secondary flow phenomenon inside pipe bends 98
Figure 5.14: Variation in bend loss coefficient for different *r/D* ratio and Reynolds number for coal-water slurry...99
Figure 5.15: Variation in bend loss coefficient for different *r/D* ratio and Reynolds number for (a) fly ash and (b) bottom ash slurries...100
Figure 5.16: Effect of additive on specific energy consumption (SEC) of coal-water slurry101
Figure 5.17: Effect of additive on specific energy consumption (SEC) of (a) fly ash and (b) bottom ash slurries 102
Figure 6.1. Geometry and meshing of pipe bend..114
Figure 6.2: Head loss variation with number of elements in mesh.......................................116
Figure 6.3: Variation of GCI index with cell size for different meshes. 117
Figure 6.4: Validation of numerical simulations with experimental results..........................118
Figure 6.5: Variation in head loss against flow velocity and solid concentration for coal–water slurry 119

Figure 6.6: Variation in head loss against flow velocity and solid concentration for fly ash slurry 120
Figure 6.7: Variation in head loss against flow velocity and solid concentration for bottom ash slurry 121
Figure 6.8: Effect of *r/D* ratio on the head loss with flow velocity for coal–water slurry 122
Figure 6.9: Effect of *r/D* ratio on the head loss with flow velocity for fly ash slurry 123
Figure 6.10: Effect of *r/D* ratio on the head loss with flow velocity for bottom ash slurry ..124
Figure 6.11: Volume fraction contours of coal–water slurry (C_w =60%) flowing at different velocities 125
Figure 6.12: Volume fraction contours of fly ash slurry (C_w =60%) flowing at different velocities 126
Figure 6.13: Volume fraction contours of bottom ash slurry (C_w =60%) flowing at different velocities 127
Figure 6.14: Volume fraction contours of coal–water slurry at different concentrations for flow velocity of 5 m/s 128
Figure 6.15: Volume fraction contours of fly ash slurry at different concentrations for flow velocity of 5 m/s...129
Figure 6.16: Volume fraction contours of bottom ash slurry at different concentrations for flow velocity of 5 m/s 129
Figure 6.17: Effect of *r/D* on volume fraction distribution of coal –water slurry having solid concentration of 60%. 130
Figure 6.18: Effect of *r/D* on volume fraction distribution of fly ash slurry having solid concentration of 60%. 131
Figure 6.19: Effect of *r/D* on volume fraction distribution of bottom ash slurry having solid concentration of 60%. 132
Figure 6.20: Effect of solid concentration of coal–water slurry on turbulence intensity at bend outlet. 133
Figure 6.21: Effect of solid concentration of fly ash slurry on turbulence intensity at bend outlet. 133
Figure 6.22: Effect of solid concentration of bottom ash slurry on turbulence intensity at bend outlet. 134
Figure 6.23: Effect of flow velocity on the distribution of turbulence intensity for coal–water slurry 135

Figure 6.24: Effect of flow velocity on the distribution of turbulence intensity for fly ash slurry 136
Figure 6.25: Effect of flow velocity on the distribution of turbulence intensity for bottom ash slurry 136
Figure 6.26: Effect of bend curvature on turbulence intensity for coal–water slurry....138
Figure 6.27: Effect of bend curvature on turbulence intensity for fly ash slurry....138
Figure 6.28: Effect of bend curvature on turbulence intensity for bottom ash slurry....138
Figure 6.29: Effect of *r/D* ratio on velocity vectors at bend outlet for coal–water slurry 139
Figure 6.30: Effect of *r/D* ratio on velocity vectors at bend outlet for fly ash slurry 140
Figure 6.31: Effect of *r/D* ratio on velocity vectors at bend outlet for bottom ash slurry 140
Figure 6.32: Velocity contours at the outlet of bend for different *r/D* ratios for coal–water slurry 141
Figure 6.33: Velocity contours at the outlet of bend for different *r/D* ratios for fly ash slurry 142
Figure 6.34: Velocity contours at the outlet of bend for different *r/D* ratios for bottom ash slurry 142
Figure 6.35: Geometry of pipe bends at different bend angles....143
Figure 6.36: Variation in head loss at different bend angles and *r/D* ratio for coal–water slurry 144
Figure 6.37: Variation in head loss at different bend angles and *r/D* ratio for fly ash–water slurry 145
Figure 6.38: Variation in head loss at different bend angles and *r/D* ratio for bottom ash–water slurry 145
Figure 6.39: Volume fraction contours of coal–water slurry at different bend angles and *r/D* ratio 146
Figure 6. 40: Volume fraction contours of fly ash–water slurry at different bend angles and *r/D* ratio....147
Figure 6.41: Volume fraction contours of bottom ash–water slurry at different bend angles and *r/D* ratio....147
Figure 6. 42: Turbulence intensity contours of coal–water slurry at different bend angles and *r/D* ratio....148
Figure 6. 43: Turbulence intensity contours of fly ash–water slurry at different bend angles and *r/D* ratio....149

Figure 6. 44: Turbulence intensity contours of bottom ash–water slurry at different bend angles and *r/D* ratio..149

LIST OF TABLES

Table 4.1: Specification of Rhelolab Q-C rheometer 65
Table 4.2: Form factors for different rheometer arrangements (Anton Par Manual, 2012) 66
Table 5.1: Specifications of positive displacement progressive pump 83
Table 5.2: Accuracy and precision values of instruments 88

NOMENCLATURES

Symbols	***Description***
C_D	Drag coefficient
C_W	Solid concentration (% by weight)
d	Diameter of solid phase
D	Pipe Diameter (mm)
e_{bb}	Coefficient of restitutions
g	Acceleration due to gravity (m^2/s)
ΔH	Head loss
K_b	Bend loss coefficient
S	Source terms
P	Pressure force
P_B	Power required for suspension (W/m)
Q	Discharge (m^3/s)
r	Radius of curvature
Re	Reynolds number
$\vec{R}$	Interaction Force
V	Velocity (m/s)
$\vec{V}$	Terminal Velocity
W	Weight (grams)
W_B	Solid flow rate (ton/hr)
Greek letters	
ϕ	Specularity coefficient
θ	Granular temperature
φ	Internal friction angle
λ	Bulk viscosity
μ	Shear viscosity
τ	Shear stress tensor
σ	Prandtl number
Subscripts	
s	Secondary phase
p	Primary phase

coll	Collision
kine	Kinectic
fric	Frictional
m	Mixture
max	Maximum
min	Minimum
w	Weight
W	Water

Abbreviations

SEC	Specific energy consumption
PSD	Particle size distribution
pH	Potential of Hydrogen
SEM	Scanning Electron Microscopy

CHAPTER 1

INTRODUCTION

Chapter 1

INTRODUCTION

Slurry pipelines are widely used in the industrial sector for transportation of solid materials. The pipelines are a universally-adopted mode for the transportation of bulk solid materials over short and long distances in the form of slurry. The slurry is the viscous mixture of pulverized solid material and a carrier fluid. Carrier fluids such as water, air, oil, etc. are used to transport the solid materials which depend on the industrial application. The slurry is transported by using an extensive slurry transportation system which is defined as a two-phase flow system that transport bulk solid materials dispersed in a liquid phase. The existence of slurry transportation system on the earth is from the day when life started. The arterial system in the body of humans and animals carries a mixture of solids suspended in blood. In recent years, transportation of bulk solid materials through a pipeline is a progressive technology. A large number of networks of pipelines are being laid down in different countries for the transportation of mineral ores, coal, mineral tailings etc. (Bai *et al.* 2001; Shankar *et al.* 2009; Zandi, 2013; Parsi *et al.* 2014; Hussain *et al.* 2016; Mishra *et al.* 2016). The slurry transportation system is classified on the basis of physical properties of solid materials and type of flow in the pipeline i.e. heterogeneous flow, homogenous flow, sliding bed flow, stationary bed flow etc. The different types of slurry pipelines are illustrated in Figure 1.1.

1.1 SLURRY TRANSPORTATION SYSTEM

The slurry transportation systems are used from more than 100 years for disposal of solid waste in mineral, power and food industries. In recent years, the development of technology in the field of the slurry transportation system has also been led to the transportation of many useful products like coal, limestone, zinc ore, iron concentrate, and various other minerals. Some of the existing pipelines are transporting up to 60 million tons/year (Liu, 2003; Ilic and Wheeler, 2017; Rehman *et al*. 2017).

In today's world, the problem of environmental pollution is faced by every country around the globe. From the ecological perspective, slurry transportation systems are more beneficial than other traditional modes of transportation. Transporting solid materials via pipelines helps to minimize the air and noise pollution, minimum ecological disturbance, reduce traffic, dust-free, and reduce energy consumption. Moreover, the acceptance of slurry transportation system for long distances is also attractive because of its economic benefits. The slurry pipelines can be laid in difficult geographic areas, operational throughout the year, requires less maintenance and operating staff, highly reliable and efficient, easy to operate, install and cross artificial-natural obstacles like mountains, rivers, railways etc.

<table>
<tr><th>MATERIAL TRANSPORTED</th><th>MATERIAL STATE</th><th>STATE OF CARRIER FLUID</th><th colspan="2">STATE OF TRANSPORTED MATERIAL</th></tr>
<tr><td>Water</td><td rowspan="6">Liquid</td><td rowspan="3">Gas</td><td colspan="2" rowspan="2">Liquid-Gas</td></tr>
<tr><td rowspan="2">Oil</td></tr>
<tr><td colspan="2" rowspan="2">Liquid-Liquid</td></tr>
<tr><td rowspan="2">Liquid wastage</td><td rowspan="3">Liquid</td></tr>
<tr><td colspan="2" rowspan="2">Liquid</td></tr>
<tr><td>Liquid goods</td></tr>
<tr><td>Solid waste</td><td rowspan="4">Solid</td><td rowspan="2">Gas</td><td rowspan="2">Solid-Gas</td><td>Pneumatic</td></tr>
<tr><td rowspan="2">Coal</td><td rowspan="2">Capsule</td></tr>
<tr><td rowspan="2">Liquid</td><td rowspan="2">Solid-Liquid</td></tr>
<tr><td>Minerals</td><td>Slurry</td></tr>
<tr><td>Gas waste</td><td rowspan="4">Gas</td><td rowspan="2">Gas</td><td colspan="2">Gas-Liquid</td></tr>
<tr><td rowspan="2">Gas products</td><td colspan="2" rowspan="2">Gas-Gas</td></tr>
<tr><td rowspan="2">Liquid</td></tr>
<tr><td>Natural Gas</td><td colspan="2">Gas</td></tr>
</table>

Figure 1.1: Different types of slurry pipelines

In the context of numerous features of the slurry transportation system, there is no technical limitation to select this way of transportation in a big way. However, this system has not been much popular because of some drawbacks such as:

- The initial cost of installation is very high.
- The slurry pipeline system is restricted only to conveying solid products.
- It requires a large quantity of carrier fluid.
- Choking and leakage of the pipeline is also a big problem.
- Ease of transporting solid products such as minerals in inaccessible geographic areas like deserts, deep sea, and mountains for reclamation of minerals.

Various benefits of slurry transportation system lead to a wide scope for future applications. Hence, there is a need to carry out extensive research that leads to designing of optimum and more reliable slurry transportation system.

1.1.1 Basic components and layout of the slurry transportation system

The transportation of the solid products through the pipeline can be done by two ways either pneumatically or hydraulically. In pneumatic transportation, the carrier fluid is the air, whereas in hydraulic transportation, the carrier fluid is a liquid. The slurry transportation system is mainly divided into three sub-systems. These three sub-systems are:

- Crushing and slurry preparation system
- Pipeline and intermediate pumping system
- Terminal or end utilization system

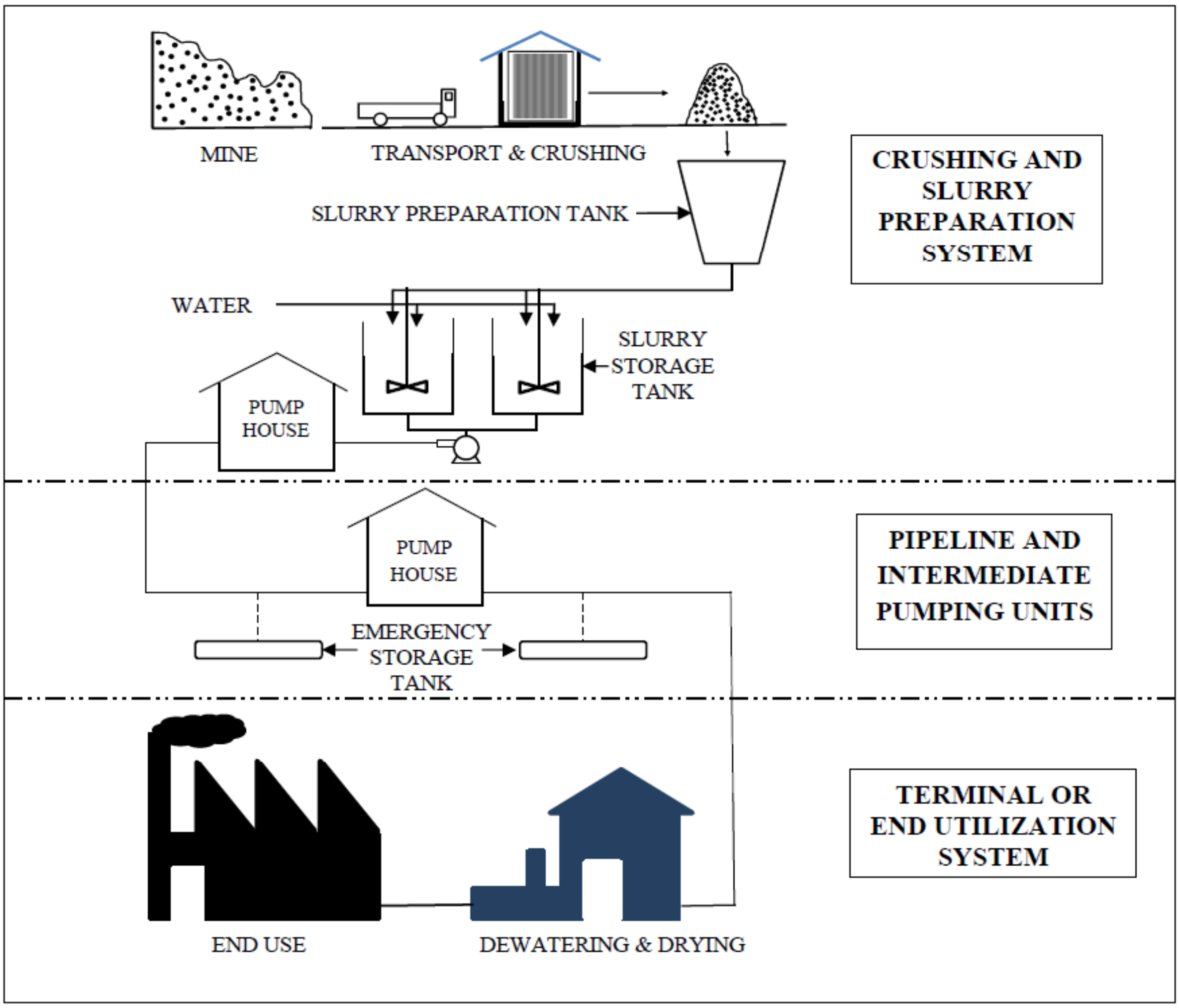

Figure 1.2: Schematic layout of the slurry transportation system

Figure 1.2 shows the schematic layout of the slurry transportation system. Initially, the minerals or any solid product is extracted from its source such as coal/ores from mine, ashes from thermal power plants. Then, the solid is subjected to grinding and crushing process to reduce them to the convenient size, which makes it feasible for transportation through the pipeline. Afterward, these solid particles are mixed with the fixed volume of the carrier fluid in the slurry preparation tanks to achieve a desired solid concentration. The slurry preparation tanks are mounted with stirrers or agitators which facilitate the uniform mixing of the solids in the carrier fluid. The slurry is then stored in the storage tanks. The capacity of the slurry storage tanks depends upon various factors like a requirement at the terminal end, the reliability of intermediate equipment etc. The long-range slurry transportation systems are also provided with intermediate pumping stations. The provision of intermediate pumping stations is determined by distance, geographical conditions and land terrain between the starting and the terminal end. The slurry transportation system is also provided with intermediate slurry storage tanks. The typical slurry storage tank is shown in Figure 1.4. In case of any breakdown, leakage or choking off the pipeline slurry is stored in these intermediate storage tanks.

At the terminal or end utilization point, the slurry is again stored in storage tanks. The slurry is then dewatered; the solid product is filtered and dried from carrier fluid as per requirement at end utilization. In the case of mineral transportation, the slurry transportation system consists of the slurry pipeline, pumping stations and storage tank at the terminal point. Whereas, coal-water slurry transportation consists of a little bit different components such as slurry preparation, pipeline, pumping units, and dewatering. In electricity power generation units, the fly and bottom ash is transported to dyke area with water as a carrier fluid at a terminal point, there is no need of dewatering.

1.2 SLURRY PIPELINE SYSTEM

In the present scenario, there is no installed coal slurry pipeline in India. Coal in being transported to thermal power plants through conventional modes of transportation like railways. However, the pipelines used for disposal of fly and bottom ash in thermal power stations are designed for conveying of low concentrated slurry. In designing, the slurry transportation system, the most important and significant area is the pipeline circuit. The slurry pipelines are laid over long distances and even in difficult geographic areas. During the installation of the slurry pipeline, many pipe-fittings are used like converging-diverging section, elbows, bends, tees etc. The *pipe bends* are the most commonly used fittings to change the direction of flow in the piping circuit. The *elbows* and *bends* used in pipelines are not same, but sometimes these terms are used interchangeably. A bend is the term, which meant from the offset that changes the direction of pipelines installed for a particular service.

The bends are generally made on mechanical bending machines either hot bending or cold bending according to desirable applications. The benefit of using pipe bends is the reduction in expenditure on expensive fittings. On the other hand, the *elbow* could be an engineered bend with specific and standard dimension. The elbow is either welded or flanged or screwed to the piping circuit. An elbow can also be 45° and 90° whereas the pipe bend can be fabricated at 45°, 90°, 135° and 180°. In other words, all bend can be categorized as elbows, but all elbows are not bends. The bends are classified into two categories mentioned below:

- *Long radius bends:* The long radius bends are mostly used for transporting highly viscous fluids such as slurry, low polymers etc. The bends having a radius-to-diameter ratio (*r/D*) > 1.5 falls into the category of long radius bends.
- *Short radius bends:* These bends are most commonly used where head loss due to the frictional loss has to be maintained a minimum. These are also used to minimize cost and space consumption. The bends having *r/D* ≤ 1.5 falls into the category of short radius bends.

1.3 TYPES OF MEDIA FLOWS INSIDE PIPELINES

There are two types of the media flow inside the pipe bend, which are single-phase flows and multiphase flows. The details are highlighted as follows:

- *Single-phase flows:* In single-phase flow, the occurrence of the hydraulic gradient inside the pipe bend is mainly due to centrifugal force acting on flowing fluid. The fluid flowing inside the pipe moves from the center of the pipe to the extrados wall and comes back from the extrados wall to the intrados wall. This result into the formation of double spiral flow in bend. Single-phase flows could be the flow of air, water, oil or gas.

- *Multiphase flows:* In multiphase flow, a number of phase moves inside the pipe bend in either heterogeneous or homogeneous form. In a wide range of applications, the most commonly observed flow is *two-phase flow*. These flows are more complicated as compared to single-phase flow due to centrifugal forces induced and stratify on different phases. The head loss in the two-phase flow is influenced by a number of process parameters. Till now, there is no generalized approach or model which could calculate these parameters precisely. Multiphase phase flows include solid-liquid slurry flow, solid-gas flow, liquid-liquid flow and gas-liquid flow.

1.4 FLOW REGIMES IN TWO-PHASE SLURRY FLOW

The two-phase solid-liquid slurry flow is a mixture of solid particles having different particle size range. The different size of solid particles in mm, cm, micro or nano-scales possesses different specific gravities. The settling or decomposition of solid particles does not occur if the density of solid particles is nearly the liquid phase; also the particles are smaller in size. However, solid-liquid slurries blended with finer and coarser solid particles having specific gravity more than carrier fluid. The solid-phase starts to settle down from the suspended liquid-phase. These solid particles in two-phase flow start accumulating on the bottom of the slurry pipeline and result in different flow regimes. These flow regimes depend upon various flow parameter like flow velocity, solid concentration, slurry density, slurry viscosity etc. The various types of flow regimes or patterns with concentration and velocity profiles are shown in Figure 1.3. These flow regimes or patterns are discretized into five different categories as shown below.

1.5.1 Fully dispersed-symmetric or homogeneous flow

The solid-liquid slurry flow is said to fully dispersed-symmetric or homogeneous if the flow parameters like specific gravity, solid concentration, flow velocity etc. don’t have any gradient along the flow cross-section and length of a slurry pipeline. In the case of homogeneous flow, the slurry acts as a single-phase flow. This type of slurry flows is generally observed at higher flow velocities and for the very fine solid particulate slurry.

1.5.2 Fully dispersed-asymmetric or heterogeneous flow

The decrease in flow velocity results in reduction in turbulence as well as lift forces inside the pipeline. This result in an asymmetric or heterogeneous flow, also the concentration gradient exists along the cross-section of a pipeline. In heterogeneous flow, the solid particles are unevenly distributed in the slurry. The concentration of the solid particles is more at the bottom of the pipeline as compared to the top region. Hence, the flow velocity profile becomes skewed at the bottom half of the pipeline due to the accumulation of solid particles.

1.5.3 Asymmetric flow with rolling & saltation motion

Furthermore, a decrease in flow velocity results into more settling of solid particles at the base of the pipeline. The solid particles start rolling and salting on the bottom of the pipe. The concentration and flow velocity profiles become more skewed. This type of flow regime is generally observed in slurries having coarser solid particles and low flow velocities.

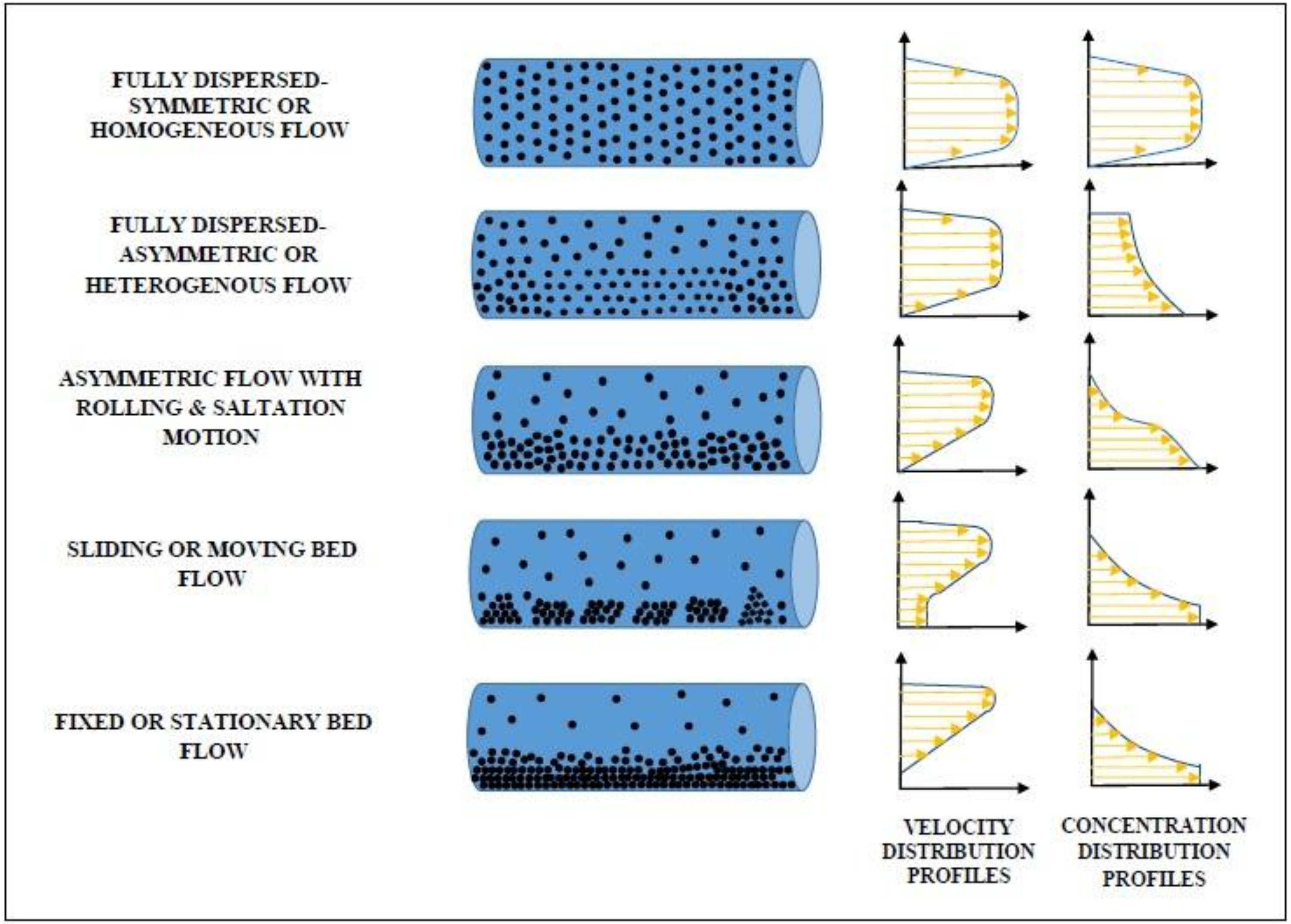

Figure 1.3: Various types of flow regimes or patterns

1.5.4 Sliding or moving bed flow

The flow velocity at which the solid particles unable to rebound back in flowing media after striking pipe wall results into moving bed flow. The solid particles start accumulating on the bottom of the pipe and form dunes. These dunes move in flow direction with a lower rate as compared to completely suspended solid particles. Solid particles above these dunes experienced saltate-roll motion. Further decrease in flow velocity results in the formation of stationary dunes.

1.5.5 Stationary or fixed bed flow

The stationary dunes formed during sliding bed flow have been acting as a building block for stationary bed flow. The lowermost settled solid particles result into the formation of a static bed as the flow velocity further decreased. The rapid settling of solid particles tends to increase the thickness of stationary bed, hence flow cross-sectional area decreased. This results into increase in flow velocity and scours formation. Also, the head loss is increased and there is a chance of chocking of the pipeline. These flow regimes are valid for equisized solid particles. In practical application none of the slurries in composed of equisized solid particles, but slurries are multi-particulate in nature.

1.5 COMPLEXITIES DUE TO TWO-PHASE FLOW INSIDE PIPE BEND

In designing of the slurry transportation system, the most important and significant area is the pipeline and intermediate slurry pumping system. The most critical part in designing and economic operation of the slurry pipeline is *pipe bends*. The bends used in slurry flow applications results in higher head loss as compared to the straight pipeline for equal cross-section and mean length. The head loss in pipe bends is increased to higher magnitudes for slurry flow at high solid concentrations.

Different type of pipe bends are used in mining, chemical, ore processing industries, and ash disposal unit in thermal power stations. Generally, the bend angles preferred in industrial applications are 45°, 90°, 135° and 180°. Pipe bends are further classified into short and long radius bends. The use of 90˚ pipe bends in slurry transportation is most frequent in industries. The use of 90˚ pipe bend could not be fully avoided due to space and geometrical constraints. All types of geometries are used in industries. There is a need for detailed investigation for geometrical configuration of pipe bends for two-phase flow at higher concentrations to minimize head loss.

The flow characteristics of all type of minerals and solid waste slurries are not possible to predict from available correlations. Therefore, the designing of a slurry pipe bend is mainly based on the experimental data procured from pilot plant test loops and other lab scale testing results. In the present scenario, the minerals and solid wastes like coal, iron ore, zinc tailing, lead ore, coal ash etc. are transported at very lean solid concentrations of 5-20% (by weight). These attempts have resulted in the consumption of large quantity of carrier fluid and energy. Hence, the whole system becomes inefficient as well as uneconomic. The head loss in the pipe bends is depends on different factors like frictional head loss due to the length of bend, losses occurs due to change on direction of flow and losses due to sudden enlargement and contraction in bends. The expansion and contraction in the pipe bends occur due to un-reamed ends of pipeline that are screwed to the pipe bends. The losses occur due to friction and un-reamed ends are same for different type of bends. Whereas, the losses occurs due to change in the direction of flow is different for different bends. The head loss is less for pipe bend having bend angle of 135° as compared to pipe bend having 90° bend angle. The effect of *r/D* ratio also contributes to head loss. The present study is focused on the optimum *r/D* ratio of pipe bend for the flow of high concentrated slurry to minimize head loss.

1.6 MOTIVATION BEHIND PRESENT STUDY

In the present scenario, the prime focus of industries is to convey slurry at high solid concentrations with minimum head loss. Head loss depends upon the various properties of slurries. In thermal power plants, three different solids are transported namely coal, fly ash and bottom ash. The transportation of coal-water slurry at high concentrations has several industrial applications such as coal combustion, gasification and liquefaction processes. The power consumption required for slurry conveying constitutes the major operational overall cost of plants (Ihle 2016; Wu *et al.* 2015). Due to this, researchers have focused on decreasing the hydraulic losses that occur during transportation. The estimation of rheological behavior of slurry helps to optimize energy consumption as well as water requirements. Rheological behavior helps to calculate the flow parameters and Reynolds number of slurry suspensions which could be helpful in flow analysis through pipe bends. So, it is required to perform the detailed analysis of the rheological behavior of slurries to estimate their role in head loss characteristics.

The transportation of bulk materials through pipelines is a developing technology in many countries. Now-a-days, the solid materials can be transported through pipelines at higher as well as lean concentration (Jacobs *et al*. 2014). There are many advantages of hydraulic conveying of dense mixtures through the pipeline, as conveying systems requires lesser space, low manpower and is environment-friendly. Solid particles mixed with liquid phase mainly water to form slurry (Bantin and Streat, 1970; Singh *et al.* 2018a). Transportation of solid matter through pipelines is more beneficial because it minimizes pollution as compared to traditional transportation. Moreover, this system requires minimum man power and maintenance cost. Presently slurry conveying system is used to transport mineral ore, mineral tailings, fly and bottom ash in thermal power stations etc. (Chen *et al.* 2009a; Ganeshan and Panda, 2017; Kaushal *et al.* 2012; Singh *et al.* 2018b). From recent decades, the main focus of the researchers/designers is to decrease the hydraulic losses that occur during the transportation of slurries. Execution of this new slurry-conveying strategy requires the least energy requirements, low pollution, optimum design, minimum losses to handle and transport the slurry at high solid loadings.

Furthermore, the presence of multi-phase fluids in a pipeline leads to extreme changes in flow characteristics when compared to single-phase fluid (Tian *et al.* 2014). Literature includes many investigations carried out on head loss characteristics for the flow of solid-liquid slurry in straight pipelines. However, very few studies have been carried out to investigate the effects of head loss on the performance characteristics of pipe bends for the flow of a solid-liquid suspension. Furthermore, the designing of pipe bends is an essential prospect for the hydraulic conveying of solid matter in the context of choking of the pipeline. The use of 90° bends in slurry transportation is restricted because it causes high head loss, also very high pumping power is required to overcome this resistance. However, due to space and geometrical constraints, the use of 90° bends cannot be eliminated entirely, though it could be minimized. So, there is needed to investigate the head loss characteristics of different slurries in pipe bends.

Computational methods/techniques are growing day-by-day. Computational fluid dynamic (CFD) tools offer the utmost rational frame-work for defining high concentration slurries. Head loss characteristics in the slurry pipeline for tailings and ores have been successfully predicted universally using commercial CFD tools by various researchers. CFD tools provide the interactive contours and profiles, which gives additional information that could not be possible from the experimental analysis. So, it is also necessary to generate a CFD code for prediction of the head loss in the slurry.

1.7 THESIS OUTLINES

The present investigation and its results are written in thesis is divided into seven chapters. The brief content of each chapter is given below:

Chapter 1 presents the general introduction about slurry and slurry transportation system through pipelines. This chapter also covers necessary components of the slurry transportation system with various flow regimes or patterns of solid-liquid flow.

Chapter 2 presents the literature review related to leaching and mineralogical characteristics of different slurries. The detailed literature about rheological characteristics, head loss characteristics, design and development of pilot scale test loops, and numerical simulation of multi-phase slurries. This chapter also comprises of gaps in the literature, objectives of the study and detailed methodology adopted to carry out dissertation work.

Chapter 3 presents the characterization of the solid-liquid slurry of coal and coal-ash along with the information about the collection of samples, bench-scale equipment and testing methods. This chapter also explains the various properties of coal and coal-ash slurry such as surface morphology, particle size distribution, static settled concentration, specific gravity, and pH value.

Chapter 4 presents the rheological characteristics of coal, fly and bottom ash at different solid concentrations lies in the range of 30-60% (by weight). This chapter also includes the effect of additives on the rheological behaviour of solid-liquid slurry.

Chapter 5 includes the experimental investigation on head loss characteristics of coal, fly and bottom ash suspension for flow through 90˚ pipe bends possessing *r/D* ratio from 1.5-2.5. This chapter also includes the study of bend loss coefficient, the effect of additives on head loss, and specific energy consumption.

Chapter 6 covers the study of head loss characteristics for optimization of *r/D* ratio of pipe bend for conveying various slurries using ANSYS-Fluent. The Multiphase phenomenon in the pipe bend is simulated using the Eulerian approach with standard SST k–ω turbulence modeling scheme. Simulation studies are also performed to analyze the influencing parameters like Reynolds number and solid concentration of different slurries namely coal, fly ash and bottom ash.

Chapter 7 lists the summary of findings on the basis of present research work, outlines, and broad conclusions drawn from experimental and numerical results. This chapter also includes valuable suggestions and recommendations for future work.

CHAPTER 2

LITERATURE REVIEW

Chapter 2

LITERATURE REVIEW

In India, the electric power is generated mainly from coal-based power plants. Coal is transported in thermal power plants by two modes either by automobiles/locomotives or by pipelines. The pipeline is a universally-adopted mode for transportation of bulk solid materials over short and long distances by using carrier fluids (Woodcock and Mason, 1987). Carrier fluids such as water, air, oil, etc. are used to transport the solid materials, depending upon the industrial application (Li *et al.* 2002; Singh *et al.* 2018a; Singh *et al.* 2018b). Use of pipelines is widely accepted for transporting solid materials due to its low maintenance, economic efficiency, reliability and year-round availability. A pipeline system operating under optimum conditions not only results in minimum energy-consumption but also minimal adverse effects on the environment (Meriem-Benziane *et al.* 2012; Singh *et al.* 2016a; Singh *et al.* 2016b). Pipelines have a wide range of applications in the industrial sector for conveying solid particles with the help of carrier fluids. Examples include the disposal of fly and bottom ash in thermal power plants, the transportation of mineral ore in the mining industry, and the disposal of mineral tailings in mineral processing units (Williams, 1983).

In thermal power plants, another aspect of solid transportation is the disposal of solid waste produced after coal combustion. The use of coal in thermal power station leads to the generation of a large amount of solid waste in terms of fly ash and bottom ash (Kumar *et al.* 2017a, Kumar *et al.* 2018a). The deposition of large quantity of fly ash and bottom ash from coal-based power stations leads to a severe problem. Nowadays, the fly ash is used in cement industries, road embankments, production of high volume composites etc. But the utilization of the bottom ash is still very less. The bottom ash is only used in landfilling **(**Kumar *et al.* 2018a, Singh *et al.* 2018c). However, the production of coal ash after combustion of coal is leveled off. The bottom and fly ash is generally conveyed to dyke area located at a far distance from power station by using pump and pipeline system (Kumar *et al.* 2014). This leads to the consumption of huge power to run slurry pumps, so there is a need to develop cost-efficient slurry disposal system. The two-phase flow of solids and liquids generally exhibits very complex flow characteristics. The interaction of solid particles leads to the formation of internal structure those results in complex behavior.

Therefore, a literature survey is carried out in this chapter to study the previous investigations carried out by different researchers presented to understand the present state of knowledge. In this survey, the literature includes the studies about physico-chemical, mineralogical, rheological behavior of different slurries, head loss for different slurries experimentally with and without additive and computational analysis of head loss. The detailed discussion on literature has been given in the following sections.

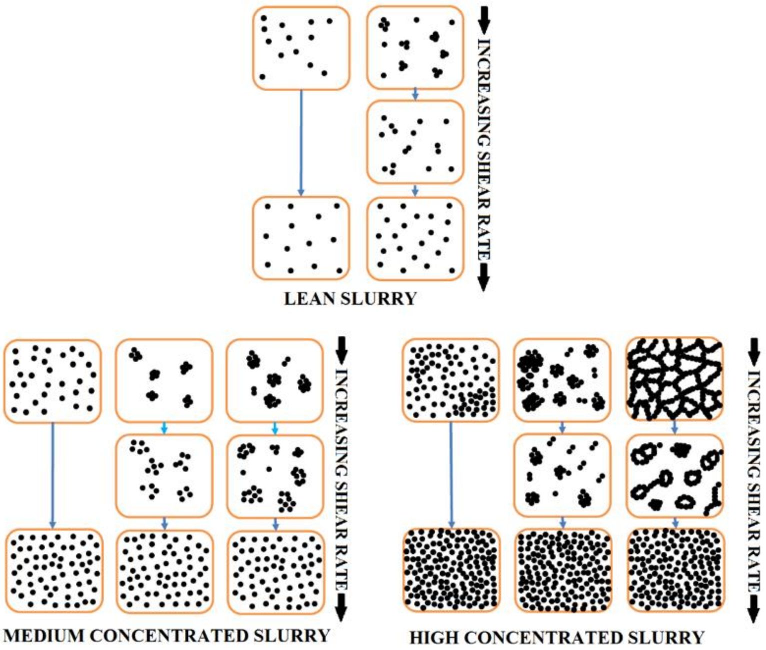

Figure 2.1: Dispersion of solid phase under action of shear rate in two phase slurries

2.1 RHEOLOGICAL CHARACTERISTICS OF VARIOUS MINERAL AND SOLID WASTE SLURRIES

The study of flow behavior and deformation of fluid under the effect of external force is known as rheology. Rheological characteristics of solid-liquid slurries play a most dominant role in designing of the slurry pipeline system and flow analysis inside pipelines. The rheological behaviour of slurry is function of numerous flow parameters such as solid concentration, shear rate, specific gravity, porosity, water adsorption capacity, viscosity etc. In previous years, several investigations (Naik *et al.* 2009; Zhu *et al.* 2013; Panda and Swain, 2014; Li *et al.* 2015; Pani *et al.* 2015) have been carried out to determine the rheological characteristics of multi-particulate slurry at different solid concentrations with and without additives. The change in the shear rate of slurry leads to alter the microstructure of solids in the liquid phase. The complete dispersion of solid-phase takes place with an increase in shear rate. The concept of dispersion with the shear rate is illustrated in Figure 2.1. A critical review of significant work carried out in this field which has been discussed as follows:

Many investigators have studied the rheological behavior of the different slurries (Mooney, 1951; Roscoe 1952; Williams 1953; Einstein 1956; Rutgers 1962; Moreland 1963; Landel *et al.* 1965; Thomas 1965; Krieger 1968; Schrick *et al.* 1972; Wilson, 1982). The rheological behavior of coal-water slurry suspensions has been investigated in many studies (Shao *et al.* 2012; Ganeshan and Panda 2017). The rheological behavior of slurries depends on solid concentration, yield stress, shear rate, particle size, shape, and properties of the liquid (Moreland 1963; Horsley 1982; Sive *et al.* 1987). Kwak *et al.* (2005) investigated the effect of concentration on flow behavior and depositional geometry of tailings and kaolinite pastes. They used a flume apparatus to simulate the paste deposition. They noticed that the residual stress obtained from a stress-time profile is not a good measure of yield stress. Results showed that the stress (measured at the transition between the elastic and viscoelastic region) and the maximum stress are valid measures due to the independency of the vane size used in the rheometer. Verma *et al.* (2006) studied the effect of particle size range on flow characteristics of coal ash suspension. They reported that fly ash exhibits Non-Newtonian flow at concentration above 40% (by weight).

Yoon *et al.* (2009) studied the effect of additive on the rheological characteristics of coal-water slurry. The solid concentration and temperature were varied within the range of 60-70% and 20-50˚C respectively. Figure 2.2 shows the schematic layout of the viscosity meter used in their study. The dosage of four different additives namely methyl methacrylate, polypropylene glycol based, polypropylene and sodium naphthalene was added in 0-0.8% (by weight). They reported that sodium naphthalene was the best additive for high concentrated coal-water slurries. Senapati *et al.* (2013) investigated the rheological measurements of fly ash water slurry at a higher concentration range of 62-65%. The pseudo-plastic flow behaviour of slurry was observed by them. Panda and Swain (2014) studied flow behaviour of low-rank Indian coal-water slurries. An empirical correlation was developed between solid concentration and apparent viscosity. Result showed the exponential increase in slurry viscosity above 50% (by weight) solid concentrations. Lee *et al.* (2017) performed various viscometer tests to describe the rheological behavior of tailings-slurries mixed with fly ash. They proposed the models for prediction of rheological behavior of these slurries with the help of root mean square error (RMSE). They noticed that the shear stress of specimen increases with increase in the amount of fly ash in tailing slurry. Also, the specimen mixtures have a lower value of shear stresses at high temperatures. Kumar *et al.* (2017b) studied the effects of additives to improve the rheological properties of bottom ash. They reported that sodium sulfate was better additive then Henko detergent. With the addition of 0.4% sodium sulfate, the flow characteristic of bottom ash was improved.

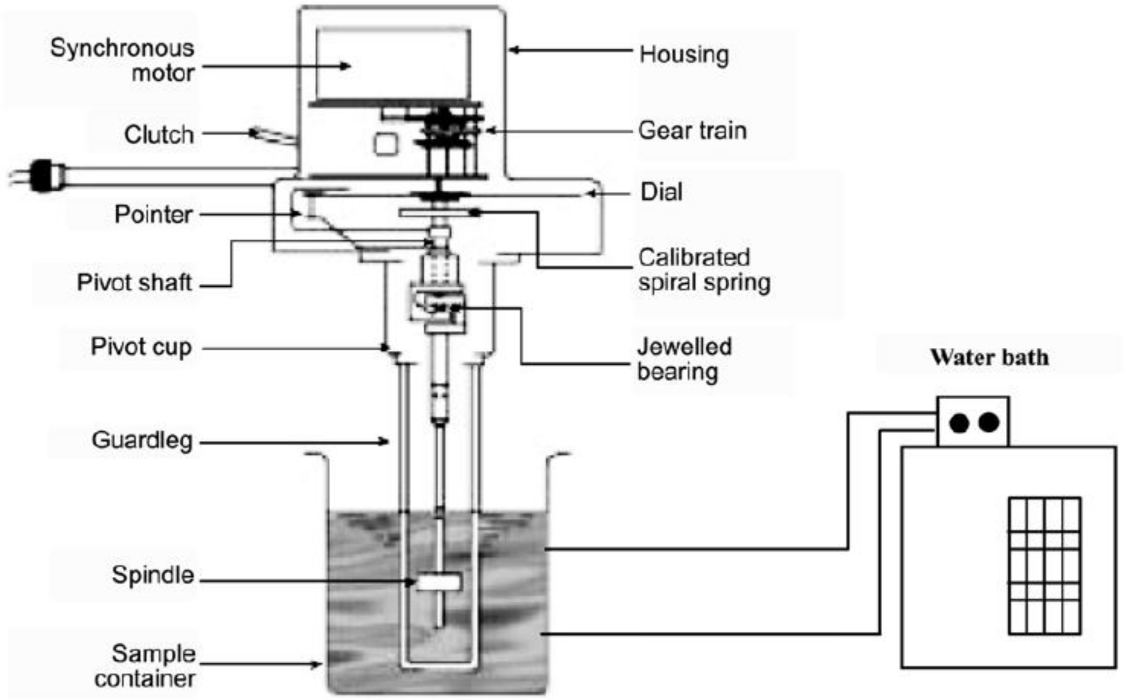

Figure 2.2: Schematic illustration of viscosity meter used by Yoon *et al.* (2009)

Many of the researchers have investigated the rheological behavior of slurries using different additives. Mosa *et al.* (2008) studied the effect of various additives namely sulphonic acid, sodium tri-polyphosphate and sodium carbonate on the rheology of coal water slurry. They found that sulphonic acid was the best among all additives. The sulphonic acid helps to improve the rheological characteristics of aqueous coal suspension. Senapati *et al.* (2008) determined the rheological behaviour of coal fly and bottom ash. They observed that fly ash suspension exhibits pseudo-plastic behaviour while power law model was found to be best to determine the viscosity of bottom ash. Chandel *et al.* (2009) analyzed the rheological behaviour of fly ash water suspension with the use of an additive. They found that with the use of sodium hexametaphosphate the apparent viscosity of slurry decreased. They reported that the viscosity of slurry was influenced by particle size range and solid concentration. Bbrenganca *et al.* (2009) reported that apparent viscosity of coal ash suspension depends on solid concentration, potential of hydrogen, range of solid particle size and properties of carrying liquid. Vlasak *et al.* (2009) determined the effect of sodium hexa-meta-phosphate on the rheological behaviour of fly ash water slurry. They reported that the addition of a small amount of additive resulted in an appreciable decrease in apparent viscosity of the slurry suspension. Zhu *et al.* (2013) investigated the effect of starch-based dispersants on the physical and chemical properties of the coal-water slurry. Three different types of dispersants namely styrene, naphthalene sulfonate and natural sodium lingo-sulfonate are used. Results showed that the apparent viscosity of a solid suspension decreases with the addition of a small amount of styrene. However, the addition of styrene improved the static settlement of coal-water slurry. Chen *et al.* (2015) investigated the rheological properties and stability of lignite washery tailing suspensions (LWTS) with the help of a rotational viscometer and a pipeline test system. They reported that the stability and apparent viscosity of LWTS increase with increasing solid concentration. Li *et al.* (2015) performed an experimental study to improve the flow properties of low-rank coal water slurry by mixing it with medium-rank coals. The presence of weak acidic groups, high water adsorption capacity and high mineral density are significant parameters that affect the rheological characteristics of low-rank coal. Coal-water slurry exhibits Newtonian flow behavior for a solid concentration range of 10-30%. However, at high concentrations (i.e. above 40%) pseudo-plastic flow nature was observed. Pani *et al.* (2015) studied rheological characteristics of fly ash collected from Jindal power, Rajgarh. They performed rheology of 50-60% concentrated fly ash water slurry with Ghari detergent powder and sodium silicate as an additive. Results show that slurry exhibits Bingham plastic behaviour and a gradual decrease in apparent viscosity was observed with the addition of sodium silicate and Ghari detergent. The sodium silicate was found a better additive as compared to Ghari detergent powder. Slatter *et al.* (2015) studied the rheological behavior of different types of tailings (coarse and fine). They added two different types of flocculants in slurries during the experiments. They concluded that from the sample-B (fine slurry), the rheological behavior was mostly similar for both the flocculants. On the other hand, the sample-A (coarse slurry) was sensitive to both the flocculants. Hence, this material showed evidence of structural rebuild of polymeric agglomerates. Merill *et al.* (2017) performed a feasibility-study on hyper-spectral characterization to estimate the rheological properties of mineral suspensions. They performed a set of rheology tests for slurries having different compositions. They combined three minerals (from five minerals) and observed that the viscosity of a bentonite suspension (15% vol.) decreases by addition of bentonite from another source. Kumar *et al.* (2017c) analyzed the effect of sodium sulphate and henko detergent on the rheology of botton ash water slurry. The dosage of additive was varied within the range of 0.2-0.6%. The solid concentration of bottom ash slurry was kept in range of 10-60% (by weight). The considerable decrease in apparent viscosity was observed with both the additives but the percentage decrease was more with the use of sodium sulfate.

From above literature, it is also noticed that limited work is reported on study of flow characteristics of bottom ash, fly ash and coal water slurry at higher solid concentration. There is a need to develop a method to reduce the transportation cost for slurry disposal at high concentration. Also, the design of the slurry conveying system is a function of numerous parameters like the density of solid and liquid particles, flow rate, flow behaviour etc. The complete knowledge of rheological behaviour helps to design and operate the slurry disposal system an optimum conditions.

2.2 EXPERIMENTAL ANALYSIS OF HEAD LOSS FOR DIFFERENT SLURRIES

In previous decades, studies have been carried out to investigate the head loss characteristics of solid-liquid suspension for flow through pipelines. Several researchers (Mosa *et al.* 2008; Seitshiro *et al.* 2012; Ravelet *et al.* 2013) have studied the head loss characteristics of the flow of different types of slurries in slurry pipelines using pilot plant test loops. A typical hydraulic conveying system consists of a pipeline circuit, a heavy-duty pump, and other devices like pressure transducers, flow meters, data acquisition system etc. (Chandel *et al.* 2010). An overview is carried out to elaborate on the experimental investigations performed by various researchers:

Several investigators (Sive *et al.* 1987, Chandel *et al.* 2009; Chandel *et al.* 2010; Sahoo *et al.* 2010) have investigated the effect of head loss for the flow of multi-particulate slurries. Bantin and Streat (1970) investigated the dense-phase conveying of solid-liquid slurry through vertical and horizontal pipes and observed that it is feasible to transport the dense phase at a high velocity with low- head loss. Mukhtar *et al.* (1995) investigated head loss across 90˚ pipe bend for the flow of iron ore and zinc tailing slurry. They reported that bend loss coefficients for the flow of slurry show lesser value as compared to water, and losses in the bend increase as flow velocity increased. Fangary *et al.* (1997) studied the effect of fine particulate slurry on flow characteristics of polydisperse phosphate slurry. They developed a pilot plant test loop for conducting the experiments as shown in Figure 2.3. Three different pipe having diameters of 1, 1.5, and 2 inches are used in their study. They reported that the head loss at higher flow velocities was more in case of fine particulate slurry-flow as compared to the coarser particulate slurry. Also, the mixing of coarser solid particles in fine particulate slurry leads to decrease head loss even at higher solid concentrations. Mishra *et al.* (1998) studied the effect of head loss across conventional and modified pipe bends. They reported that head losses across modified bends are greater than conventional bends. They also reported that modified pipe bends with an area ratio of 2 showed a marginal increase in head loss and also showed very low wear of pipe material.

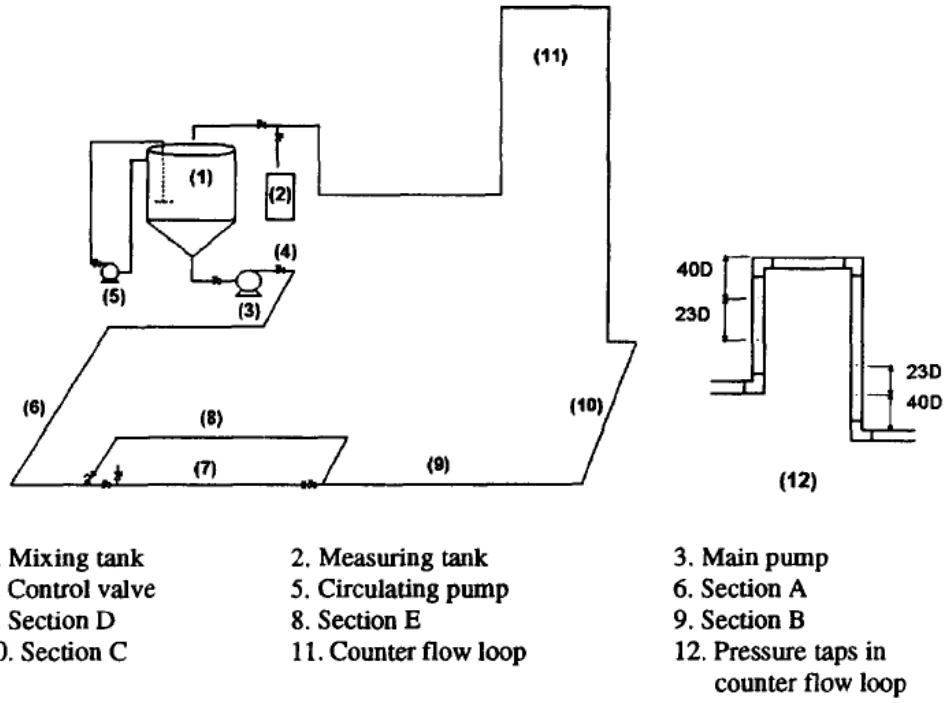

Figure 2.3: Schematic diagram of pilot test rig developed by Fangary *et al.* (1997)

Kumar *et al.* (2000) determined head loss characteristics of coal ash water slurry through a horizontal pipeline. They carried out the experimental work on the pilot plant test loop established at thermal power station NCPP, Dadri, India (shown in Figure 2.4). The pipeline is 160 m long with a diameter of 155 mm. They reported that both fly and bottom ash can be transported at high solid concentrations of 50%. Also, the addition of bottom ash in fly ash water leads to decrease in head loss at higher solid concentrations whereas the slurry flows at higher solid concentrations leads to reduce uneven wear of pipeline material. Li *et al.* (2002) studied the stabilization of fly ash water slurry in the pipeline. The deposition stability of slurry was measured by mixing four different additives such as S-130, S-194 (rhamsan gums), vanzan, and carboxymethyl cellulose. They reported that the addition of 0.2% (by weight) of S-194 leads to effective stabilization of aqueous fly ash slurry. The extensive long molecular chains of S-194 resulted in an effective network structure that helps to reduce the deposition of fly ash particles. They also proposed the effective slurry transportation system with additive feeding mechanism.

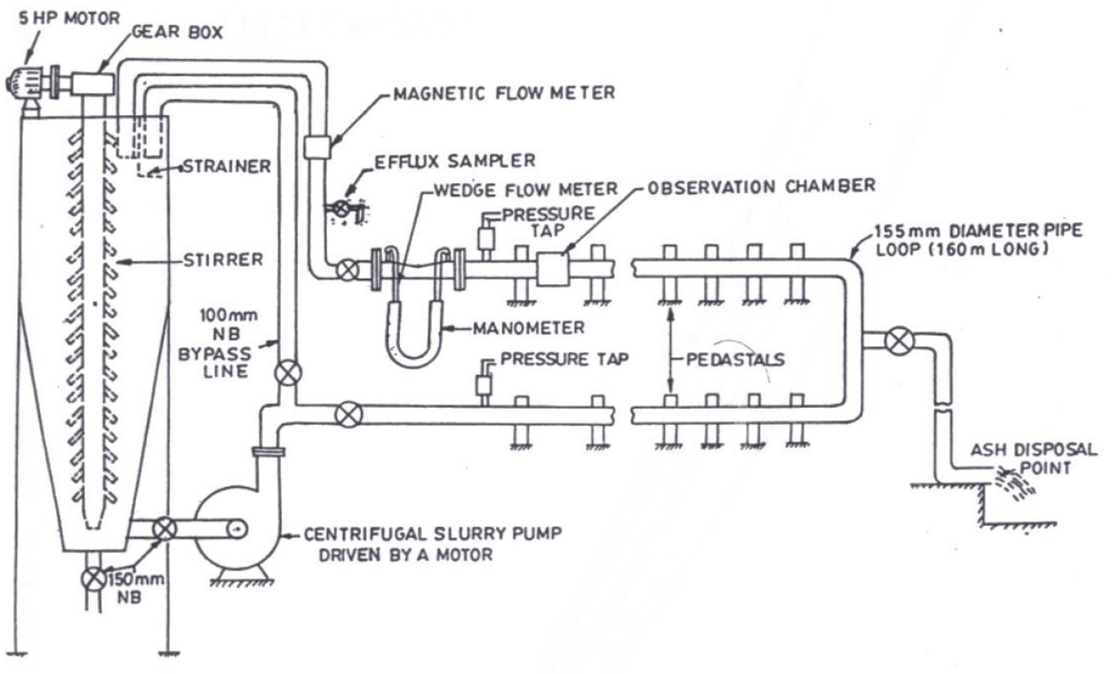

Figure 2.4: Schematic diagram of slurry loop at NCPP, Dadri (Kumar et al. 2000)

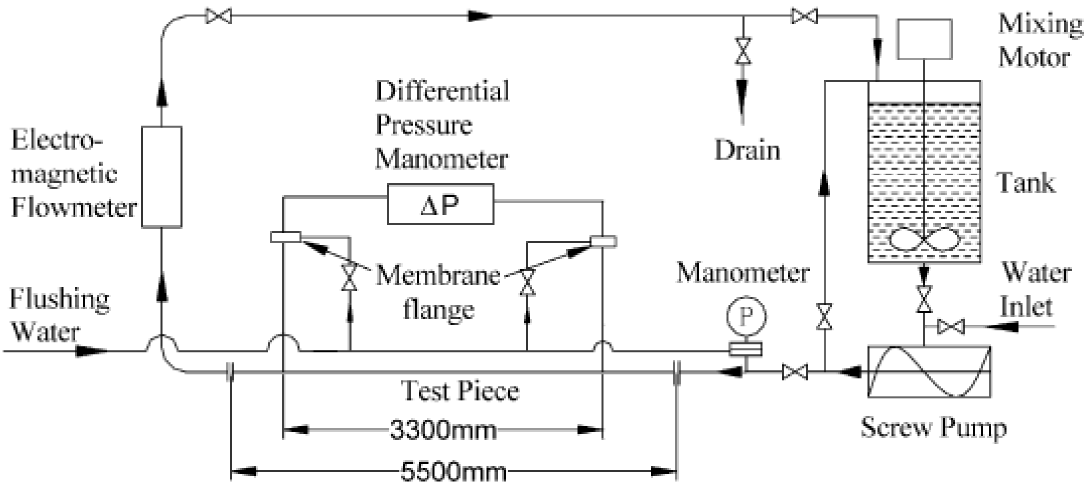

Figure 2.5: Experimental test loop developed by Lu *et al.* (2002)

Lu *et al.* (2002) analyzed the friction losses inside the horizontal pipeline for the flow of coal water slurry. The line diagram of test loop used in experimentation is shown in Figure 2.5. The solid concentration was varied within the range of 22.1-33.5% (by weight). They proposed a generalized Reynolds number for Non-Newtonian slurries. Also, the friction loss factor was determined from the generalized Reynolds number. Kumar *et al.* (2003) investigated the head loss characteristics of fly ash water slurry for flow through a horizontal pipeline. The solid concentration varied in the range of 10-60% (by weight). A 160 m long pilot plant test loop (shown in Figure 2.6) was developed to perform the extensive experimentation. They found that head loss was increased with solid concentration and flow velocity. Also, the addition of coarse bottom ash particles in fly ash slurry leads to a decrease in specific energy consumption for slurry transportation. The optimum blending of bottom ash in fly ash slurry lied in range of 4:1 to 3:2.

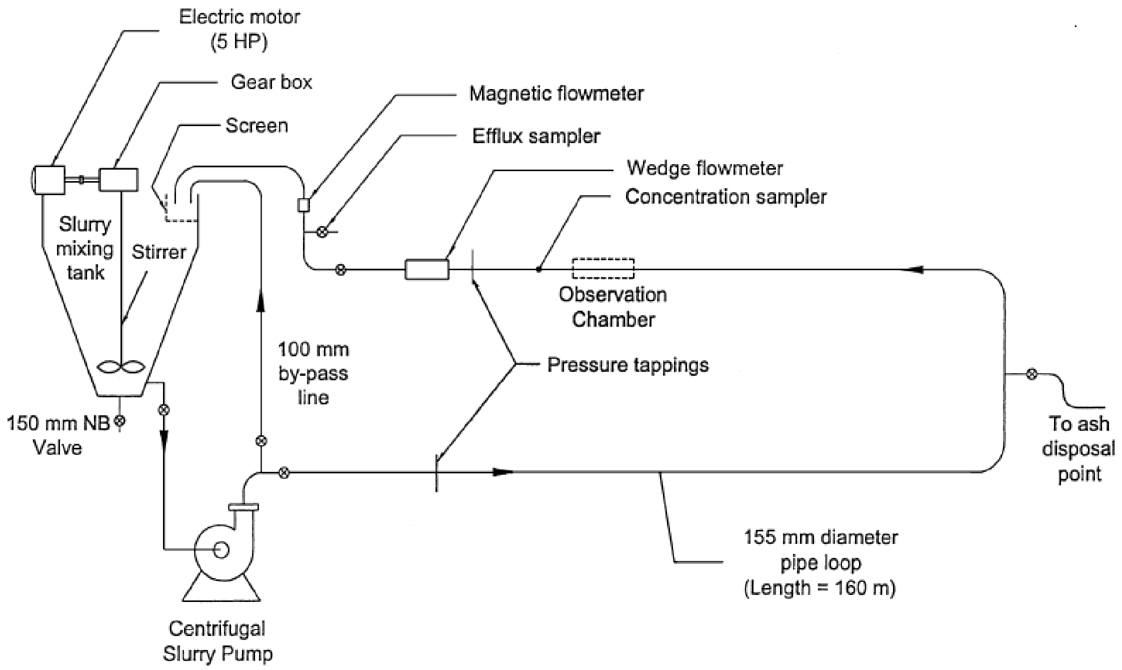

Figure 2.6: Schematic illustration of pilot plant test loop developed by Kumar *et al.* (2003)

Azzi and Fridel (2005) proposed a prediction model for two-phase flow of air-water based on the experimental data. The head loss experiments are performed on plexiglass 90˚ bends having diameter of 30 mm with radius of curvature of 120, 180, 240 and 300 mm. The pilot test facility used in their work in shown in Figure 2.7. They reported that the proposed model substantially showed lower deviations in predicted values as compared to models available in literature. Also the proposed model includes the geometrical parameters of bend and effect of two-phase flow on head loss characteristics.

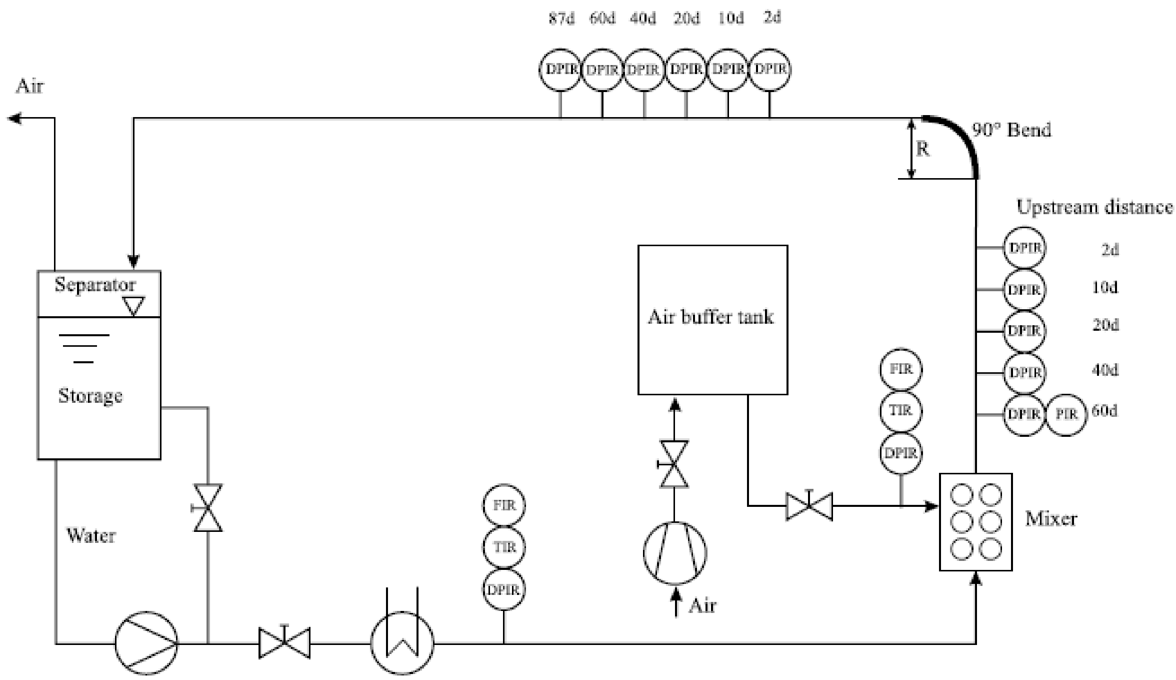

Figure 2.7: Experimental test facility developed by Azzi and Fridel (2005)

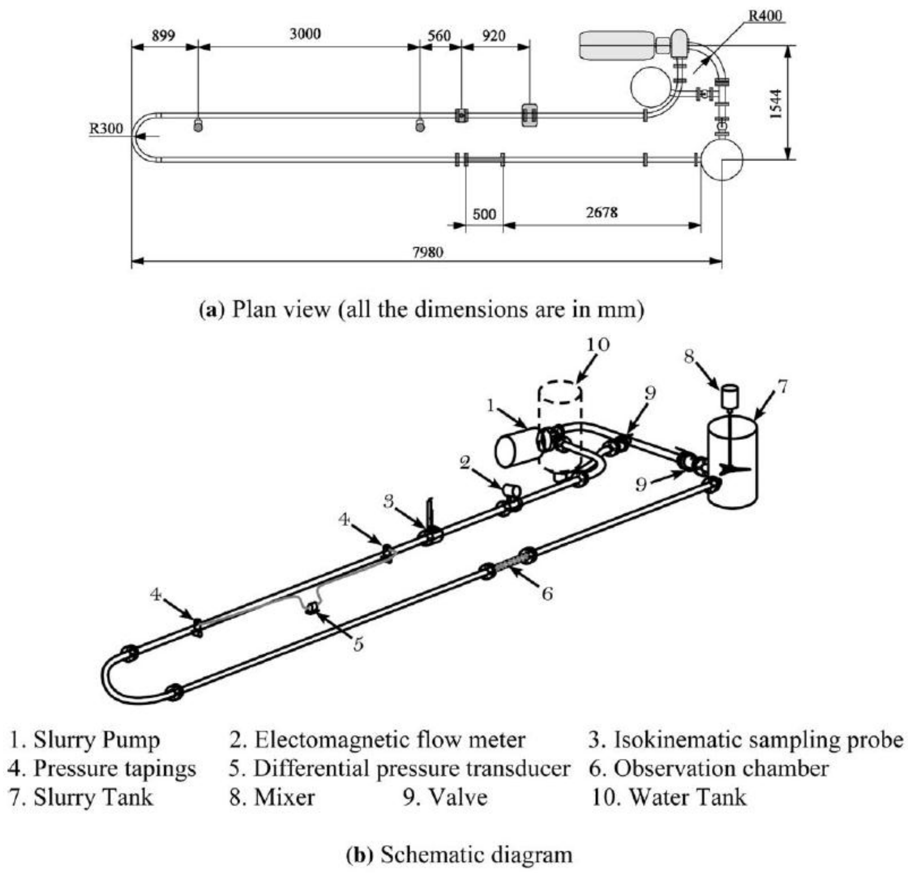

Figure 2.8: Schematic view of test loop developed by Kaushal *et al.* (2005)

Kaushal *et al.* (2005) investigated the effect of glass beads slurry on head loss through a horizontal pipeline. The glass beads of mean particle diameter were taken as 440 μm and 125 μm. A 22 m long test rig (shown in Figure 2.8) is used in the study. The head loss was studied at a solid concentration of 50% and a flow velocity of 5 m/s. They reported that head loss was decreased for glass beds slurry as concentration was increased except for flow velocity of 5 m/s. The sliding bed flow was observed for the flow of 440 μm particulate glass beads slurry. Spedding and Benard (2007) investigated the head loss characteristics of air-water flow in the horizontal-vertical bend elbow having an internal diameter of 26 mm with a curvature radius of 17 mm. The schematic representation of the bend used in the study is represented in Figure 2.9. They observed that head loss in the bend shows a significant difference as noticed in the straight pipeline in a vertical direction. This difference in found due to the complex flow regimes structure in the bend. A general correlation based on experimental results was also developed for head loss in bends in terms of Reynolds number.

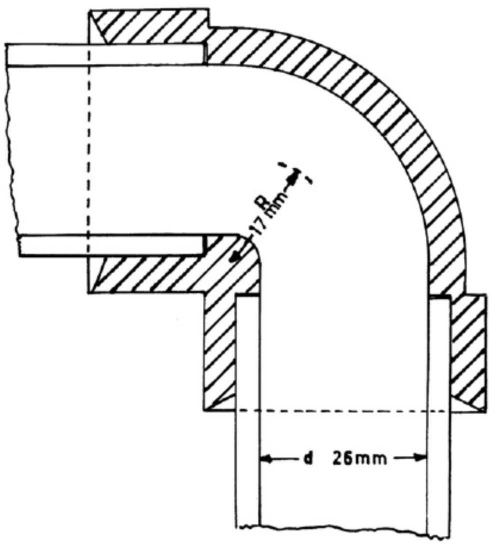

Figure 2.9: Schematic representation of bend used by Spedding and Benard (2007)

Verma *et al.* (2006) studied head loss behaviour inside 50-mm horizontal pipe and 90˚ bend for conveying of fly ash-water suspension. The solid concentration and flow velocity were taken in the range of 50-65% and 1.0-3.5 m/s respectively. The schematic representation of the closed pilot plant test loop used in experimentation is illustrated in Figure 2.10. It was found that relative head loss was increased with flow velocity and solid concentration inside pipe and bend.

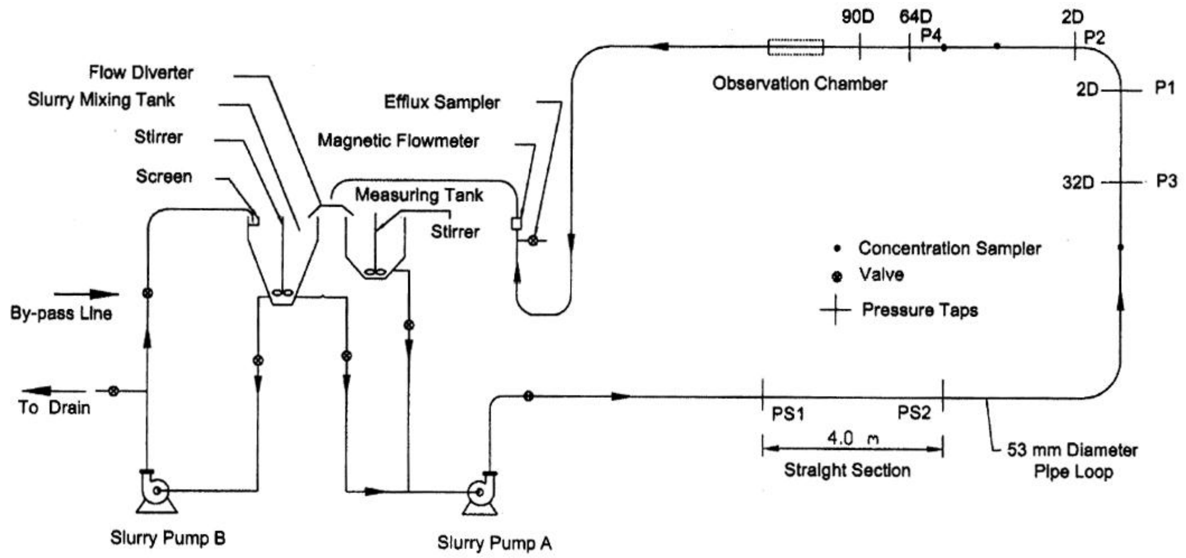

Figure 2.10: Schematic illustration of pilot plant test rig developed by Verma *et al.* (2006)

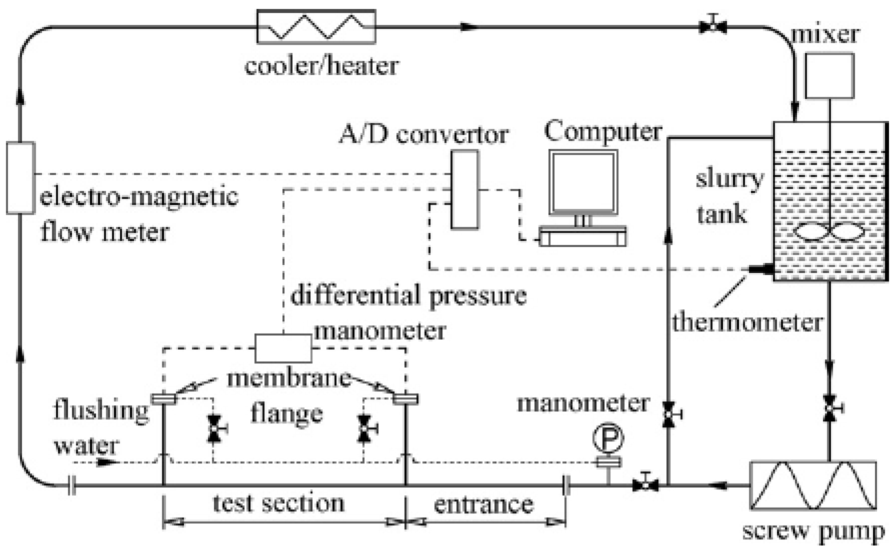

Figure 2.11: Schematic diagram of experimental test loop developed by Chen *et al.* (2009)

Chen *et al.* (2009a) studied the effect of solid concentration, temperature and particle size on slip velocity of coal water slurry suspension. The solid concentration was kept in the range of 65.3-68.2% (by weight). Three pipelines of diameter 25, 32 and 50 mm were used in the study. The schematic diagram of the pilot set up is shown in Figure 2.11. They found that slip velocity is decreased by increasing solid suspension, particle size and slurry temperature. Vlasak and Chara (2009) investigated the flow and head loss behaviour of different sand slurries. They reported that sand slurries show Newtonian flow behaviour at higher solid concentrations. Chandel *et al.* (2009) investigated the effect of additives on the head loss and rheological properties of fly ash-water slurry for flow through a straight 40 mm pipeline at higher solid concentration. Their experimental data show good agreement with analytical data obtained by the Darby and Melson (1981) algorithm. It was also observed that the head loss and flow characteristics of slurry were improved with the addition of soap-based additives.

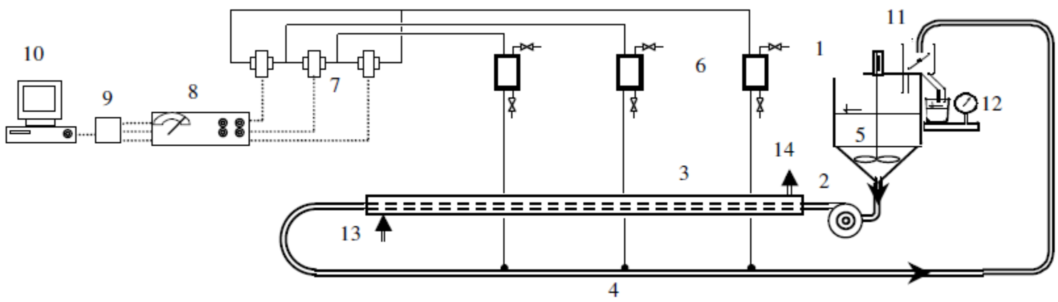

1	holding tank	8	three channels carrier frequency amplifier
2	screw pump	9	analogue/ digital converter
3	double pipe heat exchanger	10	computer
4	test section	11	flow divider vessel
5	stirrer	12	measurement of discharge & density
6	sedimentation vessels	13	cooling water inlet
7	differential pressure transducers	14	cooling water exit

Figure 2.12: Schematic illustration of experimental setup developed by EI-Nahhas *et al.* (2009)

EI-Nahhas *et al.* (2009) analyzed the effect of particle size on hydraulic conveying of sand-water slurry. Three different sorts of sand slurry having d_{50} particle size of 0.2, 0.7 and 1.4 mm were used in experimentation. The experimental work was carried out on a laboratory scale test loop having a pipe diameter of 26.8 mm. The schematic diagram of the test loop is shown in Figure 2.12. The decrease in the specific energy consumption was observed with increase in solid concentration. They mentioned that it was economic to convey slurry at higher solid concentrations.

Chandel *et al.* (2010) studied the effect of coal ash slurries at higher solid concentrations on head loss through the horizontal pipeline. The solid concentration of coal ash water slurries was kept in the range of 50-70% (by weight). The pilot plant test loop of 42 mm diameter and 50 m long (shown in Figure 2.13) was used in study. They reported that head loss was increased with solid concentration and flow velocities. Also, the mixture of fly and bottom ash in ratio of 4:1 leads to effective slurry transportation. However, the specific energy consumption was decreased to a solid concentration of 65%.

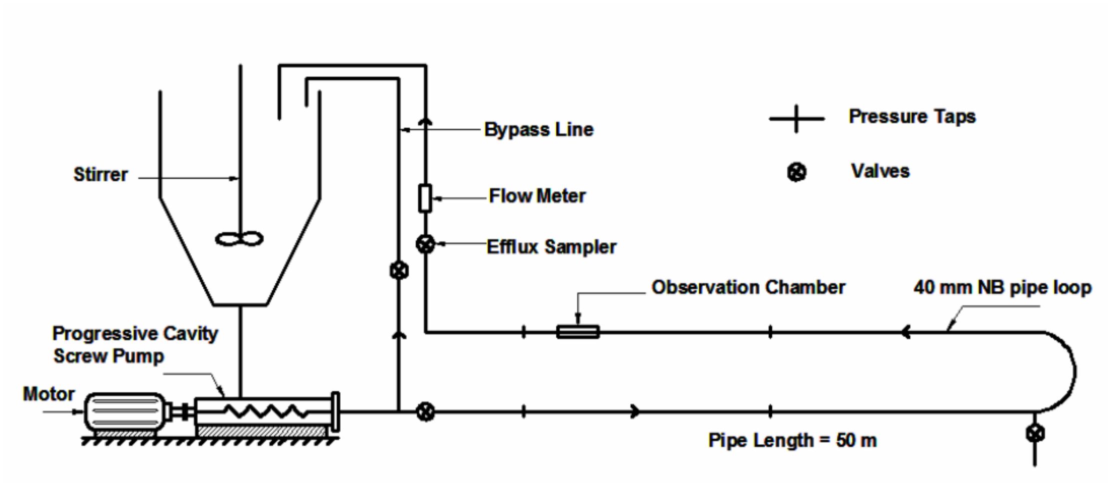

Figure 2.13: Schematic diagram of pilot plant test rig developed by Chandel *et al.* (2010)

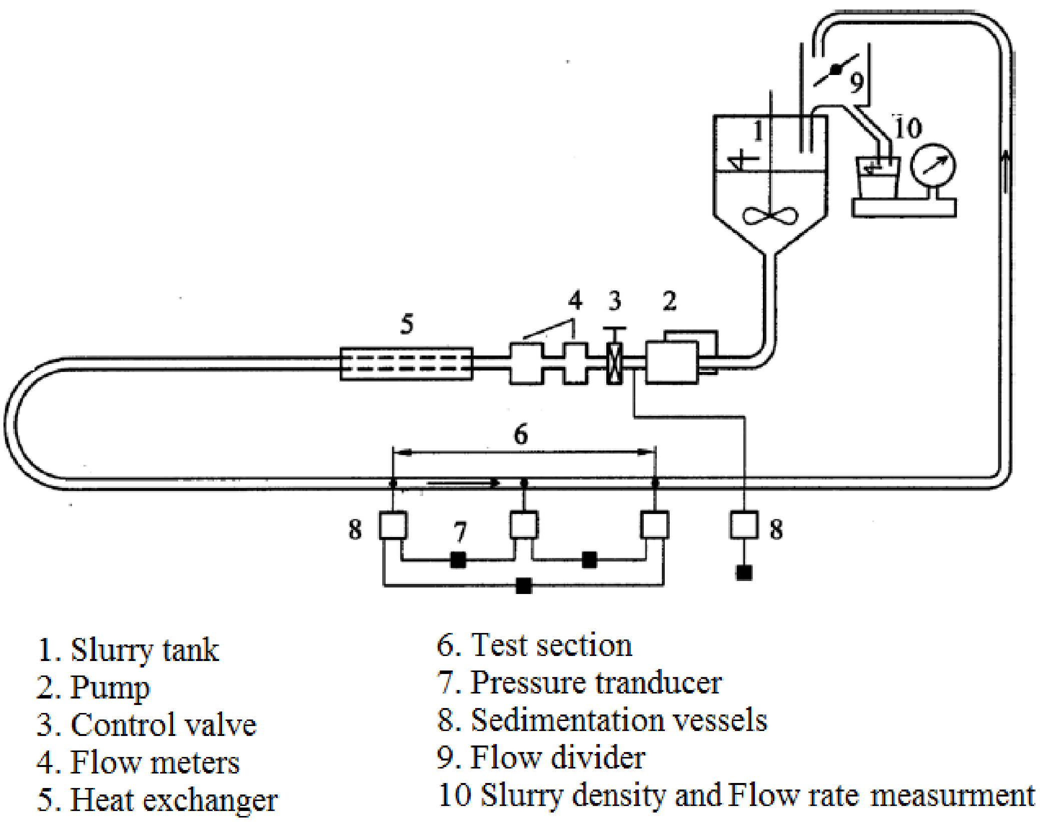

Figure 2.14: Layout of experimental test loop developed by Vlasak and Chara (2011)

Vlasak and Chara (2011) determined the flow and head loss characteristics of three different slurries namely sand, stony dust and sand-stony dust. The solid concentration was varied in the range of 6-51%. The layout of laboratory scale pilot loop is shown in Figure 2.14. They reported that coarse slurries lead to higher head loss as compared to finer one. Also, the addition of finer sand particles in coarser slurry helps to reduce the hydraulic losses up to 50% during transportation. Slatter (2011) developed the new modeling approach for fluid characteristics. The schematic view of test rig is shown in Figure 2.15. The concentration of the clay suspension was varied in range of 2-10% (by volume). He reported a new modeling approach for fine particulate slurries shows dynamic similarity for a wide range of fluid properties.

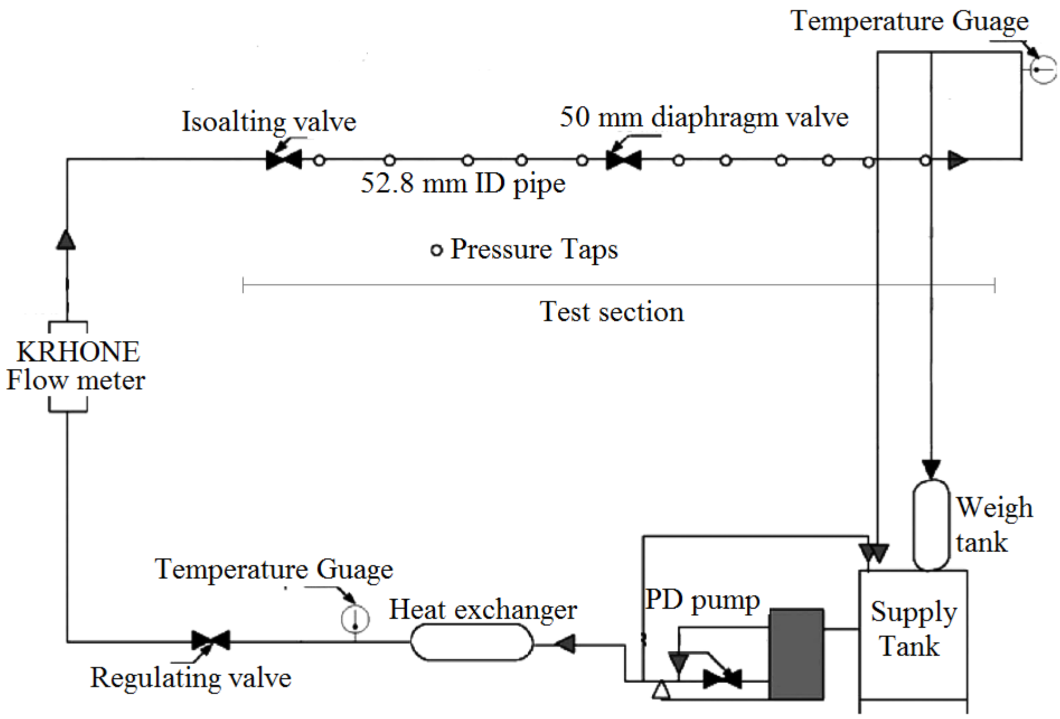

Figure 2.15: Schematic illustration of test rig developed by Slatter (2011)

Eltoukhy (2013) studied head loss characteristics for the flow of sand-water slurry through a straight 50.8 mm pipeline. They found that head loss increased with increase in solid concentration and pipe roughness. They also identified that finer sand-particulate slurry showed higher head loss than coarser slurry. Hashemi *et al.* (2014) investigated the fluctuation in flow velocity and solid concentration for sand-water slurry. The solid concentration and flow velocity were taken in the range of 20-35% (by weight) and 2-5 m/s respectively. The pilot plant test rig (shown in Figure 2.16) was used to carry out the experimentation. They reported that fluctuation of solid concentration and turbulence was more near the wall due to particle wall interactions.

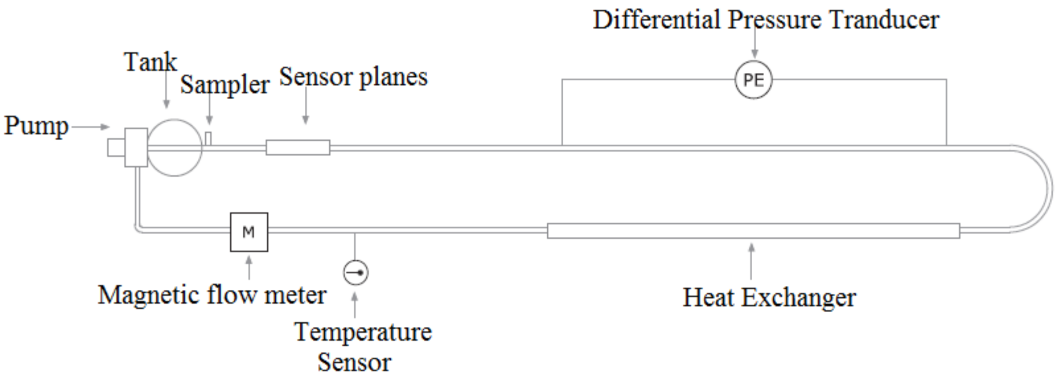

Figure 2.16: Schematic layout of horizontal pipe-loop developed by Hashemi *et al.* (2014)

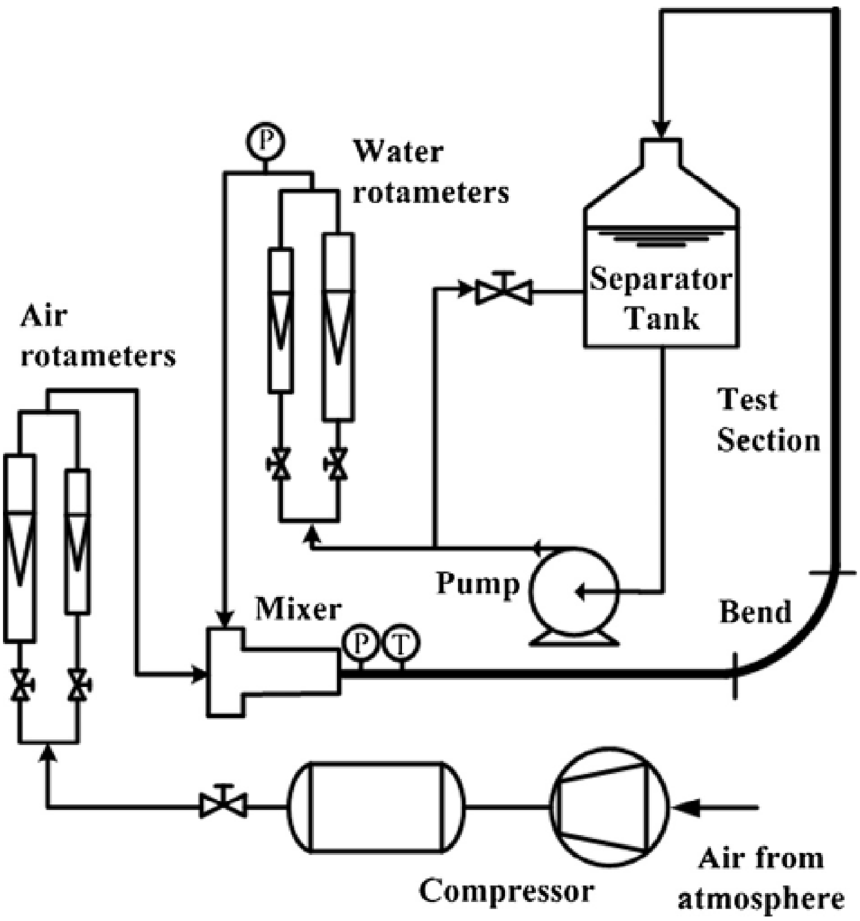

Figure 2.17: The test facility developed by Saidj *et al.* (2014)

Saidj *et al.* (2014) investigated the flow behaviour of the air-water mixture on horizontal-vertical pipe bend experimentally. The 34 mm diameter bend made of an acrylic resin having *r/D* ratio of 5 was used in experimentation. The velocity of the air and water was varied within the range of 0.3-4 m/s and 0.21-0.91 m/s. The schematic representation of the test setup is shown in Figure 2.17. They found that slug, plug and stratified flow patterns were observed in the horizontal pipeline. However, in the vertical pipeline slug and churn flow regimes were noticed. They also reported that the prediction of correlation developed by Nicklin *et al.* (1962) was more reliable for the study of slug flow in horizontal pipelines. Kim *et al.* (2014) investigated the head loss characteristics of air-water two-phase flow in the 90˚ pipe bends. The experimental setup was developed with a pipe diameter of 5.08 cm having vertical, horizontal and bend sections. They found that distribution of the bubbles at the outlet of the bend was strongly correlated to bend effects. Also, the dissipation characteristics for horizontal-vertical bend were a function of air-water flow rates. Wu *et al.* (2015) performed experimentation and simulation study on head loss characteristics of cement-fly ash slurry in a horizontal pipeline. The pilot test loop with a diameter of 120 mm and a length of 35 meters was used to perform experimental analysis. Figure 2.18 depicts the schematic diagram of the test loop. They reported that slurry exhibits Bingham plastic flow behaviour for a solid concentration range of 78-79.5% (by volume). They mentioned that an increase in volume rate leads to a significant increase in head loss in pipeline.

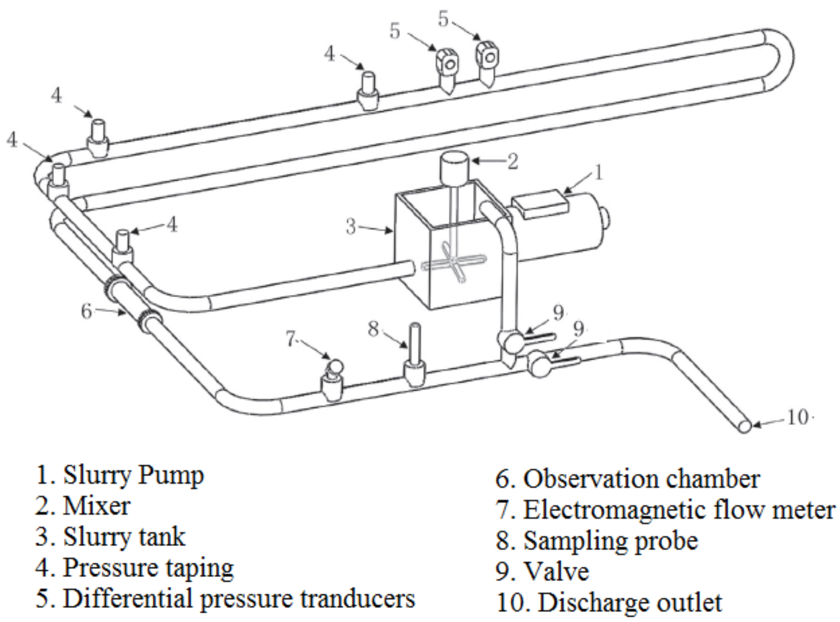

Figure 2.18: Layout of experimental test rig developed by Wu *et al.* (2015)

Senapati and Mishra (2015) investigated the effect of the addition of bottom ash on the rheological behaviour and head loss characteristics of fly ash-water slurry. They observed that the apparent viscosity and head loss inside the pipeline was decreased with the addition of coarser particles (bottom ash) in a fine particulate slurry (i.e. fly ash slurry). Autee and Giri (2016) investigated the head loss in pipe bends for the flow of two-phase flow (air-water). The main objective of their work was to develop the correlation of small diameter (4.0-8.0 mm) pipe bends having bend angle range of 90-180˚. The experimental test setup used during the study is shown in Figure 2.19. The use of these bends is limited to heat exchanger applications. They found that the already available correlations in literature were limited to particular applications and geometrical parameters.

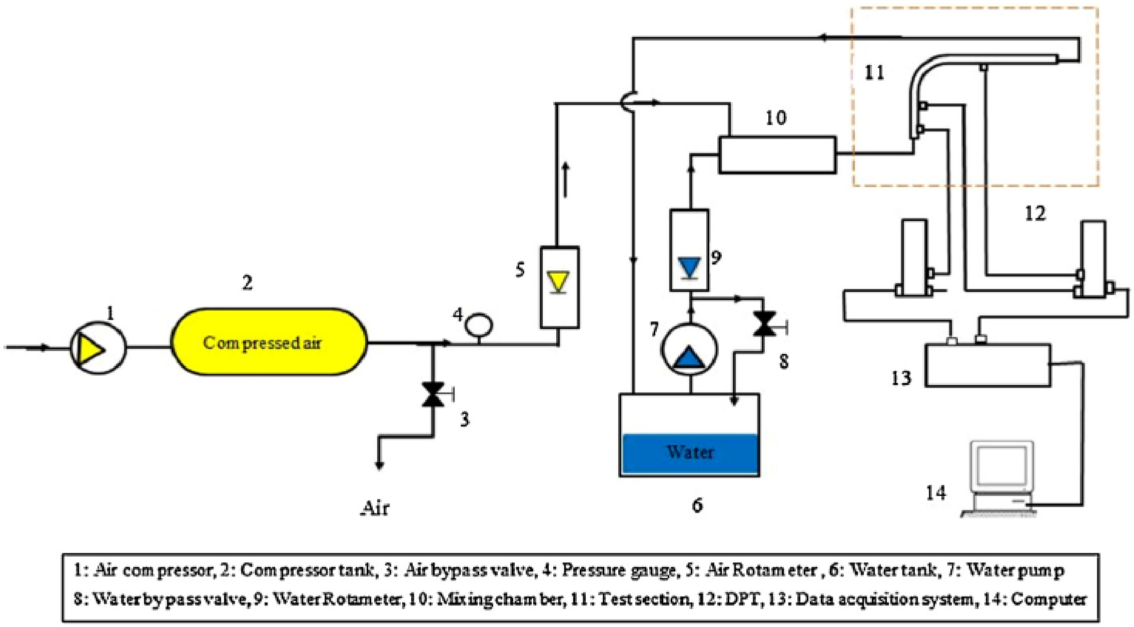

Figure 2. 19: Schematic representation of test setup used by Autee and Giri (2016)

Aleksandrov *et al.* (2017) studied the efficiency of polyurethane coated pipeline over the steel pipeline. The operational cost of the pipeline was estimated from specific energy calculations. Results showed that polyurethane coated pipelines were better than traditional steel pipes. Kumar *et al.* (2017c) studied head loss in the slurry pipeline with the addition of bottom ash for the flow of fly ash water suspension. Bottom ash acts as a better additive than sodium sulfate and detergent.

From the literature survey, it could be said that the transportation of bulk materials through a pipeline is a progressive technology. In recent years, the conveying of solid materials through pipelines is preferred at high concentrations (Jacobs, 2014; Bain and Bonnington, 1970). The hydraulic conveying of dense mixtures has many advantages. Pipeline conveying systems are dust-free, require less space and require less operating staff. However, they create a need for high-quality equipment such as pumps, pressure transducers, flow-measuring devices and control systems (Schaan *et al.* 2000; Wu *et al.* 2015; Qi *et al.* 2018). Transporting solid particles via pipelines is more beneficial than other traditional methods because it helps to minimize pollution. Moreover, pipelines can be laid in difficult geographic areas, reduce traffic, require little maintenance and are reliable and operational throughout the year (Charles and Redberger, 1962; Singh *et al.* 2018a).

From the literature review conducted on experimental investigations of pressure drop, it has been noted that head loss in the pipeline for the flow of slurry suspension is a complex phenomenon. It has been noticed that the head loss characteristic for the pipe bend is also limited. So, an investigation is required to study the head loss characteristic for the flow of coal-water slurry suspension.

2.3 COMPUTATIONAL ANALYSIS OF HEAD LOSS CHARACTERISTICS

Head loss prediction in slurry pipelines is different from single-phase pipe flow because of the existence of solid phase leading to an extreme change in flow structure. Some work has already been performed on the head loss for slurry flow in pipes based on the pilot plant tests (Biswas *et al.* 2000; Gandhi *et al.* 2001; Verma *et al.* 2006; Chandel *et al.* 2009; Kumar *et al.* 2014). The gradual development of computational techniques such as Computational Fluid Dynamics (CFD) offers an ease to analyze such phenomenon with lesser cost (Desai *et al.* 2008; Pietrykowski *et al.* 2013; Bialy *et al.* 2017). CFD simulations give a cost effective way to grasp the complicated fluid flow and is universally accepted by investigators to solve the complex flow problems (Wang *et al.* 2013; Chen and Wheeler, 2015). Numerical simulation of head loss in the pipeline can provide information about the fluid flow characteristics that helps in designing and optimization of a particular piping system. A comprehensive literature survey was carried out on head loss characteristics of different slurries. Head loss in the horizontal pipeline and pipe bends has been investigated by many researchers (Mishra *et al.* 1998; Verma *et al.* 2006; Chandel *et al.* 2010) for the flow of different solid materials.

Many investigators (Ling *et al.* 2003; Kaushal *et al.* 2012; Ma *et al.* 2015; Chen *et al.* 2018) have performed the numerical simulation to investigate the head loss characteristics in horizontal straight pipeline for the flow of solid-liquid flow. Ling *et al.* (2003) investigated the silica/sand-water slurry flow characteristics in the horizontal pipeline using RNG k-ε

turbulence model. They applied the 3D ASM multiphase approach for the fully developed flow of solid-liquid mixture**.** The pipeline was discretized into a block-structured grid (as shown in Figure 2.20) and control volume approach was adopted to solve governing equations. The validation of the simulation results were done with experimental data. They reported that numerical results were found good agreement with experimental data. Also, the post-processing part of CFD helps to study the two-phase flow characteristics in a better way.

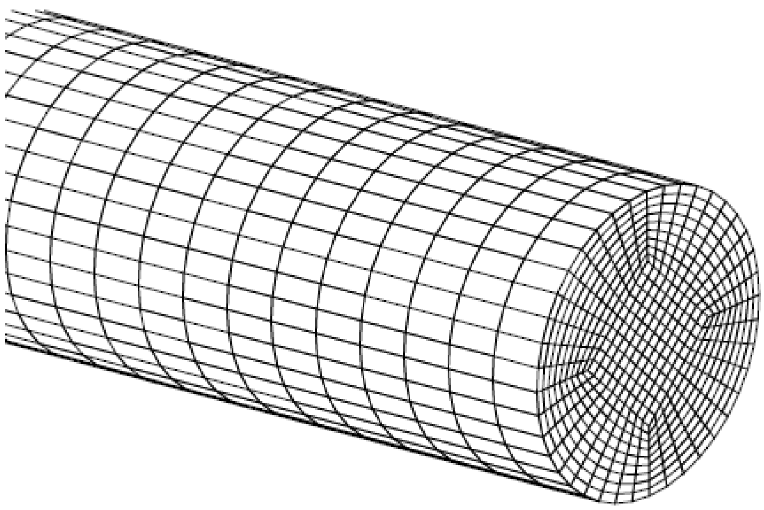

Figure 2.20: Unstructured meshing of horizontal pipe done by Ling *et al.* (2003)

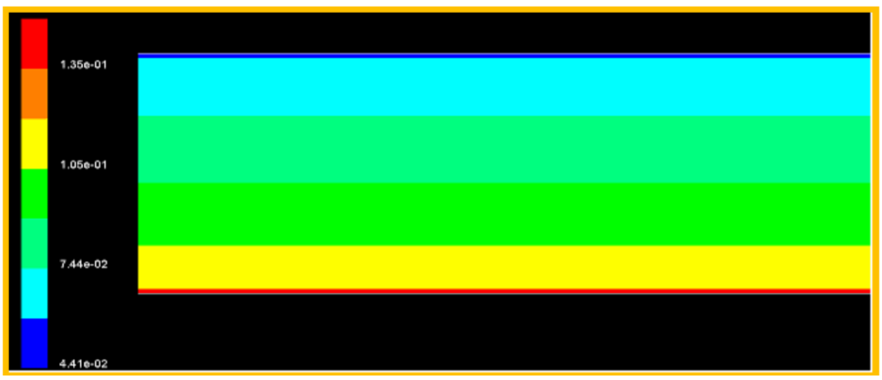

Figure 2.21: Volume fraction profile for straight pipeline studied by Lahiri and Ghanta (2008)

Lahiri and Ghanta (2008) performed the numerical simulation of zinc-tailing water slurry using CFD. Numerical results were validated with experimental data of Kaushal and Tomita (2002). The two dimensional models of the horizontal pipeline was developed in CFD. Euler-

Euler approach with Standard *k-ε* model was used to carry out the simulation results. They found that simulation results were made reasonably good agreement with experimental data. Figure 2.21 represents the concentration distribution profile inside the pipeline. They reported that due to the difference in solid concentration along a vertical plane, the settling velocity and drag coefficient varies with concentration. Chen *et al.* (2009b) studied the head loss characteristics of the coal-water slurry suspension in the horizontal pipeline. They compared the numerical results with experimental data available in the literature. The Eulerian multiphase turbulence modeling approach with RNG *k-ε* model was found good agreement with experimental results. The effect of particle size and flow velocity on head loss was studied by them. They reported the solid particles were more uniformly distributed at higher solid concentrations. Also, the variation of fine particles along vertical diameter was more uniform as compared to coarser. The distribution of solid concentration and axial velocity profiles was not only affected by gravity but also by particle-particle interaction which also plays very important role. Ekambara *et al.* (2009) investigated the flow characteristics of two phase solid-liquid slurry through the horizontal pipeline using CFD. The simulations were performed for solid concentration, particle size and pipe diameter range of 8-45% (by volume), 90-500 μm, and 50-500 mm respectively. CFD results were compared with experimental data of various researchers (Roco and Shook, 1983; Schaan *et al.* 2000; Gillies and Shook, 2000; Gillies *et al.* 2004; Kaushal and Tomita, 2002). Simulation results found excellent agreement with experimental results. They observed that the variation in the volume fraction of solid particles inside pipeline was a function of particle size, flow velocity and solid concentration. Eesa and Barigou (2009) studied the flow characteristics of solid-liquid flow through the pipeline using ANSYS CFX 10.0 in a horizontal pipeline. The numerical simulations were carried out for coarse particles having a size of 5-10 mm with a solid concentration of 41% (by volume) in the pipeline having a diameter of 45 mm. The Eulerian-Eulerian multiphase approach was adopted during the study.

The numerical results were found good agreement with simulation data. They reported that maximum volume fraction of solid particles were found at the bottom of pipe whereas the maximum velocity of solid particles were not at the center of the pipeline rather it was found at the top most part of pipeline. Lahiri and Ghanta (2010) developed a general flow model for solid-liquid flow using numerical code CFD. The numerical results were validated with experimental data of Kaushal *et al.* (2005) for slurry of glass beads. The Euler-Euler approach with standard k-ε turbulence modeling scheme was used to carry out numerical simulations. A series of simulations were carried out on FLUENT 6.2. They reported that the proposed model was suitable for two phase flow as the model showed good agreement with experimental results.

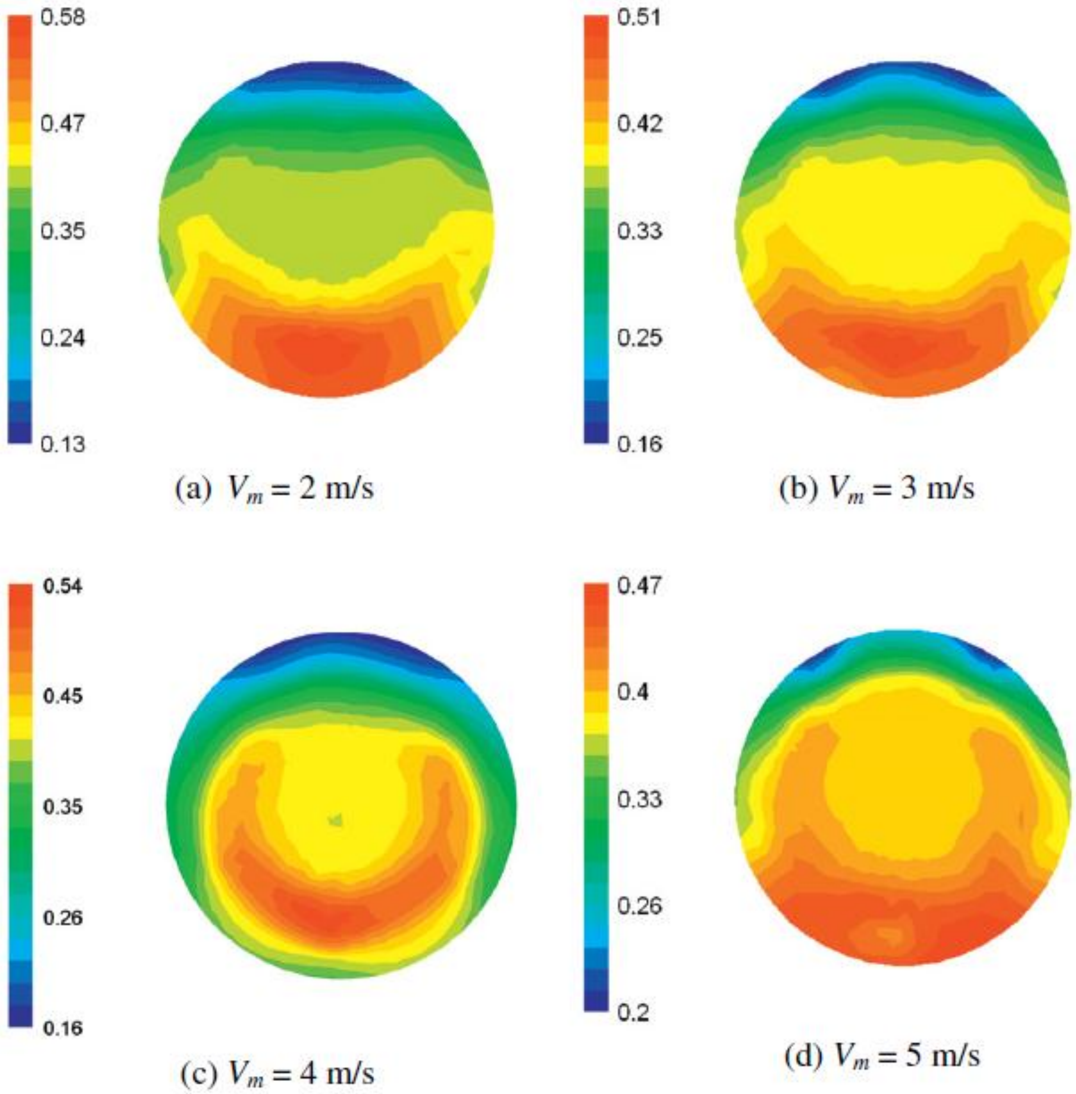

Figure 2.22: Solid concentration contours for volume fraction of 40% in straight pipeline studied by Kaushal *et al.* (2012)

Kaushal *et al.* (2012) studied the flow characteristics of glass beads-water mixture in the horizontal pipeline using *k-ω* shear stress transport (SST) model. The modeling results were validated with experimental data. The solid concentration was kept in the range of 0-50% for flow velocity of 5 m/s. They reported that results obtained from the Eulerian model show better agreement with experimental data as compared to the mixture model. Figure 2.22 shows the solid concentration contour obtained at a volume fraction of 40% for varying flow velocities. They mentioned that the SST *k-ω* scheme was most appropriate turbulence model at high solid concentration. Kumar *et al.* (2012) carried out the series of simulation to study two-phase slurry flow in the horizontal pipeline using CFD. The mean particle size was taken as 440 μm with a solid concentration of 30%. The flow domain was discretized into a non-uniform unstructured mesh. The RNG *k*-*ε* turbulence modeling scheme with ASM was adopted to predict the flow characteristics. They reported that the simulation results show good agreement with experimental data. Messa and Malavasi (2013) performed the numerical simulation for the flow of solid-water slurry through upward-facing channel. The concentration of solid was kept in the range of 5-20% (by volume). The numerical results obtained by the Eulerian multiphase approach show good agreement with experimental data.

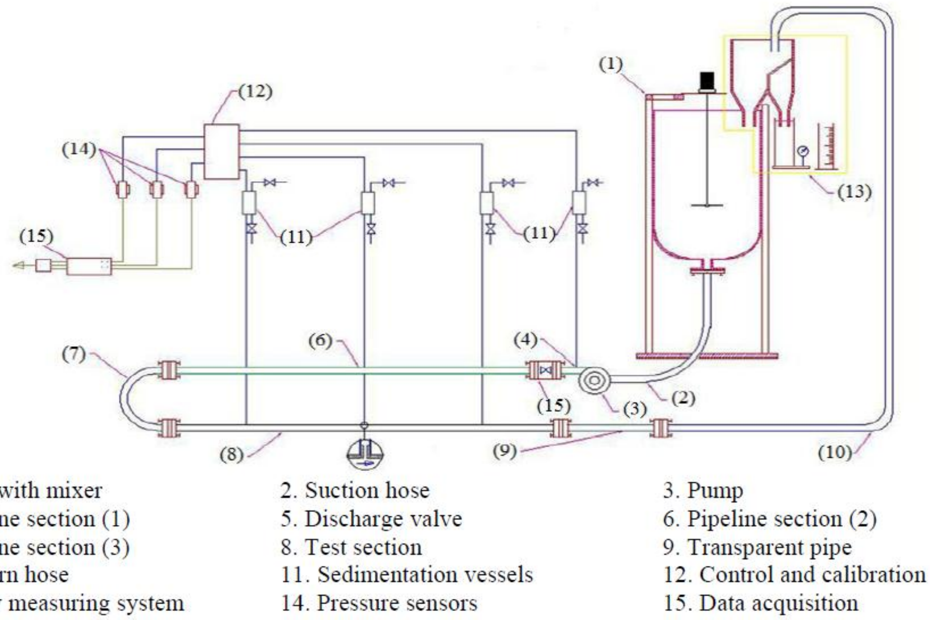

Figure 2.23: Schematic layout of experimental test loop developed by Nabil *et al.* (2013)

Kim *et al.* (2013) performed detailed numerical simulation foe flow of sand water slurry through the horizontal pipeline. The Eulerian granular multiphase scheme with *k*-*ε* turbulence model was used in simulations. The flow domain was divided into the hexahedral non-uniform mesh. The mean particle size of sand particle was taken as 0.54 mm with a slurry density of 2650 kg/m^3. They reported that a decrease in the Reynolds number and an increase in solid concentration lead results in head loss along the straight pipeline. Nabil *et al.* (2013) investigated the flow characteristics of sand-water flow though pipeline using CFD simulation. Experiments were carried out on pilot plant loop (shown in Figure 2.23) to validate numerical results. The Eulerian approach with *k*-*ε* turbulence modeling scheme was adopted during simulations. The mean particle size was taken as 0.2, 0.7 and 1.4 mm. The solid concentration and flow velocity were kept in the range of 5-30% (by volume) and 0.5-5.0 m/s respectively. They reported that results show good agreement with coarser and medium particulate slurry at low solid concentrations of 5-10%. Pinto *et al.* (2014a) performed a numerical study by using two-phase Eulerian approach and k-ε turbulence scheme by combining the population balance models at steady-state. They designed a CFD code for settled-bed of tailing thickeners having a thickness of 120 m diameter. They found that an excessive increase of the turbulence results in breakage of particle-aggregate and reduces the torque range of the tailing thickeners. Wu *et al.* (2015) determined the flow characteristics of coal, cement and fly ash slurries using CFD. The solid concentration and flow rates were varied in the range of 78-79.5% and 60-90 m^3/h. The numerical results had shown good agreement with experimental results obtained from the pilot plant test rig. They reported that head loss was increased with solid concentration and flow rate. The Darcy friction factor was also increased as head loss increased due to frictional resistance. Gopaliya and Kaushal (2015) investigated the effect of particle size on the flow characteristics of sand water slurry in the horizontal straight pipeline. The concentration of slurry was kept in the range of 15-45%. The particle size of sand was taken as 0.18, 0.29, 0.55 and 2.4 mm. The modeling of pipeline having a diameter of 53.2 mm and length of 2.7 m was done in GAMBIT. The flow domain was discretized into hexahedral mesh with convergence criteria of 10^{-3}. They reported that head loss was increased with solid concentration and flow velocity irrespective of particle size. Ofei and Ismail (2016) studied the effect of particle size and solid concentration on the velocity profile, concentration profile and frictional gradient for the flow of two-phase slurry in the horizontal pipeline. They found that the Eulerian approach with k-ε turbulence modeling scheme was most suitable for two-phase applications as compared to other models in CFD. They also reported the effect of various flow parameters on pipeline wear and agglomeration of the solid particle in pipeline. Rawat *et al.* (2016) investigated the impact of coal ash on head loss for flow through a straight pipeline. The modeling of pipe was done in a FLUENT module of ANSYS. After the validation of various turbulence models, the SST k-ω showed a reasonable agreement with experimental results. They reported that head loss was increased with the flow velocity**.** Chen *et al.* (2017) performed a simulation study using computational fluid dynamics (CFD) technique. They employed a three-dimensional backfill pipeline transport model to study pipeline transport properties. Results show that TFSB (3-phase foam slurry backfill) can maintain a steady-state condition during pipeline transportation. Che *et al.* (2017) performed bench scale as well as pilot plant tests to understand the deposition of a paste of iron-ore tailings. They found that for the dry-surface disposal of iron-ore tailing paste requires a slurry concentration above 70%. They also found that tailing-paste after deposition in the TSF (tailing storage facility) forms an angle of repose of 2.0-2.5% which features the good flowability and no particle segregation. Mishra *et al.* (2017) performed the series of numerical simulations on the straight pipeline for the flow of coal and copper-ore water slurry. The particle size range of coal and copper ore was taken as 70.5-275.7 μm and 40.1-278.5 μm respectively. The volume fraction was taken in the range of 0.08-0.19. They observed the maximum head loss for coarser copper ore and finer coal water slurry.

CFD simulations give a cost-effective way to grasp the complicated fluid flow and is universally accepted by investigators to solve the complex flow problems (Gandhi *et al.* 2001). Numerical simulation of head loss in a pipeline can provide information about the fluid flow characteristics that helps in design and optimization of particular piping system. Many investigators have performed the numerical simulation to investigate the head loss characteristics in slurry pipeline bends for the flow of solid-liquid flow. Hossain *et al.* (2011) investigated the deposition of the solid particles in the horizontal pipeline for turbulent flow. They modeled 3D loop with four ninety-degree bends using FLUENT 6.2. They explained the effect of flow velocity and particle size on deposition characteristics in their study. They reported that coarser particles show maximum deposition as compared to finer ones. Also, the depositions of solid particles were at the bottom of pipe bend for an upstream section whereas at downstream section maximum deposition was seen at an angle of 60˚ from the bottom. Ma and Zhang (2012) numerically studied the head loss characteristics for the flow of tertrabutylammonia bromide slurry in various pipe fittings like a pipe, bend, sudden contraction and expansion sections. The concentration was kept in the range of 10-30% (by weight). They reported that the loss coefficient for bend, sudden expansion and contraction was decreased with the flow velocity. Also, the increase in mass fraction results in an increase in loss coefficient. Mazumdar (2012a) performed the numerical simulation for two-phase flow of air and water using CFD in pipe elbows. The diameter of elbows was taken as 6.35 and 12.7 mm. They reported that the numerical results showed reasonable prediction with experimental and empirical correlation results. The schematic experimental test set is shown in Figure 2.24. Mazumder (2012b) investigated the flow characteristics for the flow of single phase (water) and two-phase (water-air) fluid in the elbow of 12.7 mm diameter. They reported that experimental results showed good agreement with empirical models of Chisholm (1983) and Benbell *et al.* (2009). Tebowei *et al.* (2018) numerically studied the flow characteristics sand water slurry through inclined V-bends. The Eulerian-Eulerian model with *k-ε* turbulence modeling scheme was adopted in their study. They reported that the settling of sand particles was significant for V-bend as compared to a horizontal pipe. The sand particles were settling at a higher rate in V-section even at high flow velocities. They also found that the correlations available in the literature for settling velocity in horizontal pipelines were not valid for V-type pipe bends.

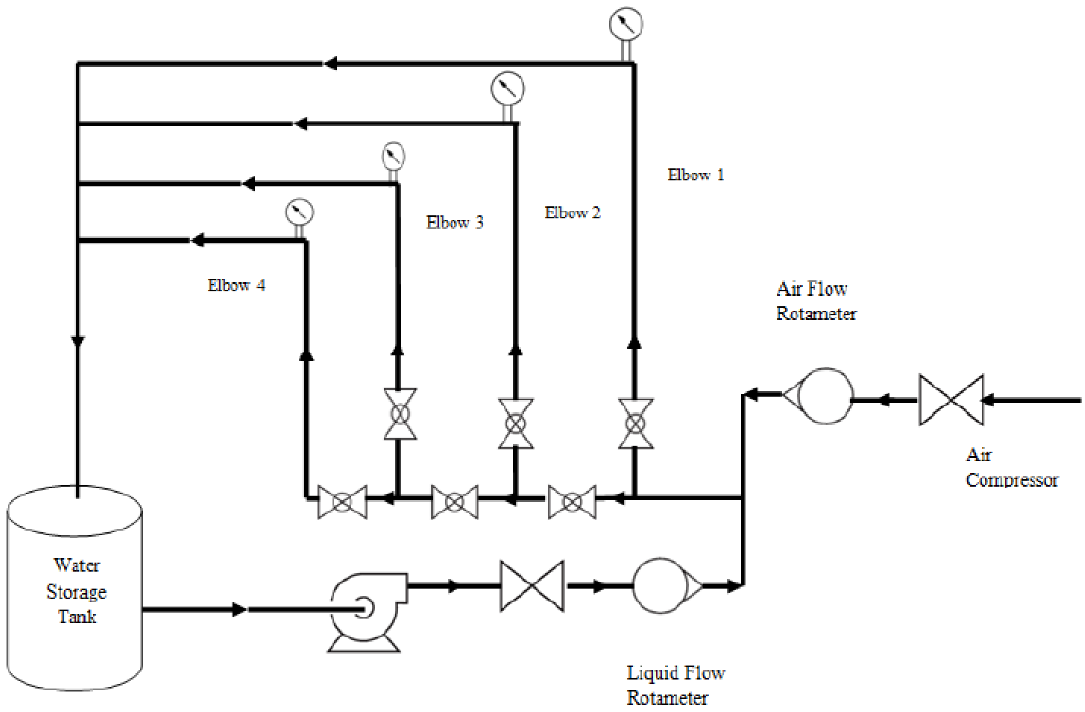

Figure 2.24. Schematic illustration of pilot plant test loop developed by Mazumdar (2012)

Numerical simulation studies were carried out by different researchers (Ling *et al.* 2003; Chen *et al.* 2009b; Pinto *et al.* 2014b) using CFD codes to predict head loss in horizontal and vertical pipelines for the flow of sand-water, coal-water, fly ash-water and various mineral ore-water slurries. The literature reveals that the Eulerian model offers the utmost rational frame-work for defining high concentration slurries (Kaushal *et al.* 2012). This model involves the interaction effects of liquid-solid, wall-solid and solid-solid particles. The only input required is the physical properties of the carrier fluid and solid material. It was also noticed from past studies that RNG *k-ε* and SST *k-ω* turbulence modeling schemes were the most appropriate for predicting the flow properties of high-concentration slurries (Rawat *et al.* 2016).

2.4 GAPS IN LITERATURE

Based on literature review, following gaps in present research on the flow characteristics of the solid-liquid slurry suspension in the pipe bend are observed.

- Due to incomplete understanding of complex solid-liquid flow phenomena in slurry pipeline bend and limited database, there is no well-established method available to predict the flow characteristics in the slurry pipeline for the flow of solid-liquid mixtures.
- Experimental studies for prediction of head loss are applicable for particular slurry and cannot predict reasonable head loss with all type of slurries or multi-particulate slurries. Also, the studies on the effect of different geometrical parameters on head loss for the pipe bend are limited.
- Head loss characteristics are studied in the past but limited to pipeline only. From the literature's point of view, very few studies are reported on head loss through sharp pipe bends.
- At present, only a few investigations have been carried out to study the head loss behavior of coal and coal-ash water suspensions for flow through a 90˚ bend. The use of a 90˚ bend is limited in industrial applications because it leads to huge loses and requires high pumping power. However, the use of 90˚ bends is not completely restricted because of geometrical and space constraints.
- Limited investigations for head loss in slurry pipe bend for the flow of solid-liquid mixture has been carried out with additives and stabilizers to improve the head loss characteristics.

2.5 PROBLEM STATEMENT AND METHODOLOGY

The comprehensive literature survey is conducted in previous sections. The gaps in literature also revealed in the field of the slurry transportation system. In this perspective, the present work is undertaken to examine the head loss and flow characteristics of three different slurries namely coal, fly and bottom ash. The rheological experiments are conducted to analyze the effect of solid concentration on flow behaviour with and without the use of an additive. The experimentation is extended to study head loss characteristics across 90º pipe bend for the flow multi-particulate solid-liquid slurry at different solid concentrations and Reynolds number. The present work also highlights the role of concentration and Reynolds number in settling velocity, bend loss coefficient and specific energy consumption for the transportation of slurry. The experimental work is typical and expensive, also limited variations are possible on the fabricated pilot test loop. Therefore, to optimize design parameters, numerical simulations are carried out by validating the numerical results with experimental data. An attempt has been made to study the head loss characteristics for conveying a solid-liquid slurry suspension using ANSYS-Fluent. The bend geometry is varied by altering the radius of curvature-to-diameter (*r/D*) ratio within the range of 1.5-3.0. The Eulerian multiphase model along with an SST k-ω turbulence scheme is adopted over different turbulence modeling schemes after validation The detailed methodology adopted during present investigation has been highlighted in Figure 2.25.

2.6 OBJECTIVES OF PRESENT WORK

On the basis of gaps found in literature and the complexities in the behavior of solid-liquid suspension flow in pipeline, it is felt that the more studies on Indian coal and coal-ash are required to be conducted for gaining more knowledge on slurry transport system in a pipeline. So, the following objectives have been set in the present study to get the necessary information on slurry transport system:

- Investigation of rheological characteristics of coal, fly and bottom ash with and without additives.
- Investigation of head loss characteristics of coal, fly and bottom ash slurry flow through a slurry pipe bend. Experiments will also be carried out to investigate the effect of Reynolds number and *r/D* ratio on head loss with and without additives.
- Optimization of *r/D* ratios of pipe bend for slurry flow using numerical simulation.

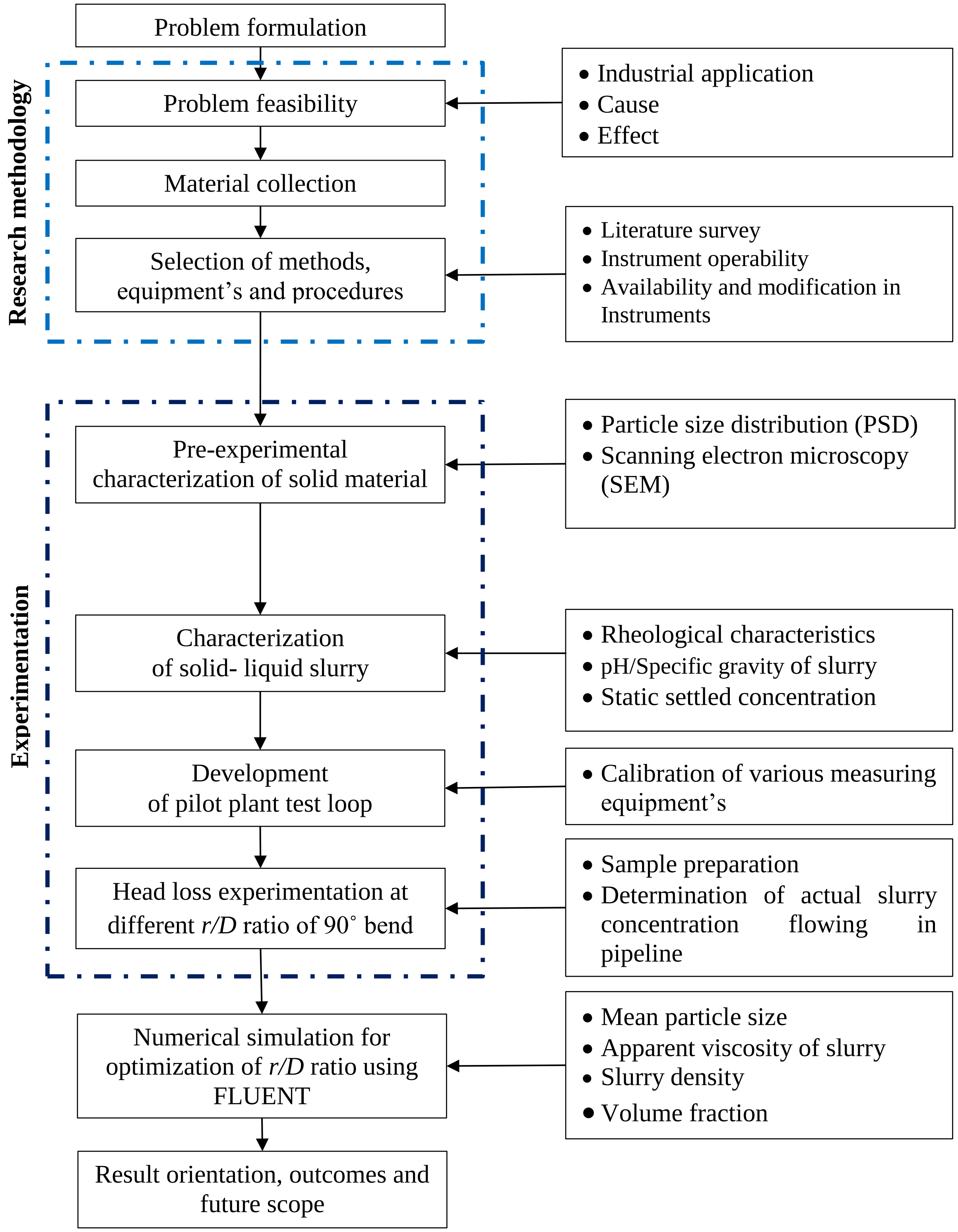

Figure 2.25: Flow chart of experimental methodology

CHAPTER 3

CHARACTERIZATION OF COAL, FLY AND BOTTOM ASH

Chapter 3

CHARACTERIZATION OF COAL, FLY AND BOTTOM ASH

The flow characteristics of solid-liquid slurry are the functions of various dynamic and geometrical parameters. The complex designing process of the slurry transportation system is directly or indirectly dependent upon these parameters. The extensive database on experimental studies of two-phase flow is required for designing a hydraulic transportation system. Form the literature review carried out in the previous chapter, it is cleared that there is unavailability of enough data for the flow of coal and coal-ash slurries at higher concentrations. Therefore, it is necessary to establish the database for different slurries so that the design methodology becomes more facile and faster. Various types of slurries are being transported though the slurry pipeline in mining industry, chemical industry and thermal power stations. The transportation of coal-water slurry suspension at high concentrations has wide applications in energy conversion systems. The huge amount of coal is being utilized in thermal power plants. In India, the coal is transported to power stations with the help of railways. There is unavailability of working or proposed a pipeline for transportation of coal-water slurry in India. Therefore, a detailed study of various properties of Indian coal is required to be performed for making this mode of transportation more popular and economic.

A large amount of solid waste is produced after the combustion of coal in the form of a fly and bottom ash at thermal power plants. The fly and bottom ash is disposed-off to the dyke area by mixing it with water through the pipelines with the help of slurry pumps. In the present scenario, the disposal of coal ash takes places at very low solid concentrations i.e. 10-15% (by weight) due to fear of chocking or effect of high concentration on various flow parameters. This leads to wastage of a large amount of water and pumping energy. Also, the leaching of heavy metals from coal-ash leads to polluting the nearby and groundwater bodies. The economical and efficient transportation of fly and bottom ash in thermal power plants is a major challenge.

The previous chapter revealed that the two-phase solid liquid flow characteristics are influenced by many parameters like specific gravity of solids, particle size distribution, slurry pH, static settled concentration, and carrier fluid. The study of microstructure, chemical composition and crystalline structure of solid particles is very important in the context of designing a slurry transportation system. In this chapter, a detailed investigation is carried out to study the various physical and chemical characteristics of solid and slurry suspensions with the help of different bench-scale tests.

3.1 COLLECTION OF COAL, FLY AND BOTTOM ASH SAMPLES

In present work, the head loss characteristics through pipe bends have been carried out for the flow of three different solid-liquid slurries made from coal, fly and bottom ash. The coal sample is procured from the Jharia coal field, Jharkhand lies in the eastern region of India. The coal fields of Jharia are situated in Damodar river valley. These coal fields are expanded in the region of 280 square kilometers. The coal mines of Jharia acts as store house of India. The major part of coal in India is coming from Jharia coal fields. These coal fields consist of 23 underground and 9 open cast large mines. The geographical location of Jharia coal mine is shown in Figure 3.1.

Figure 3.1: Location of source of coal sample (Jharia coal field, Jharkhand, India) [Image is taken from Google Earth, 2018]

Figure 3.2: Location of source of bottom ash sample (Deen Bandhu Chhotu Ram Thermal Power Plant, Yamunanagar, Haryana, India) [Image is taken from Google Earth, 2018]

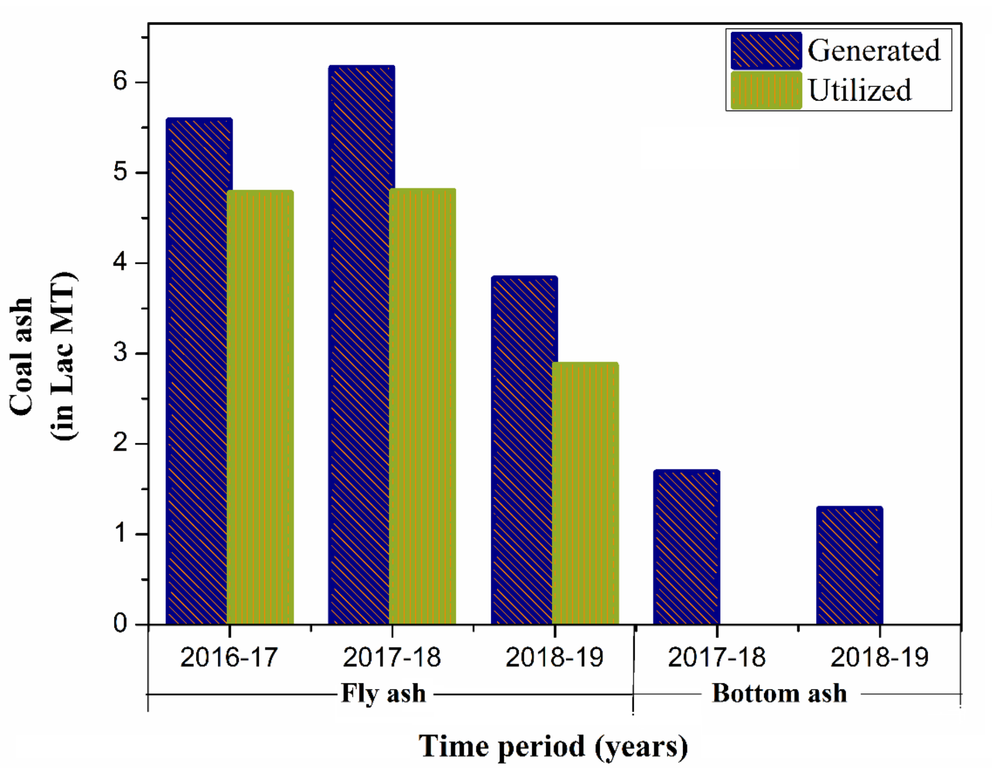

Figure 3.3: Generation and utilization of coal ash in last years at Deen Bandhu Chhotu Ram Thermal Power Plant, Yamunanagar, Haryana, India [Source: www.hpgcl.org.in]

Figure 3.4: Location of source of bottom ash sample (Deen Bandhu Chhotu Ram Thermal Power Plant, Yamunanagar, Haryana, India) [Image is taken from Google Earth, 2018]

The bottom ash sample is collected from the bottom ash hopper of the Deen Bandhu Chhotu Ram Thermal Power Plant, Yamunanagar, Haryana, India. The geographical location of Deen Bandhu Chhotu Ram Thermal Power Plant is shown in Figure 3.2. The installed capacity of this power plant is 600 MW (two units of 300 MW each). The production and utilization of fly and bottom ash in last few years is shown in Figure 3.3. The fly ash sample is directly procured from electrostatic precipitator hopper of Deen Bandhu Chhotu Ram Thermal Power Plant, Yamunanagar, Haryana, India. The coal-ash sample is not subject to any further processing like the crushing of other solid particles (coal) is done before transportation in pipelines. Figure 3.4 depicts the geographical location of Deen Bandhu Chhotu Ram Thermal Power Plant.

3.2 SURFACE MORPHOLOGY OF COAL AND COAL ASH SAMPLES

The study of mineralogical characterization helps to understand the surface microstructure, particle shape and chemical composition of collected coal, fly and bottom ash samples. In present work, the mineralogical characteristics of coal, fly and bottom ash samples are studied by various techniques/methods. The scanning electron microcopy *(SEM)* technique is used for surface morphology, energy dispersive spectroscopy technique is employed for chemical composition and crystalline characterization is studied with X-ray diffractometery *(XRD)* technique.

3.2.1 Surface morphology or microstructure analysis

The morphological analysis of coal and coal ash samples are carried out to analyze the surface microstructure. The high-resolution micrographs are obtained by using JSM 6510V model of scanning electron microcopy (*SEM*) unit manufactured by JEOL, Netherlands. This machine is available at Sophisticated Analytical Instruments *(SAI)* laboratories, Thapar Institute of Engineering and Technology, Patiala, Punjab (India). The detailed procedure and working principle of *SEM* is discussed as follows:

Sample preparation and sputter coating

The coal and coal ash samples are put in the oven at the temperature of 120±5˚C so as to remove the inhered moisture. The sample is sprinkled on the sample holder already coated with carbon tape with the help of a spatula. The excess amount of the sample is removed with the help of a small blower. Coal and coal-ash samples fall under the category of non-conducting materials, so the coating of conductive material is done before *SEM-EDS* analysis. This process of coating is called sputter coating (Lopez *et al.* 2003; Wirth, 2009).

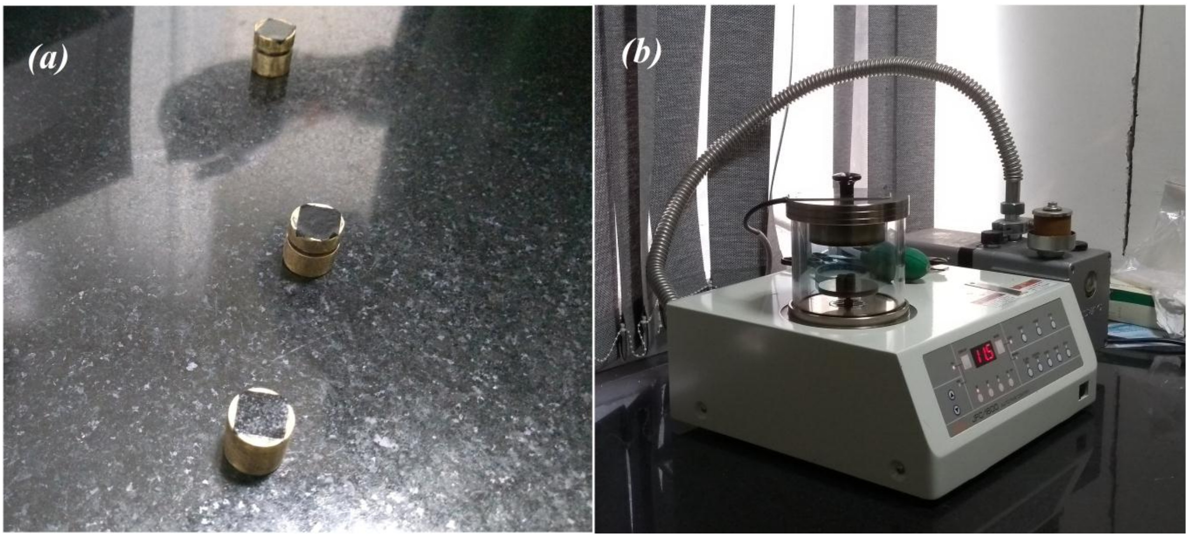

Figure 3.5: (a) Carbon tape coated sample holders (b) Auto fine coating machine manufactured by JEOL, Netherlands

Figure 3.5 shows the auto fine coating machine manufactured by JEOL, Netherlands. In sputter coating, the thin layer of gold, platinum or gold-palladium is coated on non-conducting materials. This coating operation is performed under vacuum to remove the air particle and also to increase the mean free path between solid particles. The thickness of the coating layer is kept in the range of 5-50 nm. In general, the thin layer of coating helps to provide a conduction path and also decreases the electron beam damage for sensitive samples. The samples are put in sample holders after coating and placed in the SEM unit.

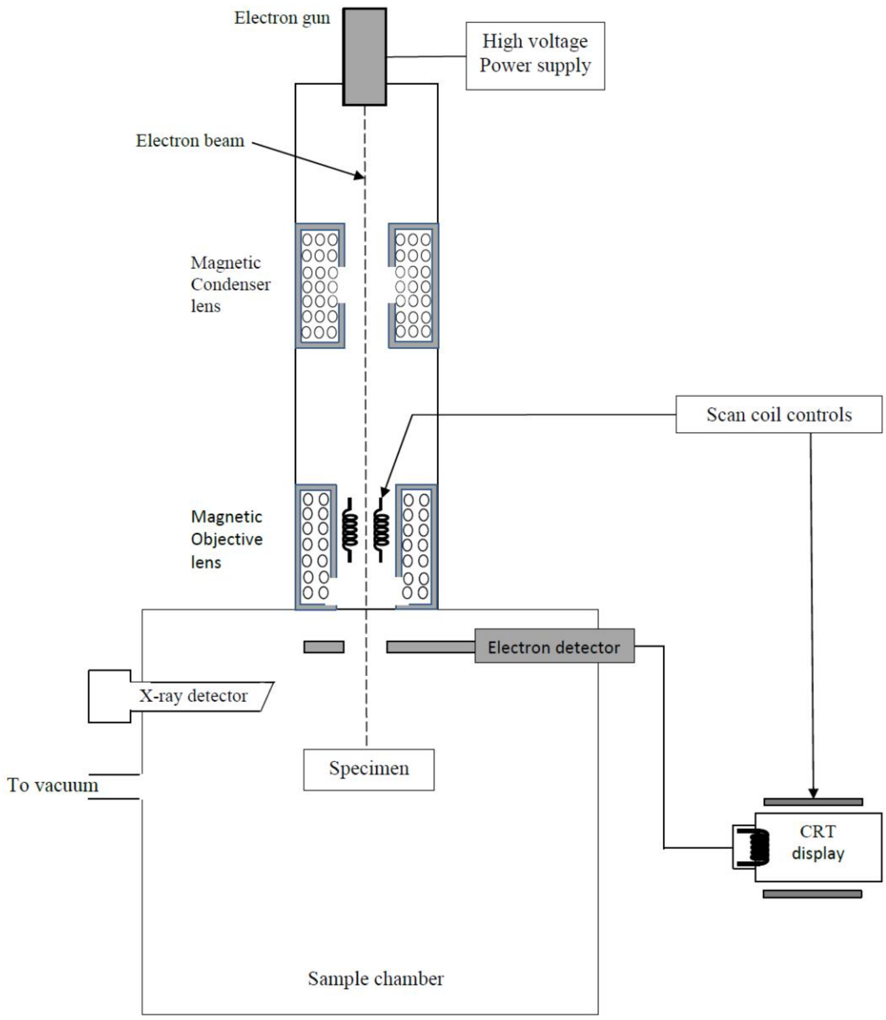

Figure 3.6: Schematic line diagram of scanning electron microcopy (SEM) unit (Skoog *et al.* 2007)

Working principle of SEM machine

The sputter-coated samples are placed in the *SEM* unit under a high vacuum of 10^{-6} torr or less. Figure 3.6 illustrates the schematic diagram of *SEM* machine with X-ray detection. The electrons are generally emitted with tungsten filament or for higher resolutions micrographs field emissions are also used. The energy level of 1-30 keV is employed to accelerate the electrons. The diameter of the electron beam ejected from tungsten filament is reduced to 2-10 nm with the magnetic objective and a condenser lens. The throughput of electron beam is determined by one or more condenser lens. However, the objective lens controls the size of the electron beam. The pair of electromagnetic scan coils are placed adjacent to the objective lens, these coils deflects the beam in x and y direction. The signal to the scan coils are controlled by digital or analog techniques. This signal is encoded and plotted in x and y positions. The electrons beam after striking the sample results into three signals namely back-scattered, X-ray emissions and secondary electrons. The *EDS* spectrum is obtained from X-ray emissions produced after striking the sample.

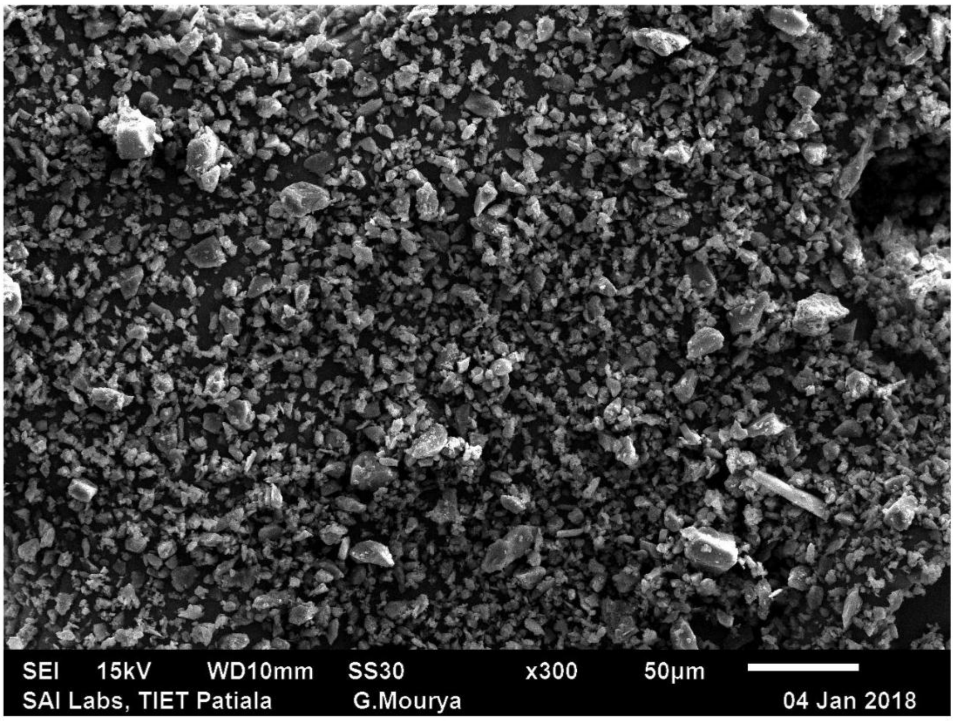

Figure 3.7: Surface morphology of coal sample (particle size < 53 µm)

SEM micrographs of coal sample

The morphological characteristics of fine pulverized coal sample having particle size <53 µm is obtained by scanning electron microscopy (*SEM*) technique. Figure 3.7 shows the *SEM* micrographs of < 53 µm coal sample. The *SEM* micrographs depict that the coal particles are non-spherical and have irregular shapes with knife edges. The rough surface of coal particles is due to the presence of carbonaceous materials and impure particles of carbon known as soot. The existences of white spots are the result of a mine fire. Similar observations are also reported by some researchers (Gupta *et al.* 2018; Juneja *et al.* 2018; Vishnoi and Mohapatra, 2018).

SEM micrographs of fly ash sample

The surface microstructure of the collected fly ash sample is shown in Figure 3.8. From the SEM micrographs, it is observed that fly ash particles have a smooth surface, regularity in shape, and spherical appearance. It is also observed that most of the fine spherical particles are agglomerated with each other. The small fine hollow spherical ash particles are known as cenospheres (Fomenko *et al.* 2011; Zyrkowski *et al.* 2016). The presence of these cenospheres in fly ash helps to develop light weight concrete having good sound absorbance tendency.

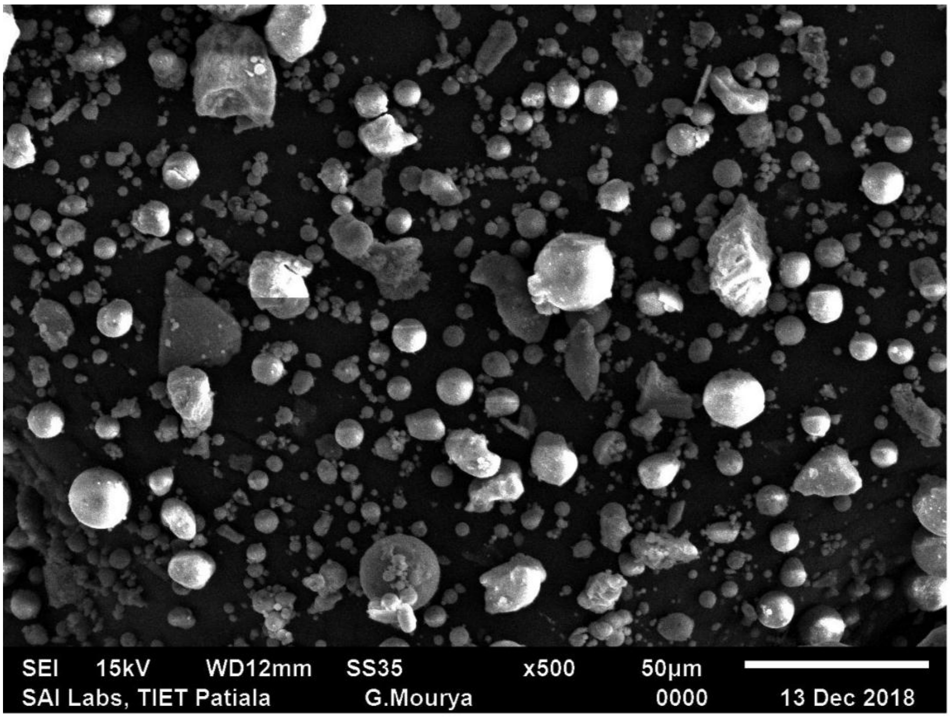

Figure 3.8: SEM micrograph of fly ash

SEM micrographs of bottom ash sample

Figure 3.9 presents the micrograph of bottom ash sample. The micrograph depicts that bottom ash particles have rough surface morphology, irregularity in shape and a porous surface. Also, bottom ash particles are dark grey in color, this shows the presence of unburnt carbon. The surface characteristics of bottom ash sample are relatively coarse as compared to fly ash. The irregularity in bottom ash particles leads to the generation of more drag forces during transportation (Asokbunyarat *et al.* 2015; Kumar *et al.* 2018a). Similar types of observations are also reported by some researchers (Mishra and Das, 2010; Mishra and Das, 2014).

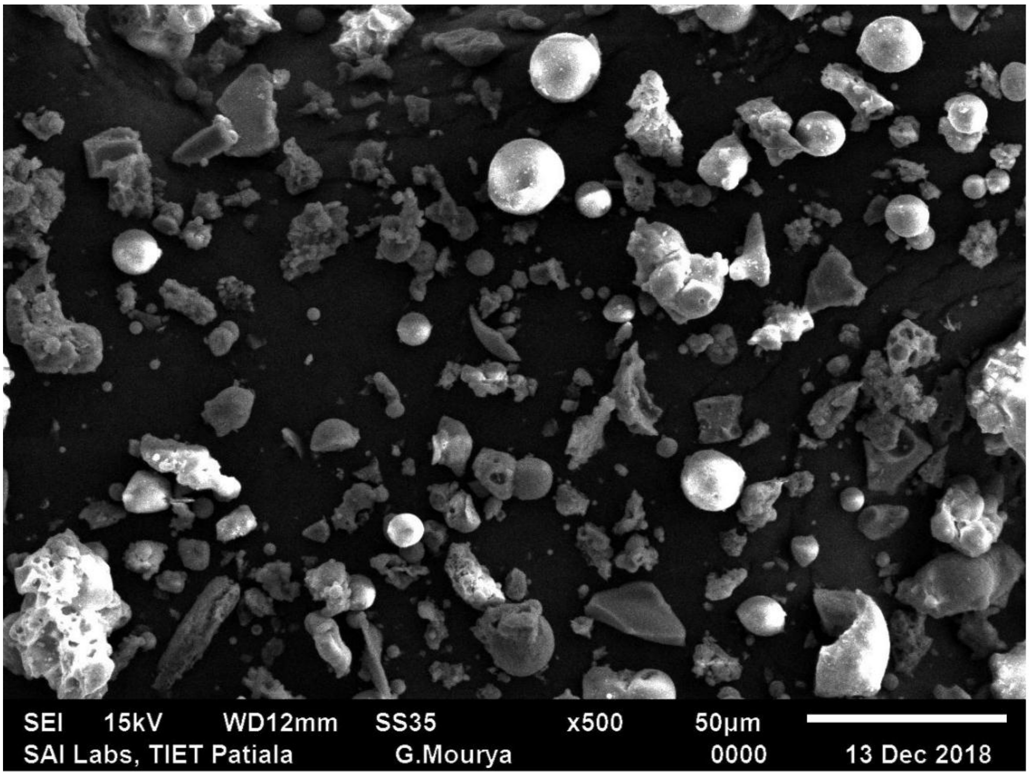

Figure 3.9: Surface morphology of bottom ash

3.3 BENCH SCALE INVESTIGATIONS

Several bench scale tests are carried out to study the particle size distribution, specific gravity, potential of hydrogen, static settled concentration, ultimate analysis, proximate analysis and leaching characteristics of slurry prepared from coal and coal-ash.

3.3.1 Particle size distribution

The particle size analysis helps to characterize the particle size distribution in the sample. The particle size distribution can be analyzed by various methods. In the present work, AS-2011 laser diffraction particle size analyzer manufactured by Aim sizer solutions, China is used to analyze the particle size distribution coal and coal-ash samples. The detailed procedure and working principle of particle size analyzer is discussed below.

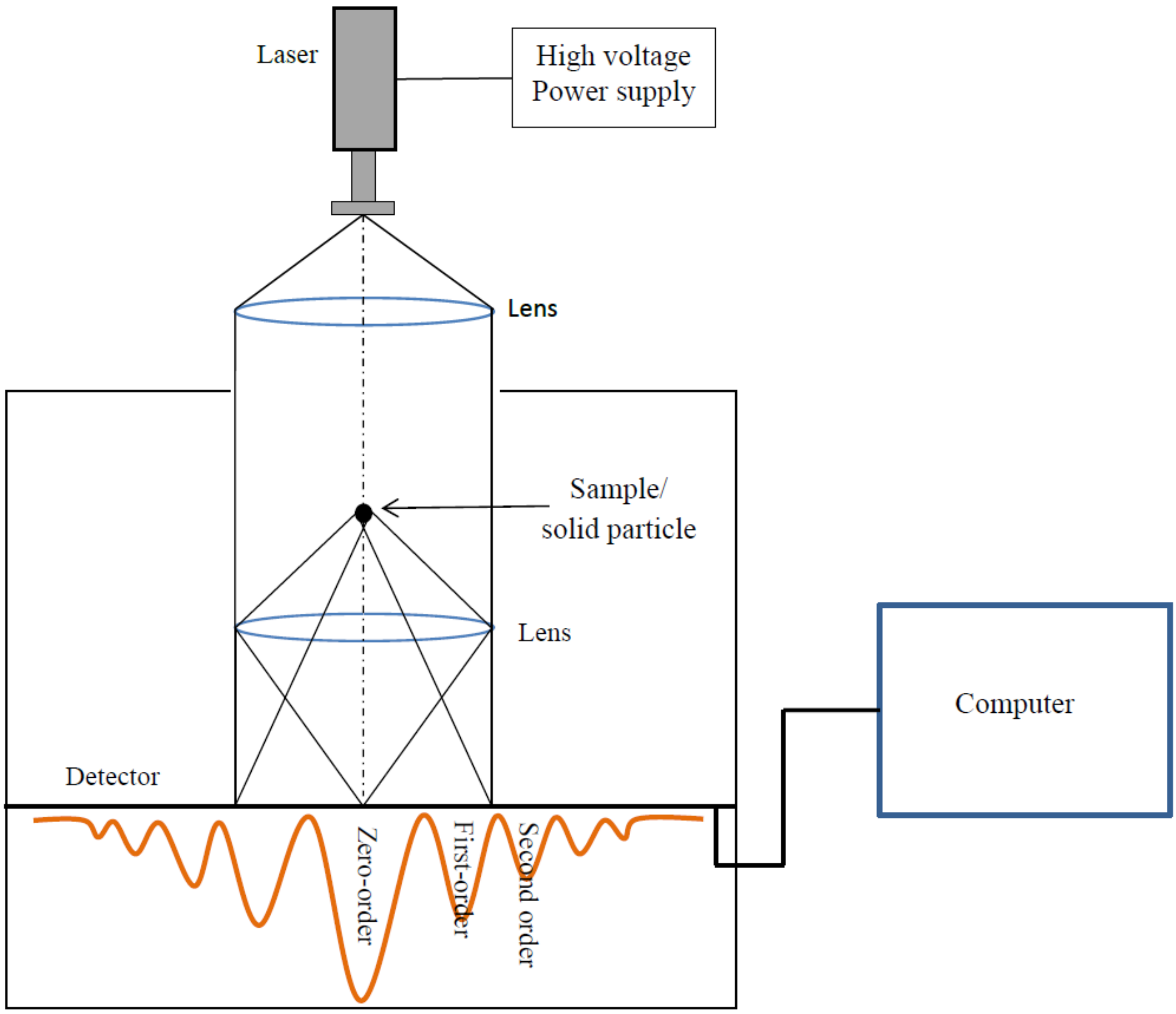

Figure 3.10: Schematic line diagram of laser diffraction particle size apparatus

Working principle and sample preparation

The laser diffraction particle size analyzer operates on the principle of Mie scattering theory. The Mie theory treats solid particles as finite objects. Figure 3.10 illustrates the typical laser diffraction particle size apparatus. The laser diffraction analyzer consists of *He-Ne* laser which passes the continuous beam through the sample. The scattering of the beam occurs while it strikes the solid particles in the sample. The scattered beam is focused on the detector array where the pattern of the diffraction is measured. Finally, the particle size distribution is obtained by analyzing the pattern with theoretical models. The oven dried sample is mixed with a fix amount of water and the solid-liquid mixture is placed in water bath ultrasonic sonicator for 15 minutes. The function of the sonicator is to disperse the accumulated solid particles in the liquid phase. After the sonication process, the sample is poured into glass cuvette. The glass cuvette is placed in front of the laser to obtain *PSD*. Each test is repeated three times to ensure the repeatability and accuracy of results.

Particle size distribution of coal and coal ash samples

The procured coal sample is initially crushed with a hammer-type coal crusher and then passed through a ball mill. The coal sample is sieved with British Standard *(BS-410)* sieves and coal samples with particle sizes < 53 μm are collected and used in experimentation. Figure 3.11 shows the percentage finer of coal, fly and bottom ash particles for different particle size. Results show that 81.63% of particles are finer than 33.95 μm, 49.94% particles are finer than 11.07 μm, and 35.98% of particles are finer than 5.05 μm for coal sample. From the results, it is noticed that all the bottom ash particles are finer than 710 μm. However, 94.95 and 15.74% particles are finer than 445 and 42.48 μm respectively. It is also observed that all the fly ash particles are finer than 500 μm whereas, 81.27% particles are finer than 163 μm. The smallest particle in the fly ash sample is noticed as 1.8 μm.

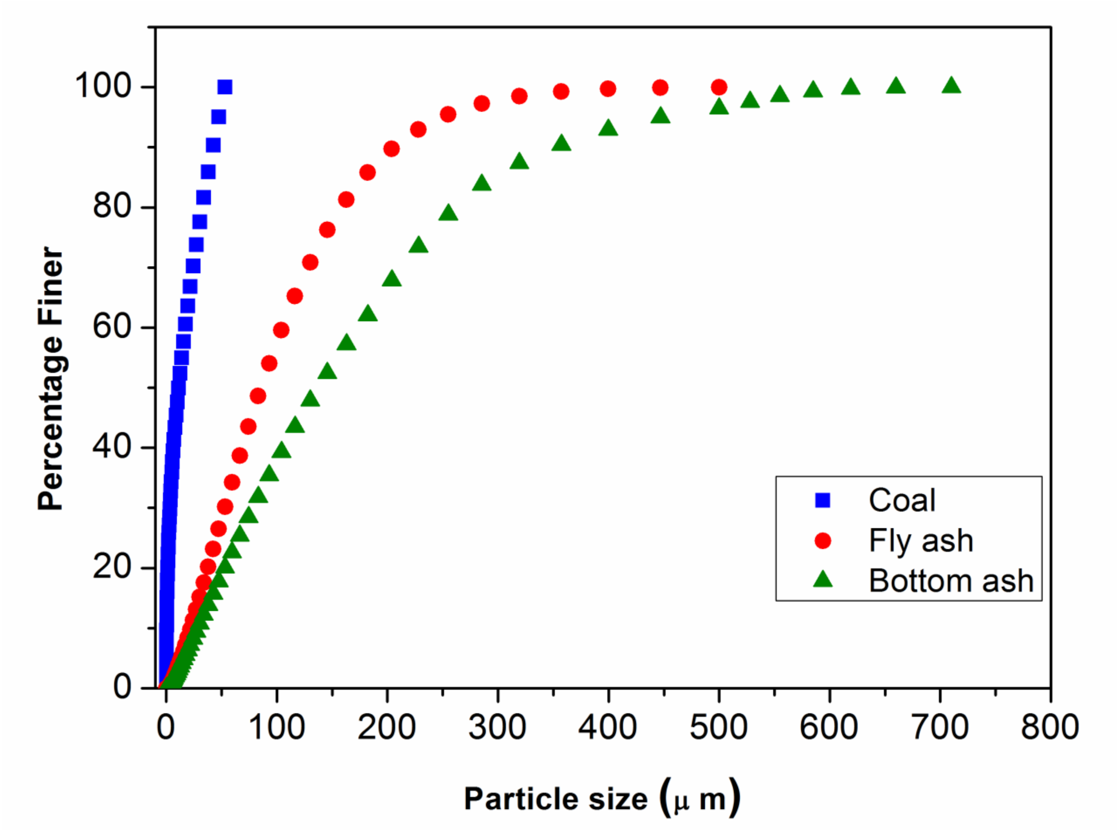

Figure 3.11: Particle size distribution of coal, fly and bottom ash samples

The particle size is one of the most critical parameter for the design of slurry transportation system. The existence of fine solid particles in the slurry results in complex flow characteristics due to colloidal nature. The solid particles undergo rotational and translational motions during the flow of slurry under the action of shear force. This leads to the formation of agglomerates and increases in particle collisions which results in an increase in slurry viscosity and viscous energy dissipation rate (Vlasak and Chara, 2007; Vlasak and Chara, 2011). The inter-particulate interactions among the solid particles are more significant for slurry having colloidal particles. These colloidal forces occur mainly due to electrostatic repulsive and van der Walls attractive forces which further evoke the non-Newtonian nature of slurry. The slurry behavior is dependent on the physical characteristics of solid particles. The knowledge of the slurry flow characteristics helps to improve economy, reliability, energy and water requirement of slurry transportation system (Nguyen and Boger, 1984; Vlasak *et al.* 2010).

3.3.2 Specific gravity of coal and coal-ash sample

The *specific gravity* is defined as the ratio of a density of sample to a density of reference material. The standard reference material is taken as water (at 4˚C). The density of a material is the ratio of weight per unit volume. The specific gravity can be mathematically expressed as follows:

$$Specific\ gravity = \frac{Density\ of\ sample}{Density\ of\ water} \tag{3.1}$$

The specific gravity plays a very significant role in flow analysis of slurry to determine one of the critical parameter in the context of choking of pipeline i.e. static settled concentration. The pycnometer method is adopted in the present study to determine the specific gravity of coal, fly and bottom ash. Initially, the moisture from coal and coal-ash samples are removed by placing them in an electric oven at a temperature of 115˚C for 1 hour. A 100 ml beaker is washed with water and dried in an oven before experimentation. Afterward, the weight of beaker (W_b) is measured by placing them it on precise electronic weighing machine having least count of 0.0001 gram. The 30 gram oven dried sample is then poured into the beaker and weight of beaker along sample is measured (W_a). The distilled water is added into the beaker to make slurry. To ensure the uniform mixing of solid in the liquid phase, the electronic stirrer is used for 10-15 minutes. The volume displaced by the addition of distilled water in solid particles is noticed. The beaker is then placed undisturbed for two hours. Later on, the weight of beaker filled with slurry (W_d) is measured again. Then, the exact weight of slurry is calculated by subtracting the weight of oven dried empty beaker form weight of beaker having slurry within it. The weight of water (W_c) is measured by filling the distilled water up to the initially marked level. The above procedure is repeated three times for every sample and then the average of each value is put in the following correlation to calculate specific gravity of coal and coal-ash sample:

$$Specific\ gravity = \frac{(W_a - W_b)}{[(W_c - W_d) + (W_a - W_b)]} \tag{3.2}$$

After calculations, the specific gravity of coal, fly and bottom ash sample is determined as 1.46±2%, 2.27±0.5% and 2.09±1.6%. The density of the slurry suspension at different solid concentrations is calculated by the following equation.

$$Slurry\ density = \frac{100}{\left\{\left(\frac{C_w}{\rho_s}\right) + \left[\left(\frac{100 - C_w}{\rho_l}\right)\right]\right\}} \tag{3.3}$$

Where C_w stands for solid concentration of slurry (by weight); ρ_s is density of solid in slurry; ρ_l is desnity of carrier fluid (water in present study).

3.3.3 Potential of hydrogen (pH)

The term potential of hydrogen or *pH* value indicates the acidity or basicity of the aqueous solution. The solution having *pH* value greater than 7 is base and less than 7 is termed as acid. However, pure water having *pH* value 7 at a temperature of 25˚C is labeled neutral solution i.e. neither base nor acidic in nature. The *pH* value of coal, fly and bottom ash samples is also determined at a different solid concentration range of 30-60% (by weight). In present work, a digital pH meter manufactured by Orino 5 star is used to determine the pH of aqueous coal and coal-ash slurry. The electrode of the *pH* meter is first filled with distilled water. Afterward, the calibration of the pH meter is done with three buffer solutions having *pH* of 3, 7 and 9. The buffer solutions are made by dissolving the buffer capsule in 100 ml of distilled water. After calibration, the electrode of *pH* meter is washed with distilled water and the *pH* value of coal and coal-ash slurries is determined. It is noticed that the *pH* of coal-water slurry varies in the range of 6.38-5.93 as solid concentration is increased from 30-60% (by weight). Also, the coal-water slurry exhibits a weak acidic nature. However, the pH value for fly and bottom ash suspensions are lies in the range of 7.62-7.42 and 7.68-7.45 respectively. From results, it is observations that both fly and bottom ash samples are alkaline in nature. This happens due to the fact that during the combustion of coal in the furnace the outermost layer of fly and bottom ash particles are get covered with a white greyish colored alkaline layer. Also, the solid concentration has very little effect on pH value for coal and coal-ash slurry.

3.3.4 Static settled concentration

The static settled concentration of solid-liquid slurry is defined as the maximum possible concentration of solid phase that occurs due to the settling of solid particles under the effect of gravity. The static settled concentration is one of the significant parameters in hydraulic conveying of multi-sized solid-liquid slurry through pipelines. The viscosity and specific energy consumption of slurry increases as the value of static settled concentration reaches maximum. The static settled concentration depends upon the various parameters like specific gravity of solid, type of carrier medium, viscosity of slurry, particle shape and size.

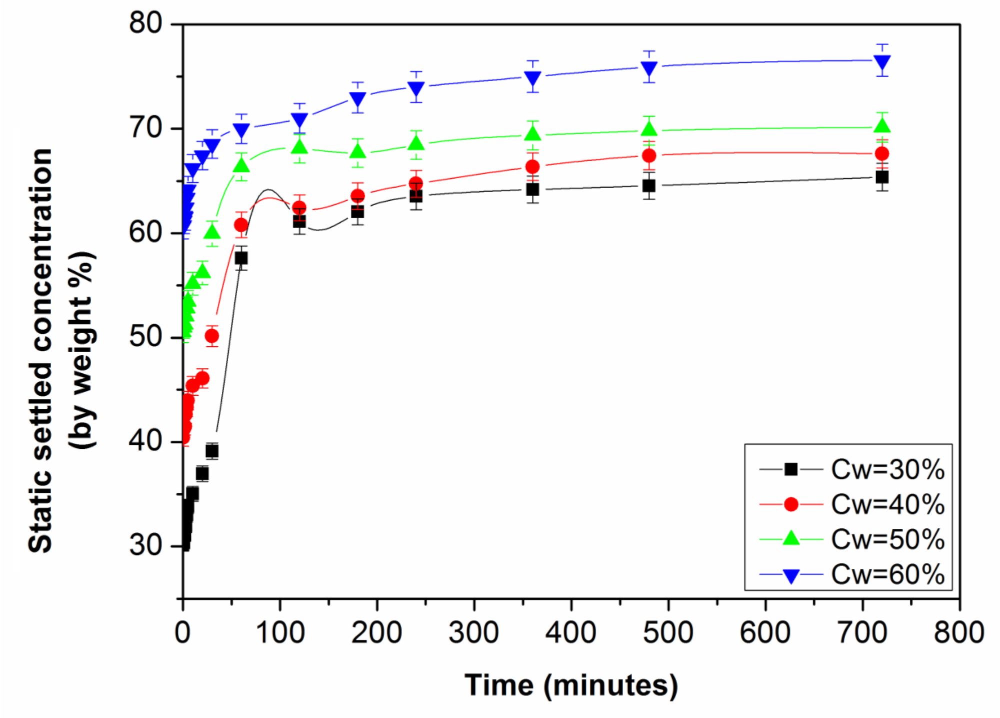

Figure 3.12: Effect of solid concentration on static settled concentration for coal-water slurry

In the present work, the gravitational settling method is adopted to determine the maximum settled concentration of coal and coal-ash slurries at a higher solid concentration range of 30-60% (by weight). Experiments are performed on a graduated 500 ml glass cylinder. The slurry of different solid concentrations is prepared and uniform mixing of solid particles is done by using stirrer. Afterward, the slurry glass cylinder is left undisturbed and slurry is allowed to settle down. The reading from the glass cylinder interface is taken after specific time intervals until no further settling occurs. All the experiments are repeated three times to ensure the repeatability and reproducibility.

Extensive experiments are carried out for fine particulate coal water slurry having particle size range <53 μm. Figure 3.12 illustrates the variation of static settled concentration with time for coal-water slurry at different solid concentrations. The maximum settled concentration for coal-water slurry is observed as 65.37, 67.61, 70.13 and 76.55% for solid concentration of 30, 40, 50 and 60% respectively. It is noticed that settling of fine coal particles is almost negligible after 240 minutes. A similar type of experiments of settling characteristics is performed for fly and bottom ash slurry for a solid concentration range of 30-60% (by weight). The variation in static settled concentration with the time period of fly ash water slurry is shown in Figure 3.13. It is noticed that maximum static settled concentration for fly ash slurry is 59.67, 62.88, 65.21 and 73.92% for a solid concentration of 30, 40, 50 and 60% respectively.

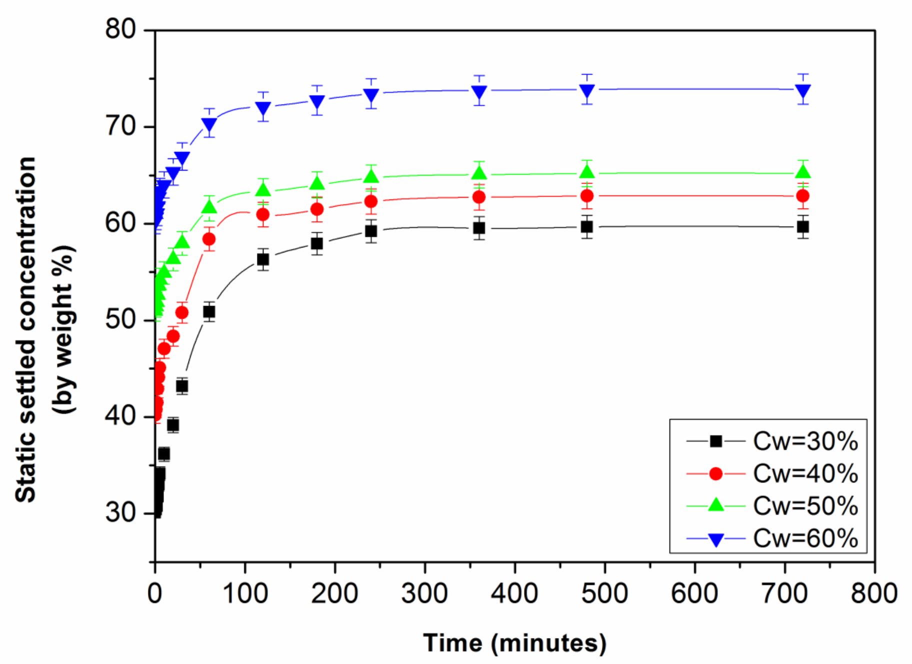

Figure 3.13 Effect of solid concentration on static settled concentration for fly ash slurry

Also for bottom ash water slurry, the maximum static settled concentration is observed as 53.79, 56.45, 58.67, and 68.58% for solid concentration of 30, 40, 50 and 60% respectively, as shown in Figure 3.14. It is observed that settling for fly and bottom ash sample is ceased after 200 minutes.

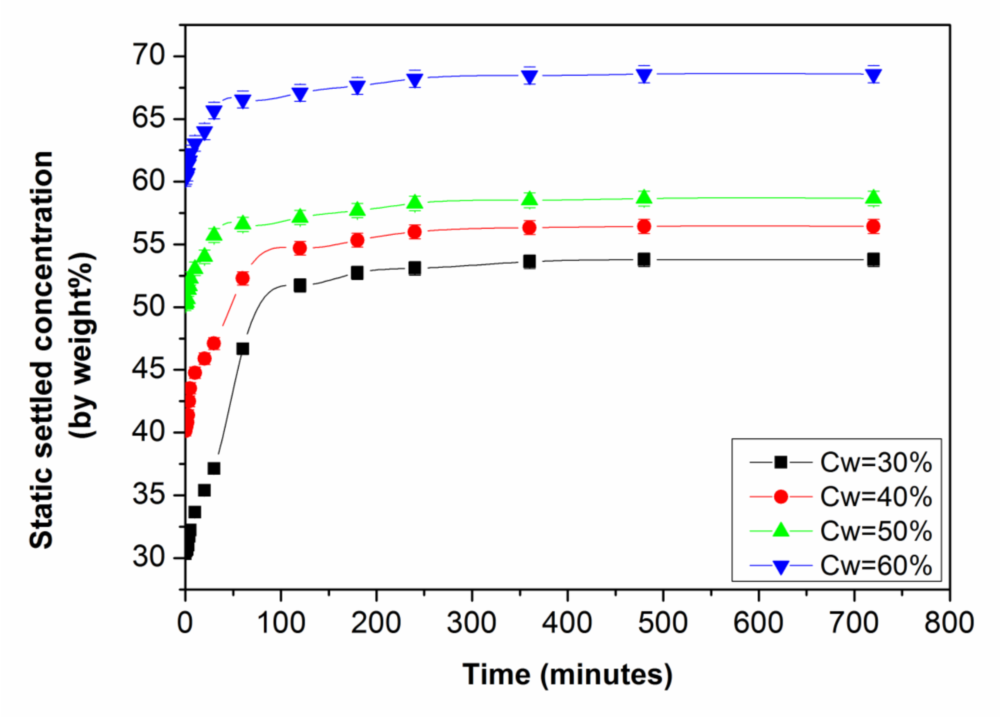

Figure 3.14: Effect of solid concentration on static settled concentration for bottom ash slurry

3.4 REMARKS

The following remarks are pointed out from this chapter:

- The coal particles are non-spherical and have irregular shapes. The fly ash particles have a smooth surface, regularity in shape, and spherical appearance. The bottom ash particles have rough surface morphology, irregularity in shape and porous.
- The rough surface of coal particles is due to the presence of carbonaceous materials and impure particles of carbon known as soot.
- The small fine hollow spherical ash particles are known as cenospheres. The presence of these cenospheres in fly ash helps to develop light weight concrete having good sound absorbance tendency. The bottom ash particles are dark grey in color this shows the presence of unburnt carbon.

- The specific gravity of coal, fly and bottom ash sample is determined as 1.46±2%, 2.27±0.5% and 2.09±1.6%.
- The maximum settled concentration for coal, fly ash and bottom slurry is observed as in range 65.37-76.55%, 59.67-73.92%, and 53.79-68.58% for a solid concentration range of 30-60% respectively.
- The *pH* of coal-water slurry varies in the range of 6.38-5.93 as solid concentration is increased from 30-60% (by weight). The pH value for fly and bottom ash suspension lies in the range of 7.62-7.42 and 7.68-7.45 respectively for the solid concentration range of 30-60%.

CHAPTER 4

RHEOLOGY OF COAL AND COAL-ASH SLURRIES

Chapter 4

RHEOLOGY OF COAL AND COAL-ASH SLURRIES

In this chapter, the rheological behavior of different slurries is investigated with and without additives. *Rheology* is the branch of fluid dynamics that deals with the study of fluid behaviour under the action of shear stress. It is the general science of fluid deformation under the action of shear force. The fluid deformation depends upon various properties like elasticity, viscosity, shear rate, intermolecular forces, drag forces, etc. The property of the material to regain its original shape after deformation under the action of an external force is called elasticity. The measure of ability of fluid to resist flow is known as viscosity. The fluid reacts to the external applied force by exhibiting viscous or elastic characteristics or more generally combinations of both mechanism. This reaction to external force is known as viscoelasticity.

The different types of rheometer are used to experimentally investigate the rheological characteristics of flowing matter such as liquid, melts, emulsions, composites and slurries. The fluids are broadly classified to two categories depending upon flow behaviour i.e. Newtonian fluid and non-Newtonian fluids. The flow characteristics of two-phase slurry in the pipeline are the function of flow behaviour of slurry suspension. The presence of different particle size ranges in slurry suspension results in a complex phenomenon. The rheological characteristics are also affected by the physical and chemical properties of solid and carrier fluid. The rheological behaviour of two-phase slurry suspension depends upon the solid concentration, solid particle size/shape, volume fraction etc. In thermal power stations, coal and coal-ash are generally conveyed through pipelines in the form of slurry. The transportation of slurry at a higher solid concentration not only economic but also decreases the negative impact of leaching in ash ponds. The increase in solid concentration results in an appreciable increase in slurry viscosity and the flow behaviour of slurry suspension is also changed. In the present study, the rheological behaviour of aqueous coal and coal-ash slurries is investigated at higher solid concentrations. The extensive experimentation is also carried out to investigate the effect of additives on the rheological behaviour and viscosity of slurry at high solid concentrations. The experimental details, range of parameters and apparatus used in the study are discussed in the following sections.

4.1 SPECIFICATIONS OF RHEOMETER

The rheological behaviour of the coal and coal-ash suspensions at different solid concentrations is investigated with the help of rheometer. The rheometer helps to plot the deformation in the fluid under the action of shear rate. Different types of rheometer are available to study the various parameter of fluid such as viscosity, shear stress, deformation rate, elasticity etc. In the present study, the Rhelolab Q-C model of rheometer manufactured by Anton Paar Ltd. Germany is used to study the flow behaviour of coal and coal-ash slurries. Figure 4.1 shows the photographic view of rheometer used during experimentation. The rheometer works on the Searle principle. The rheometer is equipped with electronically operated highly dynamic synchronous motor drive. The motor shaft is connected to the torque sensor, which measures the angular position of the shaft. The specification of the rheometer is tabulated in Table 4.1. An assembly of the torsion bar is suspended in the air to provide a hypothetical frictionless bearing. During experimentation, as the slurry offers resistance to rotation and tries to twist the torsion bar. The resultant twist is measured with angular rotation and hence the torque is obtained. The product of torque and angular velocity with the form factors C_1 and C_2 are obtained to calculate shear stress and shear rate.

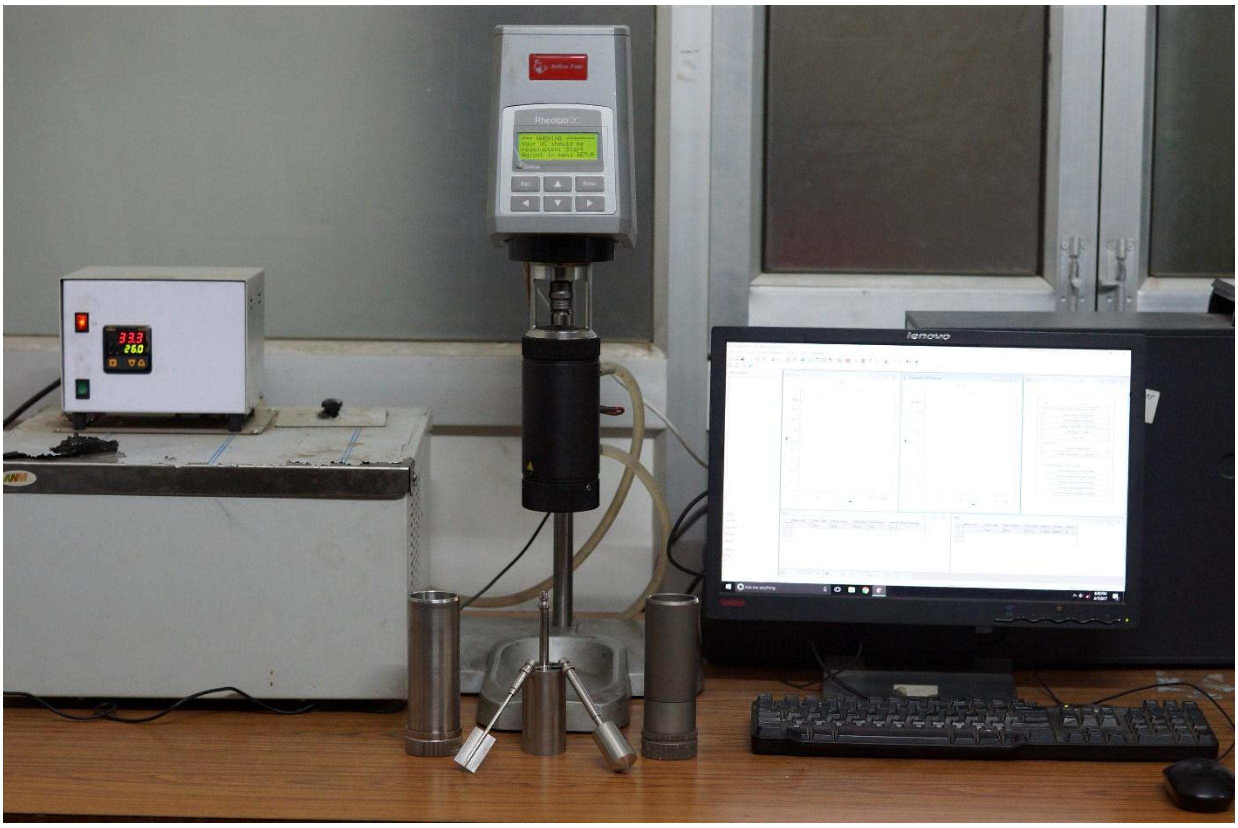

Figure 4.1: Photographic view of Rhelolab Q-C rheometer

Table 4.1: Specification of Rhelolab Q-C rheometer

S.no.	List of components	Range/Type
1	Viscosity	0.1-109 MPa.s
2	Angular speed	0.01-1200 m/min
3	Shear stress	0.5-3×107 MPa.s
4	Shear rate	0.01-4000 sec^{-1}
5	Torque	0.25-45 MN.m
6	Temperature	-20 to180˚ C
7	Motor	Synchronous motor

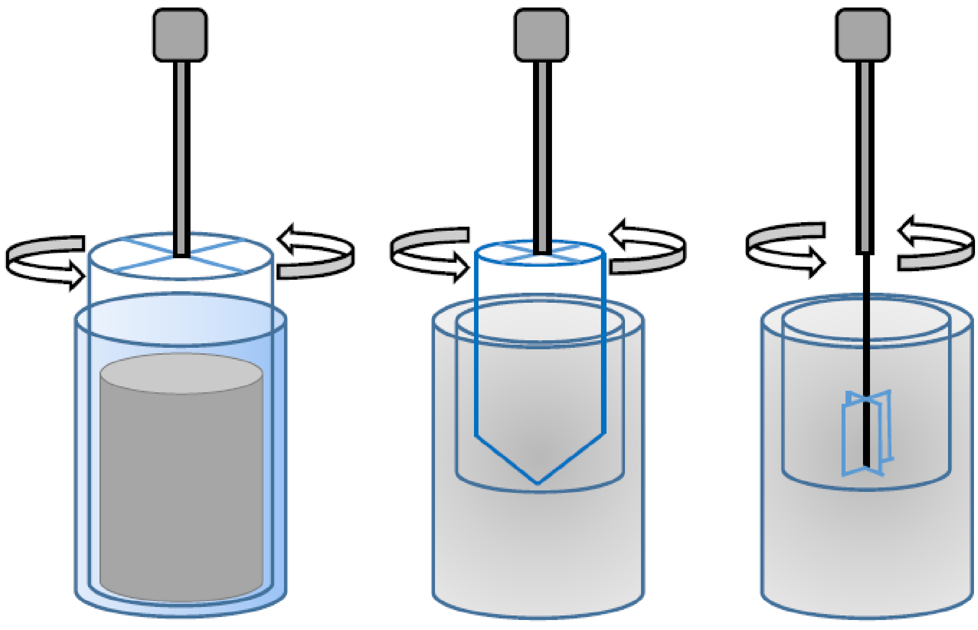

Figure 4.2: Various types of rheometer arrangements

$$Shear\ stress\ (\tau) = C_1 \times T \tag{4.1}$$

$$Shear\ rate\ (\gamma) = C_2 \times \omega \tag{4.2}$$

$$Viscosity\ (\mu) = \tau \times \gamma \tag{4.3}$$

Where T is torque and ω represents is angular velocity. The gap in the measuring system is also adjusted by the user in some type of arrangements in the rheometer like in parallel plate rheometer. The following expression is used to adjust the gap (L).

$$\gamma = \frac{C_2 \times \omega}{L} \tag{4.4}$$

The Rhelolab Q-C rheometer is equipped with three different arrangements for experimental studies of different type of slurries. Figure 4.2 illustrates the schematic diagrams of different arrangements namely co-axial cylinders, cone-plate and plate type rheometer. The form factors of all the three arrangements are listed in Table 4.2.

Table 4.2: Form factors for different rheometer arrangements (Anton Par Manual, 2012)

Types of arrangement	Form factors	
	C_1	C_2
Co-axial cylinders	$1/2\pi r^2 H$	$2r_1^2 r_0^2 / r_a^2(r_0^2 - r_i^2)$
Where r_i represents inner radius; r_o is outer radius; H is height of cylinder; $r_a = r_1 + r_0 / 2$		
Cone-plate	$1 / \frac{2}{3}\pi r^3$	$1/\theta$
Where r represents radius of cone; θ is cone angle in radians		
Plate	$1 / \frac{2}{3}\pi r^3$	$3r/4$

Figure 4.3: Uniform mixing of coal sample with stirrer

4.2 SAMPLE PREPARATION AND PROCEDURE

The rheological experiments are performed to investigate the flow behaviour and variation in viscosity of coal and coal-ash slurries at different solid concentrations. The rheological experiments are conducted for fine particulate coal-water slurry having particle size range < 53 μm. The coal falls under the category of soft solids. Being a soft solid, the viscosity of coal-water slurry increases as the particle size becomes finer. In the present study, the flow behaviour of highly viscous coal-water slurry (particle size range < 53 μm) is studied whereas, the random samples of fly and bottom ash are taken for rheological experiments. Generally, the coal-ash samples are disposed-off or utilized as obtained from ESP and bottom ash hopper. There is no prior processing of coal-ash is done before disposal like coal is pulverized before combustion in the furnace. The precise electronic type pan balance scale having the least count of ±0.001 mg is used to measure the weight of solids. The 100 ml slurry is prepared gently by mixing the measured weight of solid in water. The slurry is stirred in the 500 ml beaker with a small electronic stirrer (shown in Figure 4.3) to ensure the proper homogeneity of slurry for 15 minutes. Afterward, the slurry is poured up to the fix mark in the cylindrical bob and cup assembly. Meanwhile, the moving cylinder is mounted on the rheometer and bob-cup assembly is also coupled to the rotating spindle. As the spindle start rotating the slurry is subjected to shearing action. The rheometer is connected to the computer with LAN cable. The variation on shear stress with shear rate is displayed on the screen. Each set of experimentation is performed three times to minimize error and to ensure the repeatability-reproducibility of equipment. Furthermore, the experimentation is also conducted to study the effect of additives on flow behaviour and apparent viscosity of slurry suspension at higher concentrations.

4.3 RHEOLOGICAL BEHAVIOUR OF COAL-WATER SLURRY

The rheological behaviour of a slurry suspension plays a significant role in transportation through pipelines. Rheological characteristics of < 53 μm sized coal-water slurry are investigated for a solid concentration range of 30-60% (by weight). The apparent viscosity and shear stress of the slurry is measured up to a shear rate of 600 s^{-1}. The temperature during experimentation is kept constant at 25˚C. The temperature of rheometer is controlled with the help of temperature controlled water bath unit. Water is circulated with the help of a pump around the bob-cup assembly in which slurry is poured during viscosity measurement. The effect of an additive at solid concentration of 60% on rheological characteristics of coal-water slurry is also studied. Sulphonic acid is used as an additive in present work.

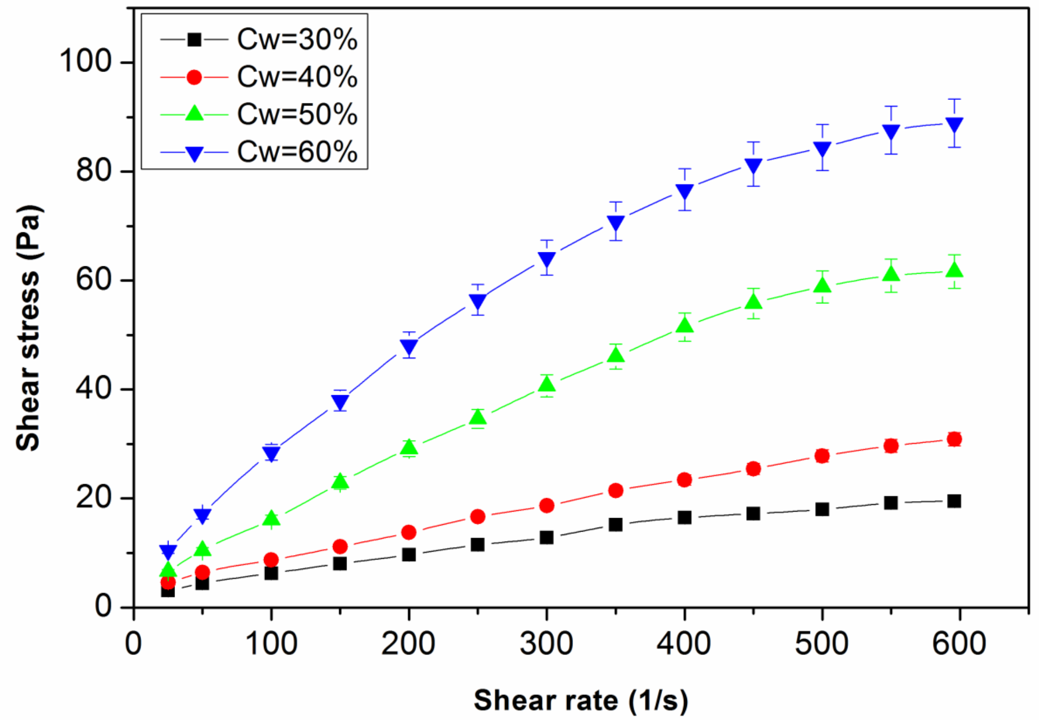

Figure 4.4: Rheogram of < 53µm fine coal-water slurry

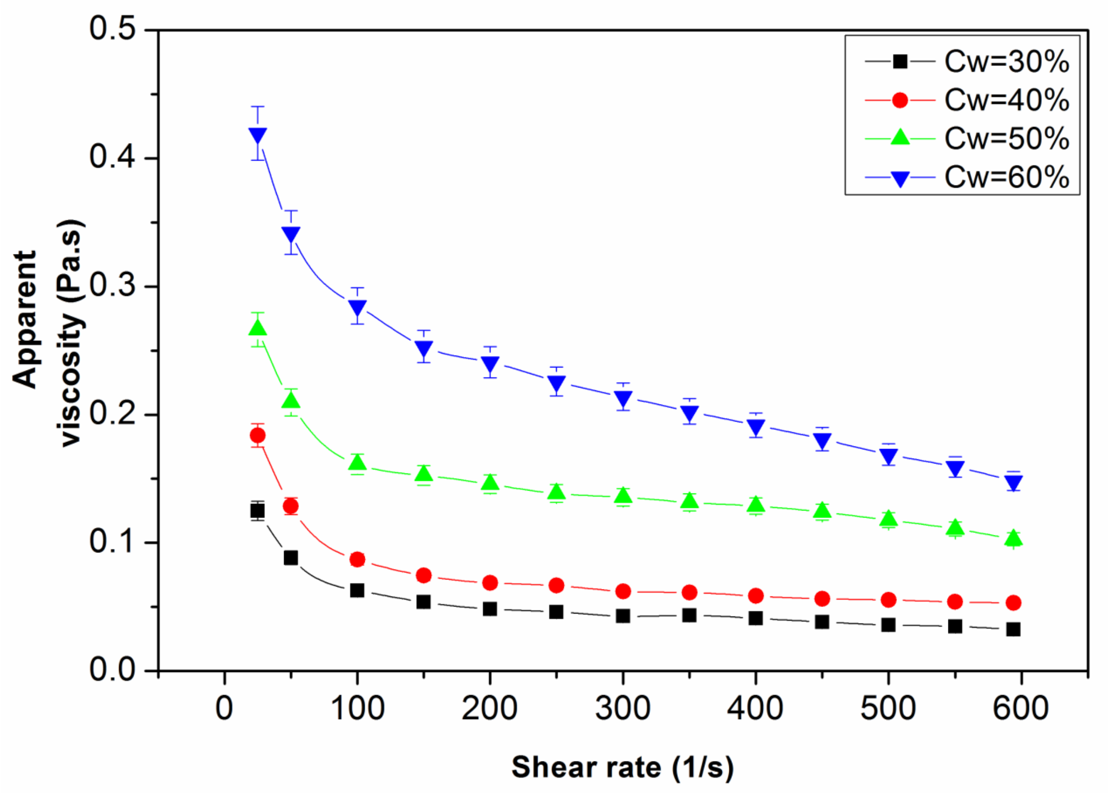

Figure 4.5: Variation in apparent viscosity with shear rate of coal-water slurry

4.4.1 Rheological characteristics of fine particulate (< 53μm) coal-water slurry

The rheological experiments are carried out for fine particulate coal-water slurry suspension having a particle size range of < 53μm for a solid concentration range of 30-60% (by weight). The rheogram of coal-water slurry at different solid concentrations is shown in Figure 4.4. From the results, it is observed that coal-water slurry exhibits Newtonian behaviour at a solid concentration of 30% (by weight). In other words, shear stress is directly proportional to shear rate at 30% solid concentration. However, at higher solid concentrations i.e. above 30% the flow behaviour shifted to pseudo-plastic flow. The apparent viscosity of the coal-water slurry is enormously affected by solid concentration. The variation in apparent viscosity with the shear rate at solid concentration range of 30-60% is shown in Figure 4.5.

The apparent viscosity of slurry increases with an increase in solid concentration. This increase in apparent viscosity is observed due to an increase in particle-to-particle interactions which further increases resistance to flow. The shear forces between particles become significant as concentration increases; hence, an increase in apparent viscosity has been noticed (Chen *et al.* 2011; Zhu *et al.* 2014). The apparent viscosity is found to be independent of shear rate at 30% solid concentration (by weight). However, coal-water slurry exhibits shear thinning behaviour at higher solid concentrations (i.e. above 30%). From the results, it is also observed that apparent viscosity decreased gradually up to the shear rate of 190 s^{-1} whereas a marginal decrease is noticed for the shear rate of 300 s^{-1} within the solid concentration range of 30-50% (by weight). A rapid decrease in apparent viscosity is noticed up to a shear rate of 370 s^{-1} at a solid concentration of 60% (by weight). Similar phenomena for coal-water slurry have been reported by various researchers (Lorenzi and Bevilacqua 2002; Yuchi *et al.* 2005).

4.4.2 Effect of an additive on the rheological behaviour of coal-water suspension

Viscosity plays a vital role in the transportation of slurry suspensions in a pipeline. Higher slurry viscosity results in very high pumping costs, so the use of additives during slurry transportation not only decreases slurry viscosity but also minimizes pumping cost.

The rheological characteristics of < 53 μm sized coal-water slurry suspension are also studied after the addition of sulfonic acid. Coal-water slurry having a solid concentration of 60% is prepared with the addition of sulfonic acid. The variation of apparent viscosity with shear rate is plotted in Figure 4.6.

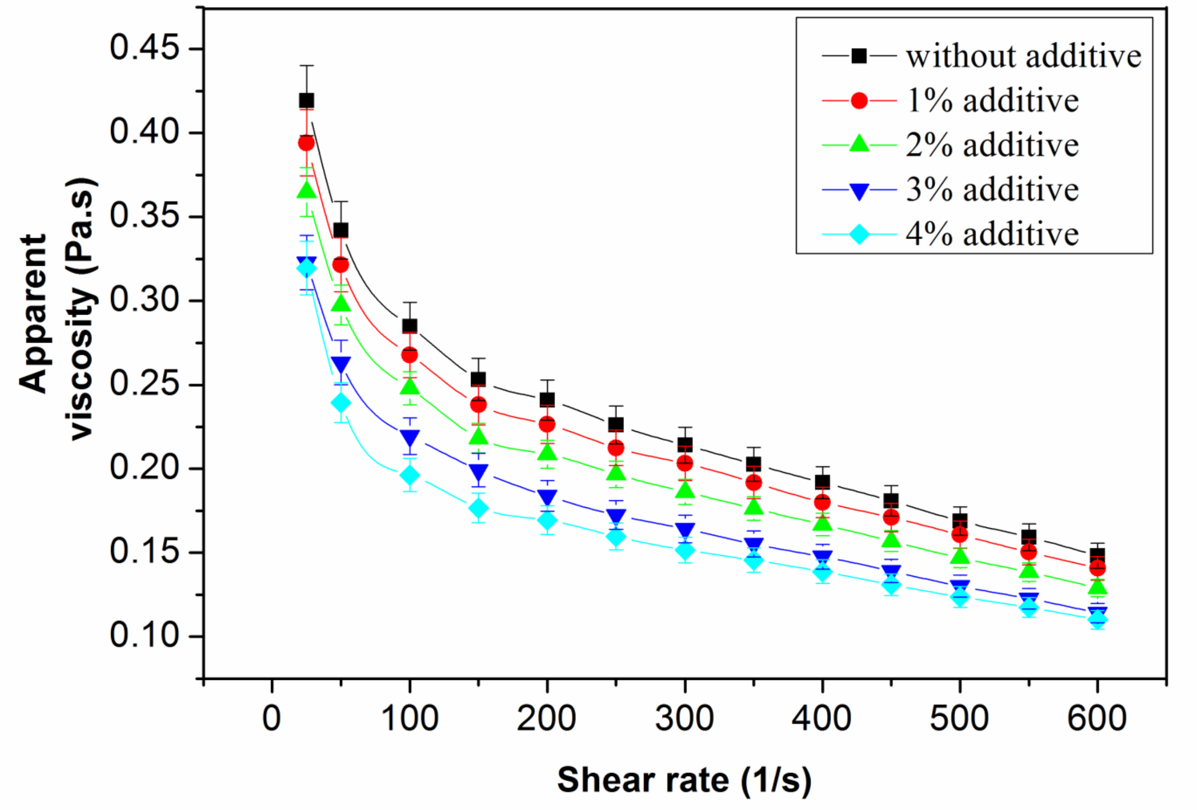

Figure 4.6: Effect of additive on the apparent viscosity of fine coal-water slurry

From the results, it is observed that the addition of a small amount of additive resulted in an improvement in the rheological properties of the coal-water slurry suspension. A drastic decrease in apparent viscosity is noticed as the amount of sulfonic acid increased from 1 to 4% (by weight). The apparent viscosity of the coal-water slurry suspension is reduced by 6.34, 13.21, 23.06 and 23.80% with 1, 2, 3 and 4% (by weight) addition of sulfonic acid, respectively at a shear rate of 25 s^{-1}. The apparent viscosity also decreased with an increase in shear rate. At a higher shear rate of 500 s^{-1}, the apparent viscosity of the slurry decreased by 4.85, 13.12, 23.18 and 26.78% with 1, 2, 3 and 4% (by weight) addition of sulfonic acid, respectively. Using the slope linear regression approach (Shah *et al.* 2018) through data points, the rate of decrease in apparent viscosity with shear rate is observed as -0.00035, -0.00032, -0.00029 and -0.00028 with the addition of 1, 2, 3, and 4% sulphonic acid respectively. As the addition of additive is increased from 0-1, 1-2, 2-3 and 3-4% the apparent viscosity is decreased by 4.85, 8.56, 11.49 and 4.92% respectively at a shear rate of 500 s^{-1}. The maximum decrease in apparent viscosity is observed with a 3% addition of sulfonic acid.

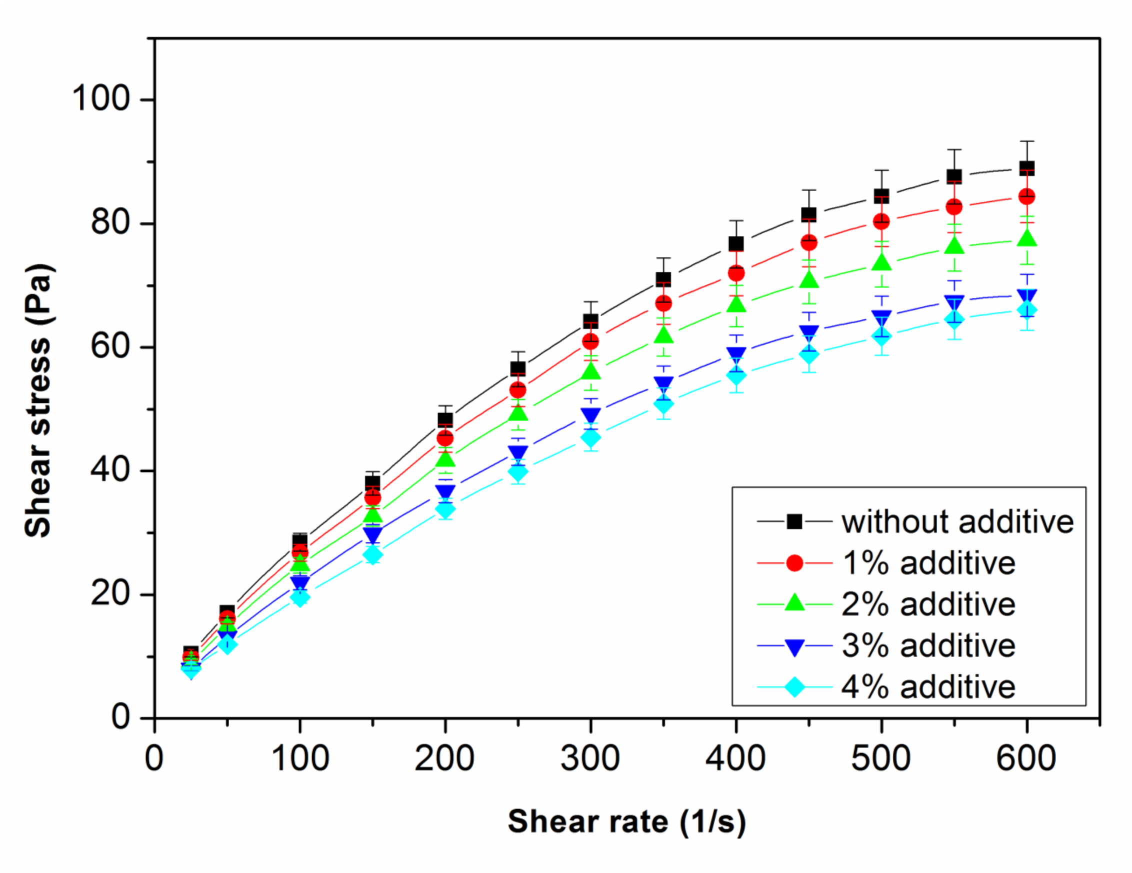

Figure 4.7: Variation shear stress-shear rate behaviour of coal-water slurry after addition of additive

It is also observed that with the addition of the additive, the flow behaviour of coal-water slurry remained unchanged at a 60% solid concentration (i.e. it exhibits pseudo-plastic behaviour as shown in Figure 4.7). Sulfonic acid is a strong acid which has the properties of detergent; due to its acidic nature, it is also hydrophilic in nature (Kosswig, 2000). Sulfonic acid helps to improve the surface properties and intermolecular interactions between solid particles of slurry suspension. The rheological characteristics of slurry suspension are affected by intermolecular forces of solid particles. These intermolecular forces arise at the solid-liquid interface and dominate the interaction among neighboring particles. The inter-particle forces contribute to the rheological characteristics of coal-water slurry suspension (Naik *et al.* 2009; Senapati *et al.* 2013; Sah, 2014; Noble *et al.* 2016). The aggregation of solid particles occurs in slurry suspension due to weak electrostatic repulsive forces. The aggregation of coal particles inside slurry results in higher slurry viscosity. The addition of sulphonic acid results in improvement of surface properties of solid particles. The addition of additive leads to an increase in the electrostatic repulsive forces by decreasing Vander-wall attraction forces and results in a fully dispersed slurry (Slaczka and Piszczynski, 2008). Hence, the rheological characteristics of coal-water slurry suspension are improved.

4.4 RHEOLOGY OF COAL-ASH SLURRY

The rheological experimentation is also conducted to investigate the flow behaviour of aqueous fly and bottom ash slurries at high solid concentrations. In the present scenario, the solid waste left after combustion of coal in thermal power plants in the form of fly and bottom ash is disposed to dyke area through pipelines at a very low solid concentration of 10-15% (by weight). This results in the consumption of large quantity of water and pumping power. Also, the leaching of heavy metals led to a negative impact on the environment. The present study is focused on transporting coal-ash slurries at high solid concentrations. The rheological behaviour of both fly and bottom ash is studied on a solid concentration range of 30-60% (by weight). Furthermore, the effect of additive on rheological characteristics is also examined, to reduce viscosity and pumping cost at high solid concentrated slurries. The experiments are conducted at a temperature of 25˚C for shear rate range of 0-600 s^{-1}.

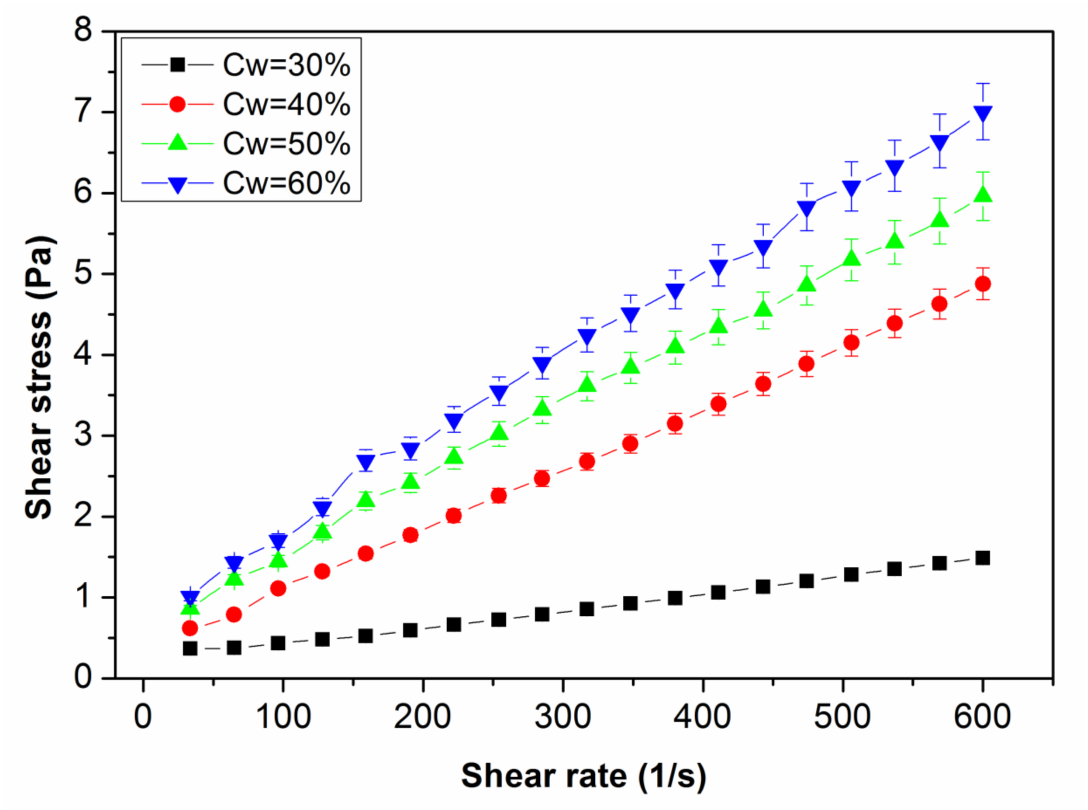

Figure 4.8: Shear stress versus shear rate plot of fly ash slurry at different solid concentrations

4.5.1 Rheological characteristics of fly ash slurry

The rheological experiments are carried out on the fly ash sample collected from ESP hopper of Deen Bandhu Chhotu Ram Thermal Power Plant, Yamunanagar, Haryana, India. The slurry of fly ash and water was prepared for a solid concentration of 30, 40, 50 and 60%. The variation in shear stress with the shear rate at different solid concentration is shown in Figure 4.8. From the results, it was seen that with the increase in shear rate, shear stress increases linearly for all concentrations of aqueous fly ash slurry. It was also observed that at higher solid concentration, the deformation of slurry starts after some yielding stress after that liner variation was noticed. This means that fly ash-water slurry shows Bingham plastic behaviour for a solid concentration range of 40-60% (by weight). The initial yielding was observed due to the formation of a continuous network by solid particles in slurry. Hence, there is a need for minimum small force to break the network that results in yielding (Navickis, 1989; Coussot and Piau, 1994). The initial yielding stress for 30% solid concentration slurry is zero. Therefore, slurry exhibits Newtonian behaviour for a solid concentration of 30%.

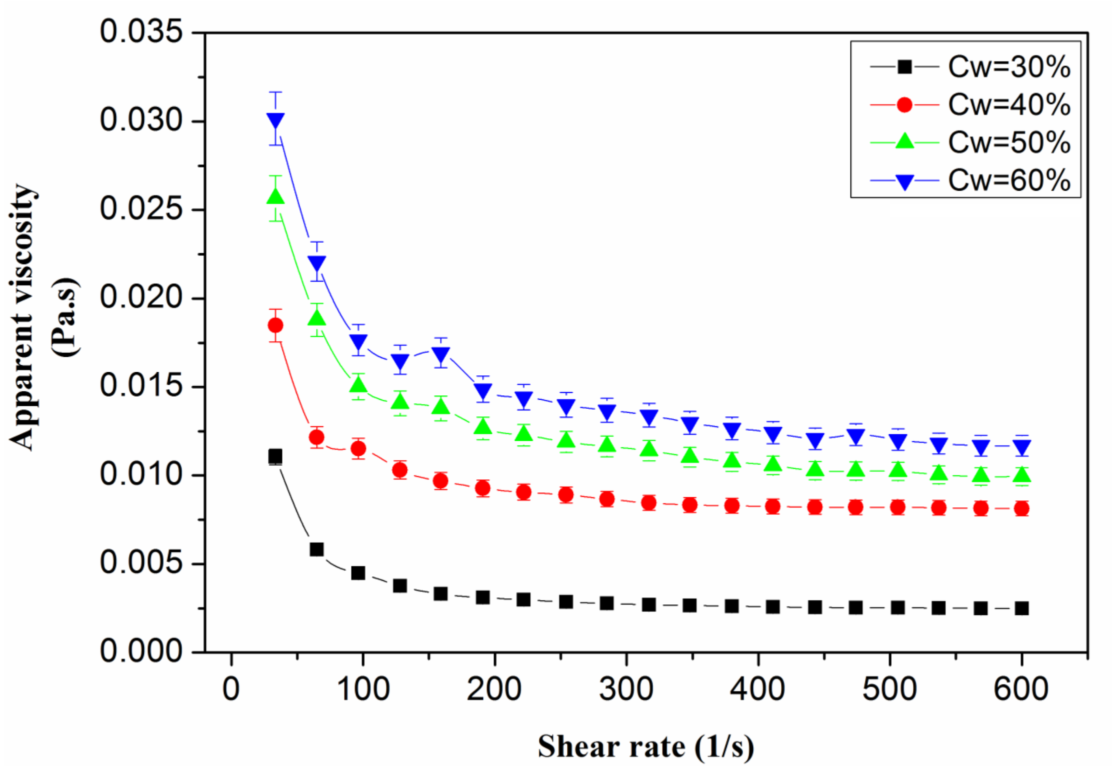

Figure 4.9: Variation in apparent viscosity with shear rate of fly ash slurry

The increase in solid concentration results in a change in flow behaviour of fly ash slurry from Newtonian to Bingham plastic. The apparent viscosity is increased by 53.45, 36.45 and

17.54% at a shear rate of 128 s^{-1} for a solid concentration of 30-40, 40-50 and 50-60% respectively. However, at a shear rate of 317 s^{-1} the apparent viscosity is increased by 58.34, 42.13 and 27.32% as the solid concentration is increased from 30-40, 40-50 and 50-60% respectively.

Figure 4.9 represents the variation in apparent viscosity with a shear rate for a solid concentration range of 30-60%. From the result data, it is observed that an increase in solid concentration results in an enormous increase in apparent viscosity. A steep hike in apparent viscosity is noticed as the solid concentration is increased from 40-60%. The increase in apparent viscosity with solid concentration is observed due to an increase in solid particles per unit volume of slurry. The increase in solid particles results in increase in particle-particle interaction. The fly ash particles are smooth-circular in shape this results into the formation of agglomeration/clusters of solid particles in the slurry. Hence, the viscosity of slurry increases which results in an increase the resistance to flow. However, the appreciable decrease in viscosity is noticed as the shear rate increased form 0-600 s^{-1}. This decrease in apparent viscosity with shear rate is observed due to rheofluidization. Figure 4.10 illustrates the mechanism of rheofluidization in solid-liquid slurries. Initially, the mixing of solid particles in fluid results in the formation of a percolating network. As the shear rate of slurry is increased, this network breakdown to cluster and at higher shear rates, uniform suspension of solid particle occurs.

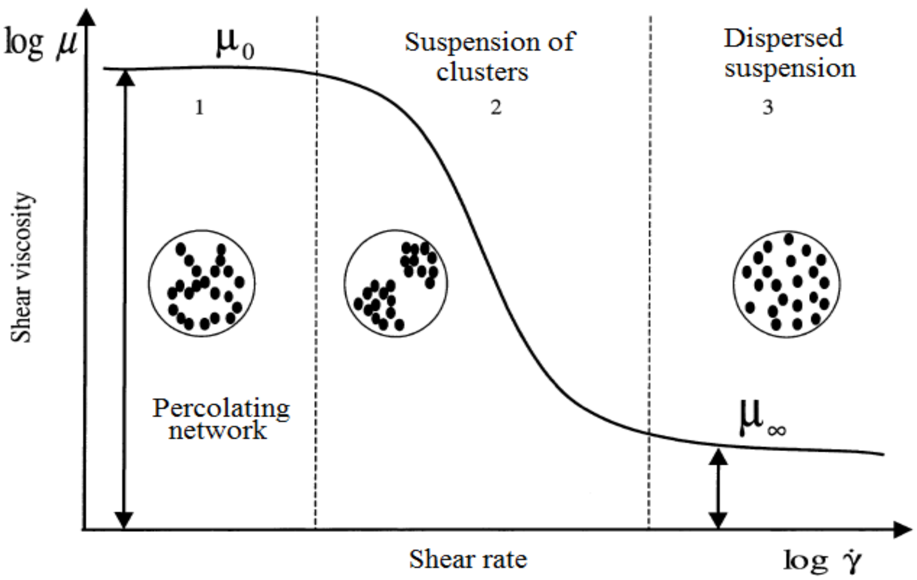

Figure 4.10: Variation of viscosity with shear rate (Perez *et al.* 2000)

4.5.2 Effect of an additive on the rheological behaviour of fly ash suspension

The fly ash is being utilized in cement industries, presence of cenospheres in fly ash helps to made light weight concrete which provides the pozzolanic nature i.e. cementing properties. However, rate of generation of fly ash is very much high as compared to the rate of utilization. Therefore, the dry fly ash left after utilization is disposed of to ash ponds. In the present study, an attempt has been made to decrease the viscosity of fly ash slurry to increase the efficiency and reduce pumping cost. Sodium triphosphate is used as an additive in fly ash slurry for a solid concentration of 60% (by weight). Figure 4.11 represents the variation in apparent viscosity with the addition of sodium triphosphate.

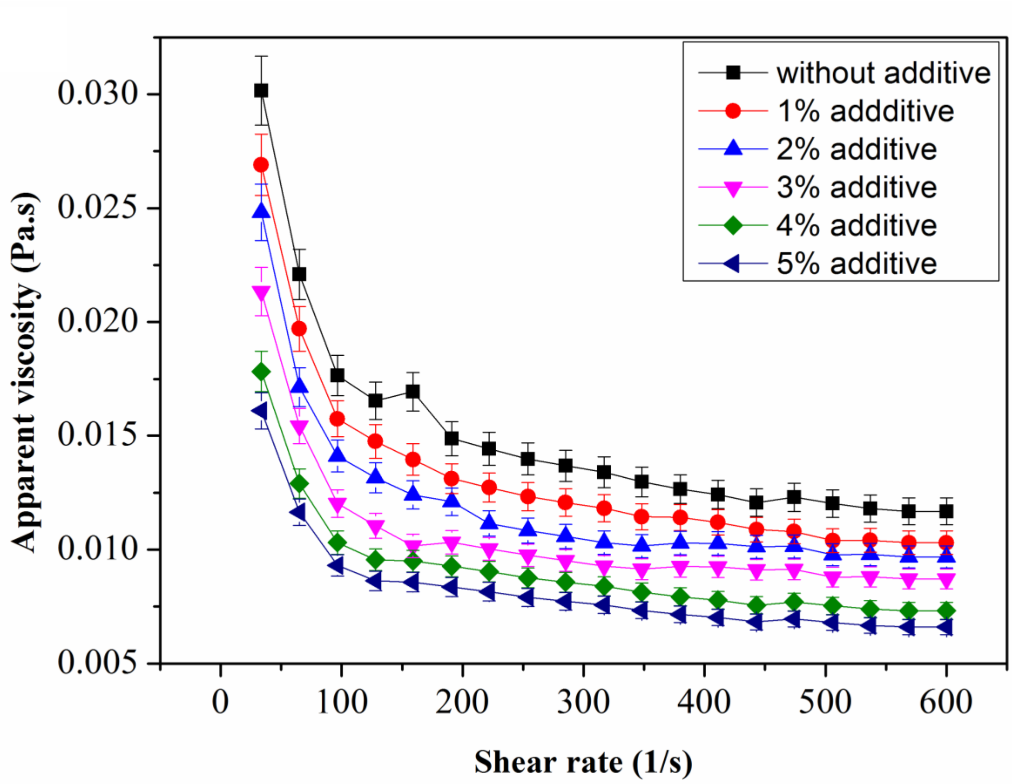

Figure 4.11: Effect of additive on the apparent viscosity of fly ash-water slurry

From the results, it is seen that the addition of additive results in an appreciable decrease in slurry viscosity. It is observed that the maximum percentage decrease in apparent viscosity is observed with 4% addition of sodium triphosphate. Furthermore, the addition of additive i.e. 5% leads to a decrease in slurry viscosity, but the percentage decrease is very less. The addition of additive helps to decrease the drag forces during transportation (Calvo *et al.* 1997). Also, the surface tension in the slurry is reduced that helps to increase the wetting and spreading of solid particles. The addition of additive also reduces the forces of attraction by forming a layer around solid particles. The sodium triphosphate acts as a strong emulsifying agent for fly ash particles. It helps the fly ash particles to remain suspended in the slurry (Schrodter *et al.* 2008). Also, the agglomeration of fly ash particles is decreased. Hence, the viscosity of fly ash slurry is reduced. The apparent viscosity is reduced by 2.55, 16.40, 29.14, 34.67, and 38.03% with addition of 1, 2, 3, 4 and 5% respectively dosage of the additive at a shear rate of 128 s^{-1}. Similarly, a gradual decrease in apparent viscosity of fly ash slurry is also noticed by 3.63, 19.16, 26.54, 29.17 and 32.81% with the addition 1, 2, 3, 4, and 5% sodium triphosphate respectively at shear rate of 317 s^{-1}. As the addition of additive is increased from 0-1, 1-2, 2-3, 3-4 and 4-5% the apparent viscosity is decreased by 5.49, 9.61, 11.25, 16.41and 5.14% respectively at a shear rate of 500 s^{-1}. The maximum decrease in apparent viscosity is observed with 4% addition of sulfonic acid.

4.5.3 Rheological characteristics of bottom ash-water slurry

The bottom ash is the inorganic and non-combustible matter present in the coal. The utilization of bottom ash in India is still very low. Mainly the bottom ash is used for landfilling purposes. In the present study, the rheological characteristics of bottom ash slurry are studied for the solid concentration range of 30-60% (by weight).

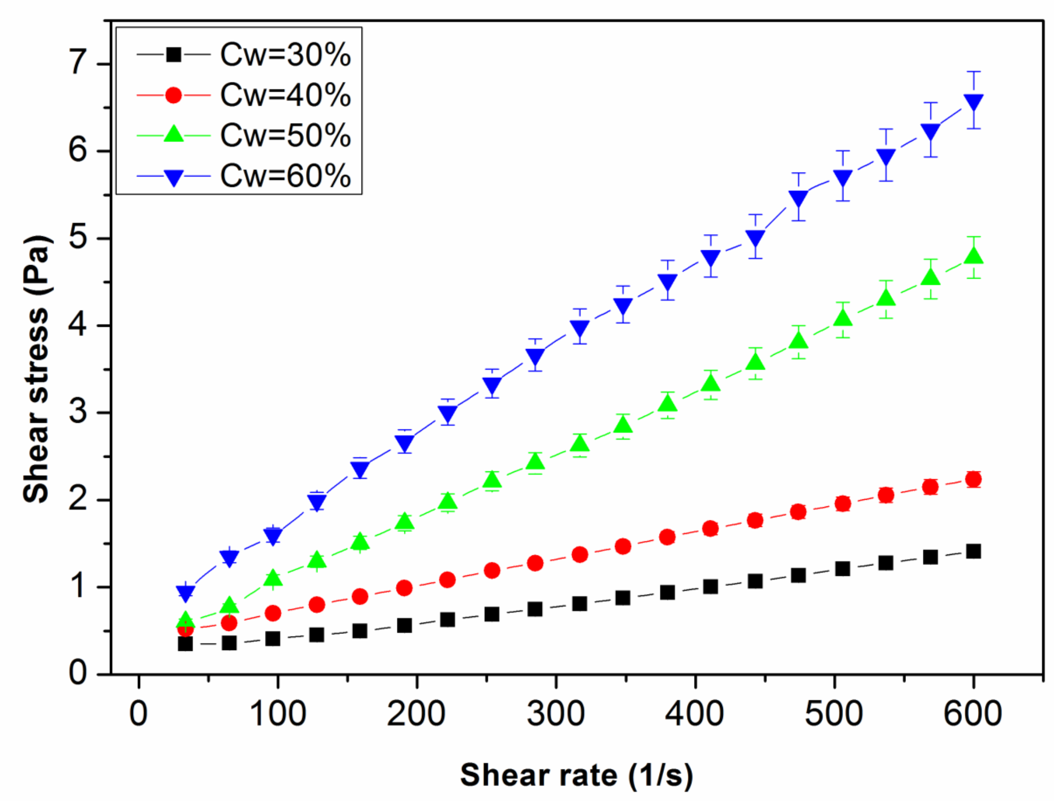

Figure 4.12: Rheogram of bottom ash slurry at different solid concentrations

Figure 4.12 shows the variation of shear stress with the shear rate at different solid concentrations. From the results, it is seen that the shear rate shows a linear variation with shear stress. The slurry exhibits Newtonian behaviour for solid suspension up to solid concentration of 30%. At the 40% concentration, the slurry shows Non-Newtonian behaviour. At a solid concentration above 40%, slurry shows Bingham flow behaviour. The yield stress for Bingham flow increases with solid concentration. The formation of clusters or gelification occurs during slurry preparation. As the bottom ash particles are porous and coarser in nature, the slurry behaves like a colloidal solution. In colloidal solution, the different type of electrochemical attraction-forces results in the creation of large bunches of solid particles. Thus during the initial deformation of slurry, a force is required to break these bunches. This restriction force is measured as yielding stress in slurry (Kumar *et al.* 2017d; Kumar *et al.* 2018b).

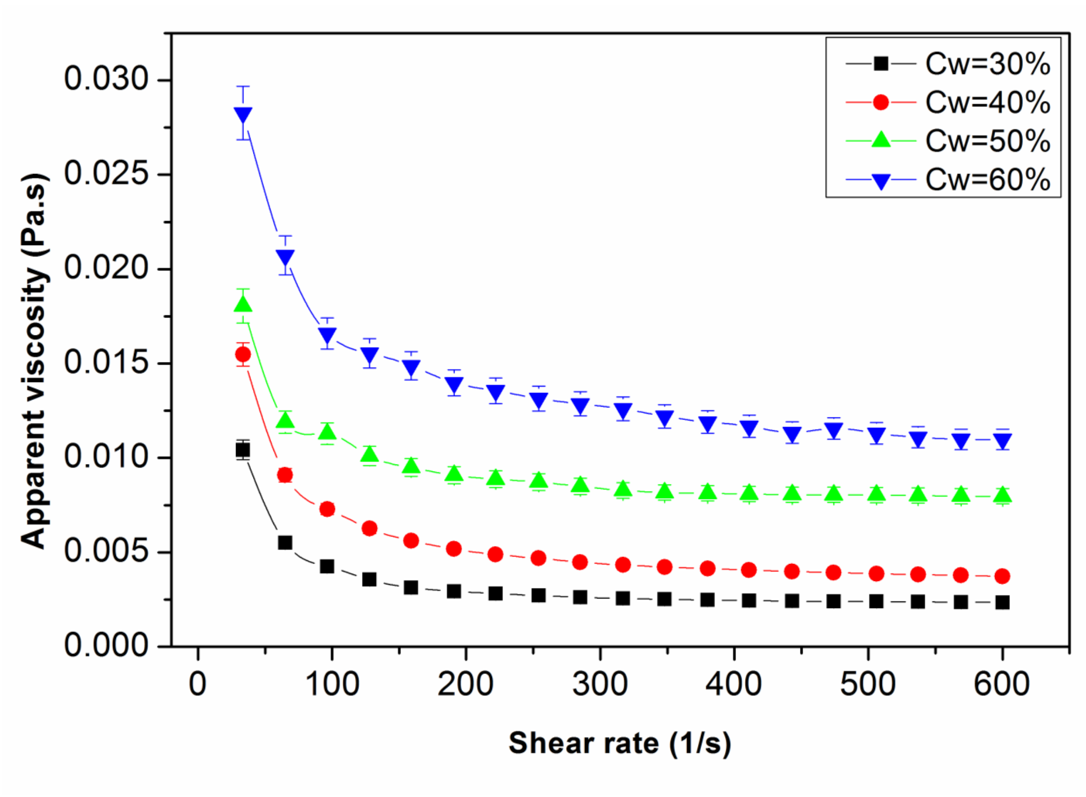

Figure 4.13: Variation in apparent viscosity with shear rate for bottom ash slurry

Figure 4.13 represents the variation in apparent viscosity with the shear rate at different solid concentrations. The viscosity slurry suspension increases with solid concentration. This increase in the slurry viscosity is observed due to an increase in the number of solid particles per unit volume of the slurry. As the number of bottom ash particles in the slurry suspension increases, the slurry becomes thicker, which leads to more resistance in the flow of slurry suspension. Therefore, more shear strain rate is required to start shearing process. Due to this reason, the high yield stress is observed at the higher solid concentration for Bingham flow characteristics. The percentage increase in slurry viscosity with solid concentration is lesser in case of bottom ash as compared to fly ash. This is observed due to the fact that fly ash particles are finer, whereas bottom ash is coarser in nature. Also, the density of fly ash is more than the bottom ash. The apparent viscosity is increased by 73.03, 81.58 and 52.82% as the solid concentration was increased from 30-40, 40-50 and 50-60% respectively at shear rate of 222 s^{-1}. However, a similar trend is noticed at higher shear rate of 411 s^{-1}, the apparent viscosity is increased from 66.40-44.45% for a solid concentration range of 30-60%.

4.5.4 Effect of an additive on the rheological behaviour of bottom ash suspension

The extensive experimentation is carried out to study the flow behaviour of bottom ash water slurry by using an additive. The effect of additive is studied at higher solid concentration i.e. 60% (by weight). In the present study, the sodium triphosphate is used as an additive. Sodium triphosphate exhibits detergent like properties and is highly soluble in water. The addition of sodium triphosphate is varied from 1-5% (by weight).

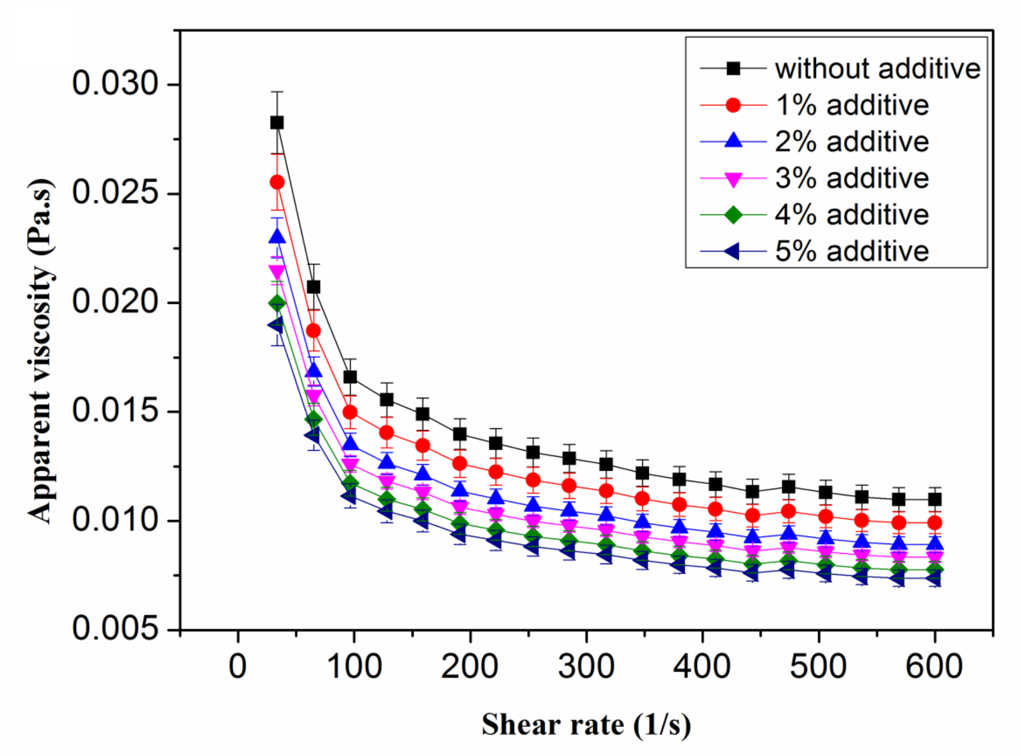

Figure 4.14: Effect of additive on the apparent viscosity of bottom ash slurry

The addition of a small amount of additive results in an appreciable decrease in the apparent viscosity of slurry, whereas the flow behaviour of bottom ash slurry suspension at 60% concentration (i.e. Bingham flow) remains unchanged. Figure 4.14 shows the variation in apparent viscosity of solid slurry suspension at a solid concentration of 60%. As the amount of additive is increased from 1 to 5%, the drastic decrease in apparent viscosity is noticed. It is also observed that the percentage decrease in apparent viscosity is less as the percentage addition of additive is increased from 4 to 5%. The maximum decrease in apparent viscosity is observed as 4% (by weight) addition of sodium triphosphate. The addition of detergent-based additives reduces the electrochemical attraction forces among the solid particles. The addition of additive results in formation of more segregated slurry. This helps to stabilize the solid particles in the liquid phase, which prevents the settling of slurry particles. The drag offered by the solid particles during transportation is also reduced. Thus, the specific energy consumption for transporting tons of bottom ash is reduced. At a shear rate of 222 s^{-1} the apparent viscosity is reduced by 9.67, 18.70, 23.99, 32.81 and 36.17% as the addition of additive is increased from 1-5% (by weight). At a higher shear rate of 411 s^{-1} the percentage decrease in slurry lies in the range of 10.93-33.56% for an additive range of 1-4%.

4.5 REMARKS

The following remarks have been addressed from this chapter:

- The coal-water slurry exhibits Newtonian behaviour at a solid concentration of 30% (by weight). The coal-water slurry exhibits shear thinning behaviour at higher solid concentrations (i.e. above 30%) that show its pseudo-plastic nature.
- The addition of a small amount of sulphonic acid resulted in an improvement in the rheological properties of the coal-water slurry suspension. The maximum decrease in apparent viscosity of coal-water slurry is noticed with a 3% (by weight) addition of sulfonic acid.
- The flow behaviour of coal-water slurry remained unchanged at a 60% solid concentration (i.e. it exhibits pseudo-plastic behaviour) with the addition of the additive.
- The fly ash slurry exhibits Newtonian behaviour for a solid concentration of 30%. The increase in solid concentration results in a change in flow behaviour of fly ash slurry from Newtonian to Bingham plastic. The fly ash-water slurry shows Bingham plastic behaviour for a solid concentration range of 40-60% (by weight).

- The bottom ash slurry exhibits Newtonian behaviour for solid suspension up to a solid concentration of 30%. The bottom ash slurry shows Bingham flow behaviour above 40% solid concentration.
- The addition of sodium triphosphate results in appreciable decrease in viscosity of bottom and fly ash slurry. The maximum percentage decrease in apparent viscosity is observed with a 4% addition of sodium triphosphate in fly and bottom ash slurry.

CHAPTER 5

EXPERIMENTAL INVESTIGATION OF HEAD LOSS CHARCTERSTICS IN PIPE BEND

Chapter 5

EXPERIMENTAL INVESTIGATION OF HEAD LOSS CHARCTERSTICS INSIDE PIPE BEND

In the previous chapters, different bench-scale tests are carried out to analyze the physical as well as rheological behavior of coal and coal-ash slurries. The rheological behavior of slurries only predicts the type of fluid, which is useful in determining the flow behavior. However, the complete phenomenon of flow inside pipe bend remains un-understood. In this context, the experiments are conducted on a pilot plant test loop to understand the complete flow behavior inside the pipe bend.

In this chapter, experiments involving head loss across horizontal pipe bend are conducted for the flow of coal and coal-ash samples at various solid concentrations of 30-60% (by weight) at different Reynolds number. The *r/D* ratio of 90˚ pipe bends is varied in the range of 1.5-2.0. This chapter covers the details and development of test loop, components of test loop, calibration of instruments installed at pipeline circuit and head loss experiments carried out at different process parameters.

5.1 DETAILS OF PILOT PLANT TEST LOOP

In the present study, the detailed experimental investigations on head loss characteristics of coal and coal-ash slurry are performed on a pilot plant test loop for slurry transportation set-up at Thapar Institute of Engineering and Technology (Patiala, Punjab, India). The three dimensional (3D) schematic diagram of the existing pilot plant test loop is represented by Figure 5.1. Figure 5.2 shows the photographic view of pilot plant set-up equipped with different flow generating, measuring and controlling deceives. The set-up consists of a conical slurry-preparation tank in which slurry of different solid concentrations is prepared. To ensure the uniform mixing of the solid in water, the slurry preparation tank is fitted with a motorized stirrer. The stirrer is run with 0.5 hp motor connected via gear box. A conical water tank is also placed adjacent to the slurry preparation tank to recover water that is lost during experimentation. This water tank is also used to clean the slurry pipeline after the experimentation so as to prevent blockage in the pilot loop and also to ensure the safe running of pump. A progressive slurry pump (manufactured by Syno Engineers Ltd. Kanpur) is used to provide the necessary driving force for pumping the solid suspension through the slurry pipeline. The specification of the slurry pump is listed in Table 5.1. A 15 HP motor coupled with a pump through gearbox is used to run the pump. The running speed (rpm) of the motor is controlled by a variable frequency device (VFD). The slurry is pumped through a pipeline that is 60 meters long and 50 mm in diameter. Three different 90˚ pipe bends having *r/D* ratio of 1.5, 2.0 and 2.5 are installed at different locations. To ensure fully developed flow in bend section the length of straight pipe before the inlet to bend is kept in the range of 15-20 times of pipe diameter. The slurry is discharged back to the slurry preparation tank after circulating through the slurry pipeline. This is done to make a closed-loop and to maintain a continuous supply of solid suspension to the slurry pump. An electromagnetic flow meter is used to measure the flow rate in the pipeline. The electromagnetic flow meter is calibrated with an ultrasonic flow sensor before experimentation. Pressure taps are installed at various locations in the pilot plant slurry transportation system to measure head loss with diaphragm-type pressure transducers. All pressure transducers and flow meters are connected to the central data acquisition system. The data acquisition system consists of 16 input ports connected to human machine interface (HMI). The HMI is programmed by Renu Electronics Pvt. Ltd. Pune, India. During experimentation, readings of pressure and flow rate are automatically stored in the data-acquisition system after every minute. In order to account the accuracy and experimental repeatability, the readings are taken for 25 minutes for a particular set of experiments. The data is transferred to the computer either by a unique I.P. address or via LAN cable.

Table 5.1: Specifications of positive displacement progressive pump

S. No.	Parameters	Range
1	Flow rate	0-60 m^3/h
2	Revolutions per minute	0-360 rpm
3	Working temperature	Up to 80˚C
4	Input power	11 kW

5.2 INSTRUMENTATION

The flow parameters for two-phase slurry flow are measured by different measuring instruments. The description, calibration, working principle and methodology for measurement is discussed follows.

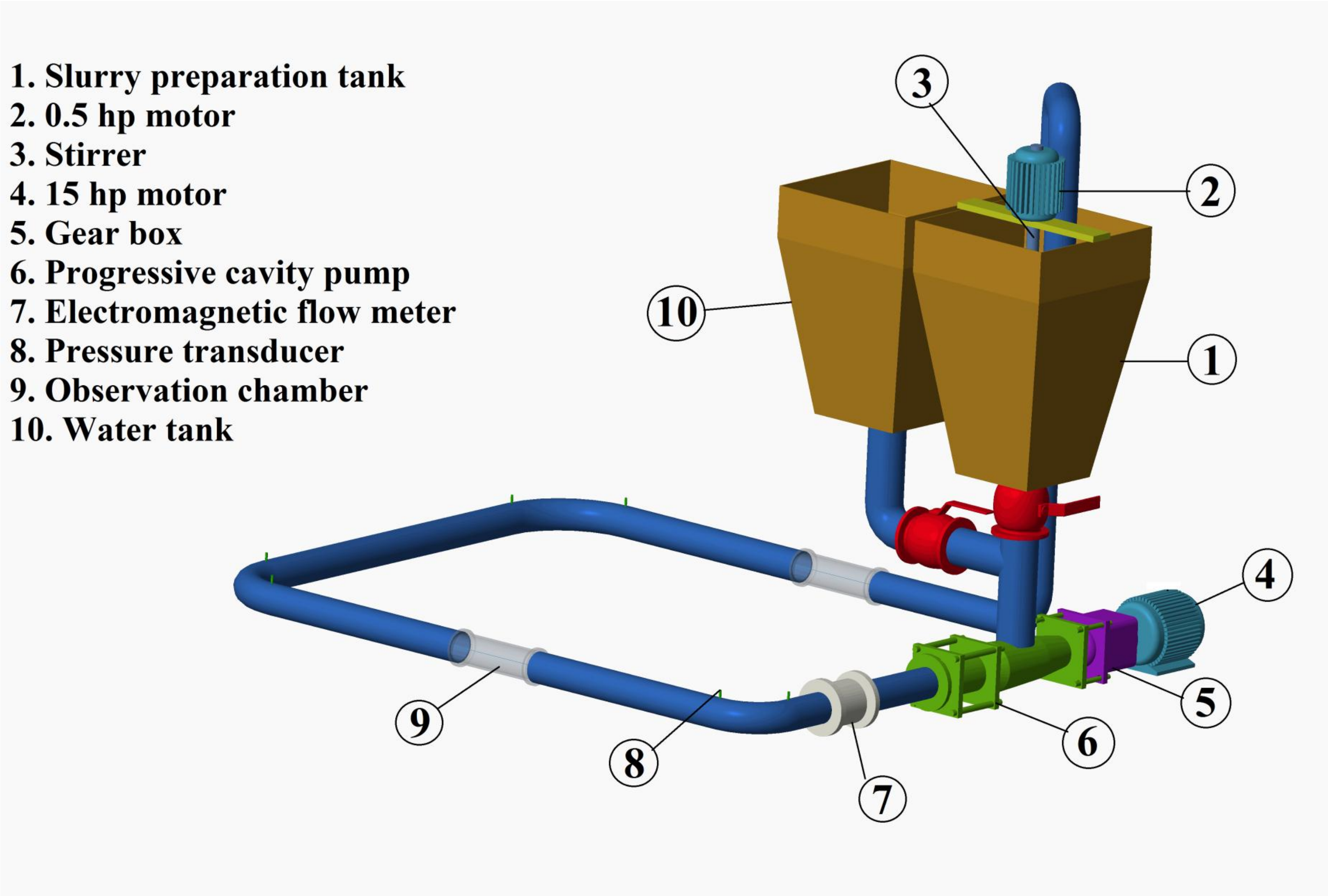

Figure 5.1: Schematic 3D view of pilot plant test loop

Figure 5.2: Photographic view of pilot plant test setup

5.2.1 Flow rate measurement

The flow rate of the two phase slurry flow at different rpm of the slurry pump is measured by an electromagnetic flow meter. The flow meter of 50 mm diameter (manufactured by IOTA Flow Systems, New Delhi, India) is installed in the pipeline. The electromagnetic flow-meter works on the principle of Faraday's law of electromagnetic induction. According to the Faraday's law when any fluid (electrically conductive) pass/flow through a magnetic field, voltage is induced in an electrode placed at right angle to the applied magnetic field. The magnitude of the voltage induced is proportional to the velocity of flowing fluid. The flow meter is connected to the display/HMI. The flow meter transmits 4-20 mA output signals to the controller. The range of the flow meter is 0-80 m^3/h for maximum pressure and temperature of 40 bar and 60˚C respectively. Initially, the calibration of the flow meter is done with ultrasonic flow meter and water is used as a fluid. Figure 5.3 illustrates the variation in the actual flow rate and indicated flow rate. The accuracy of the measurement taken from flow meter lies in the range of ±0.25%.

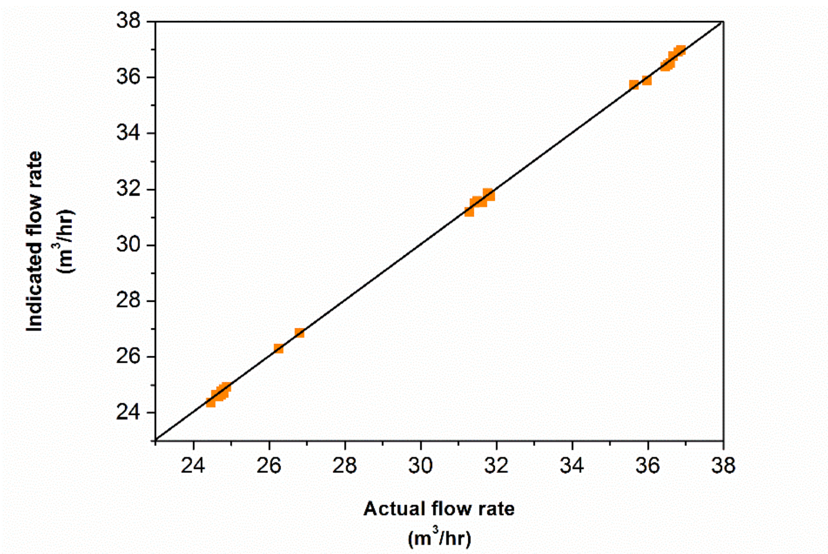

Figure 5.3: Calibration of the flow meter

5.2.2 Pressure measurement

The flush diaphragm pressure transducer (manufactured by WIKA Alexander Weigand SE and Co., Germany) is used to measure the pressure across 90˚ pipe bends having different *r/D* ratios. The pressure transducers are installed at the upstream and downstream section of every bend. The measuring range of transducer is 0-100 bar with the same output signal as of flow meter 4-20 mA. The pressure transducer operates at DC current for voltage range of 10-30 V.

Figure 5.4 illustrates the variation in actual pressure and indicated pressure (in bar). The calibration of the pressure transducer is done with a standard pressure transducer verified and tested at the laboratory. The measurements taken by pressure transducers are at the accuracy of ±0.25%.

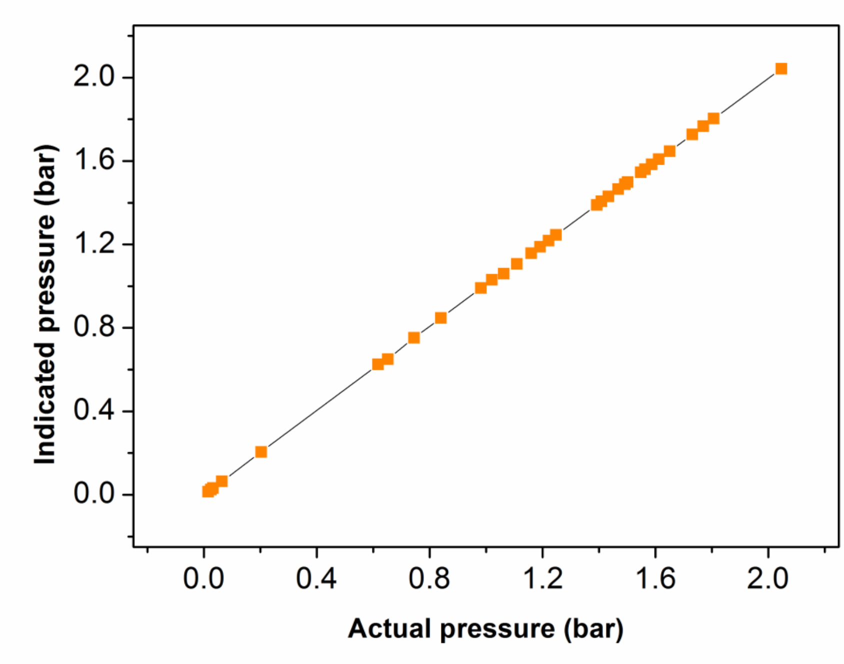

Figure 5.4: Calibration of the pressure transducer

5.3 UNCERTAINTY IN MEASUREMENTS DURING EXPERIMENTATION

The uncertainties in experimental data are always associated besides all precautions. Therefore, the analysis of all uncertainties has been carried out to quantify the maximum possible errors in experimental results. These errors in the experimentation data are due to uncertainty in measurement of instruments and in-accuracy in the geometry of apparatus. The following equations are used to estimate the uncertainty in experiments (Holman, 1994; Baird, 1995; Taylor, 1997).

$$H = H(\alpha_1, \alpha_2, \alpha_3, \ldots\ldots\ldots\ldots\ldots\ldots\ldots\ldots, \alpha_n) \qquad (5.1)$$

Where H is the parameters that depend on independent variables $\alpha_1, \alpha_2, \alpha_3 \ldots\ldots, \alpha_n$. Let δU in the uncertainty in experimental results and $\delta\alpha_1, \delta\alpha_2, \delta\alpha_3, \ldots\ldots\ldots, \delta\alpha_n$ are the uncertainties associated with independent parameters. The uncertainty in the results is calculated as:

$$\delta U = \left[\left(\frac{\partial H}{\partial \alpha_1}\delta\alpha_1\right)^2 + \left(\frac{\partial H}{\partial \alpha_2}\delta\alpha_2\right)^2 + \left(\frac{\partial H}{\partial \alpha_3}\delta\alpha_3\right)^2 + \dots\dots\dots\dots + \left(\frac{\partial H}{\partial \alpha_n}\delta\alpha_n\right)^2\right]^{1/2} \quad (5.2)$$

In present work, the head loss is the main parameter to investigate the flow characteristics of coal and coal-ash slurry. The experiments are performed at different flow rates and solid concentrations. So, the uncertainty might be associated with the equipment used for the flow equipment like pressure transducer, flow meter, weighing machine and glass beaker. The accuracy and precision values of instruments are listed in Table 5.2. The uncertainty in the head loss is calculated as 0.84%.

Table 5.2: Accuracy and precision values of instruments

S. No.	Equipment	Accuracy
1	Pressure transducer	±0.25% of full scale
2	Flow meter	±0.25% of full scale
3	Weighing machine	±0.1%
4	Glass beaker	±0.75%

5.4 EXPERIMENTAL PROCEDURE

The experiments for head loss are carried out on the pilot plant test loop. The slurry is prepared in a conical slurry preparation tank. Figure 5.5 shows the photographic view of coal and fly ash slurry inside the slurry preparation tank. The pre-calculated amount of water and solid particles are added in the slurry preparation tank to make slurry of different solid concentrations. The uniform mixing of slurry is done with the stirrer. The slurry is pumped to 60 meter long pipeline with progressive slurry pump. In order to measure the exact solid concentration of slurry flowing in the circuit, the slurry transportation system is provided with a slurry sampler. The slurry sample is taken from slurry sampler after 15 minutes start of experiment at every concentration in 1000 ml glass beaker. Figure 5.6 represents the slurry samples taken from slurry sampler to measure the actual solid concentration of slurry flowing in a test loop. The weight of slurry with beaker is noticed. Afterward, the beaker is placed on oven and weight of solid left in the beaker is also measured. Hence, the actual concentration flowing in the pipeline is calculated. The pipeline is also equipped with observation chambers of glass tube to keep eye on settling of solid particles. The pressure drop is noticed from the difference in pressure of two transducers installed at upstream and downstream of 90˚ pipe bends. The pressure drop is represented in terms of head loss and the units are meter water column (mWc).

(a) Coal-water slurry *(b) Fly ash-water slurry*

Figure 5.5: Photographic view of slurry preparation tank

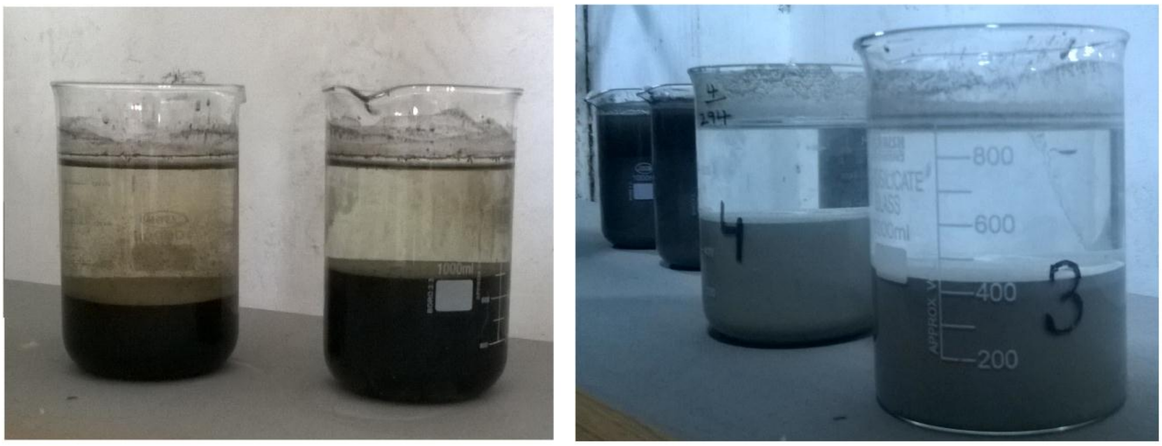

Figure 5.6: Samples collected from slurry sampler

5.5 RANGE OF PARAMETERS

The extensive experimentation for head loss across 90˚ bends is carried out for flow of < 53 μm fine particulate coal-water slurry at a higher solid concentration range of 30-60% (by weight). The flow velocity is varied in the range of 2-5 m/s. The corresponding Reynolds's number is calculated for coal-water slurry at respective solid concentrations and flow velocity. The effect of additive on head loss and specific energy consumption at higher solid concentrations of 60% is also examined in study. The physical and mineralogical characteristics of procured coal sample are already discussed in Chapter 3. The rheological behaviour of coal-water slurry at different solid concentration with and without the addition of additive is discussed in Chapter 4. Similar experimentation for head loss is carried out for fly and bottom ash slurry with and without the addition of the additive.

5.6 HEAD LOSS CHARACTERISTICS OF COAL AND COAL-ASH WATER SLURRY ACROSS 90° PIPE BEND

Experiments are carried out to investigate the head loss characteristics for the flow of < 53 μm sized coal-water slurry across 90˚ horizontal pipe bends. A slurry suspension with a solid concentration range of 30.27-60.56% (by weight) is pumped through a 50 mm pipeline. The radius of the curvature-to-diameter ratio of the pipe bends are taken as 1.5, 2.0 and 2.5. The average slurry flow velocity varied within the range of 2-5 m/s. The Reynolds number is calculated for respective flow velocities and solid concentrations. The Reynolds number range of coal-water slurry at different solid concentrations and flow velocities lies within the range of 1.45×10^4-1.36×10^5. Figure 5.7 shows variations in head loss across various pipe bends with Reynolds number at different solid concentrations for coal-water slurry.

From Figure 5.7(a-d), it is noticed that as the solid concentration of the coal-water slurry is increased from 30.27-61.56% (by weight), the head loss across all three pipe bends also increases. This increase in head loss with the increase in solid concentration occurs due to an increase in the slurry viscosity and density. A sudden increase in head loss is also found with an increase in Reynolds number irrespective of solid concentrations. At higher Reynolds number, the molecular momentum exchange between solid particles increases due to a higher level of turbulence, hence high losses occur inside pipe bend (Mishra *et al.* 1998; Chandel *et al.* 2009). From the results, it is also observed that head loss across pipe bends is a function of the *r/D* ratio. A sudden drop in head loss is found as the *r/D* ratio is increased from 1.5 to 2.0. It is observed from Figure 5.7(a) that maximum head loss at solid concentration of 30.27% is occurred in pipe bend having *r/D* ratio of 2.5 at flow velocity of 5 m/s. The increase in *r/D* ratio from 1.5-2.0 the sudden drop in head loss is observed. Figure 5.7(b) represents the head loss characteristics of coal-water slurry at solid concentration of 41.90%. A similar trend as noticed for solid concentration of 30.27% is observed but with higher magnitudes. The maximum drop in head loss is observed as 0.19 mWc for pipe bend having *r/D* ratio of 2.5 at a flow velocity of 5 m/s. The head loss characteristics of coal-water slurry at a solid concentration of 50.73% and 61.56% are shown in Figure 5.7 (c). It is observed from results that, as the *r/D* ratio of a bend is increased from 1.5 to 2.0 head loss reduced by 13.17, 16.70, 17.28 and 17.54% for a solid concentration of 30.27, 41.90, 50.73 and 61.56% at Reynolds number of 5.47×10^4, 3.35×10^4, 1.99×10^4 and 1.58×10^4 respectively. However, further increase in *r/D* ratio from 2.0 to 2.5 the head loss is increased by 16.52, 17.90, 19.12 and 21.30% for Reynolds number of 5.47×10^4, 3.35×10^4, 1.99×10^4 and 1.58×10^4 at a solid concentration of 30.27, 41.90, 50.73 and 61.56% respectively. At Reynolds number of 1.36×10^5, 8.39×10^4, 4.98×10^4 and 3.96×10^4 the head loss for coal-water slurry is decreased by 12.78, 13.68, 12.90 and 17.83% for a solid concentration of 30.27, 41.90, 50.73 and 61.56% respectively as *r/D* ratio is increased from 1.5-2.0.

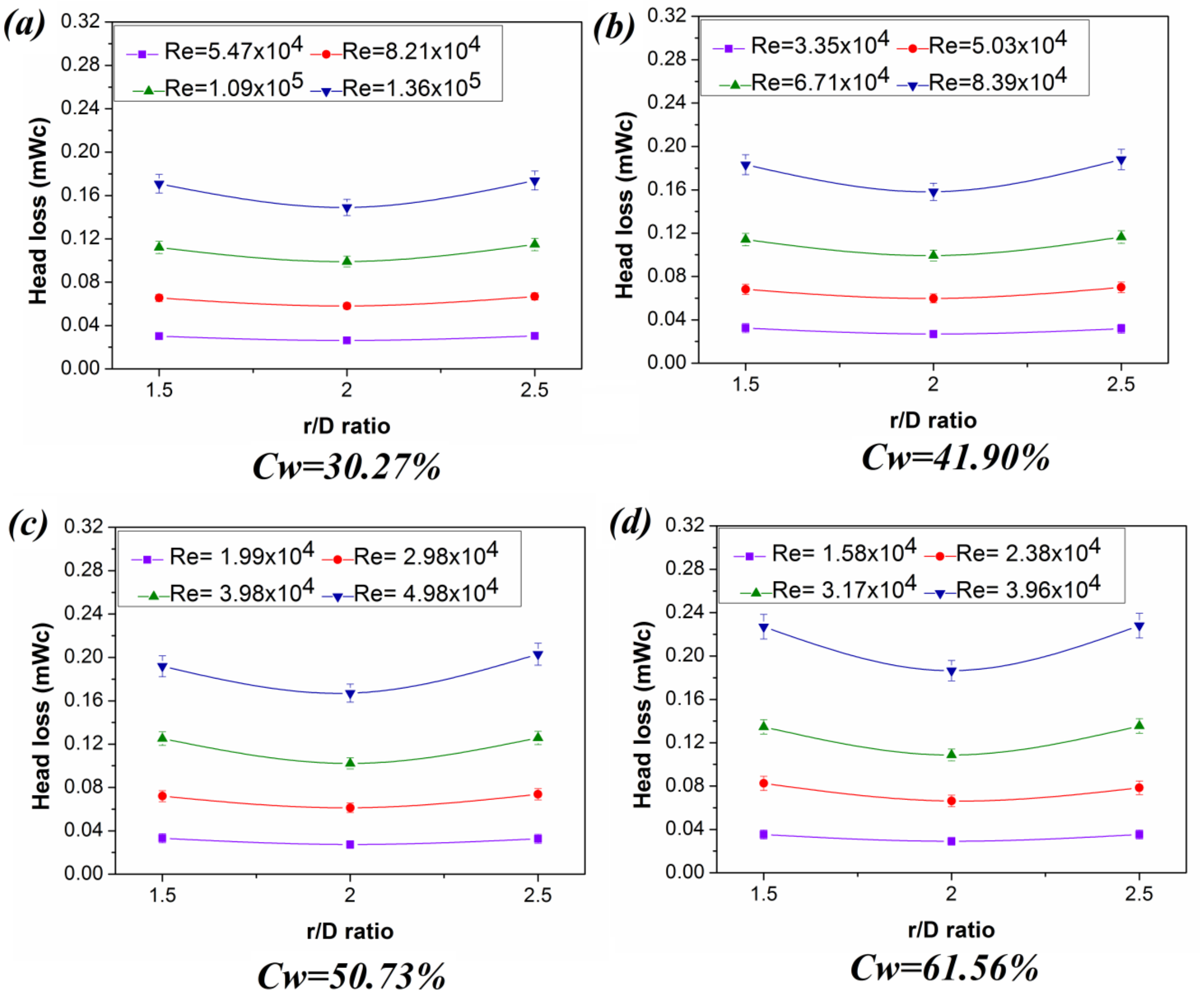

Figure 5.7: Head loss characteristics of <53 µm coal-water slurry at (a) 30.27%, (b) 41.90%, (c) 50.73% and (d) 61.56%

Using the slope linear regression approach through data points, the rate of increase in head loss with Reynolds number is observed as 0.047, 0.041 and 0.045 for *r/D* ratio 1.5, 2 and 2.5 respectively for 30.27% solid concentration whereas for 61.56% solid concentration, the rate of increase in head loss with flow velocity is noticed as 0.062, 0.051 and 0.063 for *r/D* ratio 1.5, 2 and 2.5 respectively. The abrupt drop in a head loss at *r/D* = 2.0 is due to a suppression of flow separation phenomenon inside the pipe bend. The increase in the radius-to-diameter ratio also contributed to the decrease in secondary flow intensity at the outlet of the bend. The optimum *r/D* ratio for minimum head loss in a 90˚ pipe bend is 2.0; beyond this, the increase in head loss is seen due to increase in effective length of pipe bend, losses due to friction increases.

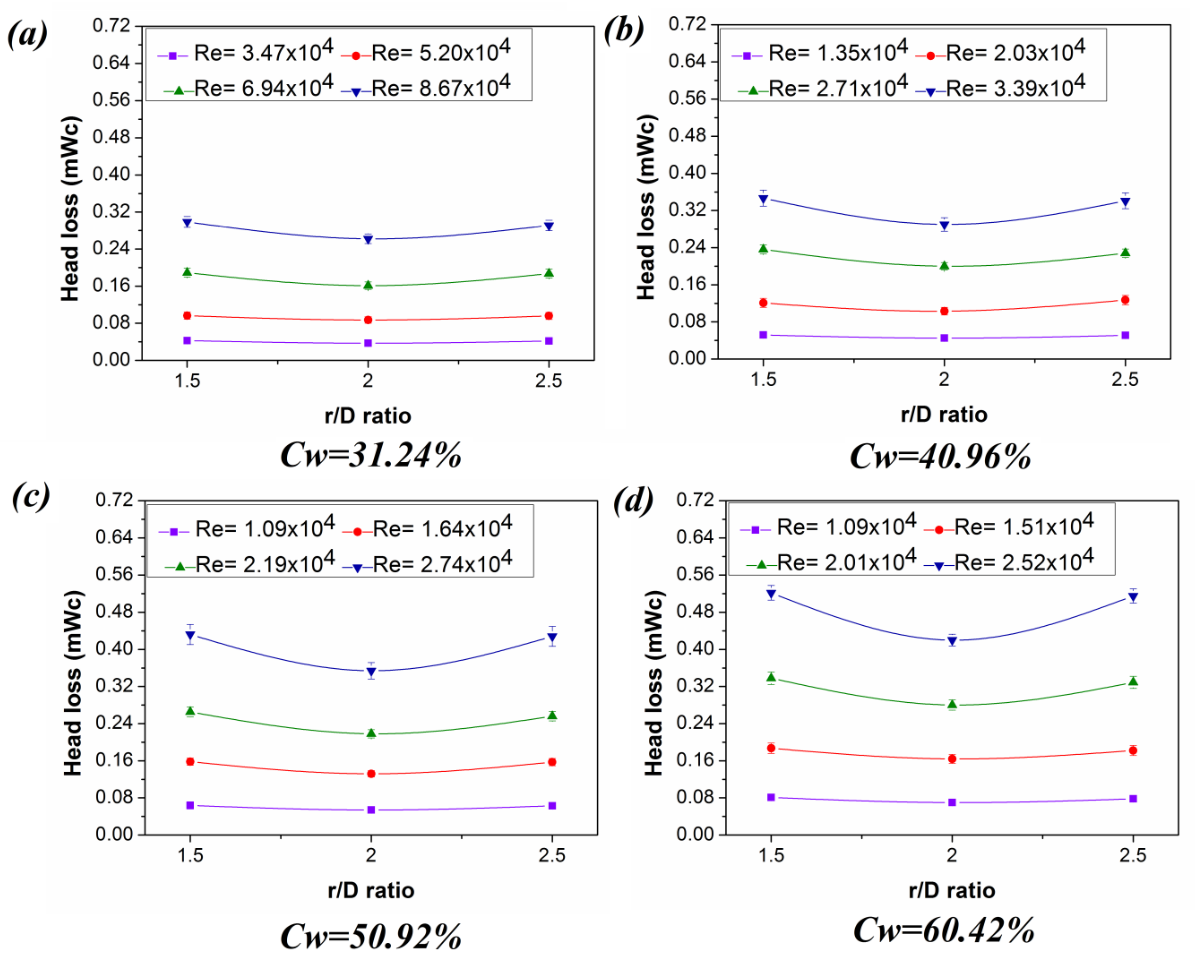

Figure 5.8: Head loss characteristics of fly ash slurry at (a) 31.24%, (b) 40.96%, (c) 50.92% and (d) 60.42%

Figure 5.8(a-d) represents the head loss characteristics of fly ash slurry for solid concentration range of 31.24–60.42% (by weight) across pipe bend having *r/D* ratio range of 1.5–2.5. The Reynolds number for flow velocity range of 2-5 m/s at different solid concentrations is lie in the range of 1.01×10^4–8.67×10^4. It is observed from results that head loss across pipe bends for fly ash slurry is more than coal-water slurry. This increase in head loss magnitude is observed due to low void fraction in fly ash particles as compared to coal particles (Ghosal, 1995; Matsunaga *et al.* 2002; Lisandy *et al.* 2016). The minimum head loss is noticed for pipe bend having *r/D* ratio of 2.0. The head loss is found the minimum for pipe bend having *r/D* ratio of 2.0. Figure 5.8(a) represents variation in the head loss for fly ash slurry at a solid concentration of 31.24%. The head loss for fly ash slurry for pipe bend having *r/D* ratio 2.0 is increased by 1.41, 1.49, 1.62 and 1.76 times as compared to the coal-water slurry for flow velocity of 2, 3, 4 and 5 m/s at 31.24% solid concentration. The variation in head loss characteristics of fly ash slurry for solid concentration of 40.96% is shown in Figure 5.8(b). At 40.96% solid concentration the head loss for fly ash slurry in pipe bend (*r/D*=2.0) is increased by 1.66, 1.72, 1.80 and 1.86 times of coal-water slurry for flow velocity range of 2, 3, 4 and 5 m/s respectively. Figure 5.8(c) shows the effect of *r/D* ratio and Reynolds number on head loss at a solid concentration of 50.92%. It is observed from results that head loss magnitude for fly ash slurry is increased by 1.94, 2.05, 2.09 and 2.15 times of coal-water slurry suspension across pipe bend having *r/D* ratio of 2.0 at solid concentration of 50.92% for flow velocity of 2, 3, 4 and 5 m/s. The variation in head loss at solid concentration of 61.42% for fly ash slurry is shown in Figure 5.8(d). The head loss for fly ash slurry at 61.42% solid concentration is increased to 2.37, 2.42, 2.49 and 2.54 times as compared to coal-water slurry for pipe bend having *r/D* ratio of 2.0 at flow velocity range of 2, 3, 4 and 5 m/s respectively. The optimum *r/D* ratio for fly ash slurry is observed as 2.0 for minimum head loss due to a decrease in secondary flows and flow separation phenomenon.

Figure 5.9(a-d) shows the variations in head loss across various pipe bends with Reynolds number at different solid concentrations for bottom ash slurry. The Reynolds number for bottom ash slurry varies within the range of 1.22×104–1.05×105. Similar phenomena of variation in head loss with *r/D* ratio as observed for coal and fly ash slurry is noticed for bottom ash slurry but with different magnitudes. The magnitude of head loss for bottom ash slurry is lies between coal and fly ash slurry. This is observed because the density of bottom ash particles is higher than coal and less than fly ash. Also, the drag offered by bottom ash particles is lesser as compared to fly ash. Figure 5.9(a) represents the variation in head loss for bottom ash slurry at solid concentration of 29.98%. It is observed from results that head loss for bottom ash slurry across pipe bend having *r/D* ratio of 2.0 at solid concentration of 29.98% increased by 1.35, 1.44, 1.50 and 1.61 times as compared to coal-water slurry for flow velocity of 2, 3, 4 and 5 m/s respectively. However, the head loss for bottom ash slurry in pipe bend (*r/D*=2.0) is increased by 1.57, 1.64, 1.70 and 1.75 times as compared to coal-water slurry for solid concentration of 41.62% (as shown in Figure 5.9(b)) at flow velocity of 2, 3, 4 and 5 m/s respectively.

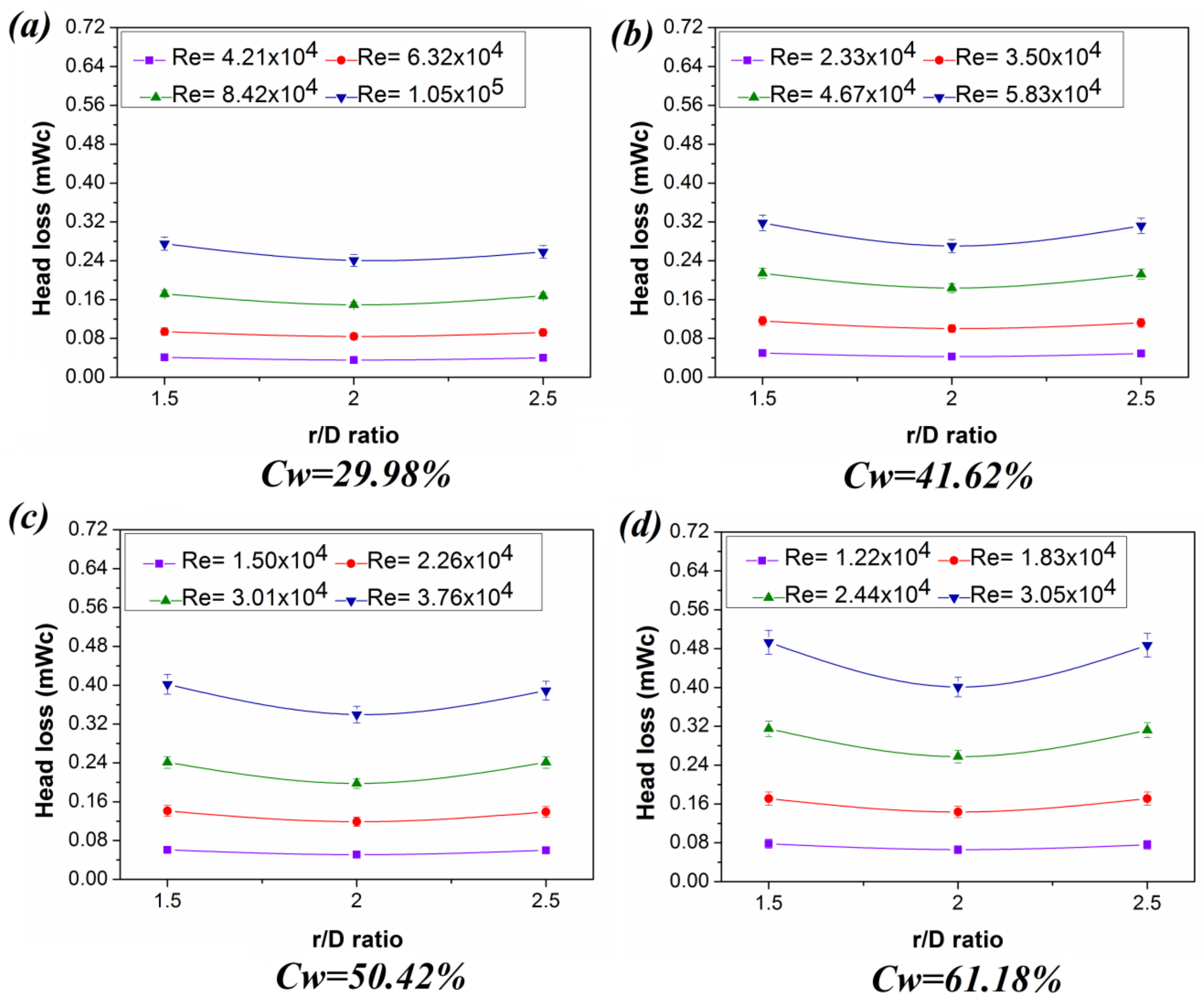

Figure 5.9: Head loss characteristics of bottom ash slurry (a) 29.98%, (b) 41.62%, (c) 50.42% and (d) 61.18%

Figure 5.9(c) represents the variation in a head loss for bottom ash slurry at a solid concentration of 50.42%. From results it is noticed that head loss for bottom ash slurry in pipe bend (*r/D*=2.0) is increased by 1.85, 1.89, 1.96 and 2.03 times as compared to coal-water slurry for flow velocity of 2, 3, 4 and 5 m/s respectively. The variation in a head loss for bottom ash slurry at a solid concentration of 61.18% is shown in Figure 5.9(d). It is observed from results that head loss in bend having *r/D* ratio of 2.0 is increased by 2.14, 2.19, 2.25 and 2.32 times at solid concentration of 61.18% for the flow velocity of 2, 3, 4 and 5 m/s respectively. The optimum head loss for flow of coal and coal-ash slurry is observed for pipe bend having *r/D* ratio 2.0. However, the order for head loss is found as fly ash > bottom ash > coal slurry.

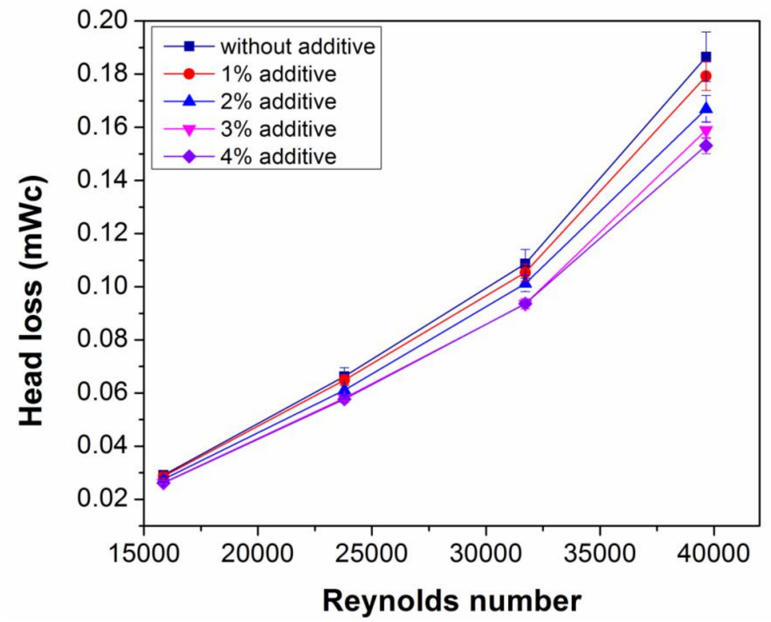

Figure 5.10: Effect of additive on head loss of coal-water slurry

5.7 EFFECT OF ADDITIVES ON HEAD LOSS CHARACTERISTICS OF COAL AND COAL-ASH SLURRIES

Experimentation across pipe bend (*r/D* = 2.0) is also extended to investigate the effect of an additive (sulfonic acid, sodium triphosphate) on head loss at a high solid concentration of coal and coal-ash slurries. Figure 5.10 represents the effect of additives on head loss characteristics of coal-water slurry. Sulfonic acid (RSO_3H) is used as an additive for coal-water slurry at a solid concentration of 61.56% (by weight). The variation in head loss with and without the use of an additive for the coal-water slurry is plotted in Figure 5.10. An appreciable decrease in head loss is noticed after the addition of a small amount of sulfonic acid. This is due to the fact that sulfonic acid exhibits surfactant like properties and is easily soluble in water (Kosswig 2002). The addition of sulfonic acid to coal-water slurry results in a reduction in the Vander Waals forces of attraction between solid particles. The increase in electrostatic repulsive forces among solid particles results in more segregated slurry (He and Laskowski, 2000; Chen *et al.* 2011; Zhu *et al.* 2014). The sulfonates ($R - SO_3^-$) of the sulfonic acid are stable in water and also non-oxidizing in nature. Hence, the head loss characteristic of slurry suspension is improved. Head loss is decreased by 4.57, 3.97, 6.61 and 6.48% with a 1% (by weight) addition of sulfonic acid (at *r/D* = 2.0).

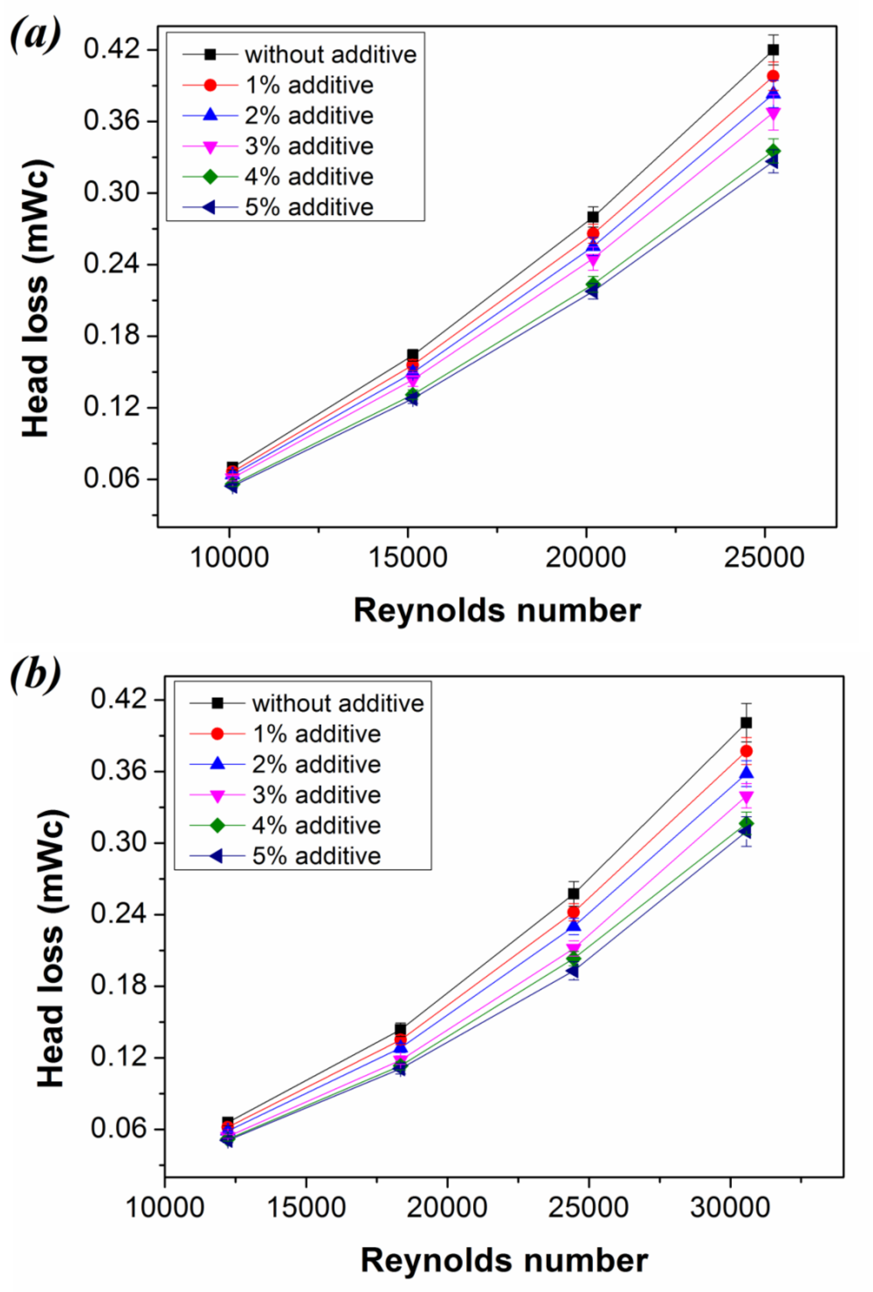

Figure 5.11: Effect of additive on head loss of (a) fly ash and (b) bottom ash slurries

A reduction of 12.52, 13.96, 17.12 and 17.09% is observed at Reynolds number of 1.58×10^4, 2.37×10^4, 3.17×10^4 and 3.96×10^4 respectively after addition of 3% (by weight) of sulfonic acid. With the addition of 4% (by weight) of sulfonic acid decrease in head loss of 13.10, 14.65, 17.97 and 18.16% are observed at Reynolds number of 1.58×10^4, 2.37×10^4, 3.17×10^4 and 3.96×10^4 respectively. The maximum percentage decrease in head loss is observed with a 3% (by weight) addition of sulfonic acid. Figure 5.11(a) represents the variation in head loss with and without the addition of an additive for fly ash-water slurry. The sodium triphosphate is used as an additive for fly ash at a solid concentration of 60.42% (by weight). The addition of additive results in a decrease in head loss without changing flow behaviour. The effect of additive (sodium triphosphate) on the head loss of bottom ash-water slurry at a solid concentration of 61.18% (by weight) is shown in Figure 5.11(b). A significant reduction in head loss is observed with small addition of additive. The sodium triphosphate ($Na_5P_3O_{10}$) is used as a component in detergents and water soluble. Sodium triphosphate is anti-corrosive, settling retarder and anti-caking in nature. The sodium triphosphate also acts as a chelating agent. The chelation is the bonding of molecules and ions with metal ions (Davies and Corbridge , 1958; Corbridge, 1960). Thus, the addition of detergent based additive helps to reduce the slurry viscosity and this leads to a decrease in head loss. The addition of sodium triphosphate forms a uniform layer around the solid particles which increases the electrostatic repulsive forces and results into more segregated slurry. Hence, the settling and head loss characteristic of slurry improves at high solid concentrations. The head loss for fly ash slurry at Reynolds number of 2.52×10^4 is decreased by 5.23, 8.80, 12.45, 20.15 and 22.21% with the addition of 1, 2, 3, 4 and 5% sodium triphosphate respectively. However, the head loss for bottom ash slurry at Reynolds number of 3.05×10^4 is reduced by 5.92, 10.62, 17.77, 21.03 and 22.73% with the addition of 1, 2, 3, 4 and 5% sodium triphosphate respectively. The maximum percentage decrease in head loss is observed with 4% addition of sodium triphosphate for fly and bottom ash slurry. However, further addition of additive also results in a reduction of head loss but percentage decrease in decidedly less.

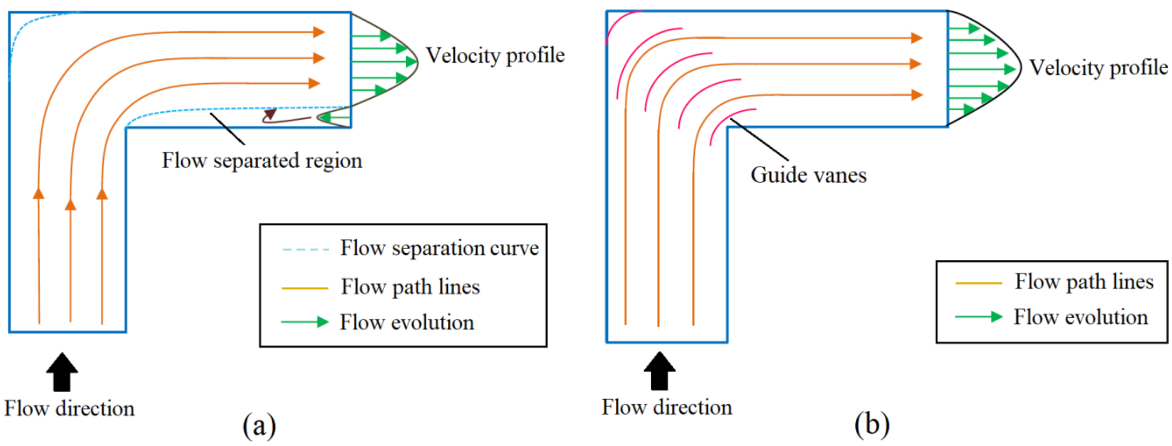

Figure 5.12: Phenomena of flow separation in 90˚ bends (Streeter *et al.* 1998)

5.8 BEND LOSS COEFFICIENT (K_b) IN PIPE BEND

The term bend loss coefficient (K_b) is associated with friction losses that are caused by separation and the axial length of a pipe bend. Generally, losses that occur inside pipe bends are comparably higher than losses that occur in a straight pipe. These losses can be attributed to the flow separation that occurs inside bends, most prominently in cases where bends are exceptionally sharp (Zhang *et al.* 2015; Dutta and Nandi, 2016; Kaushal *et al.* 2017). Figure 5.12 shows the separation of flow in sharp and smooth pipe bends. The secondary flow is another major factor responsible for higher losses in pipe bends. The unbalanced centripetal forces that arise inside bends are because of the effect of bend curvature, which generates swirling secondary flows (as represented in Figure 5.13). In the present study, bend loss is calculated by the equation (Mishra *et al.* 1998):

$$\Delta H_b = K_b \times \frac{{V_m}^2}{2g} \tag{5.3}$$

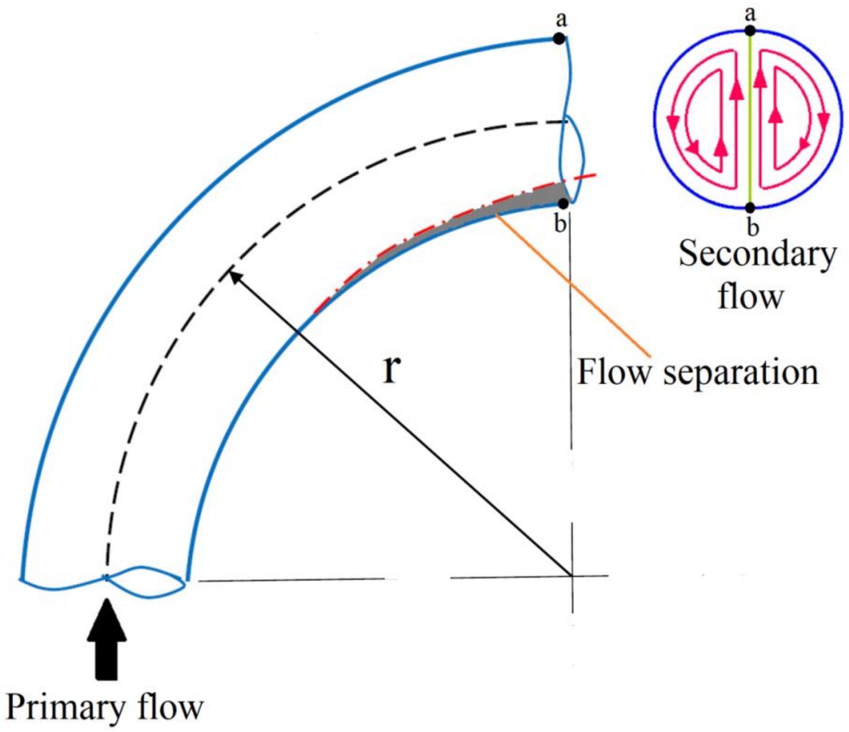

Figure 5.13: Secondary flow phenomenon inside pipe bends (Streeter *et al.* 1998)

The variation in bend loss coefficient with *r/D* ratio and Reynolds number of coal-water slurry is represented in Figure 5.14. It is observed from results that the variation in bend loss coefficient for coal-water slurry as a function of *r/D* ratio and Reynolds number for a solid concentration of 61.56% (by weight). From the results, it is observed that the bend loss coefficient is decreased with increase in Reynolds number. The 4.31, 3.04 and 1.31% decrease in bend loss coefficient is observed as Reynolds number is increased from 1.58×10^4–2.37×10^4, 2.37×10^4–3.17×10^4 and 3.17×10^4–3.96×10^4 respectively for *r/D* ratio of 1.5. It is also noticed that the bend loss coefficient is independent of flow rate at higher value of Reynolds numbers. An appreciable decrease in bend loss coefficient is seen as the *r/D* ratio increased from 1.5–2.0. The bend loss coefficient is reduced by 17.16, 17.36, 18.70 and 19.05% at Reynolds number of 1.58×10^4, 2.37×10^4, 3.17×10^4 and 3.96×10^4 as *r/D* ratio increased from 1.5–2.0. Further increase in bend curvature, increases bend loss coefficient. At lower *r/D* ratio the effect of flow separation and higher intensity of secondary flows results in higher values of bend loss coefficient whereas for higher *r/D* ratio the effective length of pipe bend contributes to higher losses inside bend.

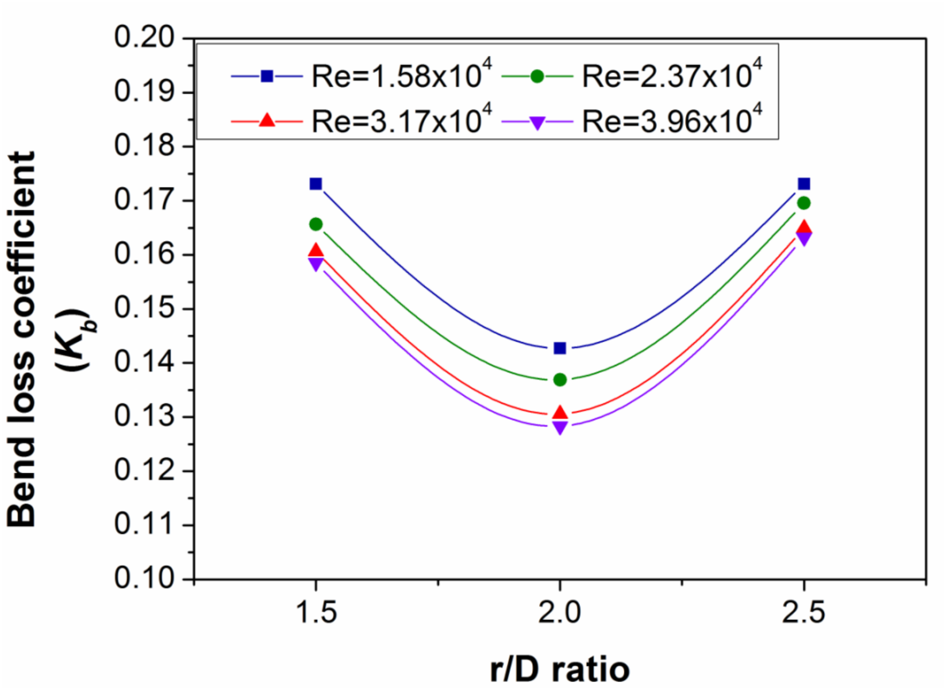

Figure 5.14: Variation in bend loss coefficient for different *r/D* ratio and Reynolds number for coal-water slurry

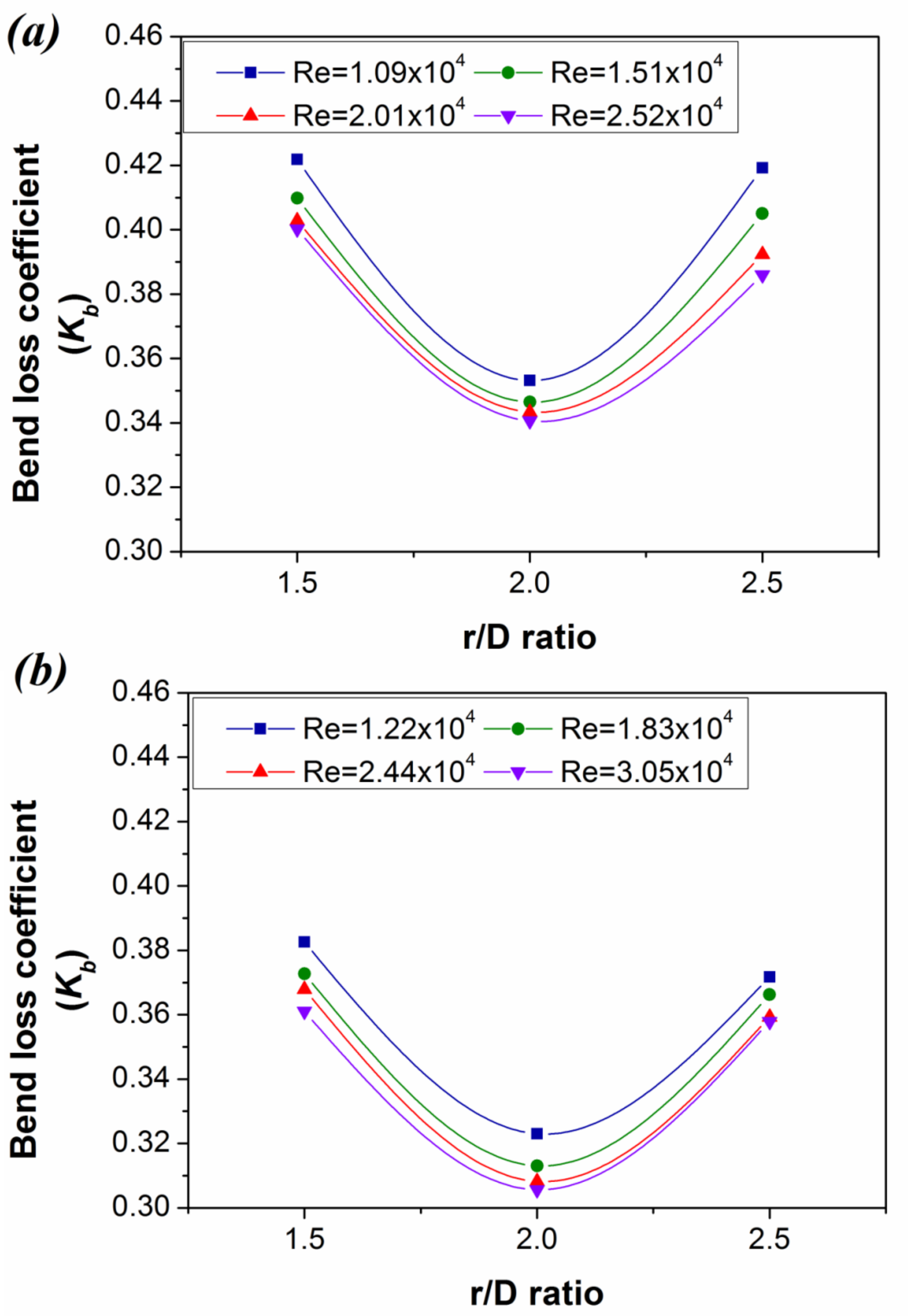

Figure 5.15: Variation in bend loss coefficient for different *r/D* ratio and Reynolds number for (a) fly ash and (b) bottom ash slurries

Figure 5.15(a) shows the effect of Reynolds number and *r/D* ratio on bend loss coefficient for fly ash slurry at a solid concentration of 60.42%. The values of bend loss coefficient for fly ash slurry are higher than coal-water slurry. This is because the specific gravity of fly ash is more as compared to coal. The bend loss coefficient of fly ash slurry for pipe bend (*r/D*=2.0) is increased by 2.47, 2.51, 2.63 and 2.66 times as compared to the coal-water slurry for flow velocity of 2, 3, 4 and 5 m/s respectively. The minimum values of bend loss coefficient are observed for pipe bend having *r/D* ratio of 2.0. Similar, results are found for bottom ash slurry as shown in Figure 5.15(b). The magnitude of bend loss coefficient for bottom ash slurry is more than the coal-water slurry whereas less than fly ash slurry. The bend loss coefficient of bottom ash slurry for pipe bend (*r/D*=2.0) is increased by 2.26, 2.28, 2.36 and 2.39 times as compared to coal-water slurry for flow velocity of 2, 3, 4 and 5 m/s respectively. Similar observations are also reported by various researchers (Mishra *et al.* 1998; Verma *et al.* 2006).

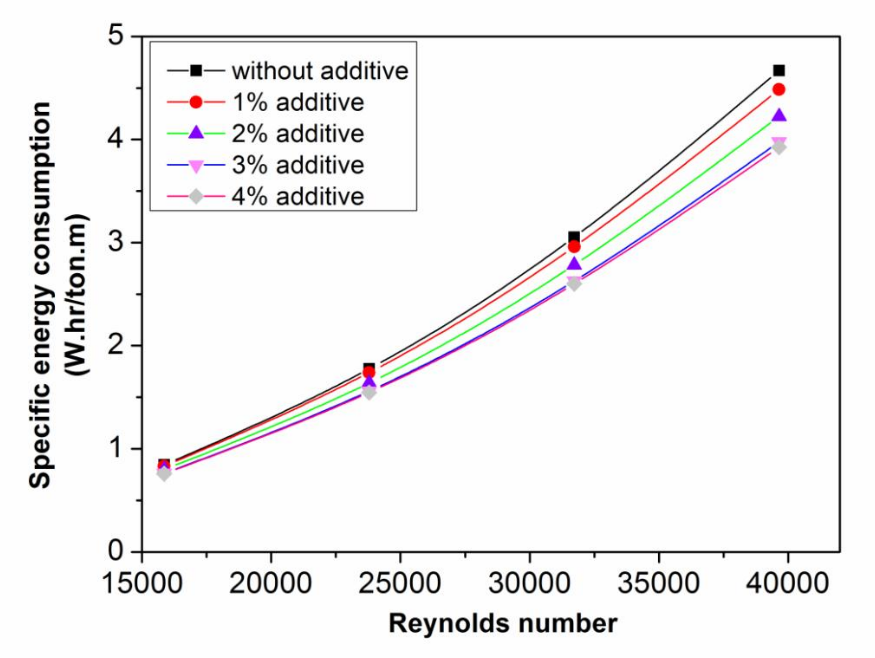

Figure 5.16: Effect of additive on specific energy consumption (*SEC*) of coal-water slurry

5.9 SPECIFIC ENERGY CONSUMPTION (*SEC*)

During the transportation of solid-liquid suspensions, solids mainly act as a payload, whereas the carrier fluid acts as a vehicle. *SEC* is generally the measure of the energy required to convey a given quantity of solid over a given distance. A slurry pipeline with low *SEC* transports solid matter more efficiently than a slurry pipeline with high *SEC* (Wu *et al.* 2010; Ihle and Tamburrino, 2012; Ihle, 2013). In the present study, *SEC* is calculated for transporting the highly-concentrated coal and coal-ash slurry through a pipe bend (*r/D* = 2.0) with and without the addition of an additive. The following relationships are used to determine the SEC.

$$P_B = Q \times g \times \Delta H_b \times \rho_m \tag{5.4}$$

$$W_B = 3.6 \times C_w \times \rho_m \times Q \tag{5.5}$$

$$SEC = \frac{P_B}{W_B} \tag{5.6}$$

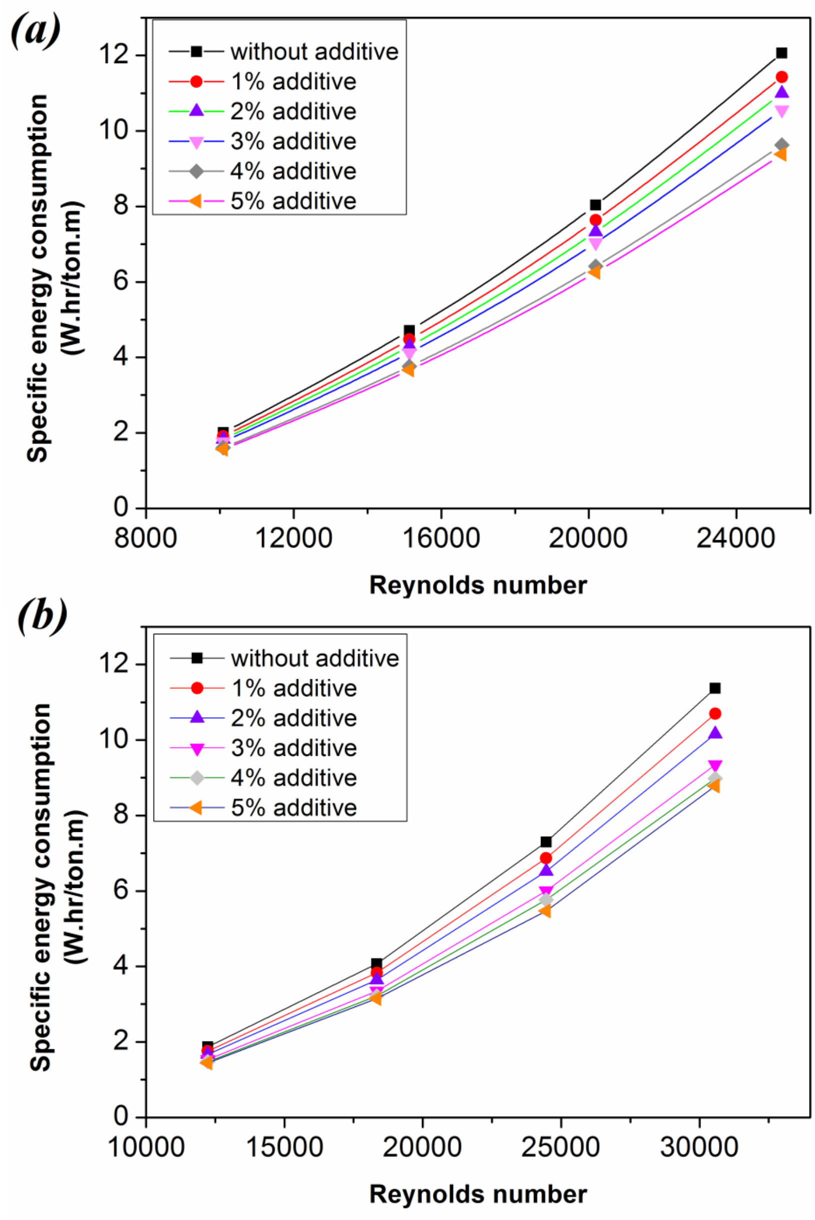

Figure 5.17: Effect of additive on specific energy consumption (*SEC*) of (a) fly ash and (b) bottom ash slurries

Figure 5.16 represents the effect of additive (sulfonic acid) and Reynolds number on SEC for coal-water slurry at a solid concentration of 61.56% (by weight). From the results, it is noticed that SEC gradually decreases with the addition of a small amount of sulfonic acid. SEC is decreased by 3.90, 9.51, 14.85 and 15.93% with the addition of 1, 2, 3 and 4% (by weight) respectively of sulfonic acid at a Reynolds number of 3.96×10^4. This decrease in

SEC is noticed due to enhancements in rheological behaviour of solid suspension with a blending of additive. The maximum decrease in SEC is noticed with 3% addition of sulfonic acid; beyond 3% the percentage decrease in SEC is comparably less. The variation in SEC with the addition of sodium triphosphate on fly and bottom ash slurry is shown in Figure 5.16(a,b). Similar results as obtained from coal water slurry are also noticed for coal-ash slurry. The considerable decrease in SEC is observed by using conveying slurry with the use of additive at higher solid concentrations. The maximum decrease of 20.15% in SEC is noticed with 4% addition of sodium triphosphate in fly ash slurry at Reynolds number of 2.52×10^4. However, for bottom ash slurry, the addition of 4% sodium triphosphate results in 21.03% reduction in specific energy consumption at Reynolds number of 3.05×10^4. Thus, it is economical to transport coal-water slurry at higher solid concentrations with the help of additives (Hashemi *et al.* 2014).

5.10 REMARKS

The following remarks are addressed in this chapter:

- The head loss across 90° pipe bends is a function solid concentration, *r/D* ratio and Reynolds number for coal and coal-ash slurries.
- The head loss is found minimum in 90˚ pipe bend having *r/D* ratio of 2.0. Further increase in *r/D* ratio results in increase in head loss.
- Head loss across pipe bends for bottom ash slurry is more than coal-water slurry and lower than fly ash slurry. This is observed because the density of bottom ash particles is higher than coal and less than fly ash.
- A significant reduction in head loss of coal-water slurry is observed with a small addition of sulfonic acid. The maximum decrease in head loss is observed with a 3% (by weight) addition of sulfonic acid.
- The addition of detergent-based additive helps to reduce the viscosity of coal-ash slurries and this leads to a decrease in head loss. The maximum decrease in head loss for fly and bottom ash slurry is observed with 4% (by weight) addition of sodium triphosphate.
- The bend loss coefficient is decreased with increase in Reynolds number. The minimum values of bend loss coefficient are observed for pipe bend having *r/D* ratio of 2.0 for coal and coal-ash slurry.
- The specific energy consumption (*SEC*) gradually decreases with the addition of a small amount of additive.

CHAPTER 6

NUMERICAL SIMULATIONS OF HEAD LOSS CHARCTERSTICS INSIDE PIPELINE

Chapter 6

NUMERICAL SIMULATIONS OF HEAD LOSS CHARCTERSTICS INSIDE PIPELINE

In previous chapters, the head loss characteristics of 90° pipe bend are experimentally evaluated on pilot plant test loop. From the previous chapter, it is noticed that the experimental evaluation of head loss is costly, time consuming and limited for a particular geometry and very few number of process parameters can be varied in pilot plant test loop. In this context, the computer enabled analysis to become more suitable in terms of flexibility, time and cost-saving. In this chapter, an attempt has been made to investigate head loss in pipe bends for conveying coal and coal ash slurry suspensions using computational fluid dynamics (CFD). The effect of flow separation and secondary flows on turbulence, flow velocity and distribution of the solid suspension inside the bend geometry is also studied with the help of contours. The mathematical model generally involves momentum, mass and energy conservation equations. In present study, water is considered as a primary phase, however coal and coal–ash are taken as secondary phase and the solution is obtained by solving the Navier–Stokes equations. The Navier–stokes equation is solved by using a commercial *CFD* code. In this chapter, the numerical simulations are performed using several turbulence models for a solid concentration range of 30–60% (by weight) and the results are validated with experimental data. The effect of various parameters has been discussed in details in the following sections.

6.1 MULTIPHASE FLOW MODEL

The multiphase flow modeling approach is used for simulation of multiphase flow problems such as solid–gas, gas–liquid, liquid–solid etc. This approach is designed with the local variables of each phase in multiphase flow. The flow problems associated with multiphase are solved by two different approaches:

- Euler–Lagrange approach
- Euler–Euler approach

The Lagrangian discrete phase modeling in FLUENT follows Euler–Lagrange approach (Ansys, 2011). In Euler–Lagrange approach the fluid phase is taken as continuum and solved by Navier–Stokes equations whereas the solution of the dispersed phase is calculated by tracking number of droplets, bubbles and particles in the flow field. This dispersed phase can able to exchange the mass, momentum and energy with the fluid phase. Euler–Lagrange approach is considered to be simpler in the case where the particle–particle interactions are neglected. The use of this model inappropriate in liquid fuel combustion, spray dryers etc. (Peng and Cao, 2016). In Euler–Euler approach the different phases exists in the flow field are treated mathematically as interpenetration continuum. In this approach, the concept of the phasic volume fraction in presented i.e. the volume of the individual phase is not occupied by other existing phases in the flow field. The volume fraction of each phase is assumed as a function of time and space and their submission is equal to one. The conservation equations of every phase in the flow field are derived to obtain set of similar equations for each phase. In Euler–Euler multiphase approach is further discretized into three different models.

- Volume of fluid (*VOF*) model
- Mixture model
- Eulerian model

The *VOF* multiphase model works on the surface tracking technique. This model is mainly designed for immiscible fluids. In this model, fluids in the flow field share a single set of momentum equations. Also, the volume fraction of each fluid is tracked in the flow domain. The *VOF* model is used for free–surface flows, the motion of a large amount of bubbles in a liquid phase, stratified flows etc. (Ndinisa *et al.*2005; Akhtar *et al.*2007). The mixture model is designed for the flow problems having two or more phases, either fluid or particulate. As in Euler–Euler multiphase approach the phases are considered as interpenetrating continua. In mixture model the dispersed phases are described by solving mixture momentum equations. The mixture model is applied to bubbly flows, cyclone separator and sedimentation applications. The most complex model in the ANSYS FLUENT is Eulerian model. This model solves the set of momentum and continuity equations for each phase present in the flow field. The interface and pressure exchange coefficients are used to achieve the coupling of various phases. The Eulerian multiphase approach is used for fluidized bed, risers and particle suspension applications.

6.2 EULERIAN–MULTIPHASE MODEL

The Eulerian model for multiphase flow generally comprises of two phases. The liquid phase i.e. water is taken as primary phase (*p*) whereas the solid phase i.e. coal is considered as secondary phase (*s*). The solid concentration of the primary and secondary phases is represented as α_p and α_s. The Eulerian model is adopted in many studies in the past to investigate the flow properties of the high concentrated slurry suspension. The major governing equations and flow constants are given below.

6.2.1 Conservation of Mass

The continuity equation for the secondary phase can be used to estimate the volume fraction of primary phase as per the following equation:

$$\frac{\partial}{\partial t}(\alpha_s \rho_s) + \nabla.\left(\alpha_s \rho_s \vec{V_s}\right) = \sum_{p=1}^{n}(\dot{m}_{ps} - \dot{m}_{sp}) + S_s \quad (6.1)$$

Here $\vec{V_s}$ represents velocity of the secondary phase (solid), $\dot{m}_{sp}$ is mass transference from secondary to primary phase and $\dot{m}_{ps}$ is mass transference from primary to secondary phase.

6.2.2 Conservation of Momentum

The momentum balance equation for secondary and primary phase is yield as.

$$\frac{\partial}{\partial t}\left(\alpha_s \rho_s \vec{V_s}\right) + \nabla.\left(\alpha_s \rho_s \vec{V_s}\vec{V_s}\right) = -\alpha_s \nabla P + \nabla.\overline{\overline{\tau_s}} + \alpha_s \rho_s \bar{g} + \sum_{p=1}^{n}(\vec{R}_{ps} + \dot{m}_{ps}\vec{v}_{ps} - \dot{m}_{sp}\vec{v}_{sp}) + \left(\vec{F}_s + \vec{F}_{lift,s} + \vec{F}_{vm,s}\right) \quad (6.2)$$

$\overline{\overline{\tau_s}}$ represents secondary phase stress–strain tensor.

$$\overline{\overline{\tau_s}} = \alpha_s \mu_s \left(\nabla \vec{V_s} + \nabla \vec{V_s}^T\right) + \alpha_s (\lambda_s - \frac{2}{3}\mu_s)\nabla.\vec{V_s}\,\overline{\overline{I}} \quad (6.3)$$

Where λ_s and μ_s denotes the bulk and shear viscosity of secondary phase, $\vec{R}_{ps}$ is interaction force among phases, $\vec{F}_s$ is external force, $\vec{F}_{vm,s}$ is virtual force, $\vec{F}_{lift,s}$ lift force and P is pressure force.

Virtual force in multiphase flow is given by.

$$\vec{F}_{vm} = 0.5\alpha_s \rho_s \left(\frac{d_s \vec{V}_s}{dt} - \frac{d_p \vec{V}_p}{dt} \right) \tag{6.4}$$

6.2.3 Solid–liquid momentum equations

The momentum exchange between the primary and secondary phase is described by the multifluid granular model of FLUENT. The momentum conservation between the solid–liquid phases is represented by equation.

$$\frac{\partial}{\partial t}\left(\alpha_s \rho_s \vec{V}_s\right) + \nabla.\left(\alpha_s \rho_s \vec{V}_s \vec{V}_s\right) = -\alpha_s \nabla P - \nabla P_s + \nabla.\bar{\bar{\tau}}_s + \alpha_s \rho_s \vec{g} + \sum_{l=1}^{n} (K_{ps}\left(\vec{V}_p - \vec{V}_s\right) + \dot{m}_{ps} \vec{V}_{ps} - \dot{m}_{sp} \vec{V}_{sp}) + (\vec{F}_s + \vec{F}_{lift,s} + \vec{F}_{vm,s}) \tag{6.5}$$

Solid–liquid exchange coefficient K_{sp} can be represented as.

$$K_{sp} = \frac{\alpha_s \rho_s f}{\tau_s} \tag{6.6}$$

Where f is a function of drag coefficient, Reynolds number and flow velocity for Syamlal–Obrien model and τ_s represents the particle relation time as defined below.

$$\tau_s = \frac{\rho_s d_s^2}{18\mu_l} \tag{6.7}$$

$$f = \frac{C_D \operatorname{Re}_s \alpha_l}{24 V_{r,s}^2} \tag{6.8}$$

Drag coefficient derived in form of Reynolds number and flow velocity is used as discussed by (Nayak and Chatterjee, 2017a). The model Syamlal–Obrien is based on measurements of particle velocities in the settled and fluidized bed with correlations which are dependent on Reynolds number and volume fraction. Symbols *s* and *p* represents the secondary and primary phase.

$$\mathrm{Re}_s = \frac{\rho_p d_s \left|\vec{V}_s - \vec{V}_p\right|}{\mu_p} \tag{6.9}$$

The exchange coefficient between secondary and primary phase is represented by equation below.

$$K_{sp} = \frac{3\alpha_s \alpha_p \rho_p}{4V_{r,s}^2 d_s} C_D \left(\frac{\mathrm{Re}_s}{V_{r,s}}\right) \left|\vec{V}_s - \vec{V}_p\right| \tag{6.10}$$

whereas $V_{r,s}$ symbolizes the flow velocity correlation for secondary phase.

$$V_{r,s} = 0.5\left(Z - 0.06\,\mathrm{Re}_s + \sqrt{(0.06\,\mathrm{Re}_s)^2 + 0.12\,\mathrm{Re}_s (2W - Z) + Z^2}\right) \tag{6.11}$$

with

$Z = \alpha_p^{4.14}$ and $W = 0.8\alpha_p^{1.28}$.

6.2.4 Shear stress in solid particles

The shear stress tensor in the solid particles contains the bulk and shear viscosity arises from solid particle momentum exchange due to collision and translational motion. The viscosity component of friction was also taken into consideration that exists when the settling of solid particles occurs during transportation. The viscosity of solids is given by the addition of colloidal, frictional and kinematic parts as discussed by researchers (Nayak and Chatterjee, 2017b; Nayak *et al.*2015; Gidaspow *et al.*1992) is considered to analyze the granular temperature as mentioned below.

$$\varphi_{ps} = -3K_{ps}\theta_s \tag{6.12}$$

The interfacial momentum exchange factor K_{ps} is represented as given below.

$$K_{sp} = K_{ps} = \frac{3}{4}\frac{\alpha_s \alpha_p \rho_p}{V_{r,s}^2 d_s} C_D \left(\frac{\text{Re}}{V_{r,s}}\right) \left|\vec{v}_s - \vec{v}_p\right| \tag{6.13}$$

and drag coefficient C_D is written as

$$C_D = \left[0.63 + 4.8\left(\frac{\text{Re}_s}{V_{r,s}}\right)^{-0.5}\right]^2 \tag{6.14}$$

Reynolds number for secondary and primary phase is stated below.

$$\text{Re}_s = \frac{\rho_p d_p \left|\vec{v}_s - \vec{v}_p\right|}{\mu_p} \tag{6.15}$$

Whereas in equation $V_{r,s}$ is terminal velocity correlation for secondary phase which is accomplished when solid particle become zero. The value of $V_{r,s}$ is calculated for $\alpha_s \leq 0.85$ and $\alpha_s \geq 0.85$ is given by equation below.

$$V_{r,s} = 0.5\left(\alpha_p^{4.14} - 0.06\,\text{Re}_s + \sqrt{\left\{(0.06\,\text{Re}_s)^2 + 0.12\,\text{Re}_s\left(1.6\alpha_p^{1.28} - \alpha_p^{4.14}\right) + \alpha_p^{8.28}\right\}}\right) \tag{6.16}$$

$$V_{r,s} = 0.5\left(\alpha_p^{4.14} - 0.06\,\text{Re}_s + \sqrt{\left\{(0.06\,\text{Re}_s)^2 + 0.12\,\text{Re}_s\left(2\alpha_p^{2.65} - \alpha_p^{4.14}\right) + \alpha_p^{8.28}\right\}}\right) \tag{6.17}$$

6.3 VARIOUS TURBULENCE MODELING SCHEMES

6.3.1 SST k–ω turbulence Model

The SST *k–ω* turbulence Model is developed by Menter (1994) from the solution of standard *k–ε* and standard *k–ω* models to obtain the formulation for turbulence flow inside for flow through pipelines. The transportation equations for turbulence flow are represented below:

$$\rho\left(\frac{\partial k}{\partial t}+\frac{\partial}{\partial x_i}(ku_i)\right)=\frac{\partial}{\partial x_j}\left(\Gamma_k\frac{\partial k}{\partial x_j}\right)+G_k-Y_K+S_K \tag{6.18}$$

and

$$\rho\left(\frac{\partial \omega}{\partial t}+\frac{\partial}{\partial x_j}(\omega u_j)\right)=\frac{\partial}{\partial x_j}\left(\Gamma_\omega\frac{\partial \omega}{\partial x_j}\right)+G_\omega-Y_\omega+D_\omega+S_\omega \tag{6.19}$$

Whereas the terms G_k represents turbulence kinetic energy generation due to the occurrence of gradients in mean velocity, Γ_k and Γ_ω are diffusivities of k and ω, which are calculated from correlations given below. Dissipation rate of k and ω is represented by Y_k and Y_ω respectively. S_k and S_ω are source terms.

$$\Gamma_k=\mu+\frac{\mu_t}{\sigma_k} \tag{6.20}$$

$$\Gamma_\omega=\mu+\frac{\mu_t}{\sigma_\omega} \tag{6.21}$$

σ_k and σ_ω are prandtl numbers for turbulent flow for k and ω respectively. μ_t is turbulent viscosity which is calculated as follows.

$$\mu_t=\frac{\rho k}{\omega}\frac{1}{\max\left[\frac{1}{\alpha^*},\frac{SF_2}{a_1\omega}\right]} \tag{6.22}$$

Here S represents magnitude of strain rate.

$$\sigma_k = \frac{1}{F_1 / \sigma_{k,1} + (1-F_2) / \sigma_{k,2}} \tag{6.23}$$

$$\sigma_\omega = \frac{1}{F_1 / \sigma_{\omega,1} + (1-F_2) / \sigma_{\omega,2}} \tag{6.24}$$

F_1 and F_2 represent the blending functions which are given as.

$$F_1 = \tanh\left[\min\left[\max\left(\frac{\sqrt{k}}{0.09\omega y}, \frac{500\mu}{\rho y^2 \omega}\right), \frac{4\rho k}{\sigma_{\omega,2} D_\omega y^2}\right]\right]^4 \tag{6.25}$$

$$D_\omega = \max\left[2\rho \frac{1}{\sigma_{\omega,2}} \frac{1}{\omega} \frac{\partial k}{\partial x_j} \frac{\partial \omega}{\partial x_j}, 10^{-10}\right] \tag{6.26}$$

$$F_2 = \max\left[2\frac{\sqrt{k}}{0.09\omega y}, \frac{500\mu}{\rho y^2 \omega}\right] \tag{6.27}$$

6.3.2 Standard k–ε turbulence Model

The Standard *k–ε* turbulence model is proposed by Launder and Splading (1972). This two-equation model is based on the transportation equations for dissipation rate (*ε*) and turbulence kinetic energy (*k*). The Standard *k–ε* turbulence model is a semi–empirical type model and the equations of the model rely on empiricism and phenomenological considerations. The dissipation rate (*ε*) and turbulence kinetic energy (*k*) are obtained by the following expressions.

$$\frac{\partial}{\partial t}(\rho k) + \frac{\partial}{\partial x_i}(\rho k u_i) = \frac{\partial}{\partial x_j}\left[\left(\mu + \frac{\mu_t}{\sigma_k}\right)\frac{\partial k}{\partial x_j}\right] + G_k + G_b - \rho\varepsilon - Y_M + S_K \tag{6.28}$$

and

$$\frac{\partial}{\partial t}(\rho \varepsilon) + \frac{\partial}{\partial x_i}(\rho \varepsilon u_i) = \frac{\partial}{\partial x_j}\left[\left(\mu + \frac{\mu_t}{\sigma_\varepsilon}\right)\frac{\partial \varepsilon}{\partial x_j}\right] + C_{1\varepsilon}\frac{\varepsilon}{k}(G_k + C_{3\varepsilon}G_b) - C_{2\varepsilon}\rho\frac{\varepsilon^2}{k} + S_\varepsilon \tag{6.29}$$

Where G_k is the measure of turbulence kinetic energy generates due to the gradients in means velocity of flow; Y_M represents the compressibility on turbulence; S_k and S_ε are source terms; $C_{1\varepsilon}$, $C_{2\varepsilon}$ and $C_{3\varepsilon}$ are constants; σ_ε and σ_k are Prandtl numbers for ε and k.

6.3.3 RNG k–ε turbulence Model

The RNG k–ε model is derived by the technique called renormalization theory. This model is similar to the standard k–ε model but have some refinements. The additional terms of ε is included in the model to improve the flow accuracy. The addition of ε terms results in more reliability and accuracy of flows (Orszag *et al.*1993). The equations of RNG k–ε model is expressed below.

$$\frac{\partial}{\partial t}(\rho k) + \frac{\partial}{\partial x_i}(\rho k u_i) = \frac{\partial}{\partial x_j}\left[\alpha_k \mu_{eff} \frac{\partial k}{\partial x_j}\right] + G_k + G_b - \rho\varepsilon - Y_M + S_K \tag{6.30}$$

and

$$\frac{\partial}{\partial t}(\rho \varepsilon) + \frac{\partial}{\partial x_i}(\rho \varepsilon u_i) = \frac{\partial}{\partial x_j}\left[\alpha_k \mu_{eff} \frac{\partial \varepsilon}{\partial x_j}\right] + C_{1\varepsilon}\frac{\varepsilon}{k}(G_k + C_{3\varepsilon}G_b) - C_{2\varepsilon}\rho\frac{\varepsilon^2}{k} - R_\varepsilon + S_\varepsilon \tag{6.31}$$

6.3.4 Realizable k–ε turbulence Model

The Realizable k–ε model is different from standard k–ε as it has an alternate formulation for turbulence viscosity (Shish *et al.*1994). Also, the equation for dissipation rate ε is derived from the exact solution of mean–square velocity.

$$\frac{\partial}{\partial t}(\rho k) + \frac{\partial}{\partial xj}(\rho k uj) = \frac{\partial}{\partial x_j}\left[\left(\mu + \frac{\mu_t}{\sigma_k}\right)\frac{\partial k}{\partial x_j}\right] + G_k + G_b - \rho\varepsilon - Y_M + S_K$$

(6.32)

and

$$\frac{\partial}{\partial t}(\rho \varepsilon) + \frac{\partial}{\partial x_j}(\rho \varepsilon u_j) = \frac{\partial}{\partial x_j}\left[\left(\mu + \frac{\mu_t}{\sigma_\varepsilon}\right)\frac{\partial \varepsilon}{\partial x_j}\right] + \rho C_1 S_\varepsilon + C_{1\varepsilon}\frac{\varepsilon}{k}C_{3\varepsilon}G_b - C_2\rho\frac{\varepsilon^2}{k + \sqrt{\nu\varepsilon}} + S_\varepsilon \tag{6.33}$$

Where

$$C_1 = \max\left[0.43, \frac{\eta}{\eta + 5}\right], \eta = S\frac{k}{\varepsilon}, S = \sqrt{2S_{ij}S_{ij}}$$

Where G_k the measure of turbulence kinetic energy generates due to the gradients in means velocity of flow; Y_M represents the compressibility on turbulence; S_k and S_ε are source terms; $C_{1\varepsilon}$, $C_{2\varepsilon}$ and $C_{3\varepsilon}$ are constants; σ_ε and σ_k are Prandtl numbers for ε and k.

6.4 DETAILS OF INPUT PARAMETERS USED IN CFD CODE

Modeling and numerical simulation for head loss across bend geometries at different *r/D* ratios is performed on a commercial Computational Fluid Dynamics (CFD) tool, ANSYS–R15.0. Figure 6.1 represents the geometry of pipe bend having a diameter of 50 mm. The length of pipe from inlet and outlet of the bend is extended to 1000 mm, to achieve a fully developed and steady flow across the bend section. Pipe material is mild steel with a density of 7850 kg/m^3. The *r/D* ratio is varied within the range of 1.5–3.0. The flowing media is possessed two–phase fluid having water as a primary phase and coal/coal–ash as a secondary phase. The viscosity of primary phase is taken as 0.001 Pa.s. The mean particle diameter of coal, fly ash and bottom ash is calculated as 16, 97 and 110 μm from the particle size distribution. The solid concentration of the coal–water suspension is calculated in terms of volume fraction as 0.22, 0.30, 0.39 and 0.49 for weight concentrations of 30, 40, 50 and 60% respectively. A multiphase Eulerian approach along with an SST k–ω scheme is adopted to determine the flow characteristics of the slurry suspension in the pipe bend.

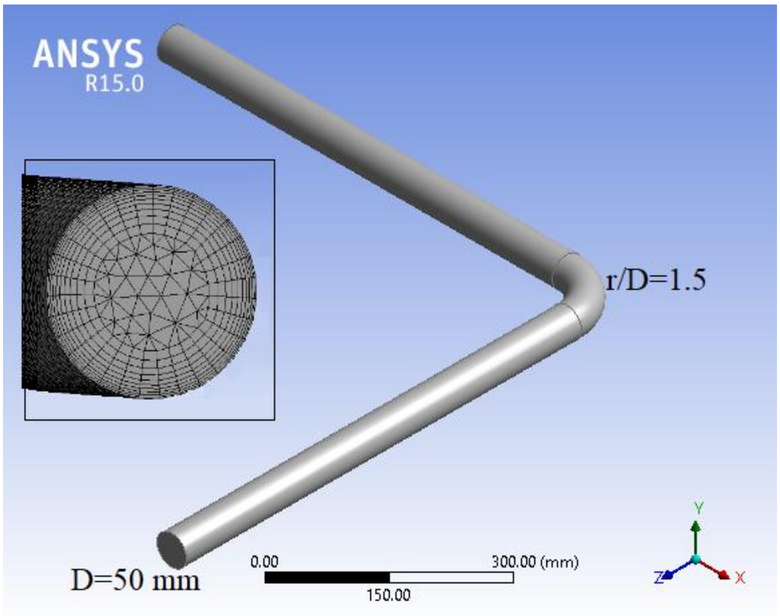

Figure 6.1. Geometry and meshing of pipe bend

6.4.1 Boundary Conditions

The calculation of domain is bonded by the three surfaces (i.e. inlet, outlet and wall). The inlet boundary of the pipe is introduced with the flow velocity and volume fraction of solid–liquid slurry suspension. The liquid and solid particle velocity at the inlet of the pipe is assumed to be uniform and solid particles are treated as uniformly distributed during flow. The shape of solid particles is considered to be angular. The liquid phase is assumed to follow no-slip condition along the pipe wall and standard functions of the wall are defined. Slip conditions between the solid particles and pipe wall are applied as outlined by Johnson and Jackson (1987).

$$\tau_{sw} = \frac{\sqrt{3}}{6}\pi\rho g\Phi\frac{\alpha_s}{\alpha_{s,\max}}\sqrt{\theta_{si}u_{siw}} \tag{6.28}$$

$$q_{wi} = \frac{\sqrt{3}}{6}\pi\rho g\Phi\frac{\alpha_s}{\alpha_{s,\max}}\sqrt{\theta_{si}}\left(u_{siw}\right)^2 - \frac{\sqrt{3}}{4}\pi\rho g\left(1-e^2\right)\frac{\alpha_s}{\alpha_{s,\max}}\theta^{3/2} \tag{6.29}$$

The outlet boundary conditions are applied at a 1000 mm long outlet cross–section of pipe geometry which has an identical grid structure. Pressure and velocity is coupled through a SIMPLEX algorithm. The surface roughness and roughness constant for the pipe wall is taken as 0.5 for CFD simulations. In the computational process, the first-order scheme is used for solving turbulence dissipation rate, head loss correction, momentum and turbulence kinetic energy. To achieve convergence of simulations in less time, the relaxation factors for momentum, pressure, kinetic energy and dissipation rate are taken as 0.7, 0.3, 0.8 and 0.8 respectively. The convergence criterion for simulation parameters is taken as 10^{-5}. All numerical simulations are performed on Intel Xenon E51607–v2, a Windows®10 based machine having a 3.41GHz processor and 16GB of RAM.

6.4.2 Grid independence test

The whole bend geometry is discretized into a number of small cells having tetrahedral cooper type structure as shown in Figure 6.1. A 10 layer boundary region with a growth rate of 20% is created near a wall so as obtain the y^+ value of 30. Grid–independence tests are carried out to optimize the population of cells in the bend geometry. Mesh is generated uniformly in ANSYS R15.0 with four different mesh sizes. The mesh sizes of 4, 5, 6 and 7 mm have 519470, 312811, 209285 and 141823 elements respectively. After mesh generation, simulations are carried out for coal–water slurries at a solid concentration of 30% (by weight) for flow velocity of 2 m/s. The mean particle diameter of coal is calculated as 16 μm.

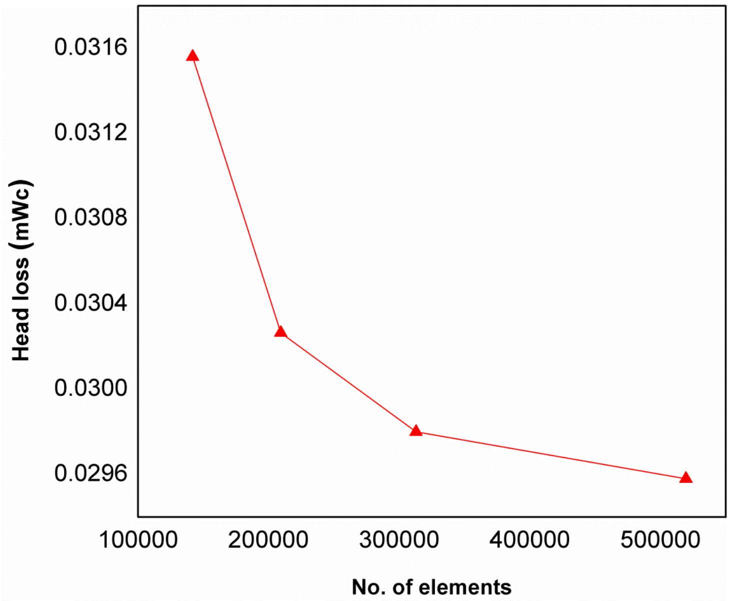

Figure 6.2: Head loss variation with number of elements in mesh

Figure 6.2 depicts the variation in the head loss as a function of the number of elements in the discretized bend geometry. The results indicate that variations in head loss become independent as the number of elements in the mesh approaches to 312811. The error occurs due to grid discretization is measured by the grid convergence index (GCI) given by Roache (1997).

$$GCI^{ab} = F_s \frac{e_r^{ab}}{r^p - 1} \tag{6.30}$$

Where e_r = relative error among two grid sizes $\left|\frac{\Delta H_a - \Delta H_b}{\Delta H_a}\right|$, and ΔH_a & ΔH_b are head loss values for two different mesh sizes, F_s = safety factor taken as 3.

In the present study, a GCI is used to calculate the variation between the head loss of two different mesh sizes. GCI is applied at three levels to determine the appropriate relative error among every mesh size. Figure 6.3 illustrates the relative error between various levels divided by grid size. From the results, it is noticed that the lowest value of GCI is 0.12 (for level 1–2). So, the mesh with an element size of 5 mm possesses the minimum relative error among the different mesh sizes used in the study.

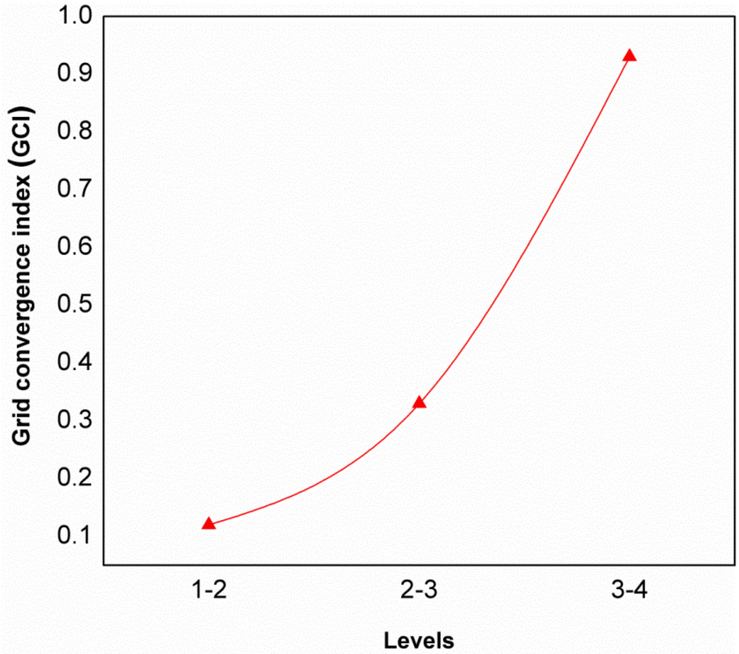

Figure 6.3: Variation of GCI index with cell size for different meshes.

6.5 VALIDATION OF NUMERICAL MODEL

The numerical simulations are performed to compare the computational results with data obtained from experimentation. Different turbulence models available in the fluent are applied by using identical boundary conditions. Numerical simulations are done on 50 mm diameter bend geometries having 1000 mm of pipe at the inlet and outlet sections of the bend. SST k–ω, Standard k–ω, Standard k–ε, RNG k–ε and Realizable k–ε modeling schemes are used to predict the head loss in 90˚ pipe bend with a radius of curvature of 75 mm. The solid concentration is taken as 60% with a mean particle size of 16 μm. The variation of experimental results with various turbulence schemes are plotted in Figure 6.4. The results indicate that the minimum deviation in head loss characteristics from experimental data is obtained as 6.81% by adopting an SST k–ω modeling scheme. The deviation between experimental results and results obtained by the Standard k–ω, Standard k–ε, RNG k–ε and Realizable k–ε modeling schemes are 7.93, 9.84, 11.25 and 13.25 % respectively. It is observed that the SST k–ω modeling scheme established a close agreement with experimental results and thus used in further investigation.

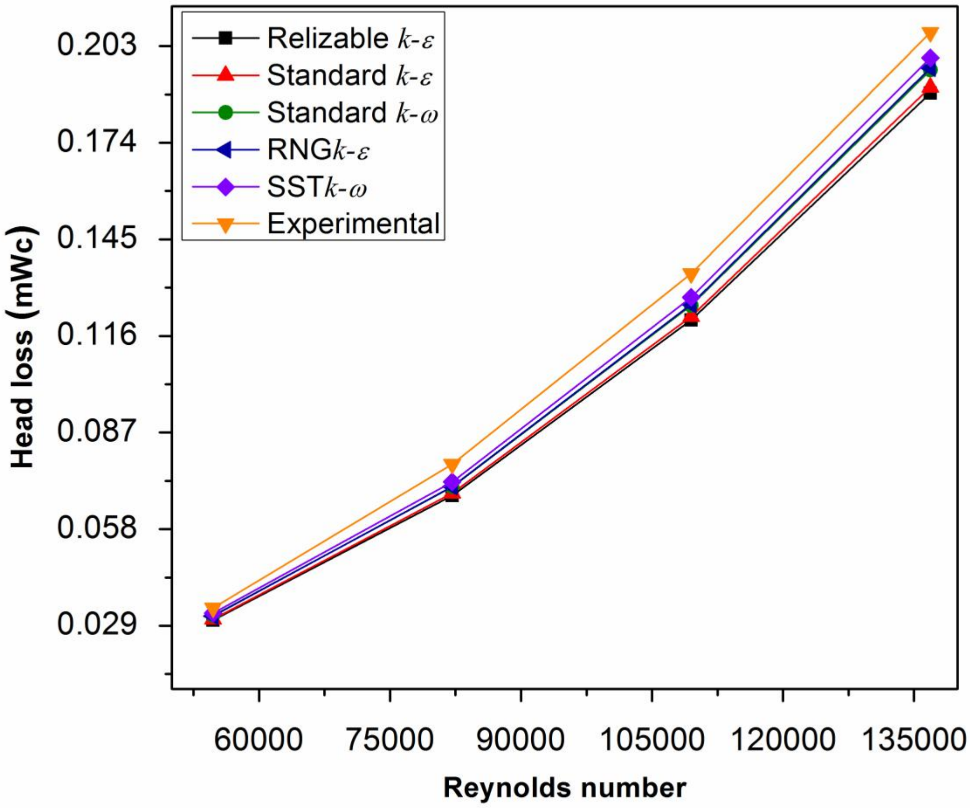

Figure 6.4: Validation of numerical simulations with experimental results.

6.6 HEAD LOSS CHARACTERSTICS OF 90˚ PIPE BEND FOR COAL AND COAL–ASH SLURRY

6.6.1 Influence of solid concentration on head loss characteristics

A series of numerical simulations are executed to examine the effect of solid concentration on head loss for the transportation of fine particulate coal–water slurry suspension. Head loss characteristics are studied across 90˚ pipe bend having an *r/D* ratio of 1.5. The solid concentration is varied within the range of 30–60% for flow velocity range of 2-5 m/s. The variation in head loss with solid concentration and Reynolds number for coal and coal–ash slurry is represented in Figure 6.5–6.7. From Figure 6.5, it is noticed that head loss is a function of both solid concentration and Reynolds number. As the Reynolds number of the slurry suspension is increased the head loss across the pipe bend also increased. This increase in head loss is examined due to an increase in turbulence. As the molecular momentum exchange in flow increases, the flow becomes disturbed and hence, losses in the flow increases, which indeed results in higher head loss. It is also observed that increase in solid concentration also enhance head loss. The rate of increase in head loss is higher as solid concentration increases from 50 to 60%. This increase in head loss with solid concentration is noted due to an increase in the slurry viscosity at higher concentrations. The viscosity is increased because number of coal particles per unit volume of water increases as the concentration of solid suspension increases (Matousek, 2009; Kaushal *et al.* 2005; Gopaliya and Kaushal, 2016). The presence of more coal particles results in a greater resistive force, which results in an increase in viscosity. The head loss is increased by 2.56, 4.12 and 10.87% as solid concentration increased from 30–40, 40–50 and 50–60% for change in Reynolds number of 1.36×10^5–8.39×10^4, 8.39×10^4–4.98×10^4 and 4.98×10^4–3.96×10^4. For a solid concentration of 60% the head loss is increased by 120.21, 76.73 and 56.35 % as the Reynolds number increases from 1.58×10^4–2.37×10^4, 2.37×10^4–3.17×10^4 and 3.17×10^4–3.96×10^4.

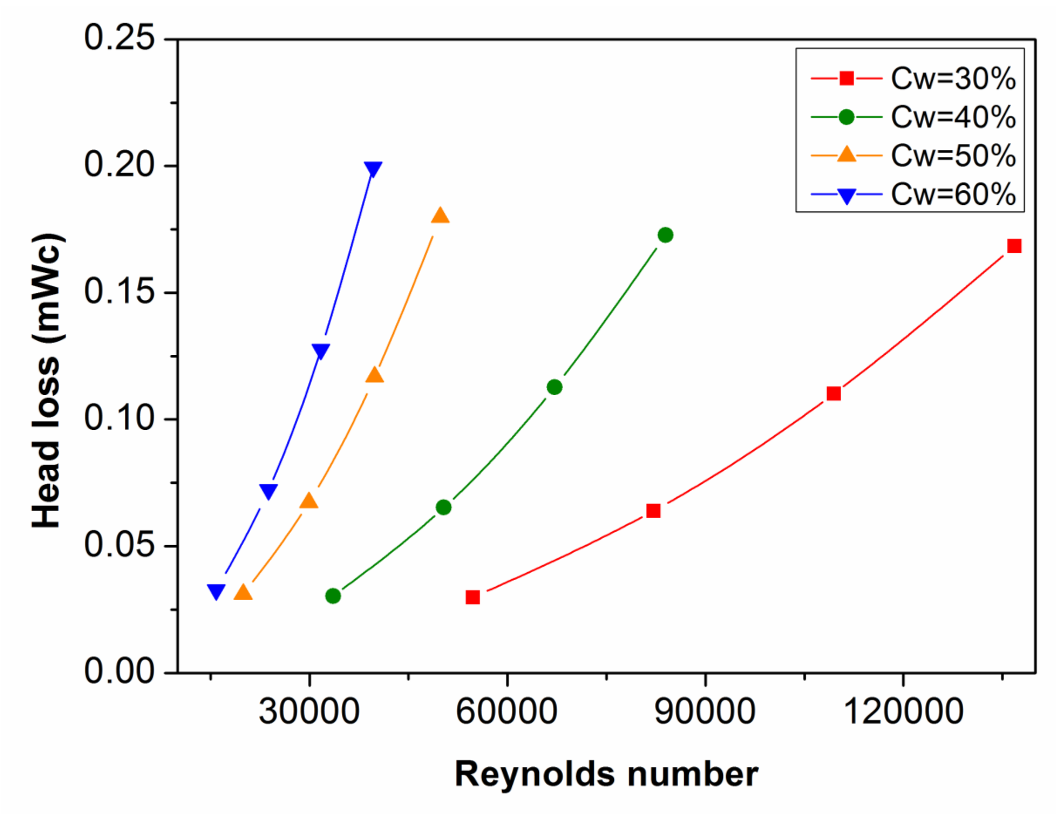

Figure 6.5: Variation in head loss against flow velocity and solid concentration for coal–water slurry

A similar set of numerical simulations are carried out for fly ash and bottom ash slurries. The solid concentration range is taken the same as coal–water slurry i.e. 30–60% (by weight). Figure 6.6–6.7 represents a similar trend as observed in the case of coal–water slurry. As the solid concentration and Reynolds number of fly and bottom ash slurry is increased, the head loss across the pipe bend is also increased. The phenomenon of change in head loss with change in Reynolds number is discussed earlier. This occurs due to an increase in turbulence inside pipe bend. From Figure 6.6, it is observed that the fly ash slurry shows high head loss than coal–water slurry. The head loss is increased about 1.41, 1.69, 2.03, and 2.46 times as compared to coal–water slurry at a solid concentration of 30, 40, 50, and 60% (by weight) for flow velocity of V = 2 m/s. As compared to coal–water slurry, head loss is 1.492, 1.778, 2.110, and 2.489 times higher at solid concentration of 30, 40, 50, and 60% (by weight) for V = 3 m/s; 1.543, 1.828, 2.144, and 2.491 times higher at solid concentration of 30, 40, 50, and 60% (by weight) for V = 4 m/s; & 1.578, 1.857, 2.186, and 2.532 times higher at solid concentration of 30, 40, 50, and 60% (by weight) for V = 5 m/s. The major difference between coal and fly ash is the shape and their density. The density of fly ash particles is higher as compared to the coal–water slurry. The spherical shaped particles provide large packing fraction in a unit volume as compare to coal particles. So, due to the large packing fraction the higher chances of settling and other attractive forces which causes the high head loss (Norton *et al.* 1986; Iyer, 2002; Elrahman and Hillemeier, 2014).

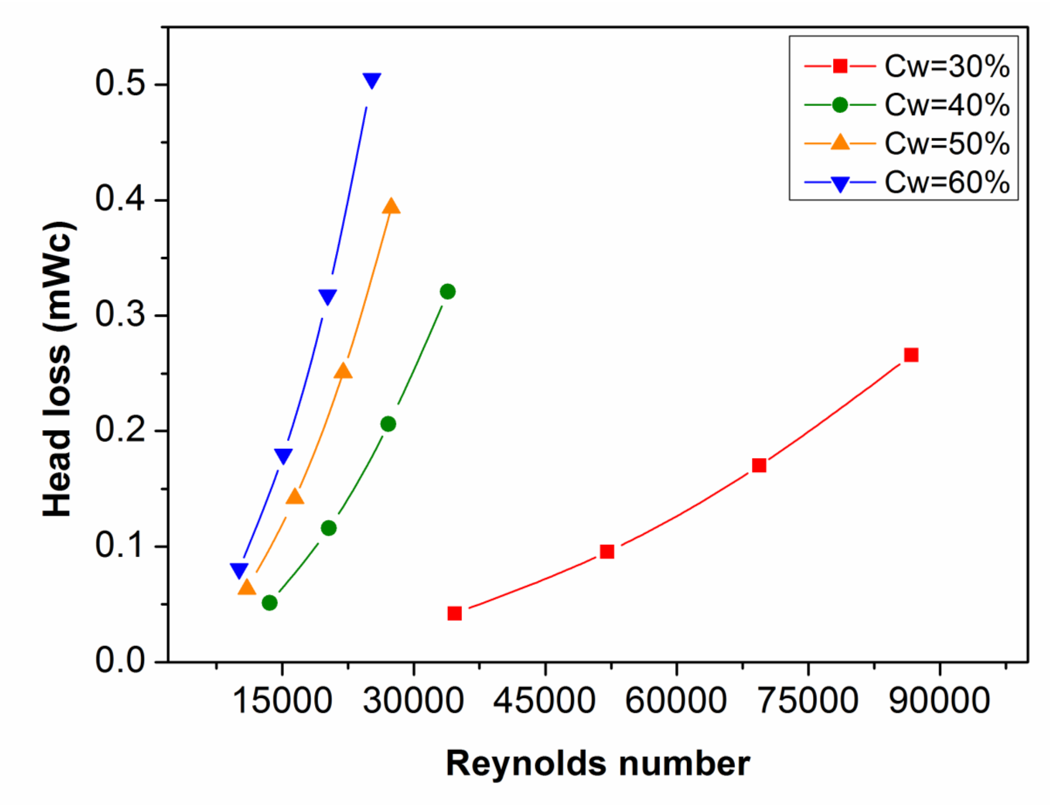

Figure 6.6: Variation in head loss against flow velocity and solid concentration for fly ash slurry

Figure 6.7 shows that the head loss occurs for the flow of bottom ash slurry is higher as compared to coal–water slurry and lower as compared to the fly ash slurry. It is seen that the head loss due to bottom ash is 1.393, 1.631, 1.938, and 2.343 times higher than coal–water slurry at a solid concentration of 30, 40, 50, and 60% (by weight) at $V = 2$ m/s. As compared to coal–water slurry, it is 1.456, 1.695, 1.985, and 2.336 times higher at solid concentration of 30, 40, 50, and 60% (by weight) at $V = 3$ m/s; 1.492, 1.727, 2.008, and 2.350 times higher at solid concentration of 30, 40, 50, and 60% (by weight) at $V = 4$ m/s; and 1.516, 1.754, 2.059, and 2.393 times higher at solid concentration of 30, 40, 50, and 60% (by weight) at $V = 5$ m/s. The order of head loss with change in concentration and velocity is as given follow:

- Fly ash > Bottom ash > Coal.

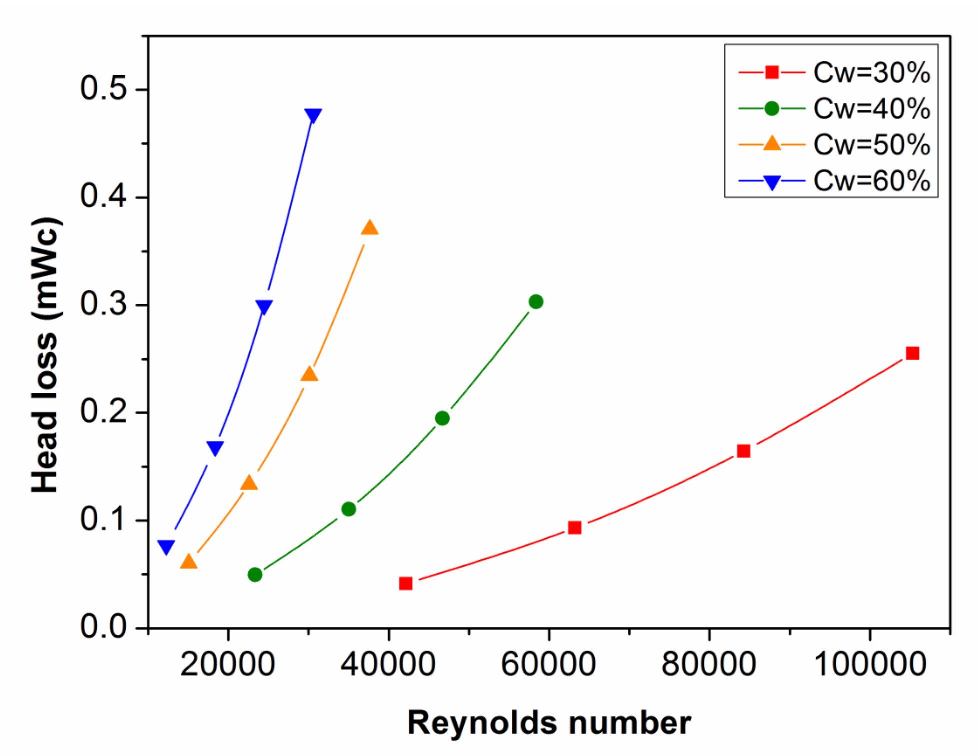

Figure 6.7: Variation in head loss against flow velocity and solid concentration for bottom ash slurry

It is also seen that bottom ash and coal slurry shows lower head loss than the fly ash slurry. The earlier discussed reason is the packing fraction and density. Apart from this reason, the comparative analysis reveals that the coal–water slurry shows the lower head loss than bottom ash. The bottom ash particles possess blocky irregular microstructure whereas coal ash particle possess knife–edge conical microstructure. The irregularities in the particle microstructure are higher in case of bottom ash particles. The irregularities in shape may impose drag forces due to flow of fluid (Mosa *et al.* 2014; Singh *et al.* 2018d). These drag forces contribute to turbulence and other losses occur due to fluid forces.

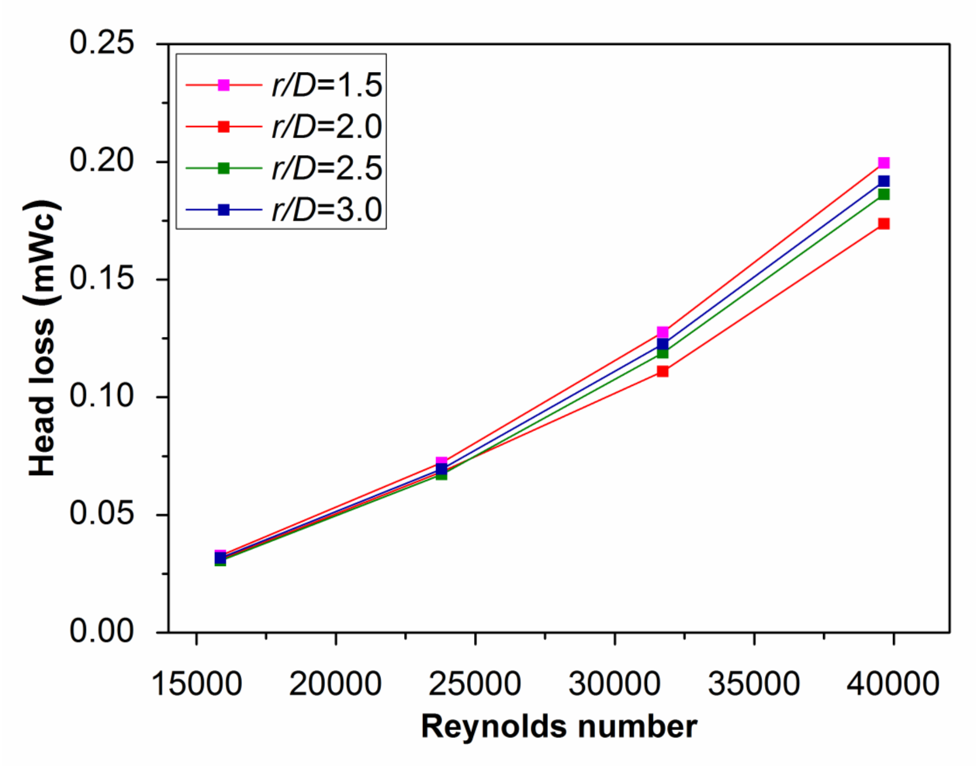

Figure 6.8: Effect of *r/D* ratio on the head loss with flow velocity for coal–water slurry

6.6.2 Influence of r/D ratio on head loss characteristics

The series of simulations are carried out on 90º pipe bends having *r/D* ratio ranging from 1.5–3.0 for flow of coal and coal–ash slurry suspension. The solid concentration of slurry is kept constant (i.e. 60% for flow velocity range of 2–5 m/s). Figure 6.8 represents the variation of head loss with *r/D* ratio and Reynolds number. From the results, it is seen that head loss in the pipe bend is enormously affected by varying the bend curvature. It is also observed that, as the *r/D* ratio is increased from 1.5 to 2.0 the head loss across the pipe bend is decreased. Moreover, further increase in the *r/D* ratio from 2.0 to 2.5 and 2.5 to 3.0 results in an increase in the head loss for the flow of coal–water slurry suspension. This decrease in head loss with an increase in *r/D* ratio from 1.5–2.0 is noticed due to a decrease in the flow separation phenomenon occurs inside the bend geometry during the flow of slurry. Also, it reduces the formation of secondary flows inside the pipe bend (Spedding *et al.* 2004; Crawford *et al.* 2007; Rohrig *et al.* 2015; Dutta *et al.* 2016). Hence, losses take place during flow is reduced, which further results in a decrease in head loss. However, as the *r/D* ratio further increased from 2.0 to 3.0, an increase in head loss is noticed. This increase in head loss is due to an increase in the effective length of the pipe bend. The increase in the length of pipe bend results in more frictional resistance for the flow of slurry. Therefore, an increase in *r/D* ratio from 2.0–3.0, further results in a higher head loss. As the *r/D* ratio is increased from 1.5–2.0 head loss is decreased by 5.23% at Reynolds number of 1.45×10^4. Furthermore, an increase in the *r/D* ratio from 2.0–2.5 and 2.5–3.0 results in an increase in the head loss by 1.39 and 3.66% respectively at Reynolds number of 1.45×10^4. At Reynolds number of 3.64×10^4 the head loss is decreased by 12.96% and increased by 7.21% as *r/D* ratio is increased from 1.5–2.0 and 2.0–2.5 respectively. Head loss is increased by 2.99% as the *r/D* ratio is increased from 2.5–3.0 at Reynolds number of 3.64×10^4. From the results, it is observed that minimum head loss is reported when the slurry is conveyed through a pipe bend having an *r/D* ratio 2.0. Rawat *et al.* (2016) have also reported a similar type of observation during the numerical analysis for the flow of solid-liquid slurry.

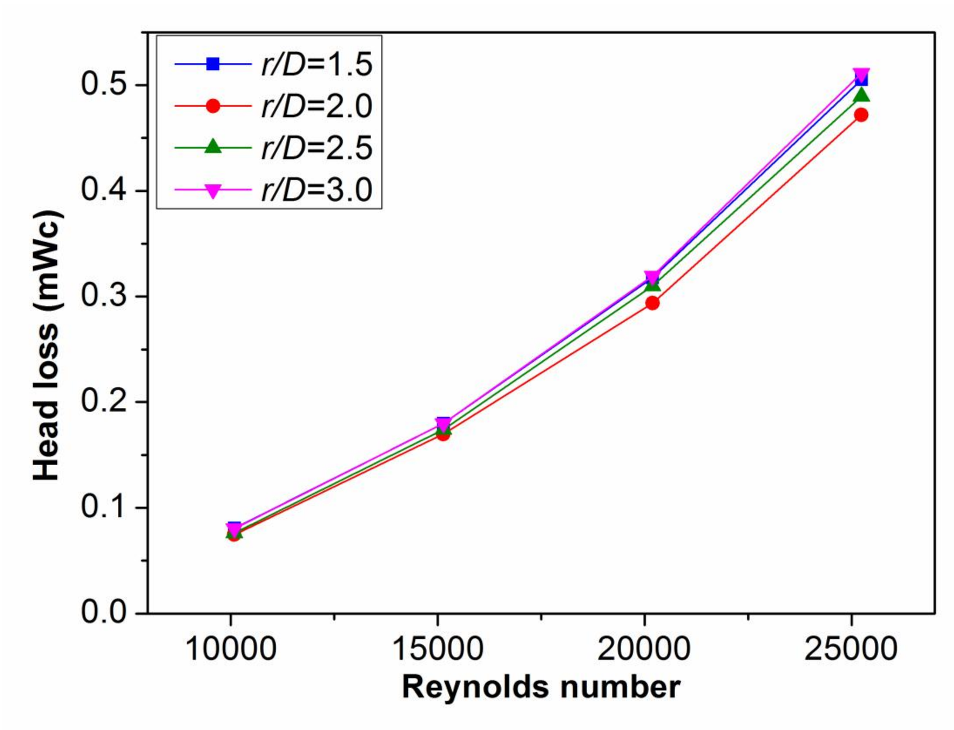

Figure 6.9: Effect of *r/D* ratio on the head loss with flow velocity for fly ash slurry

Numerical simulations are also carried out to analyze the effect of *r/D* ratio on head loss characteristics for fly ash and bottom ash slurries. The solid concentration range is taken the same as for coal–water slurry i.e. 60% (by weight). The *r/D* ratio is varied as 1.5–3.0. The effect of *r/D* ratio on head loss characteristic across 90˚ pipe bend (*D* = 50 mm) for coal–ash slurries is shown in Figure 6.9–6.10. A similar type of trend is observed as noticed in the case of coal–water slurry. The head loss is found minimum for *r/D* = 2.0.

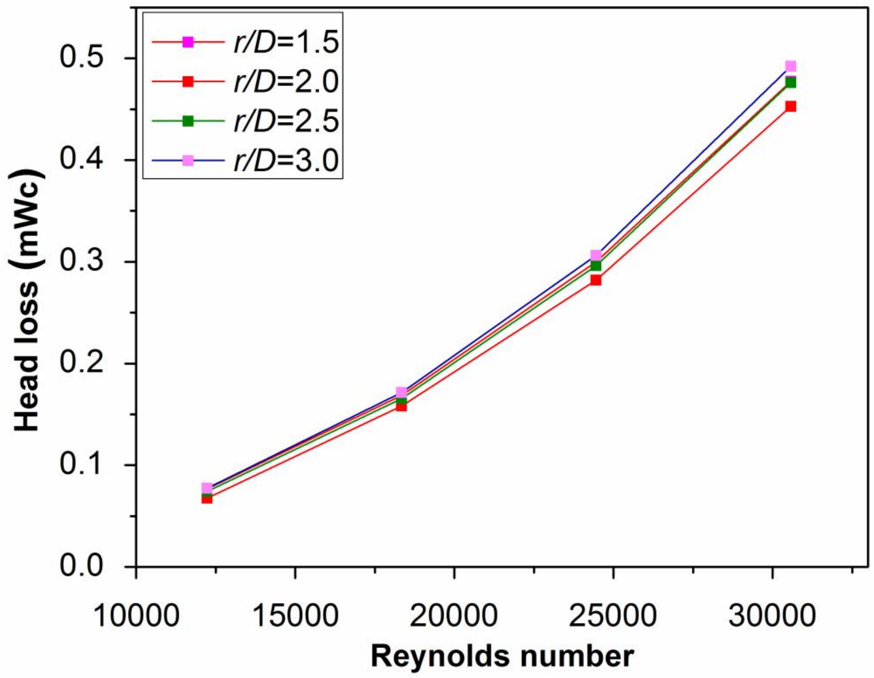

Figure 6.10: Effect of *r/D* ratio on the head loss with flow velocity for bottom ash slurry

6.6.3 Volume fraction contours

Volume fraction contours for the variation of flow velocity

The results obtained from the Eulerian approach for the volume fraction distribution of coal and coal ash slurry suspensions at various locations of bend geometry have been shown in Figures 6.11–6.13. The volume fraction contours are represented at bend locations of 0°, 30°, 45°, 60° and 90°. The inlet and outlet section of bends are considered as 0° and 90° respectively. Figure 6.11 represents the effect of flow velocity on volume fraction distribution at a solid concentration of 60% for a pipe bend having an *r/D* ratio 1.5. The contours of volume fractions are shown for a velocity range of 2–5 m/s. It is noticed that, at the inlet section of a bend, a higher concentration zone is found at the bottom of the pipe for flow velocity of 2 m/s. The higher concentration zone is shifted to the extrados wall of pipe bend as the flow proceeded from the inlet to the outlet section of the pipe bend. At the outlet of bend geometry, the volume fraction zone was almost symmetric about the horizontal axis. As the flow velocity of the slurry is increased from 2–5 m/s, the existence of higher a concentration zone at the inlet of the pipe bend is reduced. The minimum settling of solid particles is noticed at a flow velocity of 5 m/s. The minimum accumulation of solid particles is observed at the intrados region of bend, as the curvature angle is varied from 30–90°. It is observed that, at higher flow velocities, the maximum concentrated zone is reduced and forced to the extrados wall of the bend. The minimum concentrated zone is increased from the intrados wall towards the center of the pipe bend. The accumulation of the solid phase on bottom half of the pipe at lower velocities occurs due to a gravitational effect. Different researchers made similar type of observation for the flow inside pipe. (Akilli *et al.* 2001; Peters and Lith, 2004; Deng *et al.* 2005; Kuan *et al.* 2007; Spedding and Benard, 2007).

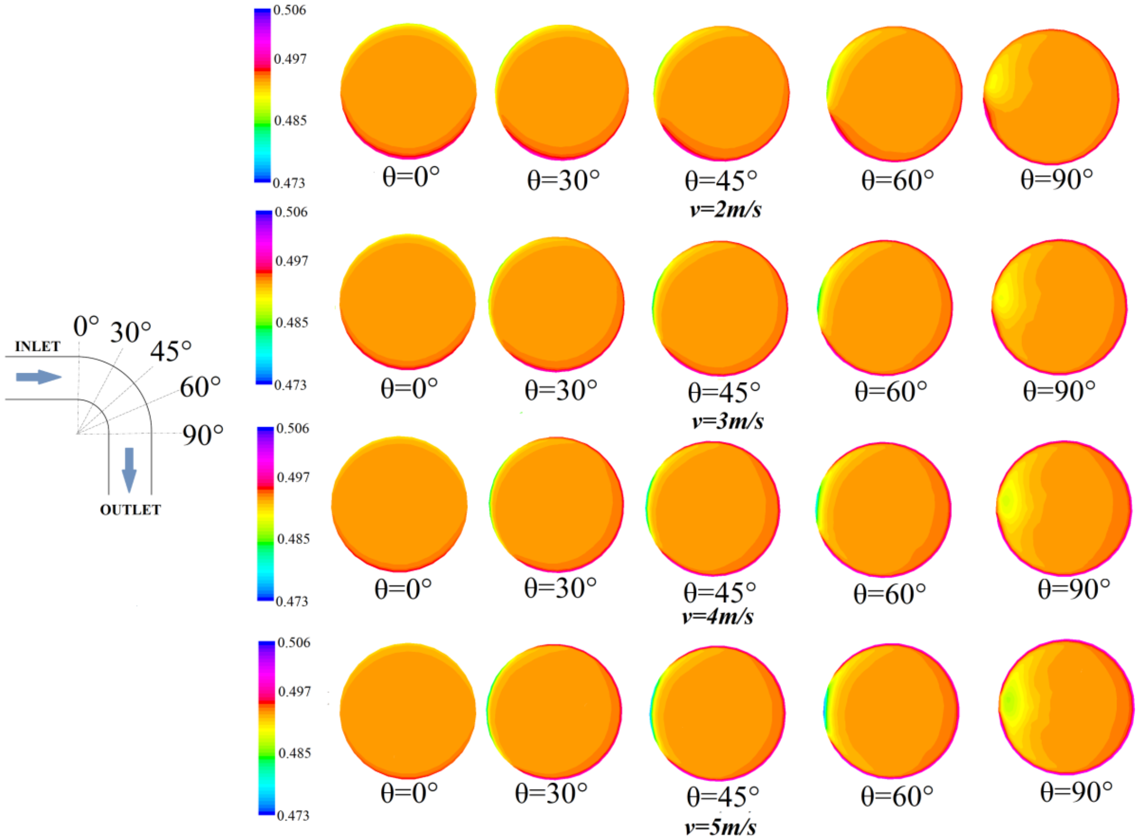

Figure 6.11: Volume fraction contours of coal–water slurry (C_w =60%) flowing at different velocities

The volume fraction contours are taken out at various bend locations of 0°, 30°, 45°,60° and 90°. The angle 0° and 90° represents the inlet and outlet section of bends. Figure 6.12 shows the volume fraction distribution at different velocities for fly ash and bottom ash slurry at C_w = 60% and r/D = 1.5. The velocity is varied in range 2 to 5 m/s. A higher concentration zone is seen at the bottom of the pipe at inlet bend section (0°). The higher concentration zone shift toward the extrados wall of pipe bend as the flow proceeded from the inlet section (0°) to the outlet section (90°) of the pipe bend. The volume fraction phenomenon doesn't change much from coal–water slurry in terms of bend locations. However, it seems to be changed as the slurry changes to fly and bottom ash. By comparison of volume fraction contours, it can be said that the volume fraction magnitude is higher for fly ash slurry. This may be due to the high density of fly ash particles. The high density of fly ash particles contributes in high settling and head losses. The lower concentration zone is observed wider in case of fly ash as compared to coal–water slurry. Similarly, the higher concentration zone observed at the extrados wall of pipe bend is also wider in case of fly ash slurry. Furthermore, the high settling is noticed at the bottom of pipe bend in case of fly ash slurry.

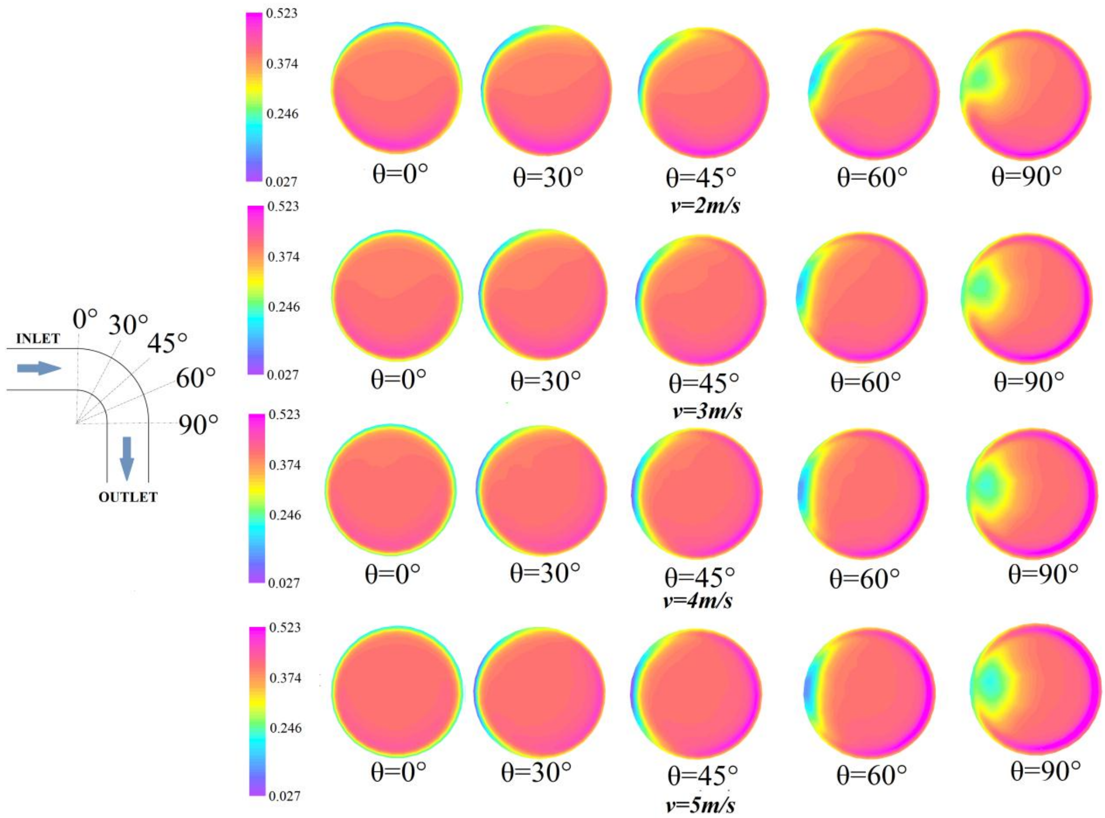

Figure 6.12: Volume fraction contours of fly ash slurry (C_w =60%) flowing at different velocities

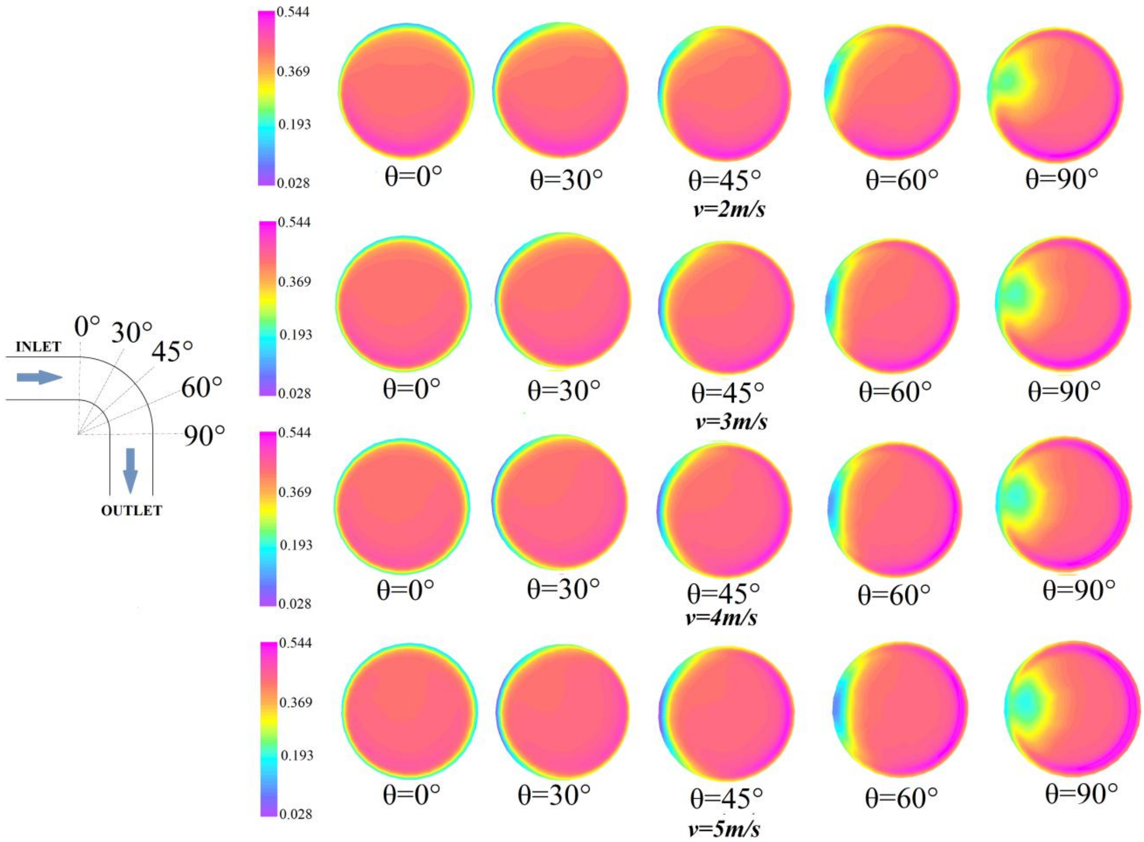

Figure 6.13: Volume fraction contours of bottom ash slurry (C_w =60%) flowing at different velocities

By comparing Figure 6.12 and 6.13, it could be noticed that the bottom ash showed a similar type of phenomenon as observed in fly ash slurry. The volume fraction magnitude of bottom ash slurry is found higher than fly ash slurry. This is observed because the bottom ash particles are coarser than fly ash as discussed in *PSD* section in chapter 3.

Volume fraction contours for the variation of solid concentration

The variation of volume fraction distribution with solid concentration is represented in Figure 6.14. The obtained volume fraction contours revealed that, as the efflux concentration is increased from 30–60%, the settling of the solid phase increased. At the inlet of bend the maximum concentrated zone is observed at the bottom of the pipe whereas, the width of the concentrated zone increased with solid concentration. It is also revealed that the higher concentrated zone is relocated from the bottom of pipe to the extrados wall as the slurry is conveyed from the inlet to outlet section of bend.

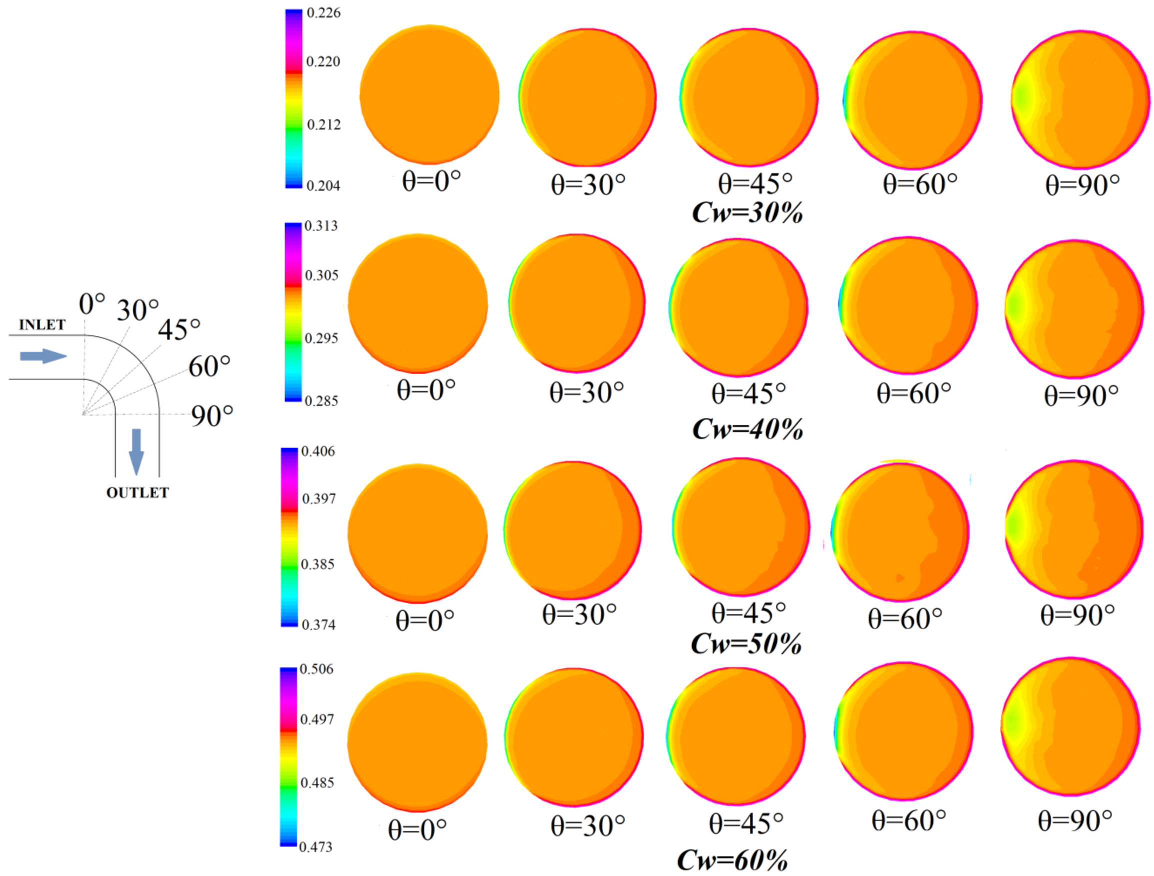

Figure 6.14: Volume fraction contours of coal–water slurry at different concentrations for flow velocity of 5 m/s

Volume fraction contours obtained at the outlet of the bend shows that the area of higher concentration zone increased along the pipe wall and also at the lower surface of pipe bend as the concentration of the slurry is increased. The volume fraction contours are taken out at various locations of pipe bend at different solid concentrations lies in range 30–60% (by weight). Figure 6.15–6.16 shows the volume fraction distribution at different solid concentrations for coal–ash slurries at V = 5 m/s and r/D = 1.5. Figure 6.15 represents the variation in volume fraction contours at different solid concentrations for fly ash-water slurry. From results, it is noticed that as the solid concentration of fly ash slurry is increased from 30-60% the colour patter of volume fraction contours for solid phase changes. The maximum accumulation at the inlet of bend is observed at the bottom side of pipe bend. However, the region of accumulation of solid phase is shifted towards the extrados wall as the flow proceeds from inlet to outlet.

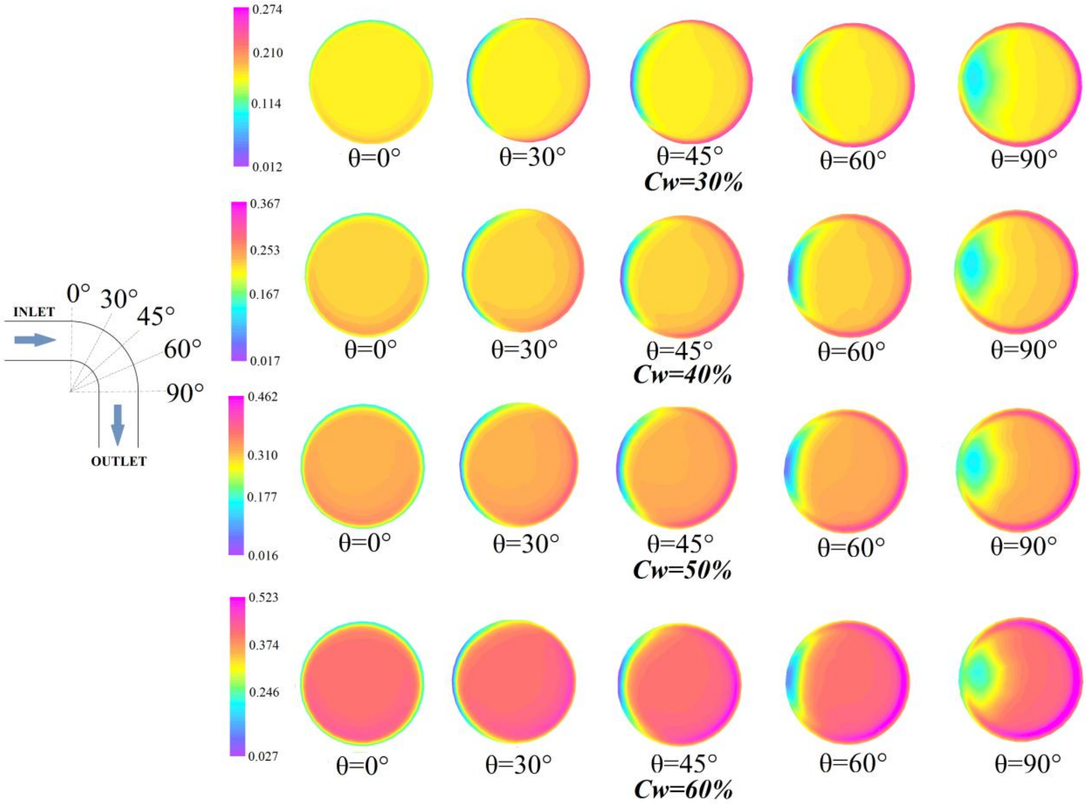

Figure 6.15: Volume fraction contours of fly ash slurry at different concentrations for flow velocity of 5 m/s

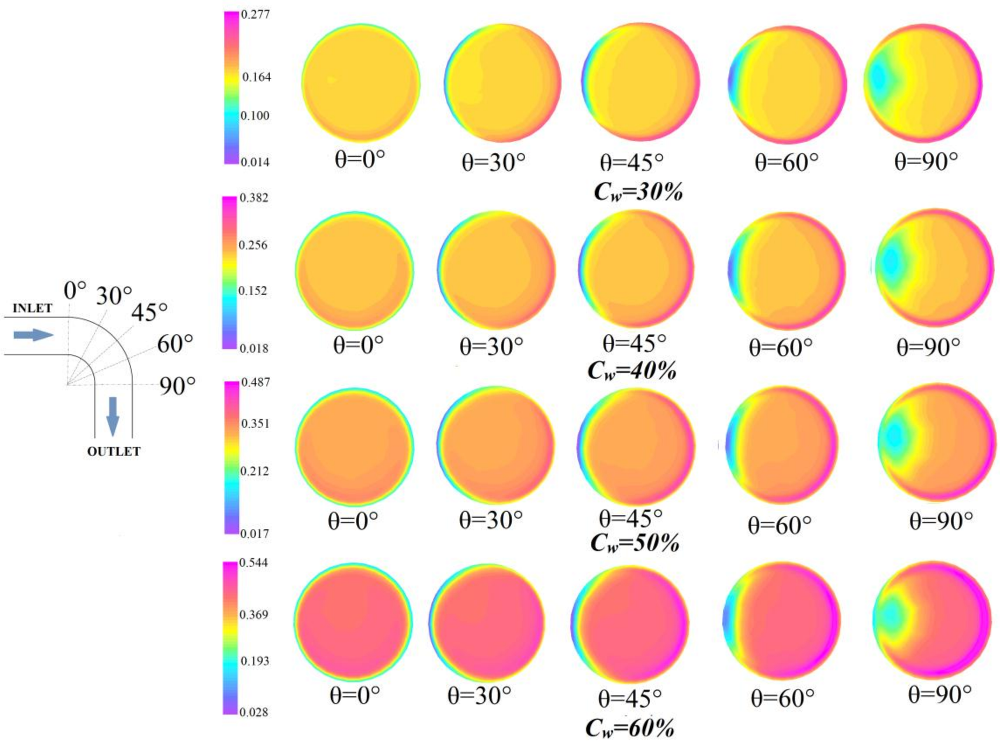

Figure 6.16: Volume fraction contours of bottom ash slurry at different concentrations for flow velocity of 5 m/s

The maximum accumulation of solid phase is observed for 60% solid concentration slurry. This is due to the presence of more solid particles in per unit volume of slurry at high concentrations. A similar phenomenon as observed for coal-water and fly ash slurry of concentrated zone's shifting is noticed in the case of bottom ash slurry as shown in Figure 6.16. By comparison, it is seen that the magnitude of efflux concentration of fly ash slurry is higher than coal–water slurry. This confirms the settling phenomenon of slurry, which dominates more in case of fly ash. At different locations of the pipe bend, the minimum concentration zone seems wider than coal–water slurry. Moreover, the solid concentration dominates in higher extent than coal–water slurry.

Volume fraction contours for the variation of r/D ratio of the pipe bend

The effect of *r/D* ratio on volume fraction distribution of coal–water slurry is shown in Figure 6.17. The result shows that, as *r/D* ratio is increased from 1.5–3.0, the lower concentration zone observed at the intrados wall of the pipe bend is decreased. This shows that flow separation and the generation of secondary flows inside the pipe bend are suppressed. From the contours, it is also seen that the high concentration zone continue decreasing as *r/D* ratio approached its maximum (i.e. 3.0).

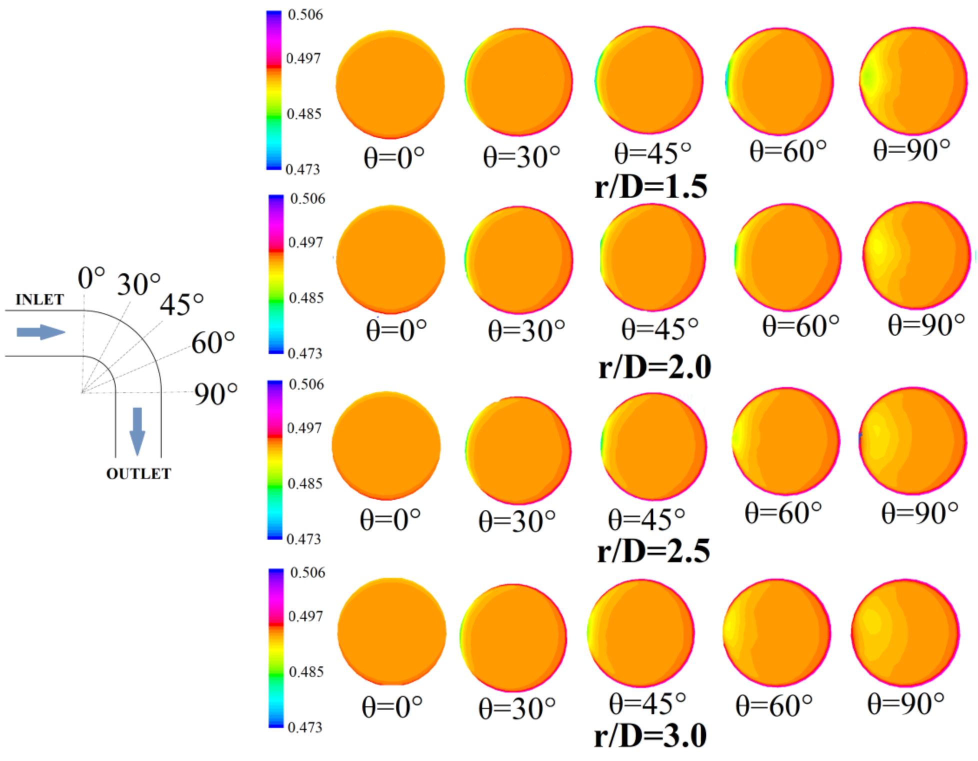

Figure 6.17: Effect of *r/D* on volume fraction distribution of coal –water slurry having solid concentration of 60%.

The effect of *r/D* ratio on volume fraction distribution of coal–ash slurries is shown in Figure 6.18–6.19. Form Figure 6.18, it is observed that with the increase in curvature bend, no change in the distribution of volume fraction of the solid phase is observed at inlet section of pipe bend. However, as the curvature of bend increased the minimum concentration zone observed at the intrados wall of pipe bend is reduced. The colour of the volume fraction contours at the intrados wall is changed to yellow from blue as the curvature of bend increased from 1.5 to 3.0.

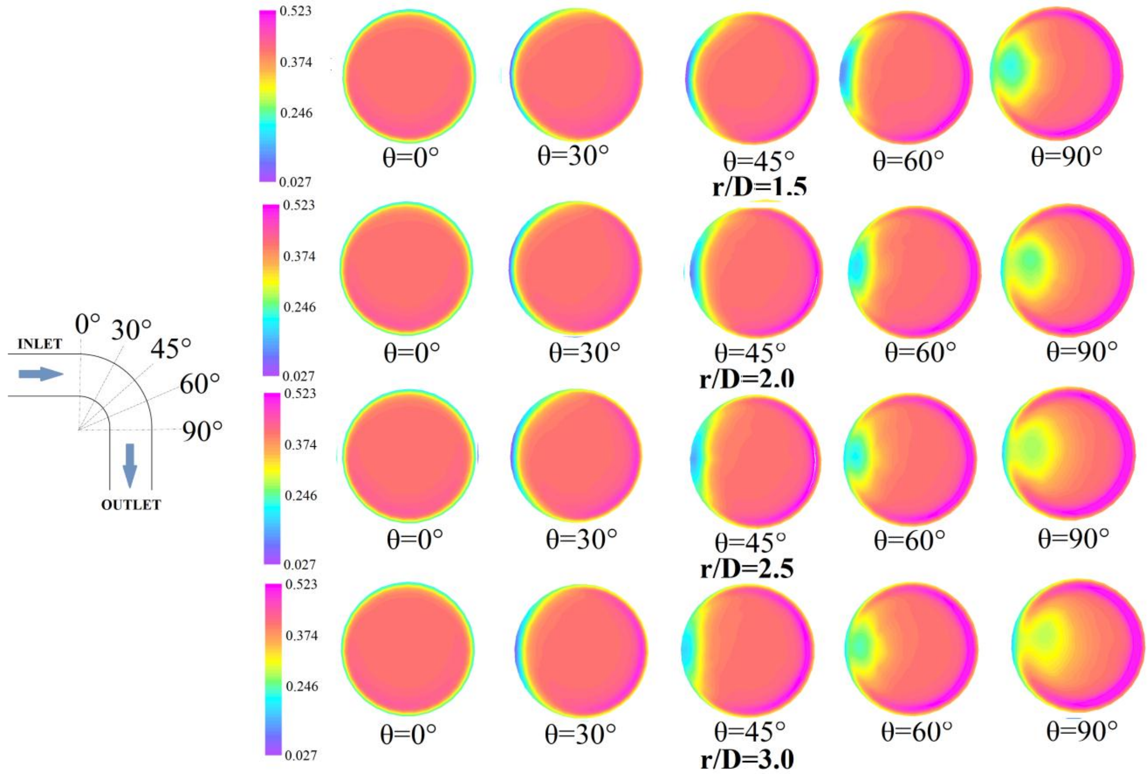

Figure 6.18: Effect of *r/D* on volume fraction distribution of fly ash slurry having solid concentration of 60%.

A similar trend, as noticed for coal-water and fly ash slurry is observed in case of bottom–ash slurries as seen in Figure 6.19. The magnitude of volume fraction varies for slurries and order of volume fraction magnitude remains the same for the variation of *r/D*. The volume fraction contours depict the complete phenomenon of settling inside the pipe bend. Thus it is observed form the analysis of volume fraction contours that the maximum efflux concentrated zone for coal and coal-ash slurries is observed at the extrados wall of pipe bend. This zone is increased with an increase in solid concentration and decreased with the increase in flow velocity. Also, the variation in *r/D* ratio shows that as the bend curvature is increased, the flow inside the pipe bend becomes more stable.

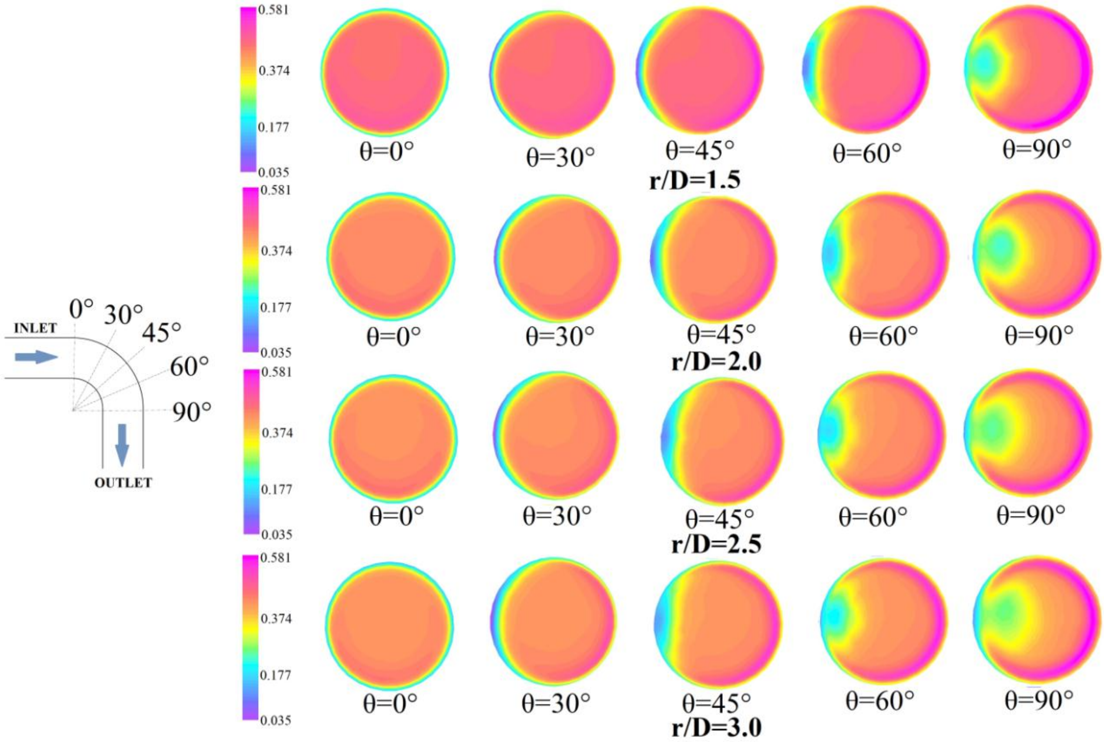

Figure 6.19: Effect of *r/D* on volume fraction distribution of bottom ash slurry having solid concentration of 60%.

6.6.4 Turbulence intensity contours

Turbulence intensity contours for the variation of solid concentration

The turbulence intensity of coal–water suspension depends upon solid concentration, flow velocity, bend geometry and momentum diffusion. Figure 6.20 shows the variation in turbulence intensity with the solid concentration of slurry suspension at various curvature angles between 0 and 90°. The contours reveal that at the inlet section of a bend the maximum intensity of turbulence occurs at the outer periphery of the bend. However, the minimum turbulence is seen at the central region of the bend section. As the solid concentration of slurry is increased from 30–60% turbulence intensity is increased and the minimum turbulence region at the center of the pipe gets reduced. This increase in turbulence with solid concentration is observed due to an increase in solid particles per unit volume of slurry. The intensification of solid particles increases solid–solid, solid–liquid and solid–wall interactions and hence turbulence is increased. A similar phenomenon of different interaction inside pipe is reported by the various researchers (Chen *et al.* 2009; Tan *et al.* 2012; Zhang *et al.* 2012).

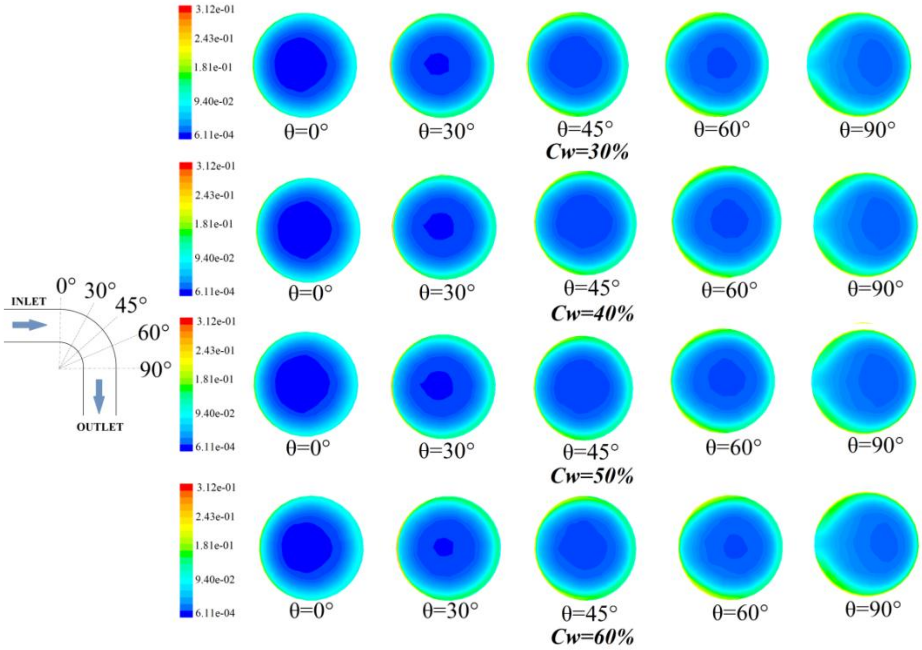

Figure 6.20: Effect of solid concentration of coal–water slurry on turbulence intensity at bend outlet.

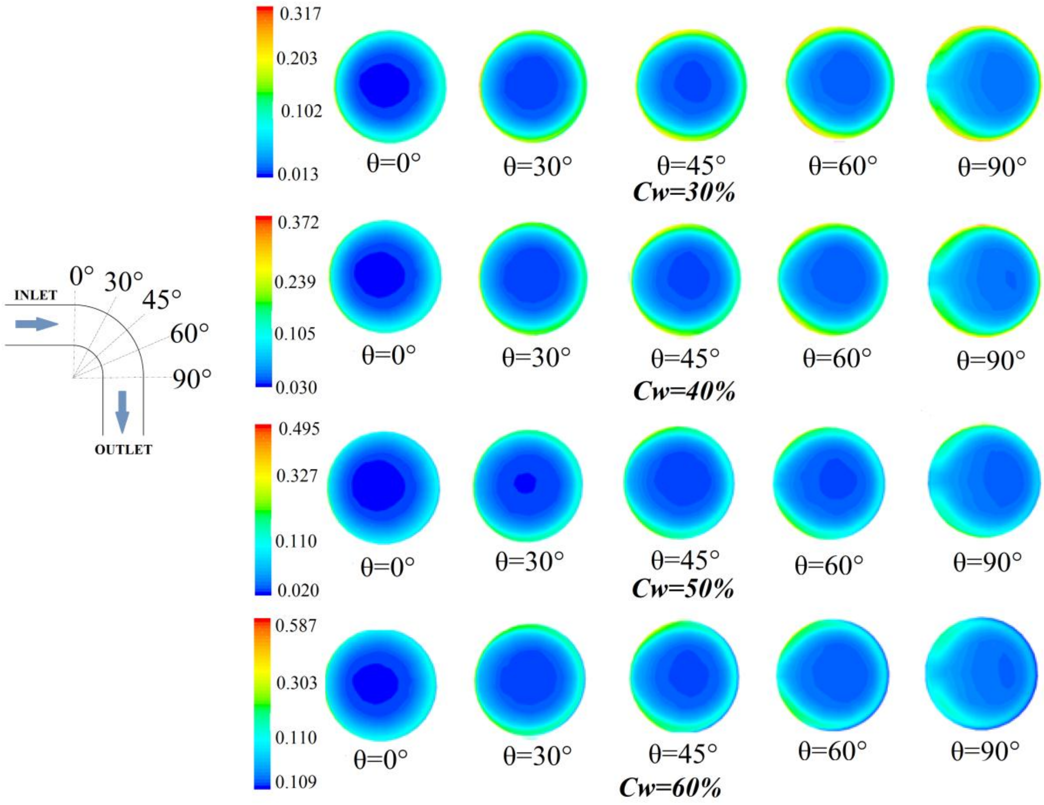

Figure 6.21: Effect of solid concentration of fly ash slurry on turbulence intensity at bend outlet.

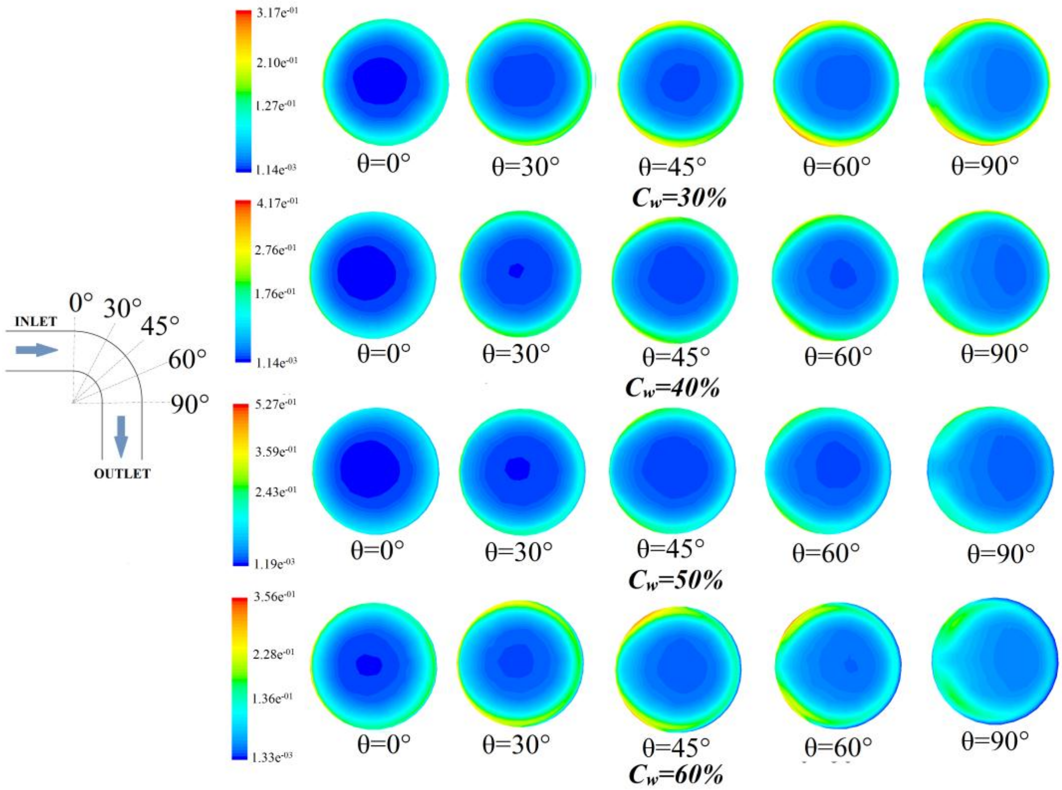

Figure 6.22: Effect of solid concentration of bottom ash slurry on turbulence intensity at bend outlet.

From the results, it is also noticed that with an increase in bend curvature angle turbulence intensity is increased at the intrados wall of the bend whereas the minimum turbulence is seen at the extrados wall. Figure 6.21–6.22 shows the turbulence intensity distribution at different solid concentrations for coal–ash slurries at V = 5 m/s and r/D = 1.5. It is observed that the magnitude of turbulence intensity due to the flow of fly ash slurry is higher as compared to coal–water slurry. Minimum turbulence zone exists at inlet section (0°) of a bend. By comparison between coal–water and fly ash slurry, it is also noticed that the minimum and maximum turbulence zones for the flow of fly ash slurry seems wider.

Turbulence intensity contours for the variation of flow velocity

Figure 6.23 shows the effect of flow velocity on turbulence intensity at a solid concentration of 60% for flow through a pipe bend having an r/D ratio of 1.5. It is perceived from turbulence contours that at a flow velocity of 2 m/s, minimum turbulence is observed in the central region of the pipe bend. At the inlet of the bend, the maximum turbulence is observed at the wall of the pipe. At the outlet, the maximum turbulence region is shifted to the intrados wall. As the flow velocity of the slurry suspension is increased from 2–5 m/s sudden increases in turbulence intensity is observed. At the inlet section, the minimum turbulence region is decreased. However, the minimum turbulence region is shifted to the extrados wall at the outlet of the bend. This variation in turbulence intensity that accompanied changes in flow velocity is due to increases in momentum exchanges among solid particles (Pietralik and Schefski, 2009; El-Gammel *et al.* 2010; Dutta and Nandi, 2016).

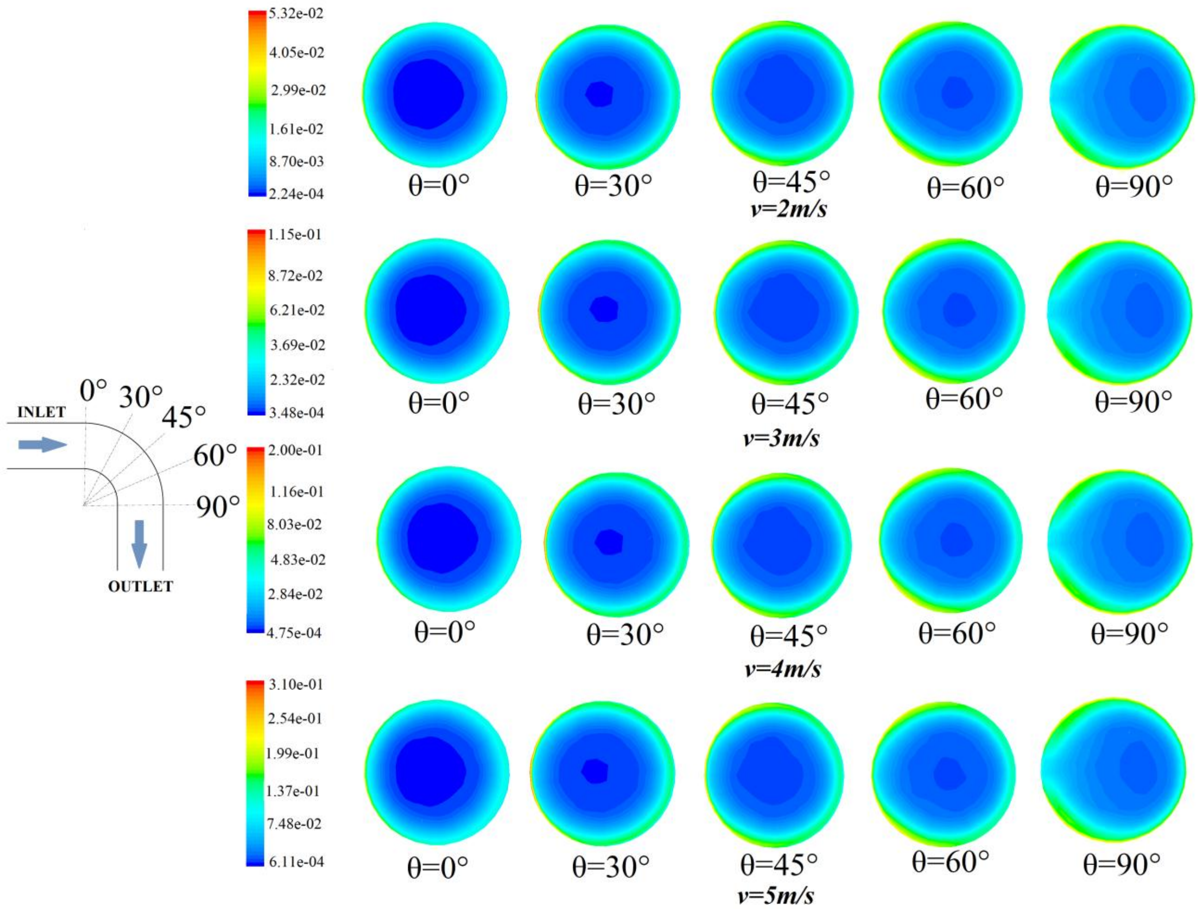

Figure 6.23: Effect of flow velocity on the distribution of turbulence intensity for coal–water slurry

Figure 6.24–6.25 shows the turbulence intensity distribution at different velocities for coal–ash slurries at C_w = 60% for flow through a pipe bend having an r/D = 1.5. It is observed that magnitude of turbulence intensity due to flow of fly ash slurry is higher as compared to bottom ash slurry.

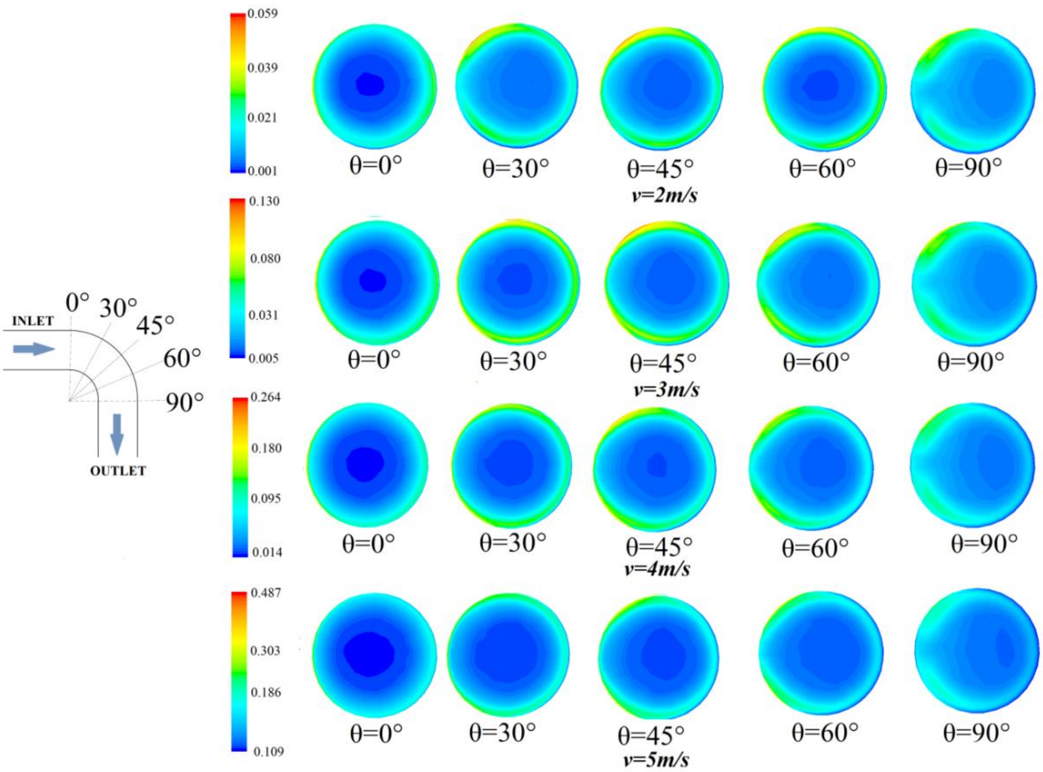

Figure 6.24: Effect of flow velocity on the distribution of turbulence intensity for fly ash slurry

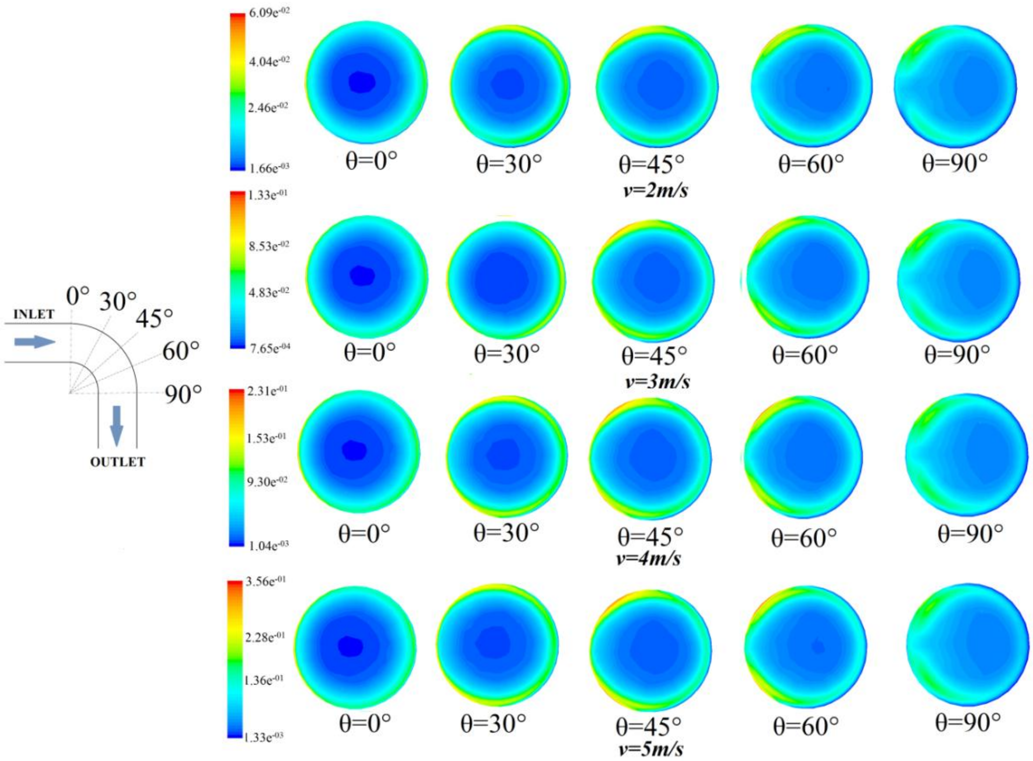

Figure 6.25: Effect of flow velocity on the distribution of turbulence intensity for bottom ash slurry

Turbulence intensity contours for the variation of r/D ratio of the pipe bend

Figure 6.26 represents the variations in turbulence intensity with *r/D* ratio. It is noticed that, as the *r/D* ratio increased the intensity of turbulence continued decreasing across the bend section. The higher turbulence zone is found at the intrados wall of a bend having an *r/D* ratio 1.5. As the *r/D* ratio approaches to 3.0, a decrease in turbulence intensity is noticed inside the pipe bend. This shows that as the curvature of a bend increases, losses occurring inside the bend due to turbulence are decreased, and thus the flow becomes more stable and uniform.

Figure 6.27–6.28 shows the turbulence intensity distribution at *r/D* ratios of pipe bend for coal–ash slurries at C_w = 60% flowing at V = 5 m/s. The *r/D* ratio is a geometrical parameter. As the *r/D* ratio is increased, the turbulence intensity phenomenon changes for different slurries. It is observed that the higher turbulence zone remains the same for all slurries. Lower turbulences zones are found wider in coal–ash slurries in comparison with coal–water slurry. At the bend exit, the yellowish color in contour is covering more area in bottom ash slurry. This indicates that the turbulence is lower on the intrados wall of pipe bend for bottom ash slurry, which is comparatively higher in case of bottom ash and coal slurry.

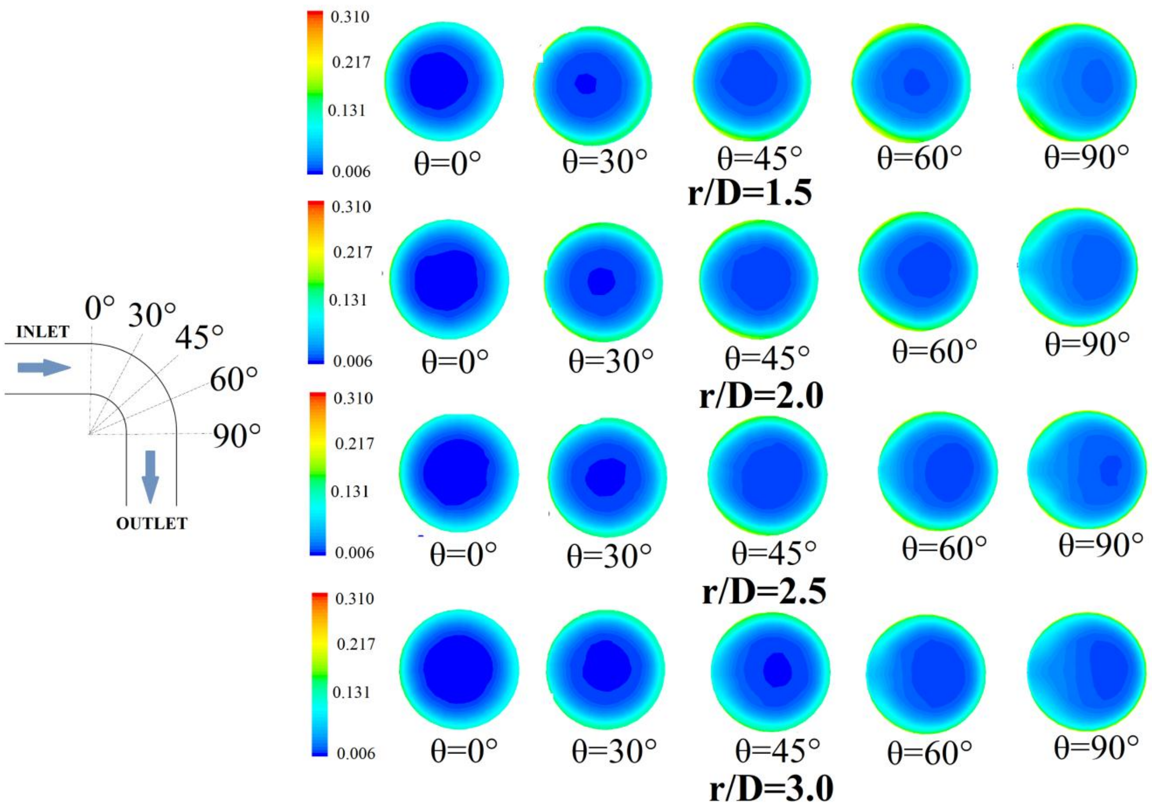

Figure 6.26: Effect of bend curvature on turbulence intensity for coal–water slurry

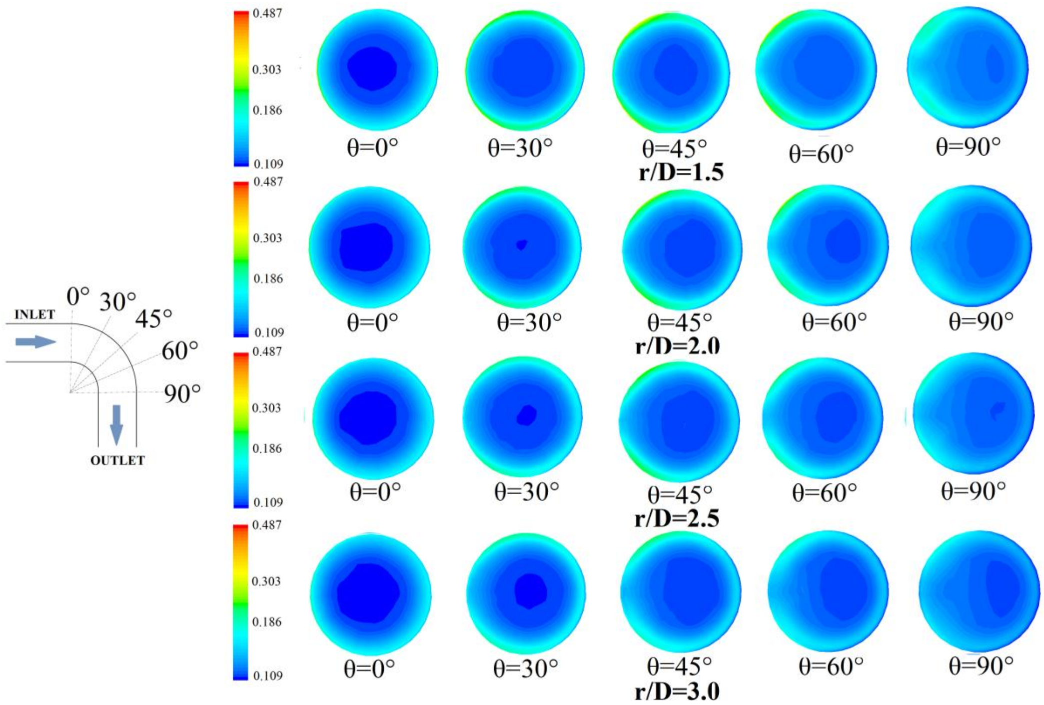

Figure 6.27: Effect of bend curvature on turbulence intensity for fly ash slurry

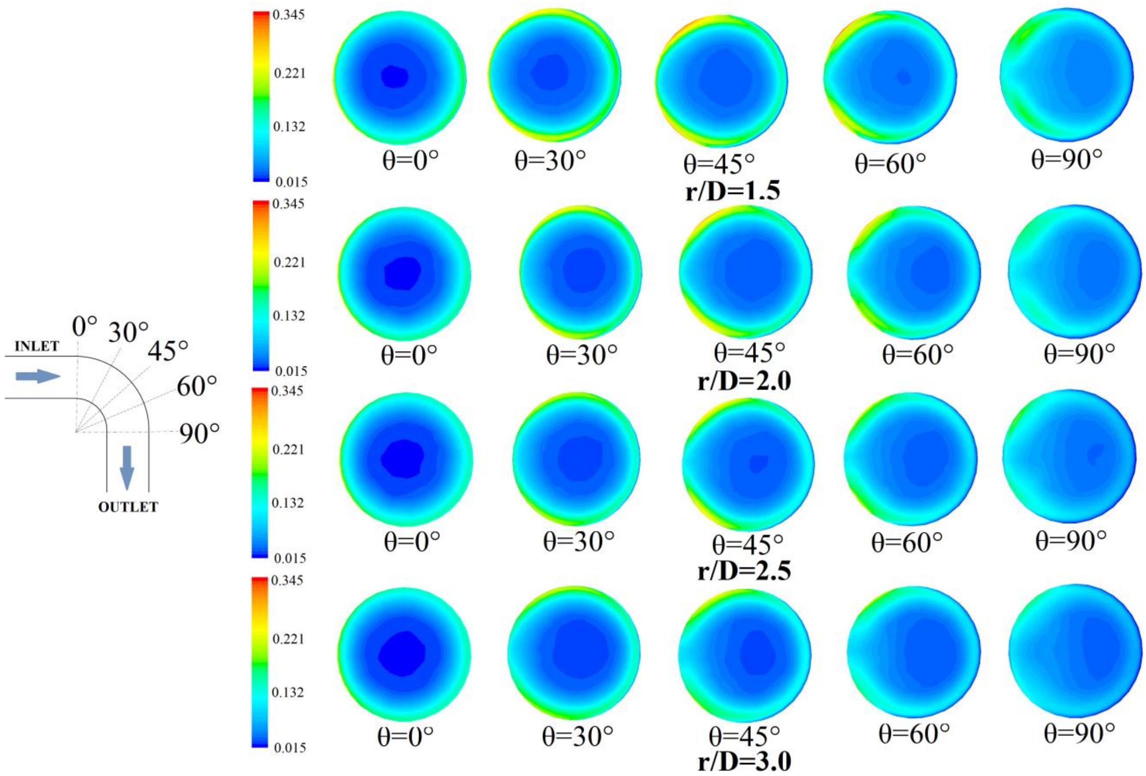

Figure 6.28: Effect of bend curvature on turbulence intensity for bottom ash slurry

6.6.5 Velocity distribution vectors and contours

Velocity vector

The distribution of velocity vectors for the flow of coal–water slurry at various curvature angles is shown in Figure 6.29. The *r/D* ratio is ranging from 1.5 to 3.0. The results illustrate that velocity is higher at the intrados region of pipe bend than at the extrados wall. The higher velocity region increased from the intrados wall to the central part of the pipe bend as the curvature angle is increased from 0 to 90°. The maximum variation in velocity magnitude is observed at curvature angles of 30–45° for a bend having an *r/D* ratio 1.5. As the *r/D* ratio increases, the magnitude of velocity at the center of pipe bend also increases. A pipe bend with *r/D* ratio 1.5 results in higher flow separation and secondary flows. As the *r/D* ratio increases, the flow separation decreases and the generation of secondary flows are also reduced. Hence, turbulence decreases, which further reduces losses and results in an increase in velocity.

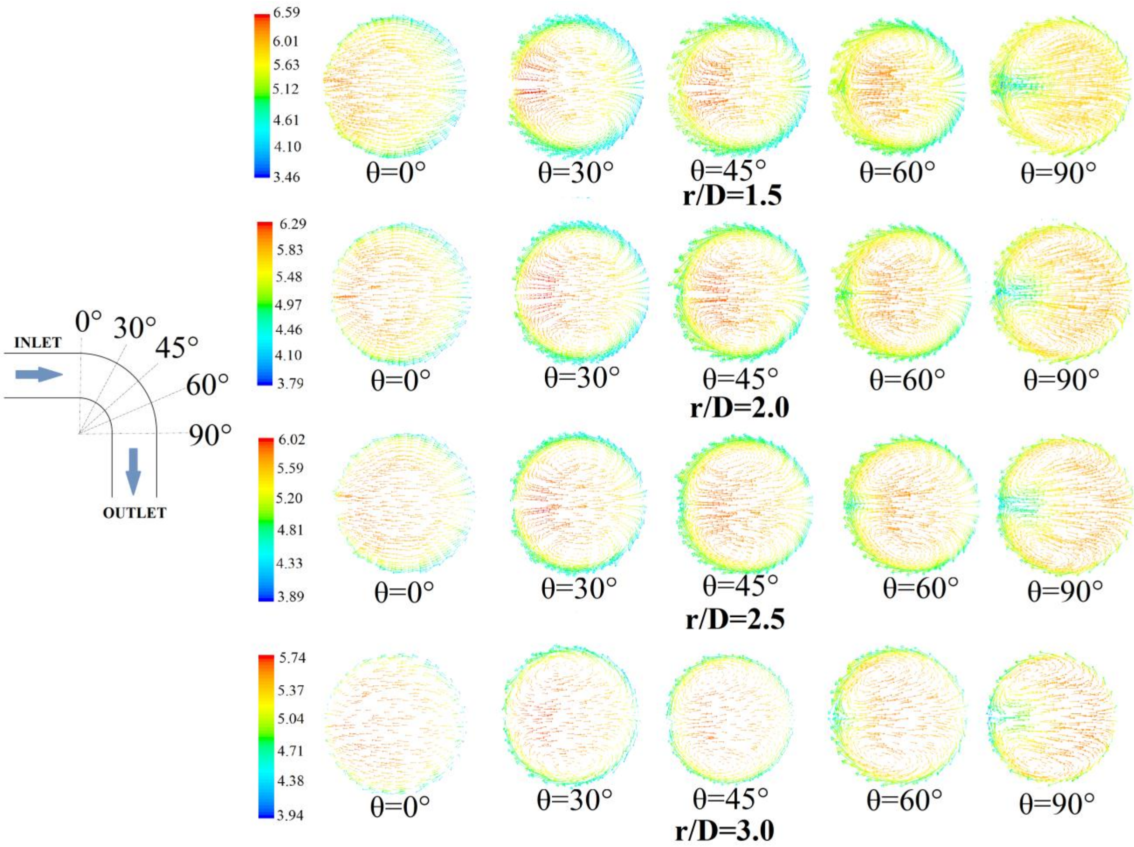

Figure 6.29: Effect of *r/D* ratio on velocity vectors at bend outlet for coal–water slurry

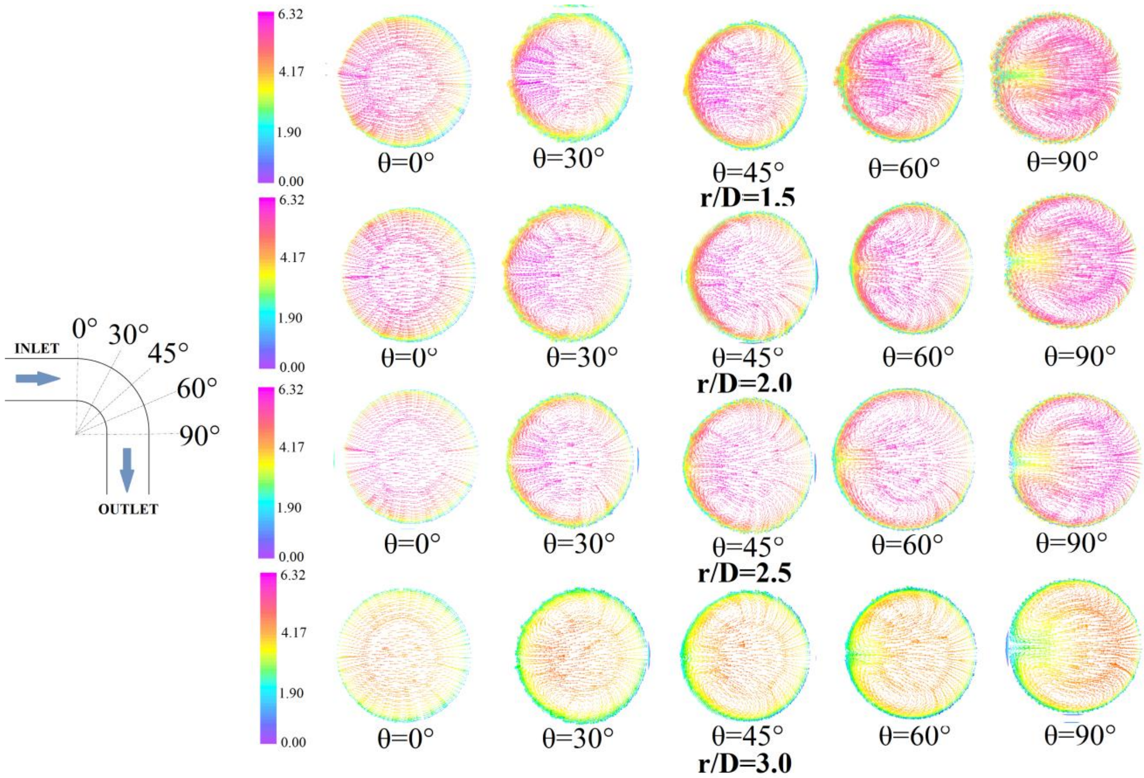

Figure 6.30: Effect of *r/D* ratio on velocity vectors at bend outlet for fly ash slurry

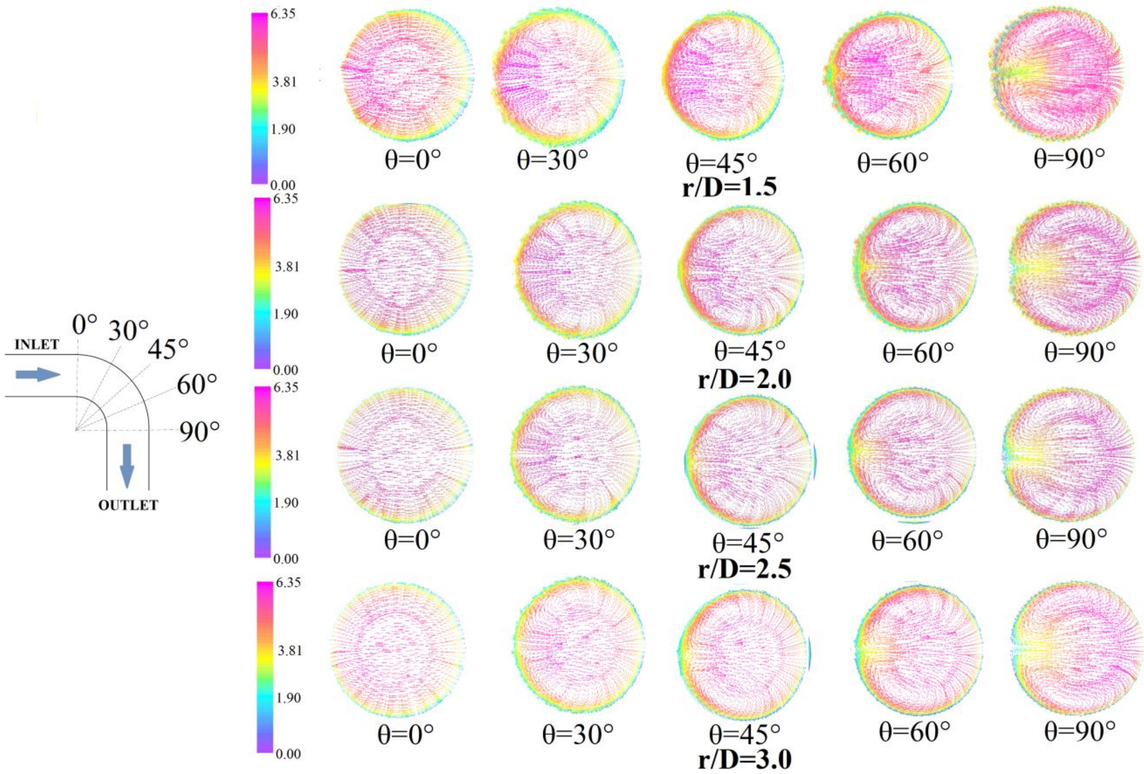

Figure 6.31: Effect of *r/D* ratio on velocity vectors at bend outlet for bottom ash slurry

The distribution of velocity vectors of the flow of bottom ash and fly ash slurry at various curvature angles is shown in Figure 6.30–6.31. By comparing the velocity vectors of coal, fly ash and bottom ash slurry, it could be observed that the flow separation is more in case of fly ash slurry than coal–water and bottom ash slurry. For the flow separation phenomenon, the *r/D* ratio dominates more as compared to the slurry type. A similar type of flow separation phenomenon is also reported by various researchers (Bozzini *et al.* 2003; Suzuki *et al.* 2008; Chen *et al.* 2015a; Solnordal *et al.* 2015).

Velocity distribution contours

Figure 6.32 represents the velocity contours for coal–water slurry at different curvature angles of pipe bends having different *r/D* ratios. From the contours, it is observed that, as the *r/D* ratio increased the flow becomes more uniform. The higher velocity region is shifted to the center of bend geometry. This indicates that pipe bends with higher *r/D* ratios have a minimal flow separation region. Figure 6.33–6.34 represents the velocity contours for fly ash and bottom slurry at different curvature angles of pipe bends having different *r/D* ratios. The trend of velocity distribution is found similar to coal–water slurry. While comparing the velocity contours of different slurry, the difference is found as the velocity magnitude which can be easily visualized by a change in color.

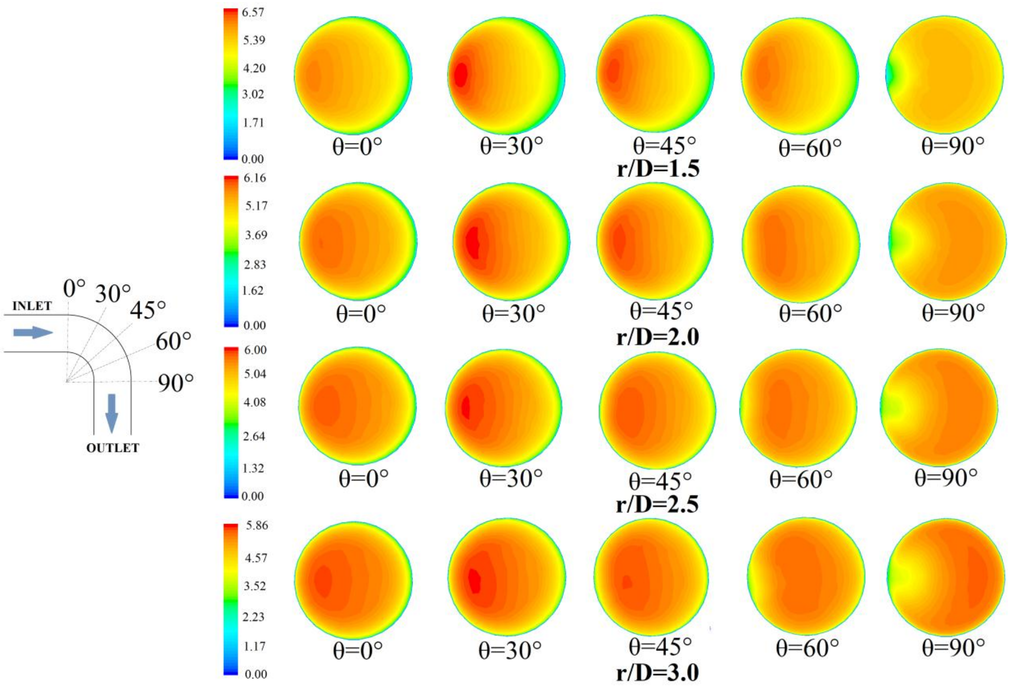

Figure 6.32: Velocity contours at the outlet of bend for different *r/D* ratios for coal–water slurry

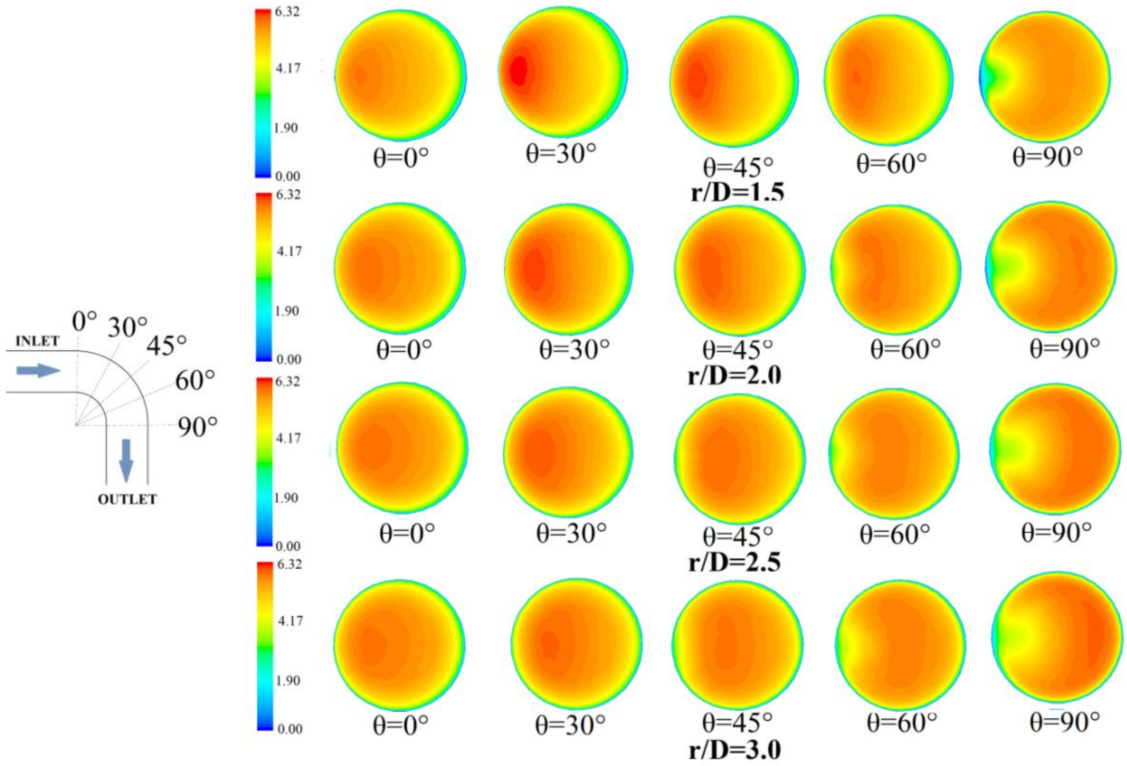

Figure 6.33: Velocity contours at the outlet of bend for different *r/D* ratios for fly ash slurry

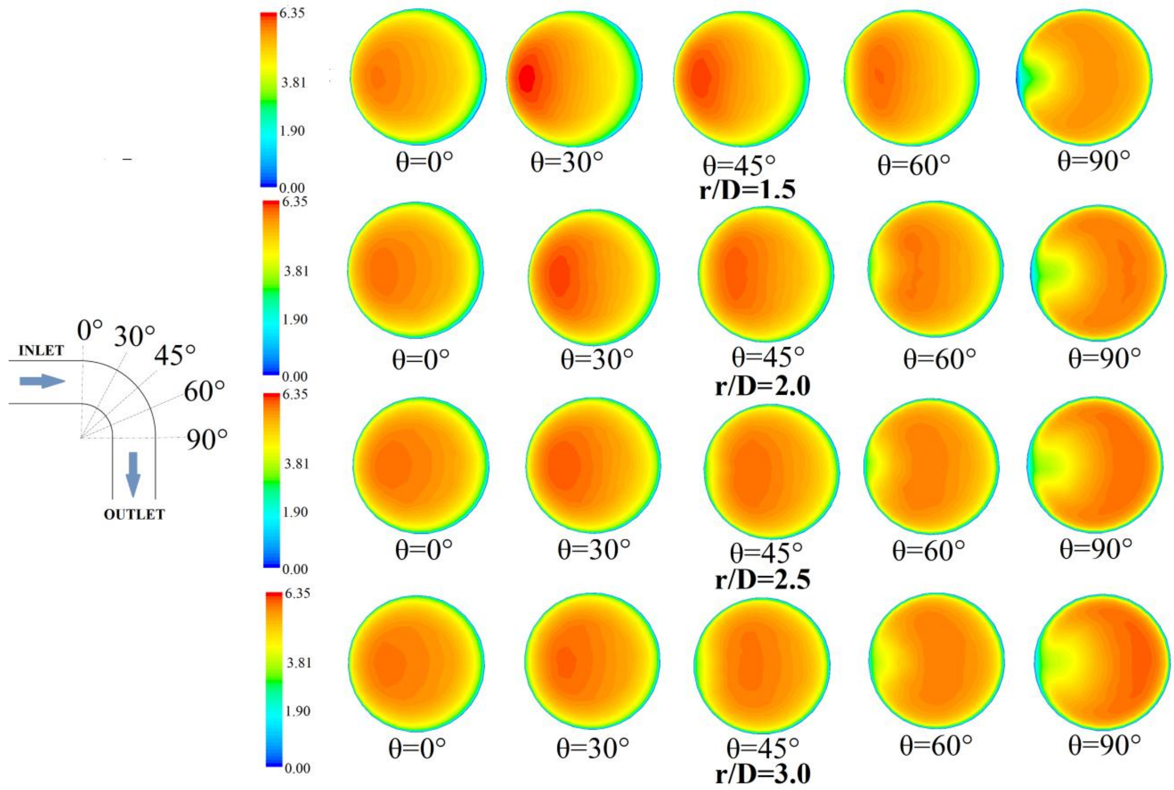

Figure 6.34: Velocity contours at the outlet of bend for different *r/D* ratios for bottom ash slurry

An another noticeable thing in the velocity contours at bend outlet (*r/D* = 1.5) is that lower velocity region is forming a shape like airfoil at intrados wall for fly ash and bottom ash slurry which remains elliptical in case of coal–water slurry.

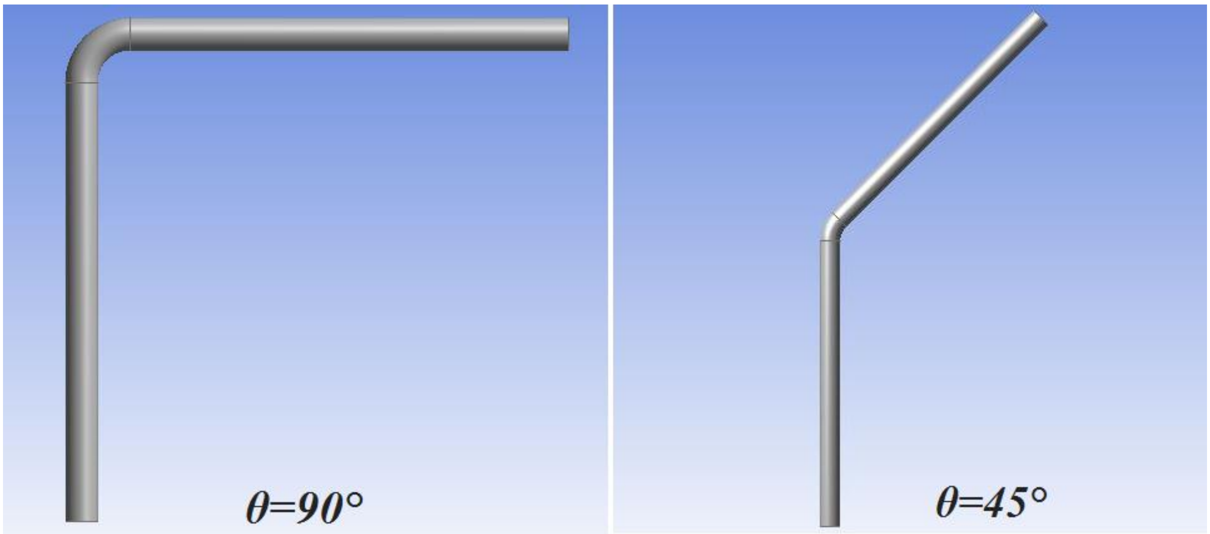

Figure 6.35: Geometry of pipe bends at different bend angles

6.7 EFFECT OF BEND ANGLE ON HEAD LOSS CHARACTERSTICS OF COAL AND COAL–ASH SLURRY

The series of simulations are carried out on different bend angles (45˚and 90˚) having *r/D* ratios ranging from 1.5–3.0 for the flow of coal and coal–ash slurry suspension. Figure 6.35 represents the pipe bends at different bend angles. The solid concentration of slurry is kept constant (i.e., 60% for flow velocity range of 5 m/s). Figure 6.36–6.38 represents the variation of a head loss with *r/D* ratio at different bend angles for coal and coal–ash slurry. Figure 6.36 shows the variation in head loss at different bend angles and *r/D* ratio for coal–water slurry at a solid concentration of 60% and Reynolds number of 3.64×10^4. From the results, it is observed that maximum head loss has occurred across 90˚ pipe bend irrespective of *r/D* ratio. However, the minimum head loss is seen across 45˚ pipe bend. Also, the minimum head loss is observed at *r/D* ratio of 2.0 for pipe bend having bend angle of 90˚. Whereas, the minimum head loss for 45˚ pipe bend is observed for bend having *r/D* ratio of 1.5. The higher head loss for 90˚ pipe bend is observed because of abrupt change in flow direction leads to the formation of turbulence. The phenomenon of flow separation and intensity of secondary flows are also very high. This leads to higher losses inside the bend and head loss is increased.

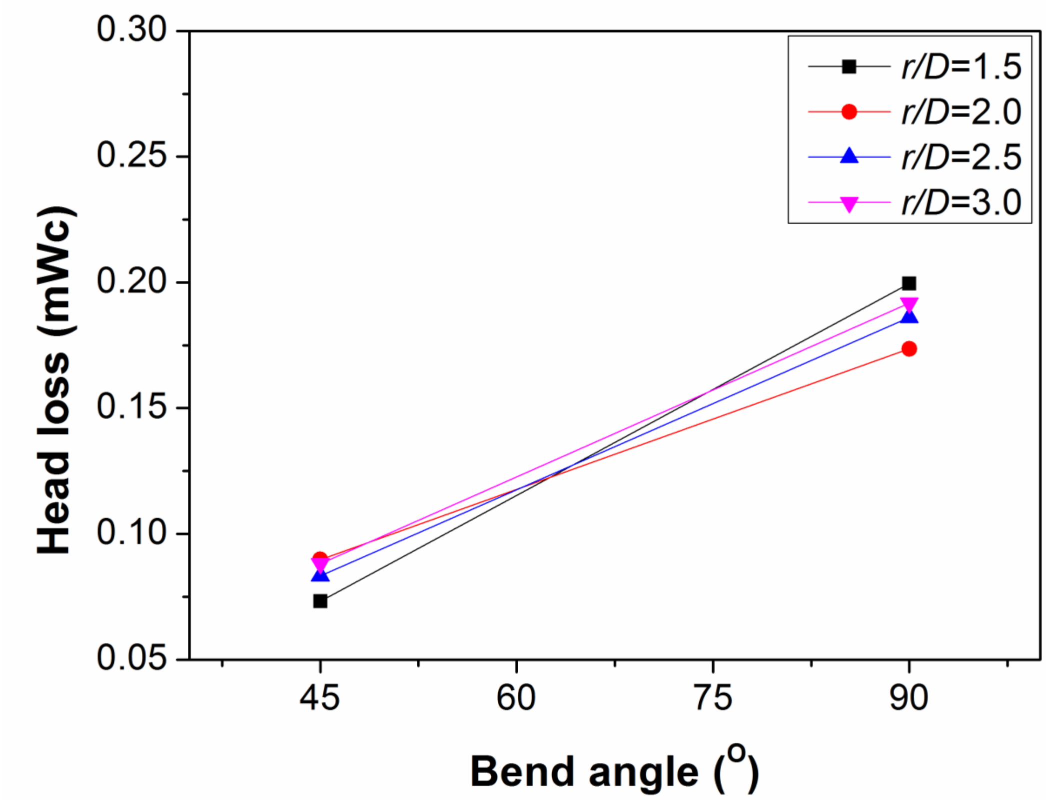

Figure 6.36: Variation in head loss at different bend angles and *r/D* ratio for coal–water slurry

However, pipe bend having 45˚ bend angle results in small diversion of slurry flow. This result in lower turbulence and also the phenomena of flow separation is decreased. The intensity of secondary flows is very less. This leads to lower head loss across pipe bend. The head loss is further increased by an increase in *r/D* form 1.5 to 3.0. This is noticed due to the increase in the effective length of pipe bend. Hence frictional losses increase with increase in length that contributes to higher head loss. Figure 6.37–6.38 represents the variation in a head loss at different bend angles and *r/D* ratio for fly ash and bottom ash slurry at solid concentration of 60%. Similar results as obtained for coal–water slurry is observed for coal–ash slurry but with higher magnitudes. From the results, it is found the *r/D*=2.0 is optimum for pipe bends having bend angle of 90˚. However, the 45˚ bend angle results in minimum head loss as compared to pipe bend having bend angle of 90˚ at *r/D* ratio of 1.5. Mandal and Das (2001) also reported that the head loss occurs in 45˚ pipe bend is generally lower as compared to 90˚ bend.

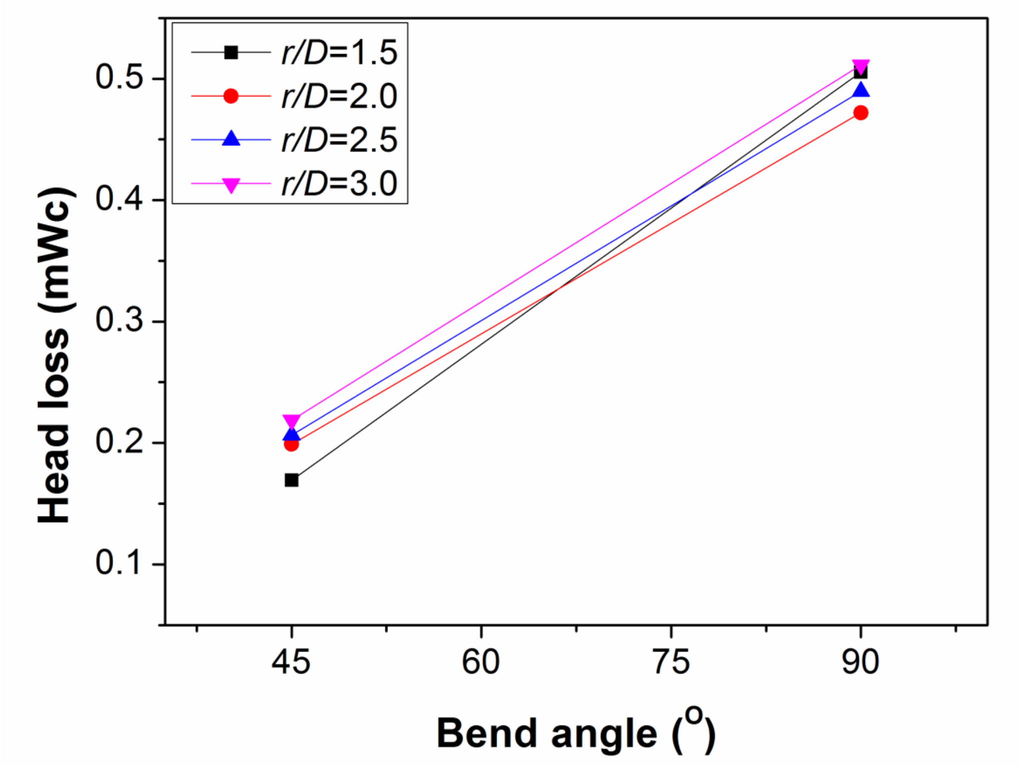

Figure 6.37: Variation in head loss at different bend angles and *r/D* ratio for fly ash–water slurry

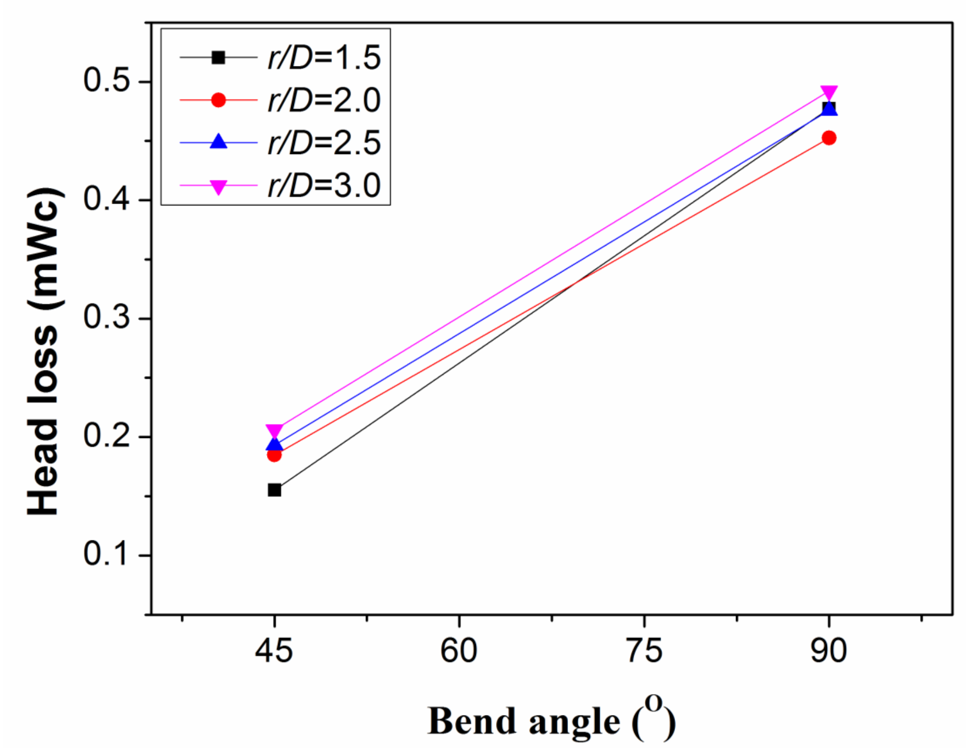

Figure 6.38: Variation in head loss at different bend angles and *r/D* ratio for bottom ash–water slurry

6.7.1 *Volume fraction contours*

The variation of volume fraction distribution with different bend angles (45˚ and 90˚) at inlet and outlet for coal and coal–ash slurry at a solid concentration of 60% and flow velocity of 5m/s is represented in Figure 6.39–6.41. Figure 6.39 represents the volume fraction contours of coal–water slurry. The contours depict that at the inlet of pipe bends the maximum efflux concentration is observed at the bottom of bend irrespective of bend angle. For the pipe bend having bend angle of 45˚ the maximum efflux concentration at the outlet of the bend is observed at the extrados region of the bend. However, the increase in *r/D* ratio for 45˚ bend angle results in a more uniform distribution of solid phase at the outlet of the bend. Whereas, for 90˚ bend angle the maximum concentrated solid phase region is noticed at the extrados wall of the pipe bend. Similar results are noticed for fly and bottom ash– water slurry. Figure 6.40–6.41 depicts the variation in efflux concentration at inlet and outlet of pipe bend having different bend angles and *r/D* ratio. It is observed from volume fraction contours that the region of maximum efflux concentration at the extrados wall of pipe bend is more in case of 90˚ pipe bend as compared to 45˚ pipe bend.

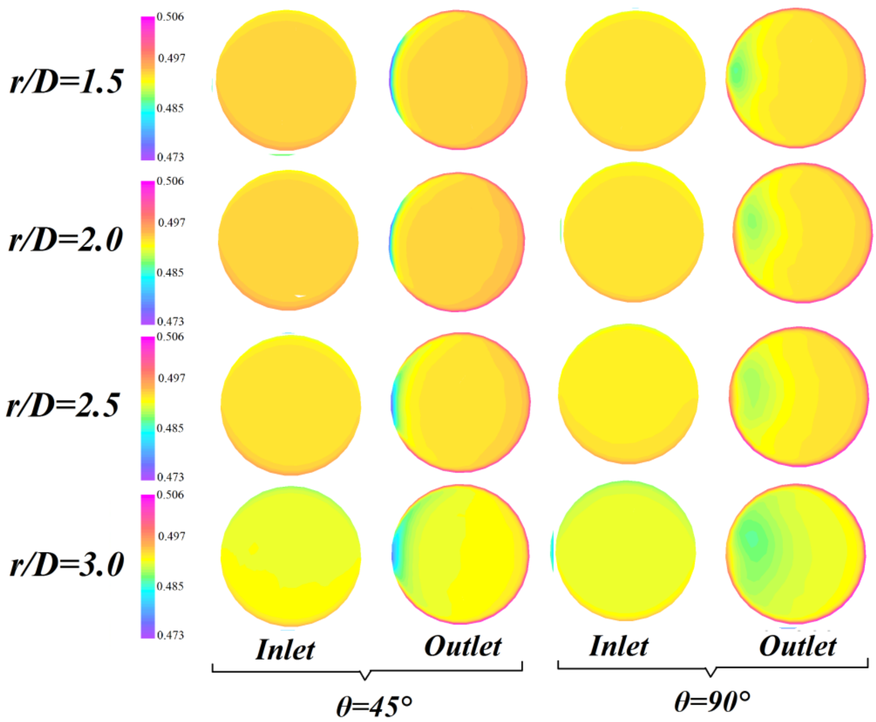

Figure 6.39: Volume fraction contours of coal–water slurry at different bend angles and *r/D* ratio

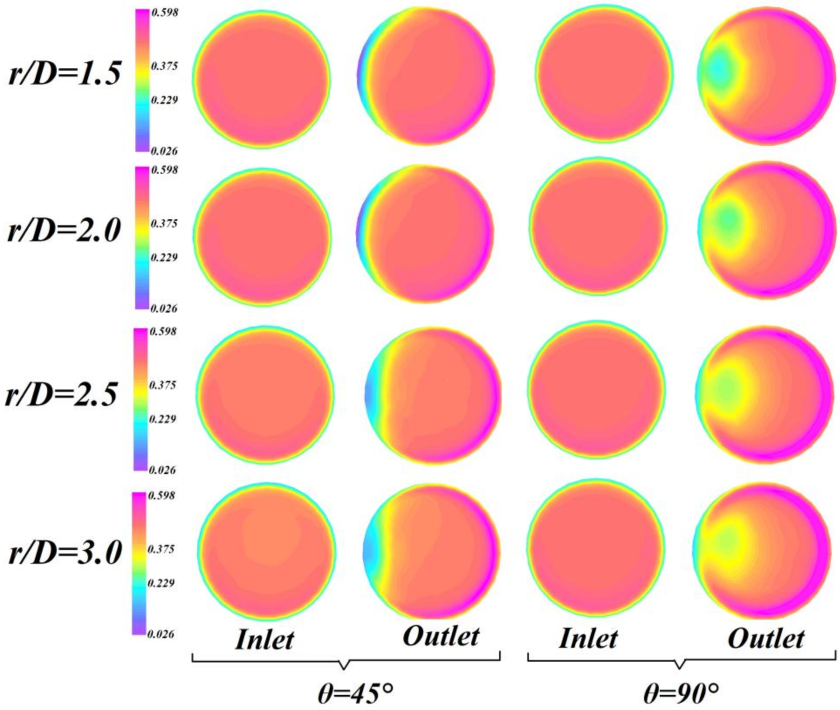

Figure 6. 40: Volume fraction contours of fly ash–water slurry at different bend angles and *r/D* ratio

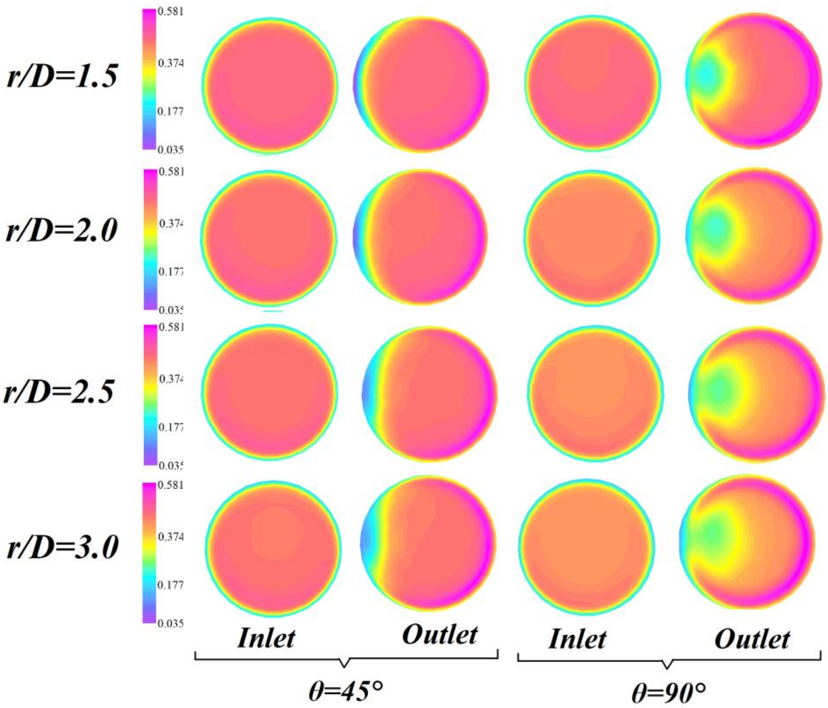

Figure 6.41: Volume fraction contours of bottom ash–water slurry at different bend angles and *r/D* ratio

6.7.2 Turbulence intensity contours

The variation in turbulence intensity of coal and coal–ash slurry suspension at different bend angles of θ=45˚and 90˚ is shown in Figure 6.42–6.44. Figure 6.42 shows the variation in turbulence intensity with varying bend angles at inlet and outlet of pipe bends for coal–water slurry suspension. The contour reveals that at the inlet section of a bend, the maximum intensity of turbulence occurs at the outer periphery of the bend. However, the minimum turbulence is seen at the central region of the bend section irrespective of bend angle. However, at the outlet of 45˚ and bend angle is the maximum turbulence region is observed at the extrados wall of pipe bend. The increase in *r/D* ratio from 1.5–3.0 results in a decrease in turbulence inside pipe bends. Whereas, the maximum turbulence region in 90˚ pipe bend is observed at the intrados wall of the pipe bend. Figure 6.43–6.44 represents the variation in turbulence for fly and bottom ash slurry. Similar contours as observed for coal–water slurry are noticed for coal–ash slurry suspension. The maximum turbulence is noticed for fly ash slurry as compared to coal-water and bottom ash slurry. In the case of 90˚ pipe bends the abrupt change in the direction of flow results in higher turbulence as compared to 45˚ bend angle. The higher turbulence in the intrados wall of 90˚ bend is observed due to flow separation and secondary flows in bends. The phenomena of flow separation occur due to the existence of pressure gradient while the fluid flows through bends. This phenomenon is more often in pipe bends having small curvature and large bend angle.

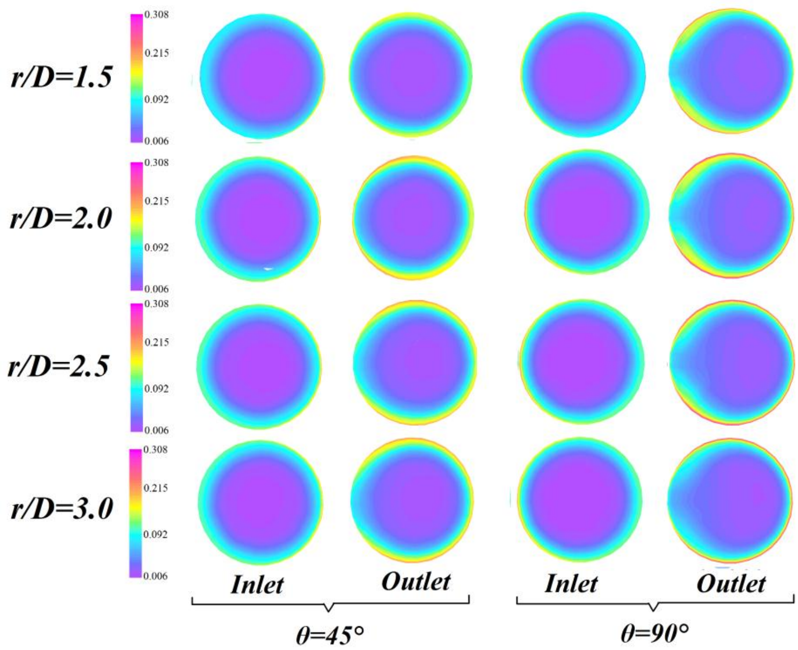

Figure 6. 42: Turbulence intensity contours of coal–water slurry at different bend angles and *r/D* ratio

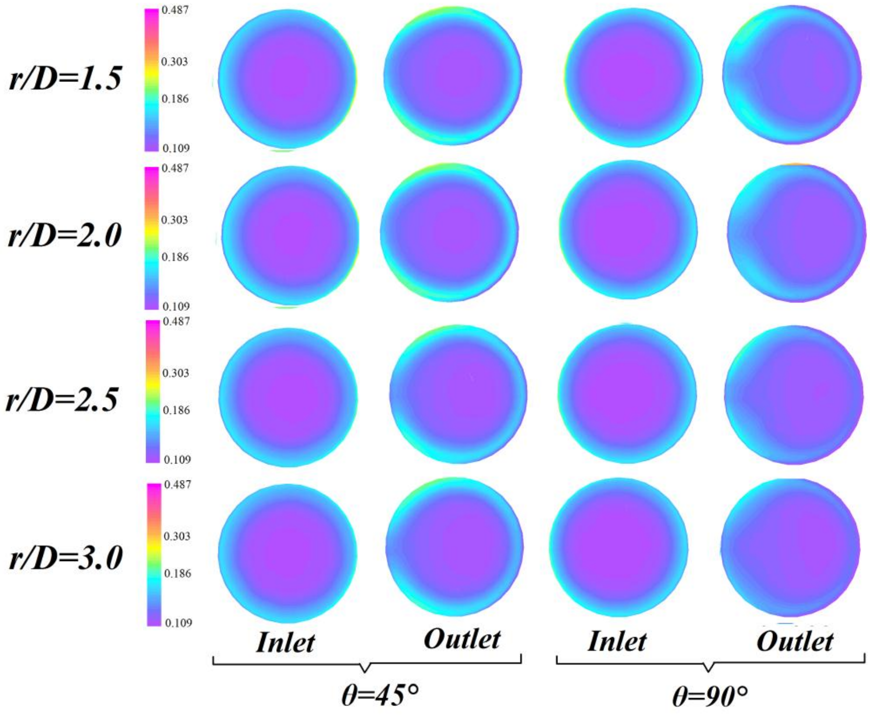

Figure 6. 43: Turbulence intensity contours of fly ash–water slurry at different bend angles and *r/D* ratio

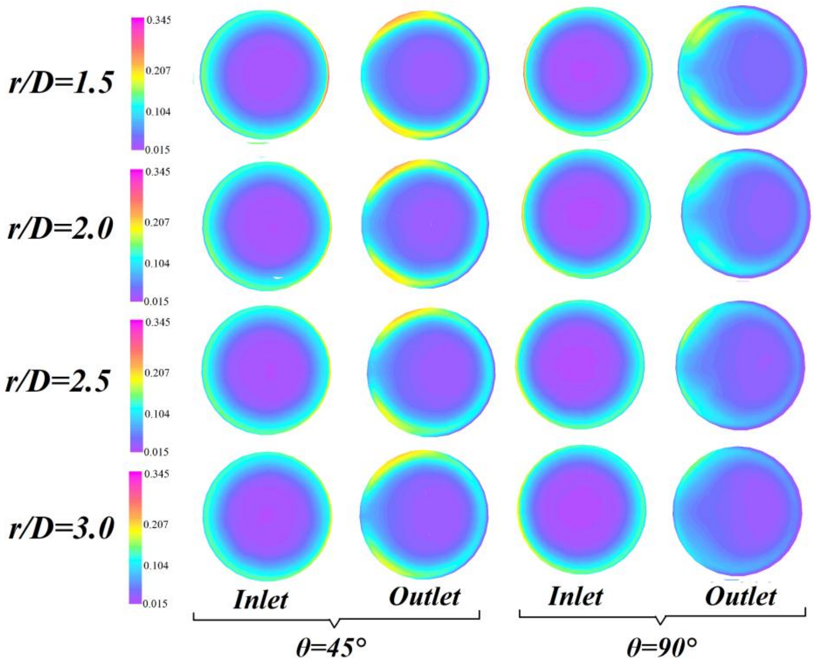

Figure 6. 44: Turbulence intensity contours of bottom ash–water slurry at different bend angles and *r/D* ratio

6.8 REMARKS

In this chapter, the head loss characteristic for coal and coal–ash slurries is successfully evaluated by using computational fluid dynamics (CFD) code ANSYS R15.0. It is observed that the SST *k–ω* modeling scheme established a close agreement with experimental results and thus used in further investigation. The remarks are pointed out from this chapter:

- The head loss is a function of both solid concentration and Reynolds number. The order of head loss with change in concentration and Reynolds number is as given follow: Coal > Bottom ash > Fly ash.
- The head loss inside the 90˚ pipe bend is enormously affected by varying the bend curvature. As the *r/D* ratio is increased from 1.5 to 2.0, the head loss across the pipe bend is decreased and increases with further increase in *r/D* ratio.
- From volume fraction contours of 90˚ pipe bend, it is observed that higher concentration zone at the inlet section is at bottom side at a lower velocity. As the flow velocity of the slurry is increased, the existence of higher a concentration zone at the inlet of the pipe bend is reduced. The minimum accumulation of solid particles is noticed at a flow velocity of 5 m/s.
- The higher concentration zone is shifted to the extrados wall of 90˚ pipe bend as the flow proceeded from the upstream to the downstream direction. At the outlet of bend geometry, the volume fraction zone is almost symmetric about the horizontal axis.
- The minimum accumulation of solid particles is observed at the intrados section of 90˚ bend, as the curvature angle is varied from 30–90°.
- The turbulence intensity contours for 90˚ bend reveals that the maximum intensity of turbulence occurs at the outer periphery of the bend at the inlet section. However, the minimum turbulence is seen in the central region of the bend section.
- As the solid concentration of slurry is increased from 30–60% turbulence intensity is increased and the minimum turbulence region at the center of 90˚ pipe bend gets reduced.
- It is also noticed that with an increase in bend curvature angle of 90˚ bend turbulence intensity is increased at the intrados wall of the bend whereas the minimum turbulence is seen at the extrados wall. The turbulence intensity inside the pipe bend decreases with an increase in *r/D* ratio.
- From velocity vectors, the velocity magnitude is found higher at the intrados region of 90˚ pipe bend than at the extrados wall. The higher velocity region increased from the

intrados wall to the central region of the pipe bend as the curvature angle is increased from 0 to 90°.

- From the velocity contours, it is observed that the flow becomes more uniform as the *r/D* ratio increased.
- By comparison of bends having different angles (45° and 90°) the head loss is found minimum in case of 45° bend.
- The optimum value of *r/D* ratio changes with change in bend angle. The observations revealed that the *r/D* ratio for 90° is found as 2.0, whereas it changes to 1.5 for 45° bend angle.

CHAPTER 7

CONCLUSIONS AND FUTURE SCOPES

Chapter 7

CONCLUSIONS AND FUTURE SCOPES

7.1 SUMMARY

The present investigation is carried out to investigate the head loss characteristics across 90˚ pipe bends for the flow of concentrated coal and coal-ash slurries. Prior to head loss experiments, different bench-scale tests are carried out to analyze the physical and chemical characteristic of solid particles. Extensive rheological experimentation is performed to analyze flow characteristics of coal-water slurry with and without the use of additive, namely sulfonic acid. Similarly, the sodium triphosphate is added as an additive in the bottom and fly ash slurry. After the rheological analysis of slurry, the head loss experiments are conducted with slurries of different solid concentrations, varying from 30-60% (by weight). During experimentation, the average flow velocity is kept in the range of 2-5 m/s. The *r/D* ratio for the pipe bend varied within the range of 1.5-2.5. Pulverized coal sample with particle size less than 53 μm is used to prepare the coal-water slurry whereas the as-collected samples fly and bottom ash are directly used to prepare the coal-ash slurries. Computational fluid dynamics (*CFD*) simulation is also carried out to obtain the flow patterns and contours. An Eulerian multiphase model with an SST k-ω approach is used for carrying out the numerical simulations for 50 mm pipe bend geometry. The effect of flow separation and secondary flows on turbulence, flow velocity and distribution of the solid suspension inside the bend geometry is also studied with the help of contours. The detailed conclusions and future scopes of this study are addressed in the next sections.

7.2 CONCLUSIONS

The following conclusions are reached from the current investigation.

- The coal particles are non-spherical and have irregular shapes. The fly ash particles have smooth surface, regularity in shape, and spherical appearance. The bottom ash particles have rough surface morphology, irregularity in shape and porosity.
- The specific gravity of coal, fly and bottom ash sample is determined as 1.46±2%, 2.27±0.5% and 2.09±1.6%. The maximum settled concentration for coal, fly ash and bottom slurry is observed as in range 65.37-76.55%, 59.67-73.92%, and 53.79-68.58% for a solid concentration range of 30-60% respectively.

- ❖ The *pH* of coal-water slurry varies in a range of 6.38-5.93 as solid concentration is increased from 10-60% (by weight). The *pH* value for fly and bottom ash suspensions are lies in the range of 7.62-7.42 and 7.68-7.45, respectively for the solid concentration range of 30-60%.
- ❖ The coal-water slurry exhibits Newtonian behaviour at a solid concentration of 30% (by weight). The coal-water slurry exhibits shear thinning behaviour at higher solid concentrations (i.e., above 30%) that show its pseudo-plastic nature.
- ❖ The addition of a small amount of sulphonic acid resulted in an improvement in the rheological properties of the coal-water slurry suspension. The maximum decrease in apparent viscosity of the coal-water slurry is noticed with a 3% (by weight) addition of sulfonic acid.
- ❖ The fly ash slurry exhibits Newtonian behaviour for a solid concentration of 30%. The increase in solid concentration results in change in flow behaviour of fly ash slurry from Newtonian to Bingham plastic. The fly ash-water slurry shows Bingham plastic behaviour for solid concentration range of 40-60% (by weight).
- ❖ The bottom ash slurry exhibits Newtonian behaviour for solid suspension up to solid concentration of 30%. The bottom ash slurry shows Bingham flow behaviour above 40% solid concentration.
- ❖ The addition of sodium triphosphate results in appreciable decrease in viscosity of bottom and fly ash slurry. The maximum percentage decrease in apparent viscosity is observed with 5% addition of sodium triphosphate in fly and bottom ash slurry.
- ❖ The head loss across 90° pipe bends increases with the increase in solid concentration of coal and coal-ash slurries. The head loss across pipe bends is a function of the solid concentration, flow velocity and *r/D* ratio. Sudden drop in head loss is found as the *r/D* ratio is increased from 1.5 to 2.0.
- ❖ The optimum *r/D* ratio for minimum head loss in a 90˚ pipe bend is 2.0; beyond this, the increase in head loss is seen due to increase in effective length of pipe bend.
- ❖ The head loss across pipe bends for fly ash slurry is more than coal-water slurry. However, the order for head loss is found as fly ash > bottom ash > coal slurry.
- ❖ The addition of sulfonic acid also results in a reduction of head loss in pipe bend (*r/D*=2.0). The head loss for coal-water slurry (C_W=61.56%) is decreased by 6.48, 11.93, 17.09 and 18.16% at a flow velocity of 5 m/s as the amount of sulfonic acid is increased from 1-4%. The maximum drop in head loss is observed with a 3% addition of sulfonic acid.

- The addition of sodium triphosphate also results in a reduction of head loss in pipe bend (*r/D*=2.0). The head loss for fly ash slurry is decreased by 5.23, 8.80, 12.45, 20.15 and 22.21% as the amount of additive is increased from 1-5%. However, for bottom ash slurry the head loss is decreased by 5.92, 10.62, 17.77, 21.03 and 22.73% as the amount of additive is increased from 1-5%. The optimum addition of sodium triphosphate is noticed as 4%.
- The specific energy consumption is decreased by 14.80, 20.15 and 21.03% by addition of additive for coal, fly ash and bottom ash slurry respectively. Thus, the addition of additive is one of the economical ways to convey the coal and coal-ash slurry at higher solid concentrations.
- The appreciable decrease in bend loss coefficient is noticed with the increase in *r/D* ratio form 1.5 to 2.0. Further increase in *r/D* ratio results in an increase in bend loss coefficient.
- The SST k-ω model shows better agreement with experimental results as compared to other turbulence models.
- From numerical simulations, it is observed that head loss increases with solid concentration and Reynolds number. However, the magnitude for head loss across 90° pipe bend is given as follows. Fly ash > bottom ash > coal.
- It is also confirmed from numerical simulations that minimum head loss is noticed for pipe bend having *r/D*=2.0.
- From volume fraction contours, a higher concentration zone is found at the inlet section of a pipe bend at bottom side at a lower velocity (2 m/s). As the flow velocity of the slurry is increased from 2 to 5 m/s, the existence of higher a concentration zone at the inlet of the pipe bend is reduced. The minimum settling of solid particles is noticed at a flow velocity of 5 m/s.
- The higher concentration zone is shifted to the extrados wall of pipe bend as the flow proceeded from the inlet to the outlet section of the pipe bend. At the outlet of bend geometry, the volume fraction zone is almost symmetric about the horizontal axis.
- The turbulence intensity contours reveal that the maximum intensity of turbulence occurs at the outer periphery of the bend at the inlet section. However, the minimum turbulence is seen at the central region of the bend section.
- As the solid concentration of slurry is increased from 30-60% turbulence intensity is increased and the minimum turbulence region at the center of the pipe gets reduced.
- The turbulence intensity inside the pipe bends decreases with an increase in *r/D* ratio.

- The velocity magnitude is greater at the intrados region of pipe bend than at the extrados wall. The higher velocity region increased from the intrados wall to the central region of the pipe bend as the curvature angle is increased from 0 to 90°.
- From the velocity contours, it is observed that the flow becomes more uniform as the *r/D* ratio increased.
- It is observed from numerical analysis that head loss in 45° pipe bend in lower as compared to 90°. Also, the optimum *r/D* ratio for 45° pipe bend is observed as 1.5.

7.3 KEY RECOMMENDATIONS

This study has raised many possibilities for practical implementation in thermal power plants. In the Indian thermal power plants situated at Northern regions, the slurries are transported at a lean concentration (10-15% by weight) which comes with many drawbacks. So to avoid such drawbacks, the slurries should the transported at high concentrations. Moreover, the present study provides a broad data which could serve as the primary data to the power stations for the installation of high concentration coal transportation and slurry disposal systems. The use of additive is one of the economical ways to convey the coal and coal-ash slurry at higher solid concentrations.

7.4 SCOPE FOR FUTURE

The present investigation is carried out to optimize the head loss characteristics across 90˚ pipe bends for the flow of concentrated coal and coal-ash slurries. It would be more beneficial to further augment the knowledge database by carrying out further work on following topics:

- To investigate the head loss problem encountered different pipe bends (45°, 60°, 135°, and 180°) bends.
- To investigate the head loss problems encountered in food, chemical and mining industries.
- Comparative analysis on flow and head loss characteristic in pneumatic and hydraulic slurry conveying systems.
- Investigation of pressure drop inside reducers, converging sections and a diverging section.
- Extension of this study to higher velocities, a wider range of impact velocity and solid concentration under different environment.
- To investigate the erosion, erosion-abrasion and erosion-corrosion inside pipe bends.

7.5 ACKNOWLEDGEMENT

I am thankful to the Science & Engineering Board (SERB), New Delhi, an autonomous organization under the Department of Science and Technology (DST), India, for providing financial support for carrying out this study. This work is supported by the Science & Engineering Board (SERB), New Delhi with grant number:-001612.2015.

REFERENCES

Akhtar, A., Pareek, V. and Tadé, M., 2007. CFD simulations for continuous flow of bubbles through gas-liquid columns: Application of VOF method. *Chemical Product and Process Modeling*, *2*(1). DOI: 10.2202/1934-2659.1011

Akilli, H., Levy, E.K. and Sahin, B., 2001. Gas–solid flow behavior in a horizontal pipe after a 90 vertical-to-horizontal elbow. *Powder Technology*, *116*(1), pp. 43-52.

Aleksandrov, V.I., Vasilyeva, M.A. and Pomeranets, I.B., 2017, October. Estimation of efficiency of hydrotransport pipelines polyurethane coating application in comparison with steel pipelines. *In IOP Conference Series: Earth and Environmental Science* (Vol. 87, No. 2, p. 022001).

Ansys, A.F., 2011. 14.0 Theory Guide. ANSYS Inc., 390.

Asokbunyarat, V., van Hullebusch, E.D., Lens, P.N. and Annachhatre, A.P., 2015. Coal bottom ash as sorbing material for Fe (II), Cu (II), Mn (II), and Zn (II) removal from aqueous solutions. *Water, Air, & Soil Pollution*, 226(5), p. 143/1-17.

Autee, A.T. and Giri, S.V., 2016. Experimental study on two-phase flow pressure drop in small diameter bends. Perspectives in Science, 8, pp.621-625.

Azzi, A. and Friedel, L., 2005. Two-phase upward flow 90° bend pressure loss model. *Forschung im Ingenieurwesen*, 69(2), pp. 120-130.

Bai, X.N., Hu, S.G., Zhang, D.F. and Qin, H.B., 2001. Advances and applications of solid-liquid two-phase flow in pipeline hydrotransport. *Journal of Hydrodynamics*, *3*, p.004.

Bain, A.G. and Bonnington, S.T., 1970. *The hydraulic transport of solids by pipeline* (No. BOOK). Pergamon Press.

Baird, D.C., 1962. Experimentation: an introduction to measurement theory and experiment design. Prentice Hall.

Biały, M., Pietrykowski, K., Tulwin, T. and Magryta, P., 2017. CFD numerical simulation of the indirect cooling system of an internal combustion engine. *Combustion Engines*, pp. 56-65.

Bantin, R.A. and Streat, M., 1970. Dense-phase flow of solid-water mixtures in pipelines. *Proceedings of Hydro transport*, *1*, pp. 1-24.

Benbella, S., Al-Shannag, M. and Al-Anber, Z.A., 2009. Gas–liquid pressure drop in vertical internally wavy 90 bend. *Experimental Thermal and Fluid Science*, *33*(2), pp.340-347.

Biswas, A., Gandhi, B.K., Singh, S.N. and Seshadri, V., 2000. Characteristics of coal ash and their role in hydraulic design of ash disposal pipelines. *Indian Journal of engineering and Material Science, 7*, pp. 1-7.

Bournonville, B. and Nzihou, A., 2002. Rheology of non-Newtonian suspensions of fly ash: effect of concentration, yield stress and hydrodynamic interactions. *Powder technology, 128*(2-3), pp. 148-158.

Bbrengança, S.R., Goncalves, M.R.F., Bergmann, C.P. and Rubio, J., 2009. Coal Ash Transportation as Paste-Like, Highly Loaded Pulps in Brazil: Characterization and Main Features. *International Journal of Coal Preparation and Utilization*, *29*(4), pp. 203-215.

Bozzini, B., Ricotti, M.E., Boniardi, M. and Mele, C., 2003. Evaluation of erosion–corrosion in multiphase flow via CFD and experimental analysis. *Wear, 255*(1-6), pp. 237-245.

Calvo, P., Remunan-Lopez, C., Vila-Jato, J.L. and Alonso, M.J., 1997. Novel hydrophilic chitosan-polyethylene oxide nanoparticles as protein carriers. *Journal of Applied Polymer Science*, 63(1), pp. 125-132.

Chandel, S., Seshadri, V. and Singh, S.N., 2009. Effect of additive on pressure drop and rheological characteristics of fly ash slurry at high concentration. *Particulate Science and Technology*, *27*(3), pp. 271-284.

Chandel, S., Singh, S.N. and Seshadri, V., 2010. Transportation of high concentration coal ash slurries through pipelines. *Inter. Archive of Applied Science and Technology*, *1*(1), pp. 1-9.

Charles, M.E. and Redberger, P.J., 1962. The reduction of pressure gradients in oil pipelines by the addition of water: numerical analysis of stratified flow. *The Canadian Journal of Chemical Engineering*, *40*(2), pp. 70-75.

Che, Y., Feng, M. and Xue, T., 2017, June. Pilot plant study of dry deposition of paste tailings in Baogang West Mine. In *Proceedings of the 20th International Seminar on Paste and Thickened Tailings* (pp. 260-266). University of Science and Technology Beijing.

Chen, L., Duan, Y., Pu, W. and Zhao, C., 2009. CFD simulation of coal-water slurry flowing in horizontal pipelines. *Korean Journal of Chemical Engineering*, *26*(4), pp. 1144-1154.

Chen, J., Wang, Y., Li, X., He, R., Han, S. and Chen, Y., 2015a. Reprint of "Erosion prediction of liquid-particle two-phase flow in pipeline elbows via CFD–DEM coupling method". *Powder Technology, 282*, pp. 25-31.

Chen, D., Jiang, X., Lv, S., Lv, G., Ma, Z., Yan, J., Yu, X., Liao, H. and Zhao, H., 2015b. Rheological properties and stability of lignite washery tailing suspensions. *Fuel*, *141*, pp. 214-221.

Chen, X. and Wheeler, C., 2015c. Computational fluid dynamics (CFD) modelling of transfer chutes: assessment of viscosity, drag and turbulence models. *International Journal of Multiphase Flow*, 69, pp. 42-53.

Chen, L., Duan, Y., Zhao, C. and Yang, L., 2009a. Rheological behavior and wall slip of concentrated coal water slurry in pipe flows. *Chemical Engineering and Processing: Process Intensification*, *48*(7), pp. 1241-1248.

Chen, L., Duan, Y., Pu, W. and Zhao, C., 2009b. CFD simulation of coal-water slurry flowing in horizontal pipelines. *Korean Journal of Chemical Engineering*, *26*(4), pp. 1144-1154.

Chen, R., Wilson, M., Leong, Y.K., Bryant, P., Yang, H., and Zhang, D.K., 2011. Preparation and rheology of biochar, lignite char and coal slurry fuels. *Fuel,* 90(4), pp. 1689-1695.

Chen, X., Zhou, J., Chen, Q., Shi, X. and Gou, Y., 2017. CFD simulation of pipeline transport properties of mine tailings three-phase foam slurry backfill. *Minerals*, *7*(8), p. 149.

Chen, W., Roberts, A., Katterfeld, A. and Wheeler, C., 2018. Modelling the stability of iron ore bulk cargoes during marine transport. *Powder Technology,* 326, pp. 255-264.

Chisholm, D., 1983. *Two-phase flow in pipelines and heat exchangers*. G. Godwin in association with Institution of Chemical Engineers.

Corbridge, D.E.C., 1960. The crystal structure of sodium triphosphate, $Na_5P_3O_{10}$, phase I. *Acta Crystallographica*, 13(3), pp. 263-269.

Coussot, P. and Piau, J.M., 1994. On the behavior of fine mud suspensions. *Rheologica Acta*, 33(3), pp. 175-184.

Crawford, N.M., Cunningham, G. and Spence, S.W.T., 2007. An experimental investigation into the pressure drop for turbulent flow in 90 elbow bends. *Proceedings of the Institution of Mechanical Engineers, Part E: Journal of Process Mechanical Engineering*, 221(2), pp. 77-88.

Darby, R. and Melson, J., 1981. How to predict the friction factor for flow of Bingham plastics. C*hemical Engineering*, *88*(26), pp. 59-61.

Davies, D.R. and Corbridge, D.E.C., 1958. The crystal structure of sodium triphosphate, $Na_5P_3O_{10}$, phase II. *Acta Crystallographica*, 11(5), pp. 315-319.

Deng, T., Patel, M., Hutchings, I. and Bradley, M.S.A., 2005. Effect of bend orientation on life and puncture point location due to solid particle erosion of a high concentration flow in pneumatic conveyors. *Wear*, *258*(1-4), pp. 426-433.

Desai, M., Channiwala, S.A. and Nagarsheth, H.J., 2008. Experimental and computational aerodynamic investigations of a car. *WSEAS Transactions on Fluid Mechanics*, 4(3), pp. 359-366.

Dutta, P. and Nandi, N., 2016. Effect of bend curvature on velocity & pressure distribution from straight to a 90° pipe bend-A Numerical Study. *REST Journal on Emerging trends in Modelling and Manufacturing*, *2*(4), pp. 103-108.

Dutta, P., Saha, S.K., Nandi, N. and Pal, N., 2016. Numerical study on flow separation in 90 pipe bend under high Reynolds number by *k*-*ε* modelling. *Engineering Science and Technology, An International Journal*, 19(2), pp. 904-910.

Eesa, M. and Barigou, M., 2009. CFD investigation of the pipe transport of coarse solids in laminar power law fluids. *Chemical Engineering Science*, *64*(2), pp. 322-333.

Einstein, A., 1956. Investigation on the theory of the Brownian movement. Dover Publications, *New York*.

Ekambara, K., Sanders, R.S., Nandakumar, K. and Masliyah, J.H., 2009. Hydrodynamic simulation of horizontal slurry pipeline flow using ANSYS-CFX. *Industrial & Engineering Chemistry Research*, *48*(17), pp. 8159-8171.

El-Nahhas, K., El-Hak, N.G., Rayan, M.A. and El-Sawaf, I., 2009. Effect of particle size distribution on the hydraulic transport of settling slurries. In *Thirteenth International Water Technology Conference. Hurghada, Egypt* (pp. 198-210).

El-Gammal, M., Mazhar, H., Cotton, J.S., Shefski, C., Pietralik, J. and Ching, C.Y., 2010. The hydrodynamic effects of single-phase flow on flow accelerated corrosion in a 90-degree elbow. *Nuclear Engineering and Design*, *240*(6), pp. 1589-1598.

Elrahman, M.A. and Hillemeier, B., 2014. Combined effect of fine fly ash and packing density on the properties of high performance concrete: An experimental approach. *Construction and Building Materials*, 58, pp. 225-233.

Eltoukhy, M.A.R., 2013. Hydraulic Gradient of Sand-Water Mixture Flow for Different Sands and Pipes. *Life Science Journal*, *10*(4). pp. 3490-95.

Fangary, Y.S., Ghani, A.A., El Haggar, S.M. and Williams, R.A., 1997. The effect of fine particles on slurry transport processes. *Minerals Engineering*, *10*(4), pp. 427-439.

Fomenko, E.V., Anshits, N.N., Pankova, M.V., Solovyov, L.A. and Anshits, A.G., 2011, May. Fly ash cenospheres: Composition, morphology, structure, and helium permeability. *In World Coal Ash Conf.–May* (pp. 9-12).

Gandhi, B.K., Singh, S.N. and Seshadri, V., 2001. Performance characteristics of centrifugal slurry pumps. *Journal of Fluids Engineering*, *123*(2), pp. 271-280.

Ganeshan, G. and Panda, D., 2017. Effect of oil viscosity on rheology of coal–oil mixtures. *International Journal of Coal Preparation and Utilization*, *37*(5), pp. 227-236.

Ghosal, S., Lund, T.S., Moin, P. and Akselvoll, K., 1995. A dynamic localization model for large-eddy simulation of turbulent flows. *Journal of Fluid Mechanics*, 286, pp. 229-255.

Gidaspow, D., R. Bezburuah, and J. Ding. 1992. Hydrodynamics of circulating fluidized beds,kinetic theory approach in fluidization. Proceedings of the 7th Engineering Foundation Conference on Fluidization, 3–8 May, Brisbane, Australia, 75–82.

Gillies, R.G. and Shook, C.A., 2000. Modelling high concentration settling slurry flows. *The Canadian Journal of Chemical Engineering*, *78*(4), pp. 709-716.

Gillies, R.G., Shook, C.A. and Xu, J., 2004. Modelling heterogeneous slurry flows at high velocities. *The Canadian Journal of Chemical Engineering*, *82*(5), pp. 1060-1065.

Gopaliya, M.K. and Kaushal, D.R., 2015. Analysis of effect of grain size on various parameters of slurry flow through pipeline using CFD. *Particulate Science and Technology*, *33*(4), pp. 369-384.

Gopaliya, M.K. and Kaushal, D.R., 2016. Modeling of sand-water slurry flow through horizontal pipe using CFD. *Journal of Hydrology and Hydromechanics*, 64(3), pp. 261-272.

Gupta, N., Luttrell, G. and Noble, A., 2018. Coal micro-pricing: optimizing the coal fuel supply chain for Indian thermal power plants. *International Journal of Coal Preparation and Utilization*, 38(8), pp. 402-421.

Hashemi, S.A., Sadighian, A., Shah, S.I.A. and Sanders, R.S., 2014. Solid velocity and concentration fluctuations in highly concentrated liquid–solid (slurry) pipe flows. *International Journal of Multiphase Flow*, *66*, pp. 46-61.

He, Y. B., and J. S. Laskowski. 2000. Rheological properties of magnetite suspensions. *Mineral Processing and Extractive Metallurgy Review*, 20(1), pp. 167–82.

Holman, J. P. 1994. Experimental methods for engineers. 6th Ed. New York:McGraw-Hill.

Horsley, R.R., 1982. Viscometer and pipe loop tests on gold slime slurry at very high concentrations by weight, with and without additives. In *Proc. of Hydrotransport* (Vol. 8).

Hossain, A., Naser, J. and Imteaz, M.A., 2011. CFD investigation of particle deposition in a horizontal looped turbulent pipe flow. *Environmental Modeling & Assessment, 16*(4), pp. 359-367.

Hussain, A., Ahmad, Z. and Ojha, C.S.P., 2016. Flow through lateral circular orifice under free and submerged flow conditions. *Flow Measurement and Instrumentation*, 52, pp. 57-66.

Ihle, C.F., 2016. The least energy and water cost condition for turbulent, homogeneous pipeline slurry transport. *International Journal of Mineral Processing*, *148*, pp. 59-64.

Ihle, C.F. and Tamburrino, A., 2012. Variables affecting energy efficiency in turbulent ore concentrate pipeline transport. *Minerals Engineering*, 39, pp. 62-70.

Ihle, C.F., 2013. A cost perspective for long distance ore pipeline water and energy utilization. Part I: Optimal base values. *International Journal of Mineral Processing*, 122, pp. 1-12.

Ilic, D. and Wheeler, C., 2017. Measurement and simulation of the bulk solid load on a conveyor belt during transportation. *Powder Technology*, 307, pp. 190-202.

Iyer, R., 2002. The surface chemistry of leaching coal fly ash. *Journal of Hazardous Materials,* 93(3), pp. 321-329.

Jacobs, B.E., 2014. *Design of slurry transport systems*. CRC Press.

Johnson, P.C., and R. Jackson. 1987. Frictional–Collisional constitutive relations for granular materials, with application to plane shearing. *Journal of Fluid Mechanics*, 176, pp. 67–93.

Juneja, P., Kumar, S. and Mohapatra, S.K., 2018. Influence of Chemical Leaching on Rheology and Ash Reduction of Indian Coal. *International Journal of Coal Preparation and Utilization*, 38(5), pp.260-270.

Kaushal, D.R. and Tomita, Y., 2002. Solids concentration profiles and pressure drop in pipeline flow of multisized particulate slurries. *International Journal of Multiphase Flow*, *28*(10), pp. 1697-1717.

Kaushal, D.R., Sato, K., Toyota, T., Funatsu, K., Tomita, Y., 2005. Effect of particle size distribution on pressure drop and concentration profile in pipeline flow of highly concentrated slurry. *International Journal of Multiphase Flow*, 31, pp. 809-823.

Kaushal, D.R., Thinglas, T., Tomita, Y., Kuchii, S. and Tsukamoto, H., 2012. CFD modeling for pipeline flow of fine particles at high concentration. *International Journal of Multiphase Flow*, *43*, pp. 85-100.

Kaushal, D.R., Kumar, A., Tomita, Y., Kuchii, S. and Tsukamoto, H., 2017. Flow of bi-modal slurry through horizontal bend. *KONA Powder and Particle Journal*, p. 2017016.

Kim, C. and Han, C., 2013. Numerical simulation of hydraulic transport of sand-water mixtures in pipelines. *Open Journal of Fluid Dynamics*, *3*(4), p. 266.

Kim, J., Yadav, M. and Kim, S., 2014. Characteristics of secondary flow induced by 90-degree elbow in turbulent pipe flow. *Engineering Applications of Computational Fluid Mechanics*, 8(2), pp. 229-239.

Kosswig, K. 2002. *Surfactants in Ullmann's encyclopedia of industrial chemistry.* Wiley-VCH, Weinheim. DOI:10.1002/14356007.a25_747.

Krieger, I.M., 1968. Shear rate in the Couetta viscometer, *Transaction Society of Rheology, 12*, pp. 5-13.

Kuan, B., Yang, W. and Schwarz, M.P., 2007. Dilute gas–solid two-phase flows in a curved 90∘ duct bend: CFD simulation with experimental validation. *Chemical Engineering Science, 62*(7), pp. 2068-2088.

Kumar, K., Kumar, S., Singh, G., Singh, J.P. and Singh, J., 2017a. Erosion Wear Investigation of HVOF Sprayed WC-10Co4Cr Coating on Slurry Pipeline Materials. *Coatings*, *7*(4), p. 54/1-11.

Kumar, K., Kumar, S., Gupta, M., Garg, H.C. and Singh, G., 2017b. Measurement of flow characteristics for multiparticulate bottom ash-water suspension with additives. *Journal of Residuals Science & Technology*. *14*, pp. 11-17.

Kumar, K., Kumar, S., Gupta, M., Garg, H.C. and Singh, G., 2017c. Measurement of flow characteristics for multiparticulate bottom ash-water suspension with additives. *Journal of Residuals Science & Technology*. *14*(1), pp. 11-17.

Kumar, S., Singh, J. and Mohapatra, S.K., 2018a. Role of particle size in assessment of physico-chemical properties and trace elements of Indian fly ash. *Waste Management & Research,* 36(11), pp. 1016-1022.

Kumar, N., Kaushal, D.R., and Kumar, A., 2012. Computational Study of the Two Phase Flow in Horizontal Slurry Pipeline. *International Journal of Mechanical and Production Engineering, 1*(1)*,* pp. 2315-4489.

Kumar, R., Banerjee, S., Banik, A., Bandyopadhyay, T.K. and Naiya, T.K., 2017d. Simulation of single phase non-Newtonian flow characteristics of heavy crude oil through horizontal pipelines. *Petroleum Science and Technology*, 35(6), pp. 615-624.

Kumar, R., Bora, G.S., Banerjee, S., Mandal, A. and Naiya, T.K., 2018b. Application of naturally extracted surfactant from Madhuca longifolia to improve the flow properties of heavy crude oil through horizontal pipeline. *Journal of Petroleum Science and Engineering*, 168, pp. 178-189.

Kumar, S., Gandhi, B.K. and Mohapatra, S.K., 2014. Performance characteristics of centrifugal slurry pump with multi-sized particulate bottom and fly ash mixtures. *Particulate Science and Technology, 32*(5), pp. 466-476.

Kumar, U., Gandhi, B.K., Singh, S.N., Seshadri, V. and Gupta, V.K., 2000, November. Performance characteristics of demonstration unit for transportation of solid-liquid flow at high concentration setup at NCPP, Dadri. In *Proceedings International Seminar on Material handling Systems Indian Institute of Plant Engineers (Delhi-Haryana Chapter), November16-18, New Delhi* (pp. 126-136).

Kumar, U., Mishra, R., Singh, S.N. and Seshadri, V., 2003. Effect of particle gradation on flow characteristics of ash disposal pipelines. *Powder Technology*, *132*(1), pp. 39-51.

Kwak, M., James, D.F. and Klein, K.A., 2005. Flow behaviour of tailings paste for surface disposal. *International Journal of Mineral Processing*, *77*(3), pp. 139-153.

Lahiri, S.K. and Ghanta, K.C., 2008. Prediction of pressure drop of slurry flow in pipeline by hybrid support vector regression and genetic algorithm model. *Chinese Journal of Chemical Engineering*, *16*(6), pp. 841-848.

Lahiri, S.K. and Ghanta, K.C., 2010. Regime identification of slurry transport in pipelines: A novel modelling approach using ANN & differential evolution. *Chemical Industry and Chemical Engineering Quarterly, 16*(4), pp. 329-343.

Landel, R.F. Moser, B.G. and Baumann, A.J. 1965. Rheology of concentrated suspension: effect of surfactant, In *4th International Congress on Rheology*, pp. 663-673.

Lauder, B.E. and Spalding, D.B., 1972. Lectures in mathematical models of turbulence. London: AP.

Lee, J.K., Ko, J. and Kim, Y.S., 2017. Rheology of Fly Ash Mixed Tailings Slurries and Applicability of Prediction Models. *Minerals*, *7*(9), p. 165-176.

Li, L., Usui, H. and Suzuki, H., 2002. Study of pipeline transportation of dense fly ash-water slurry. *Coal preparation*, *22*(2), pp. 65-80.

Li, P., Yang, D., Qiu, X. and Feng, W., 2015. Study on enhancing the slurry performance of coal–water slurry prepared with low-rank coal. *Journal of Dispersion Science and Technology*, *36*(9), pp. 1247-1256.

Ling, J., Skudarnov, P.V., Lin, C.X. and Ebadian, M.A., 2003. Numerical investigations of liquid–solid slurry flows in a fully developed turbulent flow region. *International Journal of Heat and Fluid Flow*, *24*(3), pp. 389-398.

Lisandy, K.Y., Kim, J.W., Lim, H., Kim, S.M. and Jeon, C.H., 2016. Prediction of unburned carbon and NO formation from low-rank coal during pulverized coal combustion: Experiments and numerical simulation. *Fuel*, 185, pp. 478-490.

Liu, H., 2003. *Pipeline engineering*. CRC Press.

Lopez, D.A., Schreiner, W.D., De Sánchez, S.R. and Simison, S.N., 2003. The influence of carbon steel microstructure on corrosion layers: an XPS and SEM characterization. *Applied surface science*, 207(1-4), pp. 69-85.

Lorenzi, L. D., and P. Bevilacqua. 2002. The influence of particle size distribution and non-ionic surfactant on the rheology of coal water fuels produced using Iranian and Venezuelan coals. *Coal Preparation,* 22 (5), pp. 249–68.

Lu, P. and Zhang, M., 2002. Resistance properties of coal–water paste flowing in pipes. *Fuel*, *81*(7), pp. 877-881.

Ma, L., Huang, C., Xie, Y., Jiang, J., Tufa, K.Y., Hui, R. and Liu, Z.S., 2015. Modeling of erodent particle trajectories in slurry flow. *Wear*, *334*, pp. 49-55.

Ma, Z.W. and Zhang, P., 2012. Pressure drops and loss coefficients of a phase change material slurry in pipe fittings. *International journal of refrigeration*, *35*(4), pp. 992-1002.

Mandal, S.N. and Das, S.K., 2001. Pressure losses in bends during two-phase gas−Newtonian liquid flow. *Industrial & engineering chemistry research*, *40*(10), pp. 2340-2351.

Matousek, V., 2009. Concentration profiles and solids transport above stationary deposit in enclosed conduit. *Journal of Hydraulic Engineering*, 135(12), pp. 1101-1106.

Matsunaga, T., Kim, J.K., Hardcastle, S. and Rohatgi, P.K., 2002. Crystallinity and selected properties of fly ash particles. *Materials Science and Engineering: A*, 325(1-2), pp. 333-343.

Mazumder, Q.H., 2012a. CFD analysis of the effect of elbow radius on pressure drop in multiphase flow. *Modelling and Simulation in Engineering*, p. 37-45.

Mazumder, Q.H., 2012b. CFD analysis of single and multiphase flow characteristics in elbow. *Engineering*, *4*(04), p. 210.

Menter, F.R., 1994. Two-equation eddy-viscosity turbulence models for engineering applications. *AIAA journal*, 32(8), pp. 1598-1605.

Meriem-Benziane, M., Abdul-Wahab, S.A., Benaicha, M. and Belhadri, M., 2012. Investigating the rheological properties of light crude oil and the characteristics of its emulsions in order to improve pipeline flow. *Fuel*, *95*, pp. 97-107.

Merrill, J., Voisin, L., Montenegro, V., Ihle, C.F. and McFarlane, A., 2017. Slurry rheology prediction based on hyperspectral characterization models for minerals quantification. *Minerals Engineering*, *109*, pp. 126-134.

Messa, G.V. and Malavasi, S., 2013. Numerical investigation of solid-liquid slurry flow through an upward-facing step. *Journal of Hydrology and Hydromechanics*, *61*(2), pp. 126-133.

Mishra, D.P. and Das, S.K., 2010. A study of physico-chemical and mineralogical properties of Talcher coal fly ash for stowing in underground coal mines. *Materials Characterization*, 61(11), pp. 1252-1259.

Mishra, D.P. and Das, S.K., 2014. Comprehensive characterization of pond ash and pond ash slurries for hydraulic stowing in underground coal mines. *Particulate Science and Technology*, 32(5), pp. 456-465.

Mishra, R., Singh, S.N. and Seshadri, V., 1998. Pressure drop across conventional and diverging-converging pipe bends in the flow of multi-sized particulate slurries. *Indian Journal of Engineering and Materials sciences, 5*, pp. 9-14.

Stuti Mishra, Akshoy Ranjan Paul, Anuj Jain and Rakesh Mishra, 2016 "Optimal Sizing of an Ovoid Duct Transporting Solid-Liquid Mixtures", Proceedings of 6th International and 43rd National Conference on Fluid Mechanics and Fluid Power (FMFP-2016) 15-17 Dec. 2016, MNNIT Allahabad (India). ISBN No. 978-93- 5267-407-7.

Mishra, R., Ghanta, K.C., Mullick, A.N. and Sinha, S.L., 2017. Numerical prediction of flow behavior and erosion prediction of coal water and copper ore water slurries. *Journal of Advanced Research in Dynamical and Control System, 4*, pp. 2368-2388.

Mooney, M., 1951. The viscosity of a concentrated suspension of spherical particles. *Journal of colloid science*, *6*(2), pp. 162-170.

Moreland, C., 1963. Viscosity of suspensions of coal in mineral oil. *The Canadian Journal of Chemical Engineering*, *41*(1), pp. 24-28.

Mosa, E.S., Saleh, A.H.M., Taha, T.A. and El-Molla, A.M., 2008. Effect of chemical additives on flow characteristics of coal slurries. *Physicochemical Problems of Mineral Processing, 42*, pp. 107-118.

Mukhtar, A., Singh, S.N. and Seshadri, V., 1995. Pressure drop in a long radius 90° horizontal bend for the flow of multisized heterogeneous slurries. *International Journal of Multiphase Flow*, *21*(2), pp. 329-334.

Nabil, T., El-Sawaf, I. and El-Nahhas, K., 2013, November. Computational fluid dynamics simulation of the solid-liquid slurry flow in a pipeline. In *Proc. 17th International Water Technologies Conference IWTC17* (Vol. 57).

Naik, H.K., Mishra, M.K., Karanam, U.R. and Deb, D., 2009. Evaluation of the role of a cationic surfactant on the flow characteristics of fly ash slurry. *Journal of Hazardous Materials*, 169(1-3), pp. 1134-1140.

Naik, H.K., Mishra, M.K. and Rao Karanam, U.M., 2009a, May. *Rheological characteristics of fly ash slurry at varying temperature environment with and without an additive*. In Proc. World of Coal Ash Conference, pp.1-12.

Navickis, L.L., 1989. Rheological changes of fortified wheat and corn flour doughs with mixing time. *Cereal Chemistry,* 66(4), pp. 321-4.

Nayak, B.B. and Chatterjee, D., 2017a. Convective heat transfer in slurry flow in a horizontal Y-shaped branch pipe. *Powder technology*, 318, pp. 46-61.

Nayak, B.B. and Chatterjee, D., 2017b. Numerical investigation of convective heat transfer in pipeline flow of multi-sized mono dispersed fly ash-water slurry. *International Journal of Heat and Mass Transfer*, 108, pp. 1802-1818.

Nayak, B.B., Chatterjee, D. and Mullick, A.N., 2015. Numerical simulation of convective transport of fly ash-water slurry in horizontal pipe bends. *Multiphase Science and Technology*, 27, pp. 2-4.

Ndinisa, N.V., Wiley, D.E. and Fletcher, D.F., 2005. Computational fluid dynamics simulations of Taylor bubbles in tubular membranes: model validation and application to laminar flow systems. *Chemical Engineering Research and Design*, 83(1), pp. 40-49.

Nguyen, Q.D. and Boger, D.V., 1984, October. Exploiting the rheology of highly concentrated suspensions. *In Proc. IX. Int. Congress on Rheology, Acapulco, Mexico* (Vol. 813, p. 153171).

Nicklin, D.J., 1962. Two-phase bubble flow. *Chemical engineering science*, 17(9), pp. 693-702.

Noble, A., He, Y.T. and Ziemkiewicz, P., 2016. Partitioning behavior of 4-methyl cyclohexane methanol in two appalachian coal preparation plants. *International Journal of Coal Preparation and Utilization,* 36(2), pp. 69-81.

Norton, G.A., Markuszewski, R. and Shanks, H.R., 1986. Morphological and chemical characterization of iron-rich fly ash fractions. *Environmental Science & Technology*, 20(4), pp. 409-413.

Orszag, S.A., Yakhot, V., Flannery, W.S., Boysan, F., Choudhury, D., Maruzewski, J. and Patel, B., 1993. Renormalization Group Modeling and Turbulence Simulations. *In International Conference on Near-Wall Turbulent Flows*, Tempe, Arizona.

Ofei, T.N. and Ismail, A.Y., 2016. Eulerian-eulerian simulation of particle-liquid slurry flow in horizontal pipe. *Journal of Petroleum Engineering*, p. 5743471/1-10.

Panda, S. and Swain, R.K., 2014. Some aspects of the rheological behaviour of coal water slurries. *International Journal of Thermal and Environment Engineering*, *8*(2), pp. 103-107.

Pani, G.K., Rath, P., Barik, R. and Senapati, P.K., 2015. The effect of selective additives on the rheological behavior of power plant ash slurry. *Particulate Science and Technology*, *33*(4), pp. 418-422.

Parsi, M., Najmi, K., Najafifard, F., Hassani, S., McLaury, B.S. and Shirazi, S.A., 2014. A comprehensive review of solid particle erosion modeling for oil and gas wells and pipelines applications. *Journal of Natural Gas Science and Engineering*, *21*, pp. 850-873.

Pietralik, J.M. and Schefski, C.S., 2009, January. Flow and mass transfer in bends under flow-accelerated corrosion wall thinning conditions. In *17th International Conference on Nuclear Engineering* (pp. 493-501). American Society of Mechanical Engineers.

Pietrykowski, K., Grabowski, Ł., Sochaczewski, R. and Wendeker, M., 2013. The CFD model of the mixture formation in the Diesel dual-fuel engine. *Combustion Engines*, 154(3), pp. 476-482.

Pinto, M., Kemp, I., Bermingham, S., Hartwig, T. and Bisten, A., 2014a. Development of an axisymmetric population balance model for spray drying and validation against experimental data and CFD simulations. *Chemical Engineering Research and Design*, *92*(4), pp. 619-634.

Pinto, T.S., Junior, D.M., Slatter, P.T. and Leal Filho, L.S., 2014b. Modelling the critical velocity for heterogeneous flow of mineral slurries. *International Journal of Multiphase Flow*, *65*, pp. 31-37.

Peng, W. and Cao, X., 2016. Numerical simulation of solid particle erosion in pipe bends for liquid–solid flow. *Powder Technology*, *294*, pp. 266-279.

Perez, M., Barbé, J.C., Neda, Z., Bréchet, Y. and Salvo, L., 2000. Computer simulation of the microstructure and rheology of semi-solid alloys under shear. *Acta Materialia*, 48(14), pp. 3773-3782.

Peters, T.M. and Leith, D., 2004. Particle deposition in industrial duct bends. *Annals of Occupational Hygiene*, *48*(5), pp. 483-490.

Qi, C., Chen, Q., Fourie, A., Zhao, J. and Zhang, Q., 2018. Pressure drop in pipe flow of cemented paste backfill: Experimental and modeling study. *Powder Technology*, *333*, pp. 9-18.

Ravelet, F., Bakir, F., Khelladi, S. and Rey, R., 2013. Experimental study of hydraulic transport of large particles in horizontal pipes. *Experimental Thermal and Fluid Science*, *45*, pp. 187-197.

Rawat, A., Singh, S.N. and Seshadri, V., 2016. Computational methodology for determination of head loss in both laminar and turbulent regimes for the flow of high concentration coal ash slurries through pipeline. *Particulate Science and Technology*, *34*(3), pp. 289-300.

Rehman, A.U., Kumar, V.K., Jain, A., Paul, Akshoy, R., 2017 July. Performance and cavitation prediction in an industrial centrifugal pump for different working fluids. In *First International Conference on Thermal and Fluid Engineering (ICTF-2017),* 3-5 July 2017, Phuket (Thailand), pp. 36-42, ISBN No. 978-605-9546-05-8.

Roache, P. J. 1997. Quantification of uncertainty in computation fluid dynamics. *Annual Review of Fluid Mechanics*, *29,* pp. 123–60.

Roco, M.C. and Shook, C.A., 1983. Modeling of slurry flow: the effect of particle size. *The Canadian Journal of Chemical Engineering*, *61*(4), pp. 494-503.

Roscoe, R., 1952. The viscosity of suspensions of rigid spheres. *British Journal of Applied Physics*, *3*(8), p. 267.

Röhrig, R., Jakirlić, S. and Tropea, C., 2015. Comparative computational study of turbulent flow in a 90 pipe elbow. *International Journal of Heat and Fluid Flow*, 55, pp. 120-131.

Rutgers, I.R., 1962. Relative viscosity of suspensions of rigid spheres in Newtonian liquids. *Rheologica Acta*, *2*(3), pp. 202-210.

Sahoo, B.K., De, S., Carsky, M. and Meikap, B.C., 2010. Enhancement of rheological behavior of Indian high ash coal−water suspension by using microwave pretreatment. *Industrial & Engineering Chemistry Research*, *49*(6), pp. 3015-3021.

Solnordal, C.B., Wong, C.Y. and Boulanger, J., 2015. An experimental and numerical analysis of erosion caused by sand pneumatically conveyed through a standard pipe elbow. *Wear*, *336,* pp. 43-57.

Saidj, F., Kibboua, R., Azzi, A., Ababou, N. and Azzopardi, B.J., 2014. Experimental investigation of air–water two-phase flow through vertical 90° bend. *Experimental Thermal and Fluid Science*, 57, pp. 226-234.

Sah B. K., 2014. Optimization of amount of additives to minimize relative viscosity of coal-water slurry. *Journal of Applied Chemistry*. 2278-5736, pp. 58-62.

Schaan, J., Sumner, R.J., Gillies, R.G. and Shook, C.A., 2000. The effect of particle shape on pipeline friction for Newtonian slurries of fine particles. *The Canadian Journal of Chemical Engineering*, *78*(4), pp. 717-725.

Schrick, W., Smith, L.G., Hass, D.B. and Husband, W.H.W., 1972. Experimental studies on the hydraulic transport of coal. *Engineering Division of Saskatchewan Research Council, Canada*.

Schrödter, K., Bettermann, G., Staffel, T., Wahl, F., Klein, T. and Hofmann, T., 2008. Phosphoric acid and phosphates. *Ullmann's Encyclopedia of Industrial Chemistry*.

Seitshiro, I., Fujii, S., Yokoyama, N., Sato, I. and Sato, H., 2012. The Multi-Sized Slurry Flows in Horizontal Pipes: Innovated Models and Verification. *International Journal of the Society of Materials Engineering for Resources*, *19*(1-2), pp. 24-31.

Senapati, P.K., Das, D., Nayak, A. and Mishra, P.K., 2008. Studies on preparation of coal water slurry using a natural additive. *Energy Sources*, *Part A*, *30*(19), pp. 1788-1796.

Senapati, P.K., Mishra, B.K. and Parida, A., 2013. Analysis of friction mechanism and homogeneity of suspended load for high concentration fly ash & bottom ash mixture slurry using rheological and pipeline experimental data. *Powder Technology*, *250*, pp. 154-163.

Senapati, P.K. and Mishra, B.K., 2015. Bulk hydraulic disposal of highly concentrated fly ash and bottom ash–water slurries. *Particulate Science and Technology*, *33*(2), pp. 124-131.

Shah, N.A., Animasaun, I.L., Ibraheem, R.O., Babatunde, H.A., Sandeep, N. and Pop, I., 2018. Scrutinization of the effects of Grashof number on the flow of different fluids driven by convection over various surfaces. *Journal of Molecular Liquids*, 249, pp. 980-990.

Shao, S., Chen, X., Liu, H. and Wang, F., 2012. Preparation of coal slurry with alcohol fermentation wastewater. *Energy Sources, Part A: Recovery, Utilization, and Environmental Effects*, *34*(10), pp. 919-928.

Shankar, V., Eckert, P., Ojha, C. and König, C.M., 2009. Transient three-dimensional modeling of riverbank filtration at Grind well field, Germany. *Hydrogeology Journal*, 17(2), pp. 321-326.

Shih, T., Liou, W.W., Shabbir, A., Yang, Z. and Zhu, J., 1994. A new eddy viscosity model for high reynolds number turbulent flows: development and validation. NASA TM, 106721.

Singh, G., Kumar, S., Singh, M.K. and Mohapatra, S.K., 2016a. Environmental impact assessment of ash disposal system of a thermal power plant. *International Journal of Hydrogen Energy*, *41*(35), pp. 15887-15891.

Singh, M.K., Ratha, D., Kumar, S. and Kumar, D., 2016b. Influence of particle-size distribution and temperature on rheological behavior of coal slurry. *International Journal of Coal Preparation and Utilization*, *36*(1), pp. 44-54.

Singh, J., Kumar, S., Singh, J.P., Kumar, P. and Mohapatra, S.K., 2018a. CFD modeling of erosion wear in pipe bend for the flow of bottom ash suspension. *Particulate Science and Technology*, pp. 1-11.

Singh, M., Kumar, S., Kumar, S., Nandan, G. and Gupta, M., 2018b. Characterization of Iron-ore suspension at In-situ conditions. *Materials Today: Proceedings*, 5(9), pp. 17845-17851.

Singh, G., Kumar, S. and Mohapatra, S.K., 2018c. Potential Risk by Disposal of Bottom Ash from Thermal Power Plants and Minimization by Addition of $NaHCO_3$. *Bulletin of Environmental Contamination and Toxicology*, *101*(6), pp. 773-778.

Singh, J., Kumar, S. and Mohapatra, S.K., 2018d. Study on role of particle shape in erosion wear of austenitic steel using image processing analysis technique. *Proceedings of the Institution of Mechanical Engineers, Part J: Journal of Engineering Tribology*, p.1350650118794698.

Sive, A.W. and Lazarus, J.H., 1987. Hydraulic transport system design for high concentration fly ash slurries. *Coal Ash–A Valuable Resource*.

Skoog, D.A., Holler, F.J. and Crouch, S.R., 2017. Principles of instrumental analysis. Cengage learning.

Slatter, P., 2011. The engineering hydrodynamics of viscoplastic suspensions. *Particulate Science and Technology*, *29*(2), pp. 139-150.

Slatter, P.T. and Seddon, K.D., 2015, April. Evaluation of the rheology of pipe head flocculated tailings. In *Proceedings of the 18th International Seminar on Paste and Thickened Tailings* (pp. 131-137). Australian Centre for Geomechanics.

Ślączka, A. and Piszczyński, Z., 2008. Effect of selected additives on the stability and rheology of Coal-Water Slurry Fuels (CWSF). *Gospodarka Surowcami Mineralnymi*, *24*(3/1), pp. 363-373.

Spedding, P.L., Bénard, E. and McNally, G.M., 2004. Fluid flow through 90 degree bends. *Developments in Chemical Engineering and Mineral Processing*, *12*(1-2), pp. 107-128.

Spedding, P.L. and Bénard, E., 2007. Gas–liquid two phase flow through a vertical 90 elbow bend. *Experimental Thermal and fluid science*, *31*(7), pp. 761-769.

Suzuki, M., Inaba, K. and Yamamoto, M., 2008. Numerical simulation of sand erosion in a square-section 90-degree bend. *Journal of Fluid Science and Technology*, *3*(7), pp. 868-880.

Tan, Y., Zhang, H., Yang, D., Jiang, S., Song, J. and Sheng, Y., 2012. Numerical simulation of concrete pumping process and investigation of wear mechanism of the piping wall. *Tribology International*, *46*(1), pp. 137-144.

Taylor, J., 1997. Introduction to error analysis, the study of uncertainties in physical measurements.

Tebowei, R., Hossain, M., Islam, S.Z., Droubi, M.G. and Oluyemi, G., 2018. Investigation of sand transport in an undulated pipe using computational fluid dynamics. *Journal of Petroleum Science and Engineering*, *162*, pp. 747-762.

Thomas, D.G., 1965. Transport characteristics of suspensions: VIII A note on the viscosity of Newtonian suspensions of uniform spherical particles. *Journal of Colloid Science*, *20*, p. 265.

Tian, Q., He, G., Wang, H. and Cai, D., 2014. Simulation on transportation safety of ice slurry in ice cooling system of buildings. *Energy and Buildings*, *72*, pp. 262-270.

Verma, A.K., Singh, S.N. and Seshadri, V., 2006. Pressure drop for the flow of high concentration solid-liquid mixture across 90º horizontal conventional circular pipe bend. *Indian Journal of Engineering and Materials Sciences*, *13*, pp. 477-483.

Vishnoi, N. and Mohapatra, S.K., 2018. Study of particle size distribution of pulverized coals in utility boilers. *Particulate Science and Technology*, *36*(8), pp. 999-1005.

Vlasak, P. and Chara, Z., 2007. Effect of particle size and concentration on flow behavior of complex slurries. In Seventh ISOPE Ocean Mining Symposium. *International Society of Offshore and Polar Engineers*. Lisbon, Portugal, July 1-6, pp. 181-187.

Vlasak, P. and Chara, Z., 2009. Conveying of solid particles in Newtonian and non-Newtonian carriers. *Particulate Science and Technology*, *27*(5), pp. 428-443.

Vlasak, P., Chara, Z. and Stern, P., 2010. Drag reduction of dense fine-grained slurries. *Journal of Hydrology and Hydromechanics*, *58*(4), pp. 261-270.

Vlasak, P. and Chara, Z., 2011. Effect of particle size distribution and concentration on flow behavior of dense slurries. *Particulate Science and Technology*, *29*(1), pp. 53-65.

Wang, J., Zhang, T. and Wang, S., 2013. Heterogeneous ice slurry flow and concentration distribution in horizontal pipes. *International Journal of Heat and Fluid Flow*, *44*, pp. 425-434.

Williams, O.A. and Williams, O.A., 1983. *Pneumatic and Hydraulic Conveying of Solids*. M. Dekker.

Williams, P.S., 1953. Flow of concentrated suspensions. Journal *of Applied Chemistry, 3*, pp. 120-127.

Wilson, K.C., 1982. A dense phase option for coarse coal pipelining. *Journal of pipelines*, *5*, pp. 251-57.

Wirth, R., 2009. Focused Ion Beam (FIB) combined with SEM and TEM: Advanced analytical tools for studies of chemical composition, microstructure and crystal structure in geomaterials on a nanometre scale. *Chemical Geology*, *261*(3-4), pp. 217-229.

Woodcock, C.R. and Mason, J.S., 1987. Hydraulic conveying. In *Bulk Solids Handling* (pp. 478-493). Springer, Dordrecht.

Wu, D., Yang, B. and Liu, Y., 2015. Pressure drop in loop pipe flow of fresh cemented coal gangue–fly ash slurry: experiment and simulation. *Advanced Powder Technology*, *26*(3), pp. 920-927.

Yoon, S.J., Choi, Y.C. and Lee, J.G., 2009. The effect of additive chemicals on the viscosity of coal-petroleum coke-water slurry fuel for a gasification process. *Korean Journal of Chemical Engineering*, *26*(5), pp. 1259-1264.

Wu, J., Nguyen, B. and Graham, L., 2010. Energy efficient high solids loading agitation for the mineral industry. *The Canadian Journal of Chemical Engineering*, *88*(2), pp. 287-294.

Yuchi, W., Li, B., Li, W., and Chen, H. 2005. Effects of coal characteristics on the properties of coal water slurry. *Coal Preparation*, 25 (4):239–49.

Zandi, I. ed., 2013. Advances in solid–liquid flow in pipes and its application. *Elsevier*.

Zhang, T., Zhang, Y.O. and Ouyang, H., 2015. Structural vibration and fluid-borne noise induced by turbulent flow through a 90° piping elbow with/without a guide vane. *International Journal of Pressure Vessels and Piping, 125*, pp. 66-77.

Zhu, J., Zhang, G., Li, J. and Zhao, F., 2013. Synthesis, adsorption and dispersion of a dispersant based on starch for coal–water slurry. *Colloids and Surfaces A: Physicochemical and Engineering Aspects*, *422*, pp. 165-171.

Zhu, J., Zhang, G., Liu, G., Qu, Q. and Li, Y., 2014. Investigation on the rheological and stability characteristics of coal–water slurry with long side-chain polycarboxylate dispersant. *Fuel Processing Technology*, 118, pp. 187-191.

Zyrkowski, M., Neto, R.C., Santos, L.F. and Witkowski, K., 2016. Characterization of fly-ash cenospheres from coal-fired power plant unit. *Fuel*, 174, pp. 49-53.

LIST OF PUBLICATIONS

SCI/SCIE indexed publications

- Singh JP, Kumar S, Mohapatra SK. Head Loss Investigations Inside 90° Pipe Bend for Conveying Of Fine Coal–Water Slurry Suspension. *International Journal of Coal Preparation and Utilization*. 2017. https://doi.org/10.1080/19392699.2017.1415892 (I.F.:1.5).
- Singh JP, Kumar S, Mohapatra SK. Modelling of two phase solid-liquid flow in horizontal pipe using computational fluid dynamics technique. *International Journal of Hydrogen Energy*. 2017; 42(31): 20133-7. (I.F.:4.2)
- Singh JP, Kumar S, Mohapatra SK. Simulation and optimization of coal-water slurry suspension flow through 90° pipe bend using CFD. *International Journal of Coal Preparation and Utilization*. 2018. https://doi.org/10.1080/19392699.2018.1488693 (I.F.:1.5)
- Singh JP, Kumar S, Mohapatra SK. An experimental study on head loss characteristics of pipe bends for flow of coal-water slurry at higher solid concentration. *Proceedings of the Institution of Mechanical Engineers, Part E: Journal of Process Mechanical Engineering*. Sage. 2019; 233(5):1151-1161. (I.F.:1.13)

Scopus indexed

- Singh, J.P., Kumar, S., Mohapatra, S.K. and Nandan, G. Experimental Design-Based Analysis on Process Parameters for Head Loss in Pipe Bend. *In Advances in Fluid and Thermal Engineering*. Springer, Singapore. 2019; 379-388.
- Singh JP, Kumar S, Mohapatra SK, Paras V. Investigation on the Rheological Characteristics of Bottom ash-water suspension with additive. *Materials Science and Engineering*. 2018. https://doi.org/10.1088/1757-899X/455/1/012133